AN ADVANCED SYSTEM FOR THE TARGETED CLASSIFICATION OF GRASSLAND TYPES WITH MULTI-TEMPORAL SAR IMAGERY

Dissertation

zur Erlangung

des Doktorgrades der Naturwissenschaften (Dr. rer. nat.)

des Fachbereichs Mathematik / Informatik

der Universität Osnabrück

vorgelegt von:

Dipl.-Geogr. Annekatrin Metz

geb. am 23.01.1983

Osnabrück, Mai 2016

Betreuer:	Prof. Dr.-Ing. Manfred Ehlers, Universität Osnabrück
	Hon.-Prof. Dr.-Ing. Peter Reinartz, Deutsches Zentrum für Luft- und Raumfahrt e.V.
Tag der Disputation:	25.07.2016

TABLE OF CONTENTS

LIST OF FIGURES

LIST OF TABLES

ABBREVIATIONS

AA%	Percentage average accuracy
AHS	Advanced Hyperspectral Sensor
AOI	Area of interest
ASAR	Advanced Synthetic Aperture Radar
ATKIS	Authorative Topographic-Cartographic Information System
AVHRR	Advanced Very High Resolution Radiometer
BY	Bavarian Federal State
CART	Classification and regression tree
CORINE	Coordination of Information on the Environment
CSA	Canadian Space Agency
dB	decibel
DEM	Digital Elevation Model
DFA	Discriminant function analysis
DLR	Deutsches Zentrum für Luft- und Raumfahrt e.V. (German Aerospace Center)
DRG	Data range
EAFRD	European Agricultural Fund for Rural Development
EEA	European Environmental Agency
EEC	European Economic Community
EM	Electromagnetic
ENL	Equivalent number of looks
EnMAP	Environmental Mapping and Analysis Program
EO	Earth Observation
ERS	European Remote Sensing satellite
ESA	European Space Agency
ETM	Enhanced Thematic Mapper
EUNIS	European Nature Information System
FAO	Food and Agriculture Organization of the United Nations
FAOSTAT	Statistics Division of the FAO
FFH	Flora-Fauna-Habitat directive
FQ	Fine resolution Quad-polarization beam (Radarsat-2)
GeoTIFF	Geographic extensions to the Tagged Image File Format
GHz	Gigahertz
GIS	Geographic Information System
GL	Grassland
GPS	Global Positioning System
HH	Horizontal polarization on transmit, Horizontal polarization on receive
HNV	High Nature Value
HR	High resolution

HS	High resolution spotlight mode
HT	Natura 2000 habitat type
HV	Horizontal polarization on transmit, Vertical polarization on receive
Hz	Hertz
IACS	Integrated Administration and Control System
IR	Infrared
IWS	Interferometric Wide Swath
KIT	Karlsruhe Institute of Technology, Karlsruhe, Germany
km	Kilometres
KRC	Kernel-based reclassification
LC	Land cover
LiDAR	Light Detection And Ranging
LUCAS	Land Use and Cover Area frame Survey
MASD	Mean Absolute Spectral Dynamic
MaxEnt	Maximum Entropy Approach
MDA	MacDonald, Dettwiler and Associates Ltd.
MEA	Mean
MODIS	Moderate-resolution Imaging Spectroradiometer
MR	Medium resolution
MSAVE	Multi-season remote sensing for vegetation monitoring
MV	Mecklenburg Western Pomerania
NDVI	Normalized Difference Vegetation Index
NEST	Next ESA SAR Toolbox
NGL	Non-Grassland
NOAA	National Oceanic and Atmospheric Administration
NREVI	Normalized Red-Edge Vegetation Index
OA%	Percentage overall accuracy
OAA	one-against-all
OAO	one-against-one
OC-SVM	one-class support vector machines
OHM	Object Height Model
PA%	Percentage producers accuracy
PCA	Principle Component Analysis
PDF	Probability density function
PLS-DA	Partial least squares discriminant analysis
PLSR	Partial least square regression
Radar	Radio Detection and Ranging
RBF	Radial Basis Function
RE	RapidEye
RS2	Radarsat-2
S1	Sentinel-1
S2	Sentinel-2
SAC	Special Area of Conservation
SAR	Synthetic Aperture Radar
SC	ScanSAR mode
SCBD	Secretariat of the Convention on Biological Diversity
SDMT	Species Distribution Modelling Tools
SE	Shannon Entropy
SKE	Skewness

SL	Spotlight mode
SLC	Single Look Complex product
SM	Stripmap mode
SSC	Single Look Slant Range Complex product
ST	Staring Spotlight mode
SV	Support Vectors
SVDD	Support Vector Domain Description
SVM	Support Vector Machines
TDX	TanDEM-X
TIFF	Tagged Image File Format
TM	Thematic Mapper
TSX	TerraSAR-X
UCI	University of California Irvine
UN	United Nations
VAR	Variance
VH	Vertical polarization on transmit, Horizontal polarization on receive
VHR	Very high resolution
VV	Vertical polarization on transmit, Vertical polarization on receive
WI	Wetness Index

ABSTRACT

In the light of the ongoing loss of biodiversity at the global scale, monitoring grasslands is nowadays of utmost importance considering their functional relevance in terms of the ecosystem services that they provide. Here, guidelines of the European Union like the Fauna-Flora-Habitat Directive and the European Agricultural fund for Rural Development with its HNV indicators are crucial. Indeed, they form the legal framework for nature conservation and define grasslands as one of their conservation targets, whose status needs to be assessed and reported by all member states on a regular basis. In the light of these reporting requirements, the need for a harmonised and thorough grassland monitoring is highly demanding since most member states are still currently adopting intensive field surveys or photointerpretation with differing levels of detail for mapping habitat distribution.

To this purpose, a cost-effective solution is offered by Earth Observation data for which specific grassland monitoring methodologies shall be then implemented which are capable of processing multitemporal acquisitions collected throughout the entire growing season. Although optical data are most suited for characterising vegetation in terms of spectral information content, they are actually subject to weather conditions (especially cloud coverage), which hinder the possibility of collecting enough information over the full phenological cycle. Furthermore, so far only few studies started employing high and very high resolution optical time series for grassland habitat monitoring since they have become available e.g., from the RapidEye satellites, only in the recent past. To overcome this limitation, SAR systems can be employed which provide imagery independent from weather or daytime conditions, hence enabling vegetation analysis by means of complete time series. Compared to optical data, radar imagery is less affected by the physical-chemical characteristics of the surface, but rather it is sensitive to structural features like geometry and roughness. However, in this context presently only very few techniques have been implemented, which are anyhow not suitable to be employed in an operational framework.

Furthermore, to address the classification task, supervised approaches (which require in situ information for all the land-cover classes present in the study area) represent the most accurate methodological solution; nevertheless, collecting an exhaustive ground truth is generally expensive both in terms of time and economic costs and is not even feasible when the test site is remote. However, in many applications the end-users are generally only interested in very few specific targeted land-cover classes which, for instance, have high ecological value or are associated with support actions, subsidies or benefits from national or international institutions. The categorisation of specific grasslands and habitat types as those addressed in this thesis falls within such category of problems, which is defined in the literature as targeted land-cover classification.

In this framework, a robust and effective targeted classification system for the automatic identification of grassland types by means of multi-temporal and multi-polarised SAR data has

been developed within this thesis. In particular, the proposed system is composed of three main blocks: the preprocessing of the SAR image time series including the Kennaugh decomposition, the feature extraction including multi-temporal filtering and texture analysis, and the hierarchical targeted classification, which consist of two phases where first a one-class classifier is employed to outline the merger of all the grassland types of interest considered as a single information class and then a multi-class classifier is applied for discriminating the specific targeted classes within the areas identified as positive by the one-class classifier. To evaluate the capabilities of the proposed methodology, several experimental trials have been carried out over two test sites located in Southern Bavaria (Germany) and Mecklenburg Western-Pomerania (Germany) for which six diverse datasets have been derived from multitemporal series of dualpol TerraSAR-X as well as dual-/quadpol Radarsat-2 images. Four among the Natura 2000 habitat types of the Fauna-Flora-Habitat Directive as well all High Nature Value grassland types have been considered as targeted classes for this study.

Overall, the proposed system proved to be robust and confirmed the effectiveness of employing multitemporal and multi-polarisation VHR SAR data for discriminating habitat types and High Nature Value grassland types, exhibiting high potential for future employment even at larger scales. In particular, it could be demonstrated that the proposed hierarchical targeted classification approach outperforms the available state-of-the-art methods and has a clear advantage with respect to the standard approaches in terms of robustness, reliability and transferability.

ZUSAMMENFASSUNG

Angesichts des anhaltenden Verlusts der biologischen Vielfalt auf globaler Ebene ist die Überwachung von Grünland vor dem Hintergrund der Ökosystemdienstleistungen, die es bereitstellt, äußerst wichtig. Rahmenrichtlinien der Europäischen Union wie die Fauna-Flora-Habitat Richtlinie und der Europäische Landwirtschaftsfonds für die Entwicklung des ländlichen Raums mit dem in ihm enthaltenen Indikator „Landwirtschaftsflächen mit hohem Naturwert“ (HNV) sind dabei essentiell. Sie bilden den rechtlichen Rahmen für den Naturschutz und definieren Grünland als eines ihrer Schutzziele, dessen Zustand von allen Mitgliedstaaten der Europäischen Union regelmäßig bewertet und berichtet werden muss. Vor dem Hintergrund dieser Berichtspflichten ist ein harmonisiertes und vollständiges Grünlandmonitoring äußert anspruchsvoll, da die meisten Mitgliedsstaaten derzeit immer noch intensive Geländeaufnahmen oder visuelle Bildanalysen mit unterschiedlichem Detailierungsgrad für die Kartierung von Habitaten anwenden.

Daher bietet die satellitengestützte Erdbeobachtung eine kosteneffiziente Lösung, mit Hilfe derer spezifische Methoden für das Grünlandmonitoring umgesetzt werden sollen, die in der Lage sind multitemporale Aufnahmen der gesamte Vegetationsperiode zu prozessieren. Obwohl optische Daten aufgrund ihrer spektralen Eigenschaften am besten für die Charakterisierung von Vegetation geeignet sind, unterliegen sie auch dem Einfluss von Wetter (besonders der Bedeckung durch Wolken), welcher die Aufnahme ausreichender Bilder über den gesamten phänologischen Zyklus verhindert. Außerdem haben nur wenige Studien hoch- bzw. höchstauflösende optische Zeitreihen für das Grünlandmonitoring verwendet, da diese erst in den letzten Jahren verfügbar wurden, wie z.B. durch die RapidEye Satelliten. Im Gegensatz dazu stellen SAR Systeme Bildaufnahmen unabhängig von Wetterbedingungen oder der Tageszeit bereit, was die Vegetationsanalyse auf Basis vollständiger Zeitreihen ermöglicht. Verglichen mit optischen Daten sind Radaraufnahmen weniger von den physikalisch-chemischen Eigenschaften der Oberfläche beeinflusst, sondern sind eher für Struktureigenschaften wie Geometrie oder Rauigkeit sensibel. Dennoch wurden diese Daten bisher nur im geringen Maße angewendet.

Weiterhin stellen überwachte Verfahren (welche In-situ Information aller im Untersuchungsgebiet vorkommenden Landbedeckungsklassen benötigen) die präzisesten Verfahren für eine Landbedeckungsklassifikation dar. Allerdings ist die Aufnahme eines kompletten Referenzdatensatzes sowohl zeit- als auch kostenintensiv und nicht immer umsetzbar, vor allem in schwer erreichbaren Regionen. Darüber hinaus sind die Endnutzer meinst nur an wenigen spezifischen Landbedeckungsklassen interessiert, die zum Beispiel einen hohen Naturwert haben oder in Zusammenhang mit Subventionen oder Leistungen nationaler

oder internationaler Institutionen stehen. Die Charakterisierung spezifischer Grünland- oder Habitattypen, wie sie in dieser Arbeit adressiert werden, fällt in diese Kategorie, die in der Literatur als gezielte Landbedeckungsklassifikation (targeted land-cover classification) bezeichnet wird.

In diesem Zusammenhang wurde innerhalb der vorliegenden Arbeit ein robustes und effektives gezieltes Klassifikationssystem entwickelt, welches automatisch Grünlandklassen auf Basis von multi-temporalen und multi-polarisierten SAR Daten identifiziert. Speziell besteht das vorgeschlagene System aus drei Modulen: der Vorprozessierung der SAR Zeitreihendaten einschließlich der Kennaugh Zerlegung, der Ableitung bestimmter Features einschließlich der multi-temporalen Filterung und Texturanalyse, sowie der hierarchischen gezielten Klassifikation, welche aus zwei Phasen besteht. Zuerst wird eine Klassifikation auf Basis der Zusammenführung aller zu untersuchenden Grünlandklassen zu einer einzigen Informationsklasse durchgeführt, um die Fläche dieser von der restlichen Landbedeckung abzugrenzen. Danach wird eine Klassifikation innerhalb der zuvor identifizierten Flächen durchgeführt, um die spezifischen Zielklassen zu kartieren. Um das Potenzial der vorgeschlagenen Methode zu untersuchen, wurden verschiedene experimentelle Analysen in zwei Testgebieten im südlichen Bayern und in Mecklenburg auf Basis von sechs sehr unterschiedlichen Datensätzen durchgeführt. Diese wurden aus Zeitseriendaten der Satelliten TerraSAR-X und Radarsat-2 abgeleitet. Vier Habitattypen sowie die Klassen des High Nature Value Grünlands wurden als Zielklassen für die Arbeit definiert.

Insgesamt erwies sich das vorgeschlagene Klassifikationssystem als robust und effektiv für die Anwendung von multi-temporalen und -polarisierten höchstauflösenden SAR Daten zur Unterscheidung von Habitattypen und High Nature Value Grünland, welches ein hohes Potenzial für zukünftigen Anwendungen sogar auf größerem Maßstab aufweist. Im speziellen konnte gezeigt werden, dass der vorgeschlagene hierarchische gezielte Klassifikationsansatz bessere Ergebnisse als die Methoden nach aktuellem Stand der Technik erzielen konnte und daher gegenüber den Standardmethoden in Bezug auf Robustheit, Verlässlichkeit und Übertragbarkeit einen klaren Vorteil hat.

ACKNOWLEDGEMENTS

The completion of this thesis would have not been possible without the invaluable support of a large number of people and institutions whom I would like to thank:

First and foremost I would like to thank my thesis committee members: Prof. Dr.-Ing. Manfred Ehlers, Hon.-Prof. Dr.-Ing. Peter Reinartz, Prof. Dr.-Ing. Christine Pohl and Dr. Thomas Esch.

I would like to thank Prof. Dr.-Ing. Manfred Ehlers from the Osnabrueck University for his supervision, encouragement and interest in this work as well as the administrative support and his commitment to the MSAVE project.

I am also very grateful to Hon.-Prof. Dr.-Ing. Peter Reinartz, head of the department Photogrammetry and Image Analysis at the Remote Sensing Technology Institute of the German Aerospace Center (DLR), for his support, discussions and frequent feedback during the course of the thesis.

The dissertation has been written at the German Remote Sensing Data Center (DFD) of the German Aerospace Center (DLR). Thus, I would like to thank the former head of the department Land Surface (LAX), Andreas Müller, for his unquestioning support and the provision of the necessary infrastructure and resources. Furthermore, I would like to thank the head of the team Urban Areas and Land Management, Dr. Thomas Esch, for his encouragement, advice and help during all phases of the dissertation.

Moreover, I would like to thank all MSAVE colleagues, namely Stefanie Stenzel, Carina Kübert, Dr. Hannes Feilhauer, Prof. Dr. Sebastian Schmidtlein, Carsten Oldenburg and Prof. Dr. Christopher Conrad for their fruitful discussions throughout the MSAVE project duration, particularly during the field campaigns and project meetings. In addition, I am very grateful to Michael Bock from the DLR Space Administration for his encouragement, support and constructive scientific exchange.

I would also like to thank all past and current colleagues from the Institute for Geoinformatics and Remote Sensing (IGF) of the Osnabrueck University, especially Sandra Dützer, Dr. Sascha Klonus, Dr. Florian Hillen, Dr. Thomas Jarmer and Bastian Siegmann, for their always open, helpful and friendly atmosphere.

Furthermore, I would like to thank my parents, all members of my family and all my friends for their wholehearted encouragement and believe in my person.

Last but definitely not least, I am deeply grateful to (Dr.) Mattia (Marconcini) for his professional endorsement, valuable guidance and helpful criticism, but also for his unconditional love and for

his tremendous patience and sacrifices throughout the ups and downs along the way. Thank you for turning my life upside down. Without you, I would not be where I am now.

This dissertation has been carried out within the German project MSAVE ("multi-season remote sensing for monitoring vegetation") funded by the DLR Space Administration with means provided by the German Federal Ministry of Economics and Technology, under project reference number 50 EE1034.

1. INTRODUCTION

1.1. Background

Nowadays, the economic and social development strongly depends on the Earth's biological resources (SCBD, 2016c (SCBD)). Specifically, this applies not only to agriculture and forestry, but also to transportation, tourism, industry and habitation (Küchler-Krischun and Walter, 2007). Agricultural areas, for instance, provide food, incomes and livelihood as well as ecosystem services such as soil and water conservation, maintenance of soil fertility and biota, and pollination (SCBD, 2016a); forests are habitats for a variety of species, provide goods such as timber and a livelihood for humans worldwide (SCBD, 2016b); whereas tourism is depending on an intact environment and nature and reacts sensitively to natural disasters (Küchler-Krischun and Walter, 2007). Nevertheless, in order to ensure a food security with sufficient nutrition, incomes, and livelihood for all the people, an efficient production system has to be established which guarantees a sustainable use of resources and the conservation of biological diversity (Küchler-Krischun and Walter, 2007).

Biological diversity (commonly referred to as biodiversity) is the livelihood for human life: living organisms are part of the nutrient cycle as they fulfil specific functions (e.g., cleaning water and air, fertilising soils, providing food and giving impulses for innovations) (Küchler-Krischun and Walter, 2007). In particular, within the Convention on Biological Diversity (CBD) biodiversity is defined as "the variability among living organisms from all sources including, inter alia, terrestrial, marine and other aquatic ecosystems and the ecological complexes of which they are part; this includes diversity within species, between species and of ecosystems" UN (1992). In this context, variability among living organisms can be considered in terms of genetic diversity (i.e., differences within and among populations), species diversity (i.e., distribution and abundance of species), ecosystem diversity (i.e., bioregions, landscapes, habitats), and functional diversity (i.e., ecosystem robustness, resilience, goods and services) (Bennett, 2003; Pearce and Moran, 1994).

According to Küchler-Krischun and Walter (2007), it is of utmost importance to preserve biodiversity for the current and future generations since nature itself offers services which, otherwise, might be provided only with huge technical and monetary effort. These are for instance: i) the self-purification of soils and water bodies, which supports an easier and cost-efficient abstraction of drinking water if working properly; ii) the existence of high amount of natural soil fertility, which supports the decrease in fertilizer usage; iii) the percentage of urban green, which supports the natural air filtration of particulate and noxious matter (Küchler-

Krischun and Walter, 2007). Others, instead, cannot be even technically replaced like to pollinize cultivated plants as done by insects or to compensate for the services that nature gives in terms of aesthetics (beauty and characteristic of a landscape) and recreational value (Küchler-Krischun and Walter, 2007). In general, the higher the genetic variability, the greater is the productivity, carbon sequestration, retention of nutrients, and the ability of species to resist and recover from changing environmental conditions and different forms of stress, such as diseases, droughts or floods (Küchler-Krischun and Walter, 2007; SCBD, 2016a).

In this scenario, one of the largest ecosystems of the world are grasslands, which have an estimated area of 52.5 million square kilometres (equal to 40.5 percent of the land surface excluding Greenland and Antartica) (FAO, 2005). They can be defined as areas mainly covered by grass dominated vegetation with little or no tree cover (Silva *et al.*, 2008). In 2013, 35.48% of the agricultural landscape of the European Union (corresponding to 21.29% of the European land surface) were permanent meadows and pastures (FAOSTAT, 2013). As one can see in Figure 1-1, this area has slightly decreased for different reasons between 2000 (70.38 million ha) and 2013 (66.11 million ha) by 7.62%. Indeed, their major threats are i) the change of land use mainly due to the intensification of agricultural land use (e.g., due to an increased demand and production of biofuels), ii) afforestation, iii) change in livestock density, which can directly and greatly affect grasslands, iv) intensification of grassland management practises through the use of fertilisers or pesticides as well as the employment of faster and more effective mechanical mowing techniques, and v) invasive plants, which cause a loss in the habitats value (Silva *et al.*, 2008). Furthermore, livestock species, stocking densities, and timing of grazing and mowing have a strong influence on the grassland habitat and its wildlife (Silva *et al.*, 2008). This, in return, is mainly influenced by agricultural support policies, international trade negotiations, biomass production for energy, and policies on the use of genetically modified organisms, but it is also indirectly affected by the enlargement of the European Union and the implementation of nature conservation policies. All these factors majorly affect the biodiversity of grasslands (Henle *et al.*, 2008).

Preserving grasslands and their biodiversity is anyhow of great importance since they provide a variety of goods and services: i) they supply forage for wild animals and livestock, as they are used for the production of domestic animals (e.g., cattle, sheep and goats), which in return

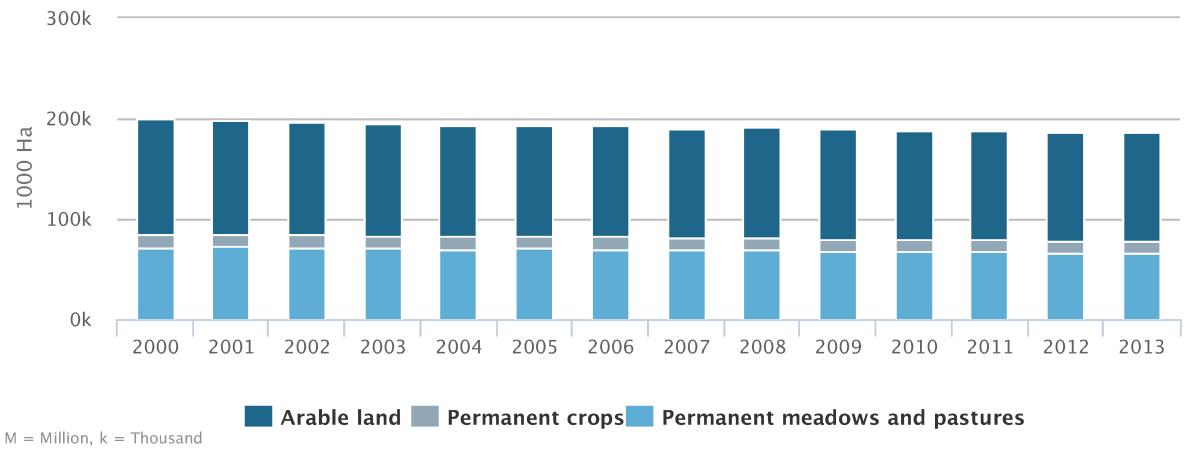

Figure 1-1: Composition of agricultural area between 2000 and 2013 within the European Union (FAOSTAT, 2013).

provide public goods like diary and meat products or wool; ii) they support nutrient cycles, iii) they are vital habitats for both flora and fauna, which they serve as biotope for breeding, wintering, or migration; iv) they are source for recreation and tourism, e.g. they attract humans with their inhabiting birds or plant diversity; v) they store nearly 34% of the global stock of carbon in their underground soils, and vi) they play a key role for an efficient hydrological cycle through preventing soil erosion, sedimentation, and dissolved solids, nutrients and pesticides, and protecting water runoff and infiltration quantity and quality (Conner *et al.*, 2001; Peeters, 2009; Silva *et al.*, 2008).

Through the loss of species, genes and habitats, human livelihood is being pressured (Küchler-Krischun and Walter, 2007) and this decrease of biodiversity is irreversible (SCBD, 2016c). Hence, the conservation of species' variety is of great concern and needs to be regulated by international directives. Reacting to this, the United Nations Environment Program (UNEP) created a Working Group of Experts on Biological Diversity in November 1988, which prepared an international legal instrument for the conservation and sustainable use of biological diversity in May 1989 (SCBD, 2016c). The Working Group's effort achieved the Conventions adoption at the United Nations Conference on Environment and Development in Rio de Janeiro in 1992 (the Rio "Earth Summit")(Küchler-Krischun and Walter, 2007).

At the European level, succeeding the Bern Convention on the Conservation of European Wildlife and Natural Habitats in 1979, the European Union Council Directive on the conservation of natural habitats and of wild fauna and flora (92/43/EEC), also known as the "Fauna-Flora-Habitat (FFH) Directive", was adopted in 1992 (Council of the European Union, 1992). Together with the Directive on the conservation of wild birds (79/409/EEC), it forms the legal framework for harmonised nature conservation within the European Union (Bock *et al.*, 2005a; Vanden Borre *et al.*, 2011). The FFH directive defines in its Article 1c natural habitat types of Community interest that "i) are in danger of disappearance in their natural range; ii) have a small natural range following their regression or by reason of their intrinsically restricted area; or iii) present outstanding examples of typical characteristics of one or more of the nine following biogeographical regions: Alpine, Atlantic, Black Sea, Boreal, Continental, Macaronesian, Mediterranean, Pannonian and Steppic". The habitat directive lists 231 natural habitat types in its Annex I, of which 91 are occurring in Germany and are included in the Natura 2000 network.

Another important aspect is the biodiversity of agricultural areas, which has majorly declined due to the changing cultivation patterns and the technological advance in the past 50 years (Gödeke and Sukopp, 2010). In the framework of the Commission Regulation (EC) No 1974/2006 on support for rural development by the European Agricultural Fund for Rural Development (EAFRD, german: ELER) of 15 December 2006 (European Commission, 2006), the European Union tries to stimulate rural development to improve the state of the environment and landscape (Gödeke and Sukopp, 2010). One of the 35 basic indicators that have been introduced with the EAFRD to integrate environmental interests into a common agricultural policy is the "High Nature Value Farmland" (HNV farmland), which belongs to the Axis 2 "Improving the environment and the countryside through land management" and is one of three biodiversity indicators (Gödeke and Sukopp, 2010; European Commission, 2006). Specifically, it has to be measured and reported by all Member states on a regular basis (Gödeke and Sukopp, 2010). Furthermore, it has been integrated in the set of indicators for the National Strategy on

Biological Diversity in Germany (Gödeke and Sukopp, 2010). The HNV indicator represents the percentage of farmland that has a high nature value with respect to the total area of farmland (Gödeke and Sukopp, 2010). "High Nature Value farmland comprises those areas in Europe where agriculture is a major (usually dominant) land use and where ... agriculture supports or is associated with either a high species and habitat diversity or the presence of species of European conservation concern or both" (Andersen *et al.*, 2003). Usually these areas are species-rich and extensively used arable land, grasslands, orchard meadows, vineyards, and fallow land (Gödeke and Sukopp, 2010).

Both, the FFH directive and the HNV farmland indicator define grasslands as part of their monitoring and conservation targets. The FFH directive requires the observation and surveillance of these natural vegetation types and their conservation status every six years (Council of the European Union, 1992), while the reporting obligation for the HNV indicator is defined with a four-year interval (Feilhauer *et al.*, 2012).

1.2. Objectives of the thesis

In the light of these reporting requirements, the need for a harmonised and thorough grassland monitoring is highly demanding for regional, national and European Union authorities as this involves a vast amount of data coming from different local sites (Bock *et al.*, 2005a). Accordingly, cost-effective methodologies have to be developed since most member states are still currently adopting intensive field surveys (Vanden Borre *et al.*, 2011) or visual image interpretation with differing levels of detail for mapping habitat distributions, which are both costly and time-consuming and depend on the interpreters' knowledge and experience (Gross *et al.*, 2009; Mander *et al.*, 2005; Thoonen *et al.*, 2010). In this framework, Earth Observation (EO) data has already proven to be effective for a frequent and spatially comprehensive monitoring of different vegetation types, which is vital to assess the actual status, identify basic trends, and mitigate major threats. In particular, with respect to traditional manual field surveys, they allow faster map production, coverage of remote areas (e.g., large wetlands or restricted military areas) and frequent repeatability (Vanden Borre *et al.*, 2011).

However, up to now most studies based on EO data employed medium-resolution (MR) optical data (Hill *et al.*, 1999; Wang *et al.*, 2013; Jensen *et al.*, 2001; Lucas *et al.*, 2007) (with pixel size in the range of 30 to 300 m) to monitor vegetation land cover, which are suitable for large scale grassland monitoring, but not of support for effectively characterising small-size heterogeneous European grassland habitats. To this purpose the employment of high resolution (HR, with pixel size between 3 and 30 m) or very high-resolution (VHR, with pixel size lower than 3 m) data are then essential. In this framework, so far only few studies started employing HR and VHR optical time series for grassland habitat monitoring since they have become available e.g., from the RapidEye satellites, only in the recent past. (Esch *et al.*, 2014a, 2014b; Stenzel *et al.*, 2014; Zillmann *et al.*, 2014; Buck *et al.*, 2015). Nevertheless, although optical times series have the most suitable spectral information for discriminating different vegetation types, their main disadvantage is the sensitivity towards weather conditions such as cloud cover, which hampers their suitability in operational applications (Blaes *et al.*, 2005).

To overcome these disadvantages, few studies started considering HR/VHR polarimetric

synthetic aperture radio detection and ranging (radar) data (SAR), which are acquired independently from weather and daytime conditions and generally allow an effective discrimination of vegetation types (Hill *et al.*, 2000; Smith and Buckley, 2011; Schuster *et al.*, 2015; Betbeder *et al.*, 2015). Compared to optical data, radar imagery is less affected by the physical-chemical characteristics of the surface, but rather it is sensitive to structural features like geometry and roughness (Woodhouse, 2006). Furthermore, the use of multiple polarisations in SAR imagery enables the collection of a higher amount of information about the scattering processes as the geometric and dielectric properties of the surface influence the backscattering of the emitted electromagnetic wave (Oliver and Quegan, 1998). The most common frequency bands for geoscience applications are X (8-12 GHz), C (4-8 GHz), and L (1-2 GHz), corresponding to a wavelength of 2.5 - 3.8cm, 3.8 - 7.5cm, and 15.0 - 60 cm, respectively (Ouchi, 2013; Woodhouse, 2006). The wavelength of the L-band is relatively long, thus, it is capable of penetrating through vegetation as well as soil and can be applied for instance to biomass estimation. Instead, X- and C-band frequencies correspond to rather short wavelengths, which can only penetrate the surface or top of vegetation, hence providing information about their structure.

Existing SAR data from historic (e.g., ERS-1/-2 and ASAR) and current missions (e.g., TerraSAR-X, Radarsat-2, or Sentinel-1) are highly diverse in terms of scale, frequency as well as polarisation modes. While the field of applications increases (as a result of their weather and daytime independency), various SAR image analysis and evaluation strategies have been developed focusing on distinct aspects and thus making it difficult to be practically applied (Schmitt et al., 2015). The development of generic algorithms, which can be employed on these diverse existing SAR data, is essential to make use of them in numerous applications. In addition, all methods applied so far solely employed few scenes, which generally are not sufficient for properly describing the dynamics of different vegetation types over time (i.e., during the phenological phase) (Metz *et al.*, 2014).

Furthermore, up to now the classifiers applied to optical and SAR data mostly rely on the availability of an exhaustive ground truth for all the land-cover classes present in the area of interest, which is rarely fulfilled both due to time and economic cost (Marconcini *et al.*, 2014; Metz *et al.*, 2014). Indeed, this task is generally challenging, expensive and, sometimes, not even feasible (Marconcini *et al.*, 2014). To this purpose, in order to reduce the amount of necessary in situ information to collect (and thus lessen related time and financial costs), new classification techniques should be designed to solely identify the only classes of interest to the user (e.g., specific habitat types) for which ground-truth information is then exclusively needed. Moreover, they should provide classification accuracies similar to those of traditional approaches (which instead require exhaustive information for all the classes present in the study area). As already discussed by Marconcini *et al.* (2014), this type of problem is referred to in the literature as targeted classification.

Accordingly, to overcome the above-mentioned limitations, here a novel automatic approach for categorising different grassland types based on polarimetric VHR SAR imagery is presented, which:

i. is capable of handling either dual or quad-polarization multi-temporal data; and

ii. supports targeted classification (i.e., it allows to exclusively identify the grassland types for which ground-truth information is available, disregarding all the other "unknown" classes present in the investigated area (Marconcini et al., 2014)).

To tackle targeted classification, normally an ensemble of one-class classifiers (i.e., specifically designed for outlining the only class for which ground truth data are available) is used, where each one is associated with a specific class of interest. Nonetheless, this represents a sub-optimal solution since: i) heuristics must be defined to effectively combine their outputs; and ii) each class is analysed separately without accounting for the information available for the other targeted classes. Accordingly, a hierarchical approach is proposed, which aims at simplifying the complex original task into two easier problems. In particular, it consists in the sequential use of:

i. A one-class classifier aimed at initially outlining the merger of all the grassland types of interest considered as a single information class;
ii. A multi-class supervised classifier aimed at discriminating the specific targeted classes within the areas identified as positive by the one-class classifier.

Experimental analyses have been carried out using multitemporal VHR SAR imagery acquired by the German X-band TerraSAR-X (TSX) satellite in 2011 and 2012 over two test sites located in southern Bavaria and Mecklenburg Western-Pomerania (Germany), as well as by the Canadian C-band Radarsat-2 (RS2) satellite in 2011 over the Bavaria study area. Four among the Natura 2000 habitat types of the FFH directive (Council of the European Union, 1992) as well all High Nature Value (HNV) grassland types (Bundesamt für Naturschutz, 2011b) have been considered as targeted classes for this study.

1.3. Structure of the thesis

This thesis is organised into 6 chapters.

In Chapter 2 an overview of the current state-of-the-art for grasslands and habitat monitoring by means of remote sensing is given.

In Chapter 3 the targeted classification system is presented. In particular, the preprocessing of the SAR data (section 3.1), the adopted feature extraction (section 3.2) as well as the proposed hierarchical targeted classification technique (section 3.3) are described into details.

In Chapter 4 a detailed overview of the input data and considered targeted classes is provided.

Chapter 5 presents and discusses the results of the intensive experimental analysis carried out for assessing the capabilities of the implemented approach.

In Chapter 6 conclusions are drawn and potential future developments are discussed.

2. STATE OF THE ART

In the last decade, Europe has experienced a significant advancement in the employment of remote sensing technologies for monitoring and assessing biodiversity and natural habitats (Turner *et al.*, 2003; Vanden Borre *et al.*, 2011; Corbane *et al.*, 2015). On the one hand this has been eased by the vast number of dedicated projects funded by national and European policy makers, such as e.g., SPIN (2001-2004, Bock *et al.* (2005a)), Habit-Change (2010-2013, Rannow and Neubert (2014)), MS.MONINA (2010-2013, Lang *et al.* (2015)), Care-X (2009-2012, Schuster *et al.* (2012)), MSAVE (2011-2014,), BIO_SOS (2010-2013, Lang *et al.* (2015)) or EU BON (2012-2017, Hoffmann *et al.* (2014)). On the other hand, it has been boosted by the increasing availability of high and very high spatial resolution multi-temporal data from multispectral and hyperspectral optical satellite sensors (e.g., RapidEye, Sentinel-2, the planned EnMAP), as well as from Radar (TerraSAR-X, Radarsat-2, Sentinel-1) and Light Detection And Ranging (LiDAR) sensors. In particular, this is progressively supporting the transition from traditional statistical classification approaches to more effective machine-learning algorithms (due to the increasing computational capabilities necessary for processing big amount of data) and is continuously fostering the development of newer more advanced methodologies (Waske and van der Linden, 2008). Nevertheless, it is worth noting that present habitat mapping programs (e.g., CORINE land cover or the NATURA 2000 Annex II habitat maps) still mainly account for visual image interpretation or field surveys, which are time and cost demanding, but also strongly depend on knowledge and experience of the operator (Mander *et al.*, 2005; Gross *et al.*, 2009; Thoonen *et al.*, 2010). Furthermore, also due to the high complexity in characterising the corresponding information classes, studies employing remote sensing techniques for mapping Natura 2000 habitats are limited to some pilot projects and case studies, hence lacking a real operative employment at larger national or continental scale (Thoonen *et al.*, 2013).

Mapping grassland species as well as characterising related parameters or indices (e.g., primary productivity, climate or habitat structure) by means of Earth Observation (EO) data is of great support for deriving key information to assess biodiversity (Turner *et al.*, 2003). In this framework, several methods have been presented in the literature for monitoring natural and semi-natural habitat types. Being this work focused of grasslands, a detailed overview of the corresponding state-of-the-art is given in the following. For a review of the methods implemented for forests, heathlands, and wetlands, the reader is referred to Corbane *et al.* (2015).

In general, grassland species occur mainly as plant societies with a great variety within each habitat (Corbane *et al.*, 2015). This makes it extremely difficult to distinguish specific types

rather than homogenous habitats, which is anyhow still a very challenging task (Corbane *et al.*, 2015; Hill *et al.*, 2005). Accordingly, the most of current research activities aim at addressing the identification, delineation and change detection of habitats (e.g., in terms of areal coverage, field size, spatial distribution and management practices) as well as the description of their status and quality; however, at present only few studies are tackling this issue by means of remote sensing techniques.

In general, national and continental land-cover maps have been derived so far by using low spatial resolution (> 300m, e.g., MODIS) or medium spatial resolution (30 - 300m, e.g. AWiFS) (Corbane *et al.*, 2015) satellite data. However, these are not suitable for a proper categorisation of grassland habitats, which, to cope with their generally small extent, ideally requires high (3 to 30 m, e.g. Sentinel-1 & 2, Landsat or SPOT) to very high (< 3 m, e.g. TerraSAR-X, WorldView-2, Quickbird) spatial resolution imagery. Moreover, given the similarity of different grassland types in their physical appearance, high frequency acquisitions over the growing season are essential for characterising their temporal behaviour, which, instead, may consistently vary e.g., due to their use associated with different mowing practices (Schlager *et al.*, 2013; Franke *et al.*, 2012; Zillmann *et al.*, 2014; Lucas *et al.*, 2007)

2.1. Habitat monitoring by means of optical data

2.1.1. Pixel-based approaches

Optical remote sensing data with a high spatial as well as temporal resolution covering large geographical areas have only become available in the last 10 – 15 years, e.g. imagery acquired by the LISS-III sensor on board of the ResourceSat-1 satellite (IRS-P6, 2003) of the Indian Space Research Organization (ISRO) with a spatial resolution of 23.5m and a revisit time of 24 days, the five identical satellites of the RapidEye constellation (2008) a with spatial resolution of 6.5m and a revisit time of 5.5 days at nadir, as well as the two Sentinel-2 satellites (one launched in 2015, the other scheduled to be launched in 2016) with a spatial resolution of 10 – 60m depending on the spectral band and a revisit time of 5 days.

Accordingly, various previous studies addressing grassland monitoring solely applied low spatial resolution satellite data for large area analyses, e.g. the NOAA-AVHRR or MODIS used to discriminate grasslands as a whole from other land-cover types (Hill *et al.*, 1999; Wang *et al.*, 2013), to estimate the aboveground biomass of grassland during the growing season (Zhao *et al.*, 2014; Yu *et al.*, 2010), to analyse grassland potential productivity dynamics and their carbon stocks (Li *et al.*, 2013), to evaluate land degradation (Tasumi *et al.*, 2014; Numata *et al.*, 2007) or to determine grassland drought (Gu *et al.*, 2007; Wan *et al.*, 2004).

In contrast, medium resolution data such as the Landsat Thematic Mapper (TM), the Landsat-7 Enhanced Thematic Mapper (ETM+) or the Advanced Wide Field Sensor (AWiFS) on board the IRS-P6 satellite have been employed more recently in a variety of studies to classify different grassland types and habitats, to determine grassland changes, to describe vegetation structure and management practises, or to evaluate grassland degradation. As an example, Jensen *et al.* (2001) performed a predictive modelling analysis based on the Fisher discriminant mapping function within three subsections of the Little Missouri National Grasslands, North Dakota, USA, to classify four grassland, five shrub land, and six woodland habitats based on six terrain indices

derived from DEM data, two Landsat TM images from 1992 and 1993, as well as nine interpolated climate variables. Sanchez-Hernandez *et al.* (2007) performed comparative classifications with support vector machines (SVM), the one-class support vector data description (SVDD) classifier, as well as a maximum-likelihood classifier using one Landsat ETM+ image from June 2000 covering the coastal saltmarsh habitat of North Norfolk (UK), which is a selected Special Area of Conservation (SAC) within the FFH directive. Wood *et al.* (2012) analysed the correlation between sample-point pixel values and image texture derived from remote sensing data (one infrared (IR) airborne image and one Landsat TM image) to describe the vegetation structure of a test site in Wisconsin (USA), which is characterised by grasslands, savannas, and woodland. Price *et al.* (2002b) assessed the suitability of several vegetation indices (the Tasselled Cap BI, GVI, and wetness index (WI), the first three components from Principle Component Analysis (PCA1, 2, 3), the Normalized Difference Vegetation Index (NDVI), the Green Ratio (GR) and the MIR Ratio) and band combinations derived from three Landsat TM images (acquired on 15th May, 2nd July and 4th September 1997) for the differentiation of six traditional grassland management practices in the Douglas County located in eastern Kansas (USA). Lucas *et al.* (2007) used four Landsat 7 ETM+ images from 2001 and 2002 to assess their suitability for habitat and agricultural land-cover mapping in the Berwyn Mountains (UK) based on a fuzzy logic decision rule classification.

To evaluate the potential of identifying land-use intensity changes in grass-dominated and woody pastures, Rufin *et al.* (2015) used spectral-temporal metrics derived from dense intra-annual Landsat time series between 1985 and 2012 in the tropical forest of Novo Progresso in Southern Pará (Brazil). To determine grassland cover change, Zha and Gao (2011) used NDVI derived from two Landsat TM images acquired in 1987 and 2000, respectively, over a study area near Lake Qinghai (China) and compared their results against in situ grass-cover measurements. Furthermore, grassland degradation was analysed by Liu *et al.* (2004), who used one Landsat TM image to derive a grassland degradation map for an area near Lake Qinghai (West China) based on NDVI and the Soil-Adjusted Vegetation Index (SAVI). Nevertheless, the limitation of these data products relies in their poor spatial resolution which does not allow a detailed analysis of specific grassland habitats, especially in areas characterised by small-size field parcels.

High and very high resolution data sets, e.g. LISS-III on board the IRS-P6 satellite, RapidEye, IKONOS-2, or Quickbird, have been used not only to distinguish grasslands from crops (as for a test site in North-East Germany (Esch *et al.* (2014a, 2014b)) or in the context of a pan-European permanent grassland map (Zillmann *et al.* (2014)), but also to classify different grassland habitats. For mapping four grassland habitat types of the Natura2000 network, Stenzel *et al.* (2014) applied a Maximum-Entropy (MaxEnt) one-class classification approach on a time series of five RapidEye images over a test site in southern Bavaria (Germany). Buck *et al.* (2013) and Buck *et al.* (2015) integrated expert knowledge in form of raster information layer into the classification approach (where they tested the maximum likelihood and SVM classifiers) to map Natura2000 grasslands types (namely dry grasslands (62xx), wet grasslands (64xx), mesophilic grasslands (65xx)), as well as intensive grassland and crops on the basis of three RapidEye scenes. Specifically, they derived biomass, homogeneity, linear structures, slope orientation, and soil moisture as additional raster information layer from an orthophoto, as well as soil map and used Land Parcel Information data (LPIS) to exclude non-agricultural areas. Schmidt *et al.*

(2014) performed a study on the number of RapidEye scenes needed to successfully classify grassland, heathland, humid meadow and woodland habitats in a test site by Döberitzer Heide in north-east Germany, which was carried out using different combinations of vegetation index derived from 24 scenes from 2009 to 2011 by means of SVMs. Moreover, investigating the same dataset, Förster *et al.* (2012) have performed a comparative study on the performances of the SVM by employing in the training phase also data from a spectral-temporal library. Keramitsoglou *et al.* (2005) applied a kernel-based re-classification (KRC) algorithm for the classification of habitat classes of the European Nature Information System (EUNIS) nomenclature (including, among others, grasslands) based on one pan-sharpened Quickbird scene for a study area in Wye Downs (England) and one IKONOS-2 image for a test site located at the river Strymon's delta (Greece). Also Kobler *et al.* (2006) applied the KRC method as second step in a three stage classification approach consisting, additionally, of a pre-classification and a final decision-tree based reclassification carried out on a test site within the Sneznik Regional Park west of Pivka (Slovenia), to map ten grassland and woodland habitats of the EUNIS nomenclature using one IKONOS image.

2.1.2. Object oriented approaches

While the above mentioned methods focused on pixel-based approaches, others focussed instead on the development of object-based approaches for discriminating grassland and other habitats mainly by means of medium and high spatial resolution data. In particular, these are based on predefined objects (e.g., from existing geodata from national topographic maps, or segmentation of homogenous regions) and have the great advantage of including additional knowledge such as region based spectral and texture features, form features or context information (Bock and Lessing, 2000).

Amongst others, Bock *et al.* (2005a) developed and assessed an object-oriented fuzzy-rule classification for habitat mapping at the regional scale (based on dual-date Landsat ETM+ scenes from 2001) and at the local scale (based on high resolution stereo camera (HRSC) scanner data from 2001) accounting for information derived from a soil and topographic map. Furthermore, Bock *et al.* (2005b) applied object-based classification for monitoring dry grasslands and wetlands by means of multi-temporal and multi-resolution EO data both at the regional (in a study site in Schleswig-Holstein, located in Northern Germany) and local level (in a study site in Wye Downs (UK)). While for the regional study a time series of Landsat TM/ETM+ scenes from the years 1990, 1995, and 2001 has been used, one pan-sharpened Quickbird image of 2002 has been employed for the local study to develop a hierarchical methodology based on fuzzy rules and nearest neighbour classification. Díaz Varela *et al.* (2008) studied the potential of the maximum likelihood classifier and the nearest neighbour decision rule for addressing both pixel- and object-based classifications of one Landsat TM image acquired over a test area in the Northern Mountains of Galicia (Spain), which is characterised by a heterogeneous landscape, also including habitats of the Natura2000 network. Franke *et al.* (2012) analysed the potential of multi-temporal RapidEye data for a large-scale assessment of grassland use intensity. Specifically, they tested two approaches to differentiate "semi-natural grassland", "extensively used grassland", "intensively used grassland", and "tilled grassland" in a managed study site in southern Germany: the first was performed based on the commercial decision tree software

See5 (RuleQuest Research Pty Ltd, Australia) and using multi-temporal NDVI, Normalized Red-Edge Vegetation Index (NREVI), and Mean Absolute Spectral Dynamic (MASD) as input parameters; the second was carried out by means of a context-based classifier. Both approaches were implemented as object-based classification systems. Also, Corbane *et al.* (2013) successfully classified two habitat types (i.e., dry improved grasslands and riparian ash woods) using two RapidEye scenes and a DEM for a test site located in Foothills of Larzac in the Southern Massif Central (France). This was possible by applying an object-oriented sparse partial least square discriminant analysis. Schlager *et al.* (2013) introduced a classification approach specific for discriminating grassland habitats in the biosphere reserve Schwäbische Alb (Germany) based on a multi-sensor remote sensing data set consisting of an orthophoto composite, 6 RapidEye scenes, and LiDAR data set as well as vector data from the Authorative Topographic-Cartographic Information System (ATKIS®) and the Integrated Administration and Control System (IACS, German: InVeKoS). Petrou *et al.* (2014) applied an object- and rule-based classification methodology to map Natura 2000 habitats (i.e., two extended coastal lagoons, numerous channels, marshes and humid grasslands) in the Le Cesine test site located in the Apulia region in south-eastern Italy. The experiments were based on a pre-existing land cover map, two multispectral images from Quickbird and WorldView-2 as well as an Object Height Model (OHM) extracted from LiDAR data.

2.2. Habitat monitoring by means of Hyperspectral data

Despite their great potential arising from the capability of fine characterisation of the spectrum (in more than 60 channels), hyperspectral data have been rarely applied for mapping grassland habitats. This is principally due to the fact that currently mostly airborne hyperspectral sensors exist, which require dedicated and costly missions for which intensive planning activities are needed. However, in the context of satellite sensors, a big advancement will be provided by the Environmental Mapping and Analysis Program (EnMAP) satellite mission which allows hyperspectral measurements over large areas; nevertheless, it is schedule to be launched not earlier than 2018.

In this scenario, few studies in the literature applied airborne hyperspectral data to address the monitoring of grasslands on small-scale test areas. Instead of directly classifying habitat types and their distribution, Schmidtlein and Sassin (2004) applied hyperspectral Airborne Visible/Infrared Imaging Spectrometer (AVIS-2) imagery acquired on 4th July 2001 to model floristic gradients within a test site in southern Bavaria (Germany) by means of partial least square (PLS) regression analyses. Specifically, they could show that floristic gradients could be modelled with a higher quality than individual species and that homogeneous reflectance does not imply homogeneous species distribution while heterogeneous reflectance implies heterogeneous formations.

Within the HABISTAT project, airborne hyperspectral imagery of the Advanced Hyperspectral Sensor (AHS) of June 2007 has been acquired for the Natura2000 test site *Kalmthoutse Heide* in Belgium and has been used to develop several techniques to map habitat types. For instance, Hufkens *et al.* (2010) applied a linear discriminant least squares classification algorithm and a subsequent spatial patch-based distribution analysis for describing the heterogeneity in the corresponding heathland habitats. Also, Thoonen *et al.* (2010) applied a kernel-based

reclassification (KRC) on a thematic land cover map derived from the above mentioned data together with habitat reference information for delineating forests, grasslands and heathlands. Furthermore, Thoonen *et al.* (2013) employed a hierarchical classification scheme to classify heathland vegetation and to characterise the structural dependencies of the heathland vegetation types and basic land-cover types by including contextual information derived by means of structured Markov-Random-Fields.

Feilhauer *et al.* (2013) used multi-seasonal field spectra measured on three test sites close to Cologne (Germany) with an ASD Fieldspec 3 JR™ spectrometer from 3 different habitat types, i.e. nutrient-poor grassland, wet heath, and floodplain meadow, to simulate mono-temporal and multi-seasonal acquisitions of eleven multispectral sensors, (namely: ASTER, HRSC-AX, IKONOS, Landsat 5 TM, Landsat 7 ETM+, LDCM OLI, Quickbird 2, RapidEye, Sentinel-2, SPOT 5, and Worldview-2) and evaluate their capability for vegetation mapping, especially of floristic gradients. Modelling was performed using partial least square regression (PLSR). Neumann *et al.* (2015) linked knowledge gained from species ordination with spectral signatures from data of the Airborne Imaging Spectrometer for Application (AISA DUAL) from 4th June 2011 in the *Döberitzer Heide* test site (Germany) to predict the existence probability of Natura2000 habitats and their conservation status by means of PLSR. Möckel *et al.* (2014) applied data from the airborne HySpex hyperspectral spectrometer from 9th July 2011 and a LiDAR dataset from the same date for the Jordtorp study site on the Baltic Island of Öland (Sweden) to differentiate three age classes of grazing management (i.e., 5–15, 16–50, and >50 years) in agriculturally used grassland based on a partial least squares discriminant analysis (PLS-DA).

2.3. Habitat monitoring by means of LiDAR data

So far, very few attempts have been done for applying LiDAR data to directly classify vegetation or grasslands. Despite its capabilities for characterising canopy structures (Zlinszky *et al.*, 2014). According to Ichter *et al.* (2014), LiDAR data are considered unsuitable for the classification of grassland types; rather, they have been mainly applied for estimating forest height and modelling canopy structure (e.g., Hollaus *et al.*, 2009; Lindberg *et al.*, 2014), and classifying shrublands (e.g., Sankey and Bond, 2011) and wetlands (e.g., Zlinszky *et al.*, 2012; Zlinszky *et al.*, 2014) Only recently, Zlinszky *et al.* (2014) evaluated the usability of airborne LiDAR data for vegetation mapping including different grassland types (of which one is a Natura2000 type) for a test site in Sopron (Hungary) employing a random forest classifier.

2.4. Habitat monitoring by means of SAR data

Similarly to optical imagery, also synthetic aperture radar (SAR) data have been successfully applied in several studies for discriminating different crop types (McNairn and Brisco, 2004; Ferrazzoli *et al.*, 1997; Blaes and Defourny, 2003; Lopez-Sanchez *et al.*, 2011; Wegmüller and Werner, 1997); however, they have been seldom employed for classifying grassland habitats. Furthermore, in such context studies accounting for multitemporal series of SAR images are extremely rare. Available data from current and past SAR satellite missions are mainly acquired in three frequency ranges: L-band (1-2 GHz; e.g., ALOS/ PALSAR, JERS-1), C-band (4-8 GHz; e.g., Radarsat-1 and Radarsat-2, ERS-2/SAR, Envisat/ASAR), and X-band (8-12 GHz; e.g., TerraSAR-X/Tandem-X, COSMO-SkyMed, PAZ). While C-band and L-band data have longer wavelength and

can penetrate through vegetation (hence being more suitable for forest analyses), X-band data are not penetrative and thus more suitable for short vegetation cover, such as grasslands. However, only in recent years the acquisition of high-temporal frequency SAR imagery has become possible, thus enabling a variety of new possibilities.

Hill *et al.* (2000) evaluated the applicability of Radarsat-1 C-band single polarisation (HH) data for monitoring grasslands in test sites located in Australia and Canada. In particular, they applied a clustering followed by a maximum likelihood classifier to different datasets obtained combining the backscattering information with texture features. The use of multiple images allowed a consistent improvement with respect to using a single one; moreover, the degree and regularity of surface roughness proved to be the most informative feature. Smith and Buckley (2011) assessed the suitability of multi-temporal Radarsat-2 quadpol imagery to classify native and improved grasslands as well as agricultural crops over a test site in southern Alberta (Canada). The classification on the Freeman-Durden decomposed data was performed by means of the See5 decision tree classifier (RuleQuest Research Pty Ltd, Australia). The results showed the potential to separate native grasslands from agricultural areas as well as native from improved grasslands and that the incidence angle of the acquisition has no influence on the classification accuracy. Schuster *et al.* (2011) showed that habitat-specific swath rules describing management practices are an important parameter in the conservation of semi-natural grasslands and can be used to indirectly map specific habitat types. They introduced a method to detect swath events based on a time series of eleven TerraSAR-X images (HH polarisation, Stripmap mode) over a nature conservation area west of Berlin (Germany) and analysed the temporal profiles of the backscattering coefficient σ^0 by applying a rule-based approach to detect swath events. Results were compared to ground-truth data as well as to habitat-specific swath rules defined to conserve Natura 2000 habitats. Furthermore, Schuster *et al.* (2015) analysed the potential of grassland habitat mapping by means of inter-annual time series data (2009-2011) of RapidEye and TerraSAR-X data acquired over a 60km^2 test site in Northern Germany. Based on individual sets of five RapidEye and 15 TerraSAR-X scenes, after masking non-grassland areas they mapped seven grassland classes with a SVM and were able to achieve overall classification accuracies higher than 90%, with Kappa coefficient greater than 0.9. Betbeder *et al.* (2015) investigated the optimal number and key dates for the acquisition of dual-polarisation (HH/VV) TerraSAR-X images to classify wetland vegetation formations in a 6.7 km^2 test site located in the Bay of Mont-Saint-Michel (France). The available eight dualpol TerraSAR-X scenes were decomposed using the Shannon Entropy (SE) calculation and a SVM classifier with a Gaussian kernel was then used to categorise six classes (of which four are wet grassland types) based on training points collected in situ. Five images proved to be the best trade-off between the number of acquisitions and the final overall accuracy; moreover the best combination was obtained using scenes acquired in February, April, May, June, and July, i.e. when plants grow actively and hydrodynamic processes are vibrant.

A variety of approaches jointly apply multi-sensor imagery from SAR and optical satellites for the classification of vegetation classes, such as crop types (Brisco and Brown, 1995; Blaes *et al.*, 2005; McNairn *et al.*, 2009), and crops combined with more general land-cover classes (Waske and van der Linden, 2008, Waske and Benediktsson, 2007), or for the estimation of herbaceous biomass (Svoray and Shoshany, 2003). Smith *et al.* (1995) analysed ERS-1 SAR data together

with Landsat TM, SPOT VIR, and airborne optical imagery to assess the combination of radar and optical data for monitoring rangeland in the Agriculture and Agri-Food Canada Research Substation at Onefour (Alberta) by means of discriminant function analysis (DFA). The combination allowed obtaining an improved categorisation of the vegetation classes with respect to considering each data type separately; moreover, while optical data proved to be more suitable to characterise the vegetation status, SAR imagery provided key information about the structure and surface topography. Also Price *et al.* (2002a) used a classification system based on the DFA to study the separability of three tallgrass land management practices in eastern Kansas (USA), where usually cool- and warm-season grass species occur, by means of three multi-seasonal Landsat TM and four multi-seasonal ERS-2 SAR images, as well as their combination. The results showed that by using Landsat TM data alone performances were better than those obtained with ERS-2 imagery and, when combined, the SAR data did not allow to increase the classification accuracy. Hill *et al.* (2005) showed the potential of improving the categorization of heterogeneous herbaceous cover in pastures and grasslands by combining independent classifications obtained by means of mono-temporal Landsat-5 TM and Jet Propulsion Laboratory AirSAR data. Experiments were performed for a test site in the Cervantes area (Australia) using an unsupervised version of the Complex Wishart classifier for the C-, L-, and P-band polarimetric SAR data as well as a principal component analysis on the green, red and near-infrared Landsat bands followed by a centroid distance measure clustering. In particular, they were able to map vegetation types based on the different sensitivity of SAR and multispectral sensors to specific vegetation characteristics. Erasmi (2013) assessed the capability of combining optical (six RapidEye scenes) and SAR (four Radarsat-2 and six TerraSAR-X scenes) data for the classification of semi-natural habitats over the study site *Schorfheide Chorin* in eastern Germany and compared the results with single sensor classifications. The object-based classification was performed by means of a classification and regression tree (CART) algorithm. Results showed that single-sensor classifications based on multi-temporal RapidEye data outperformed the once carried out with TerraSAR-X and Radarsat-2 data and demonstrated that bi-sensor combinations of optical and SAR data resulted in classification accuracies between 60.83% and 84.53% (with Radarsat-2 polarimetric data providing higher classification accuracies than TerraSAR-X).

In the above-described context, the work proposed in this thesis represents a continuation in the relatively novel research field of applying very high resolution multitemporal SAR data for classifying habitats and, in particular, specific grassland types by means of advance machine learning techniques.

3. PROPOSED METHODOLOGY

As pointed out in the introduction, the aim of the presented work is the development of a novel targeted classification system for the automatic identification of grassland types by means of multi-temporal and multi-polarised SAR data. Specifically, a scheme depicting its structure into detail is shown in Figure 3-1. In the following, a thorough description will be given for each of the three main blocks, corresponding to as many processing phases, namely: i) the preprocessing of the SAR image time series including the Kennaugh decomposition (section 3.1), ii) the feature extraction including multi-temporal filtering and texture analysis (section 3.2), and iii) the hierarchical targeted classification (section 3.3).

3.1. Preprocessing

The objective of the first phase is to preprocess the original multitemporal SAR data in the form of Kennaugh matrix decomposition elements.

Electromagnetic (EM) waves are transverse (i.e. they oscillate perpendicular to the propagation direction) and the parameter describing the direction of their oscillation is referred to as polarisation. Active radar sensors are capable of transmitting EM pulses of microwave radiation in horizontal (H) / vertical (V) polarisation and have a specialised receiving system to measure the scattered signal from the area of interest in H / V polarisation (Woodhouse, 2006). In the past, the content of SAR scenes has been generally limited to one channel since most of the commercial sensors solely acquired in single polarisation mode. Nevertheless, new instruments are now capable of acquiring in multiple polarisations, hence allowing to collect a higher amount of information about the underlying scattering processes (Alberga, 2004; Schmitt, 2012).

When dealing with multi-polarised SAR data, normally decomposition methods are used to physically explain the resulting complex scattering mechanisms; in particular, they first account for the superimposition of multiple signals and, then, aim at characterising each of them separately (Alberga, 2004; Woodhouse, 2006). All decomposition techniques take into consideration the modifications experienced by the wave during its propagation to the Earth's surface and back, which occur due to specific scattering caused by different land-cover types (Schmitt, 2012). Specifically, according to Freeman and Durden (1998) who first described this phenomenon on a physical rather than mathematical basis, three main categories exist, namely surface, double bounce and volume scattering (see Figure 3-2), which interact with each other to a greater or lesser extent during the wave propagation process. By means of decomposition methods

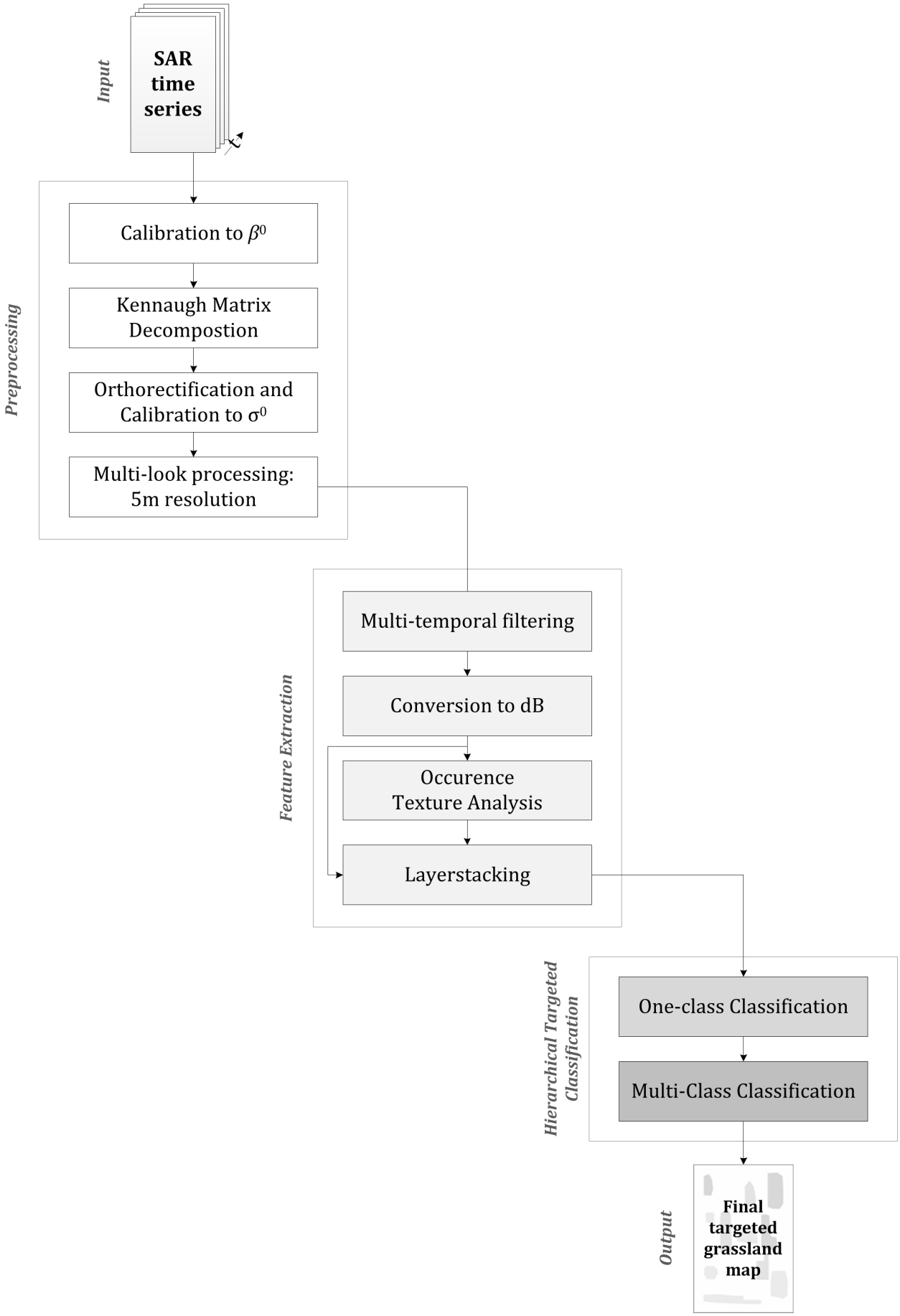

Figure 3-1: Block scheme of the proposed methodology.

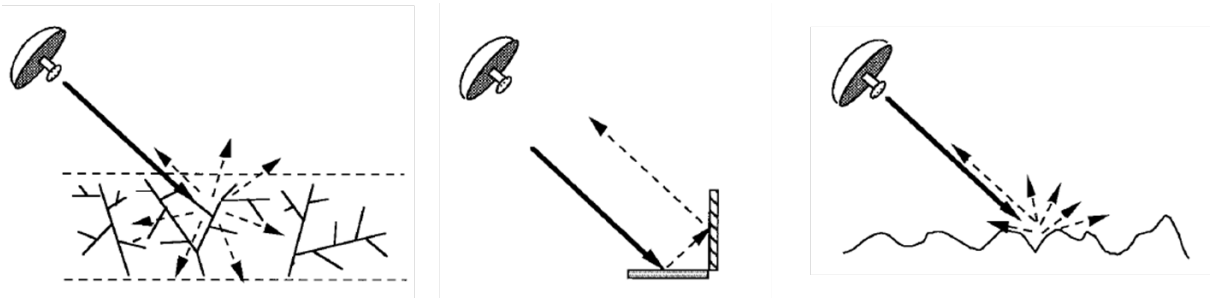

Figure 3-2: Scattering mechanisms described by Freeman and Durden (1998): volume scatter (left), double bounce scatter (middle), surface scatter (right).

the signal is deconstructed into its single original scattering mechanisms (i.e., surface, double bounce, volume), hence easing, e.g., the categorisation of the corresponding land cover (Schmitt, 2012).

As stated in Schmitt *et al.* (2015), generally decomposition techniques based on the only analysis of the backscattering amplitude are still mostly employed with quadpol data, despite various methods exploiting the phase information have been recently presented in the literature (Cloude and Pottier, 1996; Touzi *et al.*, 2004). Besides, few of these can actually be applied to dualpol data provided that specific polarisation modes are used (e.g., Cloude, 2007; Shan *et al.*, 2011; Lopez-Sanchez *et al.*, 2012). Nevertheless, it is worth noting that multi-polarisation data are nowadays most commonly acquired in dualpol mode as for instance in the case of Sentinel-1 (whose standard acquisition mode over Europe is the Interferometric Wide Swath (IWS) dual VV/VH polarisation mode (ESA, 2015b)) or TerraSAR-X (where quad-pol imagery is only experimental and just available on special order (Roth *et al.*, 2004)). In this context, the decomposition technique based on the Kennaugh matrix has the great advantage, compared to the other state-of-the-art techniques, of: i) accounting for the phase information, and ii) supporting both quadpol and dualpol data independently from the acquisition sensor and polarisation mode (i.e., HH/HV, VV/VH, HH/VV) (Cloude and Pottier, 1996; Touzi *et al.*, 2004).

Named after Edward M. Kennaugh, who first considered applying polarisation to radar data (Cloude and Pottier, 1996), the Kennaugh matrix (see equation (3-1)) mathematically characterises the linear transformation of the (send and received) polarised wave (Schmitt, 2012). In particular, it consists of the total intensity K_0 - which describes the sum of the backscattering intensity of all polarisation channels – as well as, being it symmetrical, nine intensity differences $K_1, \dots, K_9$ representing as many linear transformation coefficients (Schmitt *et al.*, 2015).

$$[K] = \begin{bmatrix} K_0 & K_4 & K_5 & K_6 \\ K_4 & K_1 & K_9 & K_8 \\ K_5 & K_9 & K_2 & K_7 \\ K_6 & K_8 & K_7 & K_3 \end{bmatrix} \tag{3-1}$$

Specifically, the Kennaugh matrix is the linear transformation of the Stokes vector g (Schmitt *et al.*, 2015) introduced by George Gabriel Stokes in 1852 (see equation (3-2)) which allows for a complete description of the polarised wave by means of its four parameters, namely I_0, Q, U, and V (Woodhouse, 2006). While I_0 reflects the total intensity of the wave, Q, U, and V describe the

state of the polarisation (Woodhouse, 2006). Q describes the trend of the wave to be of horizontal ($Q < 0$) or vertical polarisation ($Q > 0$) (Woodhouse, 2006). U and V characterise the phase difference between the horizontal and vertical elements of the wave: U describes the direction of the wave (with $U > 0$ denoting a trend to be polarised at +45° and $U < 0$ to be polarised at -45°), while V describes the circular polarisation (with $V > 0$ denoting left-handed and $V < 0$ right-handed polarisations) (Woodhouse, 2006). In particular, it holds that:

$$g_{received} = \begin{bmatrix} I_0 \\ Q \\ U \\ V \end{bmatrix} received = \begin{bmatrix} K_0 & K_4 & K_5 & K_6 \\ K_4 & K_1 & K_9 & K_8 \\ K_5 & K_9 & K_2 & K_7 \\ K_6 & K_8 & K_7 & K_3 \end{bmatrix} * \begin{bmatrix} I_0 \\ Q \\ U \\ V \end{bmatrix} send \tag{3-2}$$

As stated in Schmitt (2012), the elements of the Kennaugh matrix are calculated as:

$$K_0 = \frac{1}{2}\{|S_{HH}|^2 + |S_{HV}|^2 + |S_{VH}|^2 + |S_{VV}|^2\} \tag{3-3}$$

$$K_1 = \frac{1}{2}\{|S_{HH}|^2 - |S_{HV}|^2 - |S_{VH}|^2 + |S_{VV}|^2\} \tag{3-4}$$

$$K_2 = \frac{1}{2}(|S_{HV}|^2 + |S_{VH}|^2) + Re\,\{S_{HH}S_{VV}^*\} \tag{3-5}$$

$$K_3 = \frac{1}{2}(|S_{HV}|^2 + |S_{VH}|^2) - Re\,\{S_{HH}S_{VV}^*\} \tag{3-6}$$

$$K_4 = \frac{1}{2}(|S_{HH}|^2 - |S_{VV}|^2) \tag{3-7}$$

$$K_5 = \frac{1}{2}Re\,\{S_{HH}S_{HV}^* + S_{VH}S_{VV}^* + S_{HH}S_{VH}^* + S_{HV}S_{VV}^*\} \tag{3-8}$$

$$K_6 = \frac{1}{2}Im\,\{S_{HH}S_{HV}^* + S_{VH}S_{VV}^* + S_{HH}S_{VH}^* + S_{HV}S_{VV}^*\} \tag{3-9}$$

$$K_7 = Im\,\{S_{HH}S_{VV}^*\} \tag{3-10}$$

$$K_8 = \frac{1}{2}Re\,\{S_{HH}S_{HV}^* - S_{VH}S_{VV}^* + S_{HH}S_{VH}^* - S_{HV}S_{VV}^*\} \tag{3-11}$$

$$K_9 = \frac{1}{2}Im\,\{S_{HH}S_{HV}^* - S_{VH}S_{VV}^* + S_{HH}S_{VH}^* - S_{HV}S_{VV}^*\} \tag{3-12}$$

where S denotes the complex measurements (amplitude and phase) depending on the polarisation as defined in the Sinclair Matrix. As mentioned above, the first element K_0 represents the total intensity, while the remainder can be categorised according to how their coordinate system is oriented, i.e. parallel to the linear axes (horizontally and vertically), diagonal to the linear axes (45 and 135 degrees), or circular (in right and left rotating direction). Absorption elements (K_1, K_2, K_3) describe the loss of polarisation during the scattering process, diattenuation elements (K_4, K_5, K_6) express the change of the relation between two amplitude values, and retardance elements (K_7, K_8, K_9) characterise the phase delay during scattering in the respective direction (see Table 3-1) (Schmitt *et al.*, 2015).

For the dualpol case, missing information is set to zero, thus a reduced set of matrix elements is derived (Schmitt, 2012). Specifically, K_0 , K_2 , K_4 and K_7 are calculated for co-pol images (HH/VV) while K_0 , K_1 , K_5 and K_8 are generated for cross-pol images (VV/VH or HH/HV). As an example, for the VV/VH polarisation K_0 , K_1 , K_5 and K_8 are calculated as follows (Schmitt, 2012):

Table 3-1: Interpretation of the Kennaugh elements (Schmitt (2012)).

	Total	Parallel	Diagonal	Circular
Absorption	K_0	K_1	K_2	K_3
Diattenuation		K_4	K_5	K_6
Retardance		K_7	K_8	K_9

$$K_0 = |S_{VH}|^2 + |S_{VV}|^2 \tag{3-13}$$

$$K_1 = |S_{VV}|^2 - |S_{VH}|^2 \tag{3-14}$$

$$K_5 = Re\{S_{HV}S_{VV}^*\} \tag{3-15}$$

$$K_8 = -Im\{S_{HV}S_{VV}^*\} \tag{3-16}$$

The Kennaugh matrix decomposition is sensor and polarisation independent (i.e., it always includes K_0 and a varying number of transformation coefficients depending on the considered polarisation mode), thus being suitable for an operative application at any scale (Schmitt *et al.*, 2015).

In this framework, the automatic preprocessing chain implemented by Schmitt (2012) is employed in the first phase of the proposed methodology; in particular, it requires as input uncalibrated complex single-look images in slant range geometry (e.g., SSC (single-look slant range complex) in the case of TerraSAR-X and SLC (single look complex) in the case of Radarsat-2). First, calibration to the radar brightness β^0 is applied (Schmitt, 2012), where β^0 stands for the backscattering per unit area in slant range, hence representing the backscattering measured by the sensor not being modified based on ellipsoid or terrain Earth models (Small *et al.*, 2009). This is followed by the actual Kennaugh matrix decomposition.

All Kennaugh elements are then normalised between -1 and +1 in the hyperbolic tangent scaling (Schmitt *et al.*, 2015). Specifically, as one can notice from Figure 3-3, this is more sensitive and very precise around zero (where the hyperbolic tangent has its maximal slope), while it gets imprecise towards infinity. In this way, very big and small outlier values are not captured accurately, in contrast to values covering 95 percent of the image, which are instead well represented (Schmitt, 2012).

The Kennaugh elements are then orthorectified and calibrated to σ^0 representing the backscattering coefficient projected to the Earth's surface and depends on several factors like the incidence angle, wavelength, polarisation and properties of the scattering surface (Schmitt, 2012). Finally, they are processed to a spatial resolution calculated based on the equivalent number of looks (ENL), which is equivalent to the number of independent intensity values averaged per pixel (Oliver and Quegan, 1998) and is given by:

$$ENL = \frac{mean^2}{variance} \tag{3-17}$$

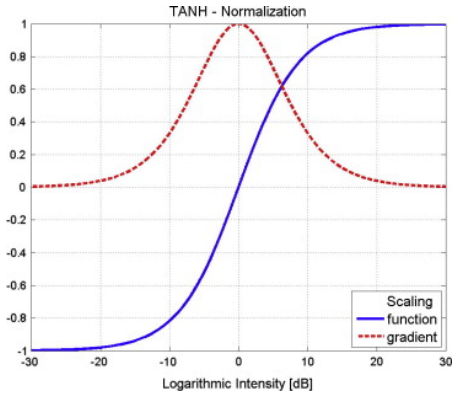

Figure 3-3: The hyperbolic tangent function (Schmitt *et al.*, 2015).

where *mean* and *variance* refer to the backscattering.

In particular, instead of pre-defining the ENL, the desired spatial resolution of the resulting geocoded images is specified and then the ENL is calculated accordingly (Schmitt, 2012). This is especially useful when working with multi-source data sets where a comparable spatial resolution is crucial. The resulting multitemporal sequence of Kennaugh elements is given then as input to the feature extraction module.

3.2. Feature extraction

3.2.1. Multi-temporal filtering

As the quality of SAR data is often influenced by the speckle (i.e., the "salt-and-pepper" granular noise typically of radar images), it is of utmost importance to properly filter them in order to avoid errors, especially when applying pixel-based methods (Quegan and Yu, 2001). Speckle occurs due to the presence of various discrete scatterers within each resolution cell which change the amplitude and phase of the backscattered wave (Oliver and Quegan, 1998). Commonly, data are filtered in the spatial domain (an overview of methods is given by Oliver and Quegan (1998)). However, with the availability of multitemporal images acquired over a given study area, it is recommended to apply a linear combination of the items composing the series so to minimise speckle while preserving both the radiometric and spatial resolution (see Figure 3-4) (Quegan and Yu, 2001). One common measure to describe the quality of the original as well as filtered images is the ENL, whose value is low for images with high speckle, while it increases for filtered data. As an example, Quegan and Yu (2001) presented a multi-temporal filter where the size of the selected moving window affects the ENL such that it saturates with a growing number of input images.

In this framework, the second phase of the presented methodology first includes the multi-temporal filtering presented by Oliver and Quegan (1998), which is applied to the sequence of Kennaugh elements defined in the first phase. In particular, given a sequence of *N* (co-registered) elements, the filtered value for the pixel at position (*x, y*) of the *n*-th item of the series for the *m*-th Kennaugh element $K_m^n(x, y)$ is given by:

$$\overline{K}_m^n(x,y) = \frac{E[K_m^n]}{N} \sum_{i=1}^{N} \frac{K_m^i(x,y)}{E\left[K_m^i\right]} \tag{3-18}$$

where $E[K_m^n]$ denotes the local mean value for K_m^n computed using a window centred at (*x, y*).

The obtained temporally-filtered Kennaugh elements are finally converted to dB in order to obtain a Gaussian distribution of the data.

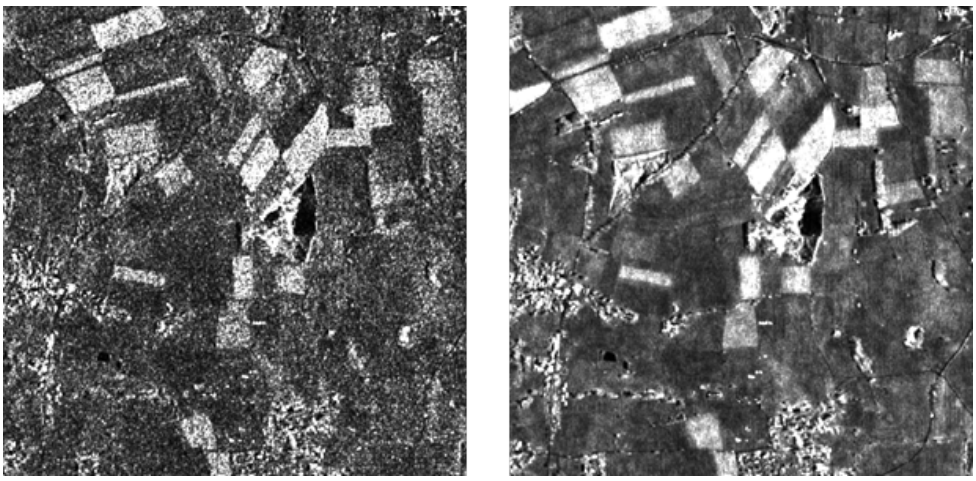

Figure 3-4: K_0 element generated from a TerraSAR-X dualpol VV/VH image (left), and corresponding multitemporally filtered image (right) derived using a window of size 11x11 pixels.

3.2.2. Texture analysis

Texture describes the spatial distribution of differences of the scattered signal within an image (Haralick *et al.*, 1973). Specifically, "It contains important information about the structural arrangement of surfaces and their relationship to the surrounding environment" (Haralick *et al.*, 1973) and carries useful information for discriminating spectrally similar land cover classes (Anys *et al.*, 1994). In such context, given the general advantages offered by including textural information when addressing land-cover classification, occurrence texture measures have been computed from the time series of the multi-temporally filtered K_0 elements. Here, only K_0 is used, since it represents the total backscattering intensity and is the most suitable element for highlighting spatial geometrical relationships (with respect to the others which describe the state of the polarisation). In particular, data range (DRG), mean (MEA), skewness (SKE) and variance (VAR) are computed, as they have proven to be particularly effective in the context of land cover classification with SAR imagery (Anys *et al.*, 1994). According to Anys *et al.* (1994), they are defined as follows:

$$\mu_0^n = MEA\ (\overline{K}_0^n) = \frac{1}{L}\sum_{i=1}^{L} x_i \tag{3-19}$$

$$\sigma_0^n = VAR\ (\overline{K}_0^n) = \frac{1}{L}\sum_{i=1}^{L} (x_i - \mu_0^n)^2 \tag{3-20}$$

$$SKE\ (\overline{K}_0^n) = \frac{1}{L}\sum_{i=1}^{L} \left(\frac{x_i - \mu_0^n}{\sigma_0^n}\right)^3 \tag{3-21}$$

$$DRG\ (\overline{K}_0^n) = MAX\ \{x_1, \dots, x_L\} - MIN\{x_1, \dots, x_L\} \tag{3-22}$$

where x_i denotes the value of the *i*–th pixel in the processing window and L its total number of pixels.

The final data set, which serves as input to the subsequent classification module, is obtained by stacking the multitemporally filtered Kennaugh elements (four in the case of dualpol data or ten in the case of quadpol data) together with the four texture features computed for K_0 (i.e., DRG, MEA, SKE, VAR) generated for each image of the original SAR time series.

3.3. Hierarchical targeted classification

Land-cover classification represents nowadays one of the major applications of satellite Earth Observation (EO) and has proven to be of valuable support in several fields like, among others, land-use managing and planning or environment protection (Waske and Braun, 2009; Marconcini *et al.*, 2014). In this context, the greater is the advancement in terms of spatial, temporal, and radiometric resolution of the EO data, the higher is the development of classification techniques (Richards, 2005).

In general, supervised approaches represent the most accurate methodological solution to land-cover classification problems, although they are highly depending on the availability of comprehensive ground truth data for all the land-cover classes occurring in the area of interest (AOI) (Fernández-Delgado *et al.*, 2014). However, this demand can rarely be fulfilled in most real-life cases since the collection of exhaustive training samples is generally difficult, expensive or not even feasible, particularly if the area under investigation is remote, inaccessible, or unfamiliar to the operator (Marconcini *et al.*, 2014; Foody *et al.*, 2006). Nevertheless, in many applications the end-users (who have increasing financial limits and time constrains) are actually only interested in very few specific targeted land-cover classes which, for instance, have high ecological value or are associated with support actions, subsidies or benefits from national or international institutions (Mack *et al.*, 2014; Marconcini *et al.*, 2014). In such cases, the collection of labelled points for the fewer classes of interest is generally faster and cheaper. The categorisation of specific grasslands and habitat types as those addressed in this thesis falls within such category of problems, which is defined in the literature as “targeted” land-cover classification (Marconcini *et al.*, 2014).

Several techniques have been presented in the literature aimed at categorising a single class of interest for which training points are solely available (Tax (2001); Khan and Madden (2014)). These methods are commonly referred to as one-class classifiers and can actually be employed also to address targeted classification problems where multiple classes of interest are investigated at a time. In particular, such task can be performed by considering an ensemble of one-class classifiers each one associated to a specific class of interest. Nonetheless, this represents a sub-optimal solution since: i) heuristics must be defined to effectively combine their outputs; and ii) each class is analysed separately without accounting for the information available for the other targeted classes.

To overcome this limitation, Marconcini et al., 2014 have recently proposed a dedicated targeted classification approach which in addition to the training points available for the classes of interest also takes into account unlabelled samples drawn from the same AOI. Specifically, the expectation–maximisation algorithm in combination with Markov random fields is used for approximating the probability density function of the targeted classes as well as that of the unknown class given by the merger of all the other land-cover types present in the study site (for which no training samples are given). However, despite the technique proved effective on different datasets, it has the great limitation of a high computational load mostly due to the employment of the *k*-means clustering for determining the most informative among all possible unlabelled points. With datasets of rather limited size as the ones investigated by the authors this aspect was not too critical (i.e., one dataset of size 600x600 pixels composed of 6 features

and another of size 512x512 pixels composed of 63 features); nevertheless, in the cases considered in this work (e.g., of the order of ~12000x6000 pixels for up to more than 100 features), it definitely hinders the employment of the technique.

To effectively perform the targeted classification of the grasslands and habitat types of interest also in the presence of large and high-dimensional datasets, a new method has been then defined which aims at simplifying the complex original task into two easier problems. In particular, the proposed approach is hierarchical and consists in the sequential use of:

i. A one-class classifier aimed at initially outlining the merger of all the grassland types of interest considered as a single information class;
ii. A multi-class supervised classifier aimed at discriminating the specific targeted classes within the areas identified as positive by the one-class classifier.

In the first phase, all labelled samples available for all targeted classes of interest are merged and used together for training the one-class classifier. This always results in a higher ratio between the amount of employed training samples and the total number of features, hence lowering the influence of the Hughes phenomenon (Hughes, 1968) (stating that for a given number of training samples, the predictive power reduces as the dimensionality increases), which arises in the presence of few training samples for one/some of the targeted classes. Moreover, assuming that the considered classes of interest belong to similar land-cover types, it is reasonable to expect that the resulting one-class classification problem is simpler to solve with respect to outlining each single class separately.

When addressing the multi-class classification task in the second phase, under the hypothesis that the previous step results in a reliable mask of the unknown class, the problem becomes then suitable to be solved by using a standard supervised classifier. Indeed, the labelled samples available for the targeted classes constitute an exhaustive training set for the remaining (unmasked) areas in the AOI.

It is worth pointing out that, theoretically, any combination of one-class and multi-class supervised classifiers might be employed. To this aim, in the following a brief overview is first given about the different families of state-of-the-art one-class classifiers and, next, the attention is focused on the two currently most largely employed techniques (i.e., the Maximum Entropy and the One-Class Support Vector Machines), which have been extensively tested in the experimental analysis described in chapter 5. Afterwards, concerning the supervised multi-class classification, details are given about the Support Vector Machines classifier, which has been selected to be adopted in the final hierarchical system for the experimental analysis carried out in this work.

3.3.1. One-class classification

One-class classifiers are designed for outlining the only class of interest for which ground-truth information is exclusively available. Despite the term "one-class classifiers" (Tax (2001); Khan and Madden (2014)) is generally used in the literature, in some studies these type of methods are also referred to as "outlier detection" (Ritter and Gallegos, 1997), "novelty detection" (Bishop, 1994), or "concept learning" (Japkowicz, 1999) as a result of the different applications from which they have been originated (Khan and Madden, 2014). However, all algorithms share two main elements: i) a measure for the distance $d(x)$ or the similarity $s(x)$ (in some cases, a probability) of a sample x to the only land-cover class of interest ω_{int} and ii) a threshold θ on $d(x)$ or $s(x)$ (Marconcini *et al.*, 2014). According to Tax (2001), one-class classifiers can be separated into three main categories, namely density, boundary or reconstruction methods.

Density methods aim at estimating the probability density function $p\ (\omega_{int}|x)$ in the complete feature space (Mazhelis, 2006) exploiting the labelled points available for ω_{int}. A generic input sample is then associated with ω_{int} if $p(\omega_{int}|x) > \theta$ or with the unknown class ω_{unk} otherwise (Mazhelis, 2006). Despite effective, these approaches might be strongly influenced by i) the selection of the threshold θ depending on the prior knowledge of ω_{int}, and ii) the data distribution type which has to be chosen a priori. Common density methods include histograms, Markov models, Gaussian and mixture of Gaussians models, Parzen density estimation, *k*-nearest-neighbours estimation and the Maximum Entropy (MaxEnt) classifier (Tax, 2001; Mazhelis, 2006; Mack *et al.*, 2014).

Reconstruction methods have been originally designed for modelling the data rather than directly performing one-class classification (Tax, 2001). Specifically, a model is chosen and fitted to the data by assumptions made on their generating process based on a priori knowledge about their distribution (Tax, 2001). When employing reconstruction methods, the empirical threshold θ is determined on the basis of the available training data for the target class ω_{int} and the reconstruction error is used for describing the distance $d(x)$ to it (Tax, 2001). Samples not fulfilling the assumptions about the resulting distribution for ω_{int} are considered as outliers and, thus, finally associated with ω_{unk} (Tax, 2001). In this context the most employed methods include, among others, the *k*-means classifier and the Principal Component Analysis (Mazhelis, 2006).

Boundary methods aim at optimising a closed boundary around the training data available for ω_{int} such that an unknown sample is assigned to ω_{int} depending on the estimated (weighted) distances $d(x)$ to most informative labelled samples in the training set (Tax, 2001). Contrarily to density methods, they generally exhibit effective performance also in the presence of a lower amount of labelled points for ω_{int}, but they might be sensitive to the scaling of the input features and thus are very dependent on well-defined distances between objects (Tax, 2001). These methods comprise the One-class Support Vector Machines (OC-SVM) and the support vector data description (SVDD) (Mazhelis, 2006).

Among all methods presented so far in the literature, the two which proved more effective suitable to be employed in the proposed hierarchical system are the MaxEnt and OC-SVM classifiers.

Maximum Entropy Classifier

Historically, the MaxEnt comes from statistical mechanics (Jaynes, 1957), but has been applied in a variety of other disciplines, such as astronomy, image reconstruction, image processing, language processing, and ecological niche modelling (Phillips *et al.*, 2004; Phillips *et al.*, 2006). In particular, it predicts the distribution of the target class by estimating the distribution of maximum entropy (i.e., the one closest to uniform) based on a given set of labelled target samples and a set of input features (Phillips *et al.*, 2004). This is done provided that the expected value of each feature corresponds to its empirical average derived from the set of labelled points of the target class (Phillips *et al.*, 2006). For vegetation or species distribution modelling, the labelled target samples refer to the ground truth training points of the class of interest and the set of features is composed of EO input imagery and/or environmental variables (e.g., temperature, soil moisture, elevation, etc.) over the geographic area of interest (Phillips *et al.*, 2004).

Let ω_{int} denote the targeted class of interest for which labeled samples are available and let ω_{unk} represent the unknown class composed of the merger of all the remaining unknown classes in the investigated area for which labelled samples are not available. In this framework, the Bayes classifier (i.e., the one minimising the probability of misclassification) is defined as:

$$p(\omega_{int}|\mathbf{x}) \underset{\omega_{int}}{\overset{\omega_{unk}}{\lessgtr}} p(\omega_{unk}|\mathbf{x}) \tag{3-23}$$

where, in the considered case, $\mathbf{x} = \langle x_1, \dots, x_D \rangle \in \mathcal{X} \subset \mathbb{R}^{\boldsymbol{D}}$, $|\mathcal{X}| = I \times J$, represents the generic D-dimensional feature vector (consisting of the multi-temporally filtered Kennaugh elements and the corresponding texture measures described in section 3.2) from the investigated dataset $\mathcal{X}$ of size $I \times J$ pixels. According to the Bayes' theorem, Equation (3-23) can be rewritten as:

$$\frac{p(\mathbf{x}|\omega_{int}) \cdot P(\omega_{int})}{p(\mathbf{x})} \underset{\omega_{int}}{\overset{\omega_{unk}}{\lessgtr}} \frac{p(\mathbf{x}|\omega_{unk}) \cdot P(\omega_{unk})}{p(\mathbf{x})} \tag{3-24}$$

$$p(\mathbf{x}|\omega_{int}) \cdot P(\omega_{int}) \underset{\omega_{int}}{\overset{\omega_{unk}}{\lessgtr}} p(\mathbf{x}|\omega_{unk}) \cdot P(\omega_{unk}) \tag{3-25}$$

which can be further reduced to:

$$p(\mathbf{x}|\omega_{int}) \underset{\omega_{int}}{\overset{\omega_{unk}}{\lessgtr}} \frac{p(\mathbf{x}|\omega_{unk}) \cdot P(\omega_{unk})}{P(\omega_{int})} \tag{3-26}$$

Figure 3-5 (a) and (b) depict a simple one-dimension example referring to Equations (3-25) and (3-26), respectively, where the area in light red corresponds to where the classifier associates the input sample to the class of interest ω_{int}. In the addressed framework no labeled samples are supposed to be available for the unknown class ω_{unk}; hence, nothing can be effectively guessed for its conditional probability density function (PDF) $p(\mathbf{x}|\omega_{unk})$ and prior $P(\omega_{unk})$; moreover, since labeled samples are only available for ω_{int}, it is not possible to accurately estimate $P(\omega_{int})$ independently from the sample size (Ward *et al.*, 2009).

In such context, the MaxEnt classifier aims at estimating a reliable approximation $\hat{p}(\mathbf{x}|\omega_{int})$ for the conditional PDF of ω_{int} and finally deriving a binary classification map based on the

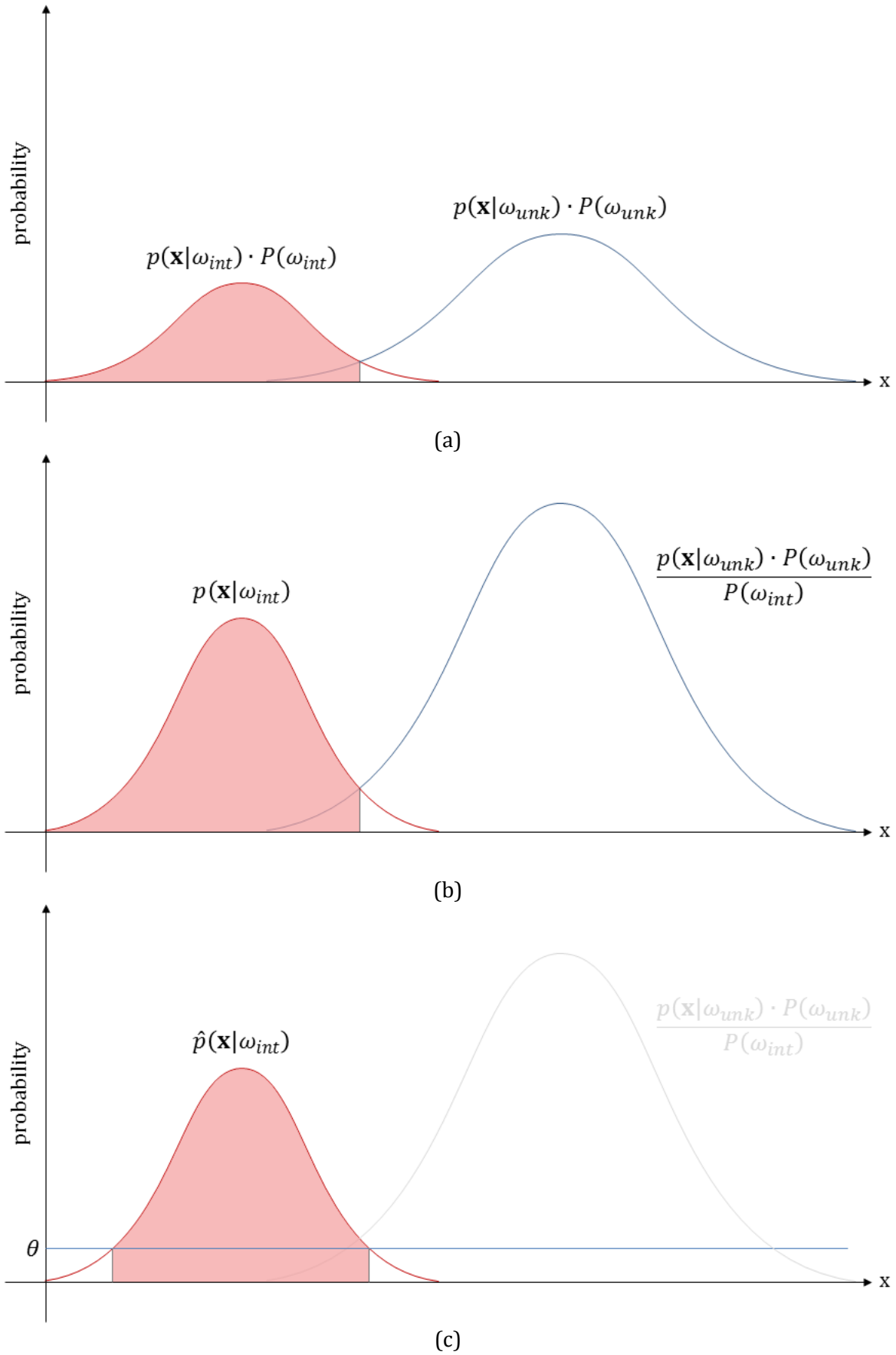

Figure 3-5: One-dimension example depicting the decision rule corresponding to equations (3-25) (a), (3-26) (b), and (3-27) (c). The area in light red corresponds to where the classifier associates the input sample to the class of interest ω_{int}.

following decision rule

$$\hat{p}(\mathbf{x}|\omega_{int}) \underset{\omega_{int}}{\overset{\omega_{unk}}{\lessgtr}} \theta \tag{3-27}$$

where the threshold θ is empirically defined by the user (see Figure 3-5 (c)).

As it can be noticed from the considered example, this approach might result in sub-optimal solutions; however, in practical applications MaxEnt proved to be very effective resulting in limited omission and commission errors (Phillips *et al.*, 2004; Phillips *et al.*, 2006; Phillips and Dudík, 2008; Evangelista *et al.*, 2009; Kumar *et al.*, 2009; Li and Guo, 2010; Morán-Ordóñez *et al.*, 2012).

The expectation of a random variable is defined as the integral of the random variable with respect to its probability measure and represents the expected average value of the random variable (Hamming, R. W., 1991). In the case of the random vector $\mathbf{x}$, the expectation is a random vector whose elements are the expected values of the respective random variables. Accordingly, in the above-described scenario, the expectation of the generic feature x_d given ω_{int} is defined as:

$$\mathrm{E}[x_d|\omega_{int}] = \sum_{\mathbf{x}\in\mathcal{X}} x_d \cdot \hat{p}(x_d|\omega_{int}) \tag{3-28}$$

Let consider the training set $\mathcal{T} = \{\bar{\mathbf{x}}|\bar{y} = \omega_{int}\}$, $\mathcal{T} \subset \mathcal{X}$, $|\mathcal{T}| = M$, where $\bar{y}$ represents the class label associated to $\bar{\mathbf{x}}$. $\mathcal{T}$ is composed of a set of M samples available a priori from the investigated dataset $\mathcal{X}$ which belong to the class of interest ω_{int}. The MaxEnt classifiers assumes that, for a given feature x_d, its empirical average computed over the available training samples can be used as a reliable estimate for its true expectation, thus:

$$\mathrm{E}[x_d|\omega_{int}] = \sum_{\mathbf{x}\in\mathcal{X}} x_d \cdot \hat{p}(x_d|\omega_{int}) = \frac{1}{M}\sum_{\bar{\mathbf{x}}\in\mathcal{T}} \bar{x}_d \tag{3-29}$$

MaxEnt exploits the maximum entropy principle first formalised by Jaynes (1957) which states that, given a set of available observations, the best approximation for the corresponding unknown probability distribution is the one whose entropy is largest (i.e., the one closest to uniform). Shannon, C. E. (1948) defined the entropy of a random variable x as:

$$H(x) = -\int p(x) \cdot \log p(x)\, dx \tag{3-30}$$

Hence, the objective of MaxEnt becomes solving the following constrained optimisation problem:

$$\begin{aligned} &\max_{\hat{p}} \left(-\sum_{\mathbf{x}\in\mathcal{X}} \hat{p}(\mathbf{x}|\omega_{int}) \cdot \log \hat{p}(\mathbf{x}|\omega_{int}) \right) \\ &\text{s.t. } \textstyle\sum_{\mathbf{x}\in\mathcal{X}} x_d \cdot \hat{p}(x_d|\omega_{int}) = \frac{1}{M}\sum_{\bar{\mathbf{x}}\in\mathcal{T}} \bar{x}_d \quad \forall d \in \{1, \dots, D\} \end{aligned} \tag{3-31}$$

By means of convex duality it is possible to demonstrate (Della Pietra *et al.*, 1997) that the conditional PDF with maximum entropy subject to the above constraints has the form of a Gibbs distribution $q_{\boldsymbol{\lambda}}(\mathbf{x})$ of the type:

$$q_{\boldsymbol{\lambda}}(\mathbf{x}) = \frac{\exp(\boldsymbol{\lambda} \cdot \mathbf{x})}{Z_{\boldsymbol{\lambda}}} \tag{3-32}$$

where $\boldsymbol{\lambda} = \langle \lambda_1, \dots, \lambda_D \rangle \subset \mathbb{R}^{\boldsymbol{D}}$ is a vector of weights and $Z_{\boldsymbol{\lambda}} = \sum_{\tilde{\mathbf{x}} \in \mathcal{X}} \exp(\boldsymbol{\lambda} \cdot \tilde{\mathbf{x}})$ a normalisation constant ensuring that $q_{\boldsymbol{\lambda}}(\mathbf{x})$ sums to 1.

In particular, $\hat{p}(\mathbf{x}|\omega_{int})$ is equal to the Gibbs distribution maximising the probability of the available training samples belonging to $\mathcal{T}$:

$$\hat{p}(\mathbf{x}|\omega_{int}) = \frac{\exp(\tilde{\boldsymbol{\lambda}} \cdot \mathbf{x})}{\sum_{\tilde{\mathbf{x}} \in \mathcal{X}} \exp(\tilde{\boldsymbol{\lambda}} \cdot \tilde{\mathbf{x}})} \tag{3-33}$$

where

$$\tilde{\boldsymbol{\lambda}} = \underset{\boldsymbol{\lambda}}{\operatorname{argmin}} \left(\ln Z_{\boldsymbol{\lambda}} - \frac{1}{M} \sum_{\bar{\mathbf{x}} \in \mathcal{T}} \boldsymbol{\lambda} \cdot \bar{\mathbf{x}} \right) \tag{3-34}$$

As generally the empirical average computed over the training samples does not equal the true expectation but solely approximates it, the constraint in (3-31) is relaxed as (Dudík *et al.*, 2004):

$$\left| \sum_{\mathbf{x} \in \mathcal{X}} x_d \cdot \hat{p}(x_d|\omega_{int}) - \frac{1}{M} \sum_{\bar{\mathbf{x}} \in \mathcal{T}} \bar{x}_d \right| \leq \beta_d \quad \forall d \in \{1, \dots, D\} \tag{3-35}$$

being β_d a given constant. This prevents the MaxEnt to overfit the training data. The optimal vector $\tilde{\boldsymbol{\lambda}}$ is then computed as

$$\tilde{\boldsymbol{\lambda}} = \underset{\boldsymbol{\lambda}}{\operatorname{argmin}} \left(\ln Z_{\boldsymbol{\lambda}} - \frac{1}{M} \sum_{\bar{\mathbf{x}} \in \mathcal{T}} \boldsymbol{\lambda} \cdot \bar{\mathbf{x}} + \sum_{d} \beta_d |\lambda_d| \right) \tag{3-36}$$

where the last term penalises large values for the weights λ_d.

In real-word applications the cardinality of $\mathcal{X}$ might be very high (e.g., in the case of remote-sensing datasets generally of the order of tens or hundreds of million pixels); thus, solving (3-36) where $\mathrm{Z}_\lambda = \sum_{\tilde{\mathrm{x}} \in \mathcal{X}} \exp(\lambda \cdot \tilde{\mathrm{x}})$ would be not feasible. Accordingly, this is generally overcome by considering a subset $\dot{\mathcal{X}} \subset \mathcal{X}$ of random "background" samples of the order of tens or hundreds of thousands pixels which practically does not result in any sensible loss of performance (Yates *et al.*, 2010; Elith *et al.*, 2011).

To further simplify the minimisation problem, Phillips and Dudík (2008) proposed to fix the constant β_d according to:

$$\beta_d = \beta \sqrt{\frac{s^2[x_d]}{M}} \tag{3-37}$$

in which $s^2[x_d]$ denotes the empirical variance for x_d computed over the available training samples $\mathcal{T}$. In this way, β_d is given by the standard error (i.e., the result of the square root term) multiplied by the single regularisation parameter β defined on the basis of the preferred confidence level (Elith *et al.*, 2011). A method for automatically determining an effective value for β based on the available labeled sampled for ω_{int} has been described in Dudík *et al.* (2004).

Several strategies exist in the literature for computing the MaxEnt conditional PDF (Darroch, J. N. and Ratcliff, 1972; Della Pietra *et al.*, 1997; Malouf, 2002; Salakhutdinov *et al.*, 2003). A simple approach capable of handling a large number of features (as in the case investigated in this work) proved to be the one employed in Phillips *et al.* (2004) and Dudík *et al.* (2004), where each weight λ_d is progressively updated at a time. Specifically, the algorithm converges to the MaxEnt conditional PDF and stops either when the value of the function to minimise in (3-36) between successive iterations is lower than a prefixed convergence threshold κ or the predefined maximum number iterations φ is reached.

Once $\hat{p}(x|\omega_{int})$ is computed for each input sample of the given dataset $\mathcal{X}$, the last step involves determining the threshold θ based on which input samples are finally associated with ω_{int} or ω_{unk} according to (3-27). To this aim, a common approach in the literature is to fix a significance level ρ and compute θ such that the maximum rejection probability (i.e., omission error) calculated over the training samples $\mathcal{T}$ available for ω_{int} is not greater than ρ (Jeon and Landgrebe, 1999; Engler *et al.*, 2004; Phillips *et al.*, 2006). In statistics, the significance level ρ is often set equal to 0.05 or 0.01 (Capraro, 2007).

One-Class Support Vector Machines (OC-SVM)

The OC-SVM algorithm was first proposed by Schölkopf *et al.* (2001) as a support vector approach for addressing novelty detection. In particular, rather than trying to estimate the probability density of the targeted class on interest ω_{int}, its aims at defining a binary function for which most of the data actually belonging to ω_{int} are mapped where the function is nonzero. This is in line with the principle of Vapnik (i.e., the co-inventor of the original SVM algorithm) stating that "we should never try to solve a problem that is more general than is actually needed" (Vapnik, 1998).

Let denote with $\mathcal{X}$ the investigated dataset of size $I \times J$ pixels, where $\mathbf{x} = \langle x_1, \dots, x_D \rangle \in \mathcal{X} \subset \mathbb{R}^{\boldsymbol{D}}$, represents the corresponding generic D-dimensional feature vector (consisting of the multi-temporally filtered Kennaugh elements and the corresponding texture measures described in section 3.2). The training set $\mathcal{T} = \{\bar{\mathbf{x}} | \bar{y} = \omega_{int}\}$, $\mathcal{T} \subset \mathcal{X}$, $|\mathcal{T}| = M$, is available and consists of M samples belonging to the targeted class of interest ω_{int}. The aim of the OC-SVM is then to find a hyperplane with maximum margin separation from the origin, which is considered as the only available sample for the unknown class ω_{unk} (for which actually no labelled points are supposed to be available). However, as it is highly unlikely that ω_{int} and ω_{unk} can be linearly separated in the original input space $\mathbb{R}^{\boldsymbol{D}}$, training points are mapped through the non-linear transformation $\phi(\cdot)$ into a high-dimensional Hilbert space [i.e., a space of dimension $N \gg D$ possessing the structure of an inner product that allows length and angles to be measured (Dieudonné, 1960)] where it is more likely that the two classes can be discriminated by means of such an hyperplane.

Any hyperplane is defined as a subspace of dimension D-1, where D denotes the dimension of its ambient space (e.g., in a 3-dimensional space hyperplanes are 2-dimensional planes; in a 2-dimensional space, hyperplanes are 1-dimensional lines). Mathematically, it can be written in the form $\mathbf{w} \cdot \mathbf{x} + \rho = 0$, where $\mathbf{w}$ is a vector perpendicular to the hyperplane and ρ is a parameter such that $\rho/\|\mathbf{w}\|^2$ denotes the distance from the origin. Accordingly, for separating

the training data from the origin one has to solve the following constrained minimisation problem:

$$\min_{\mathbf{w},\rho,\xi}\left(\frac{1}{2}\|\mathbf{w}\|^2-\rho+\frac{1}{\nu M}\sum_{i=1}^{M}\xi_i\right)$$
$$\text{s.t. } \left(\mathbf{w}\cdot\phi(\bar{\mathbf{x}}_i)\right)\geq\rho-\xi_i,\ \ \xi_i\geq 0\ \ \forall i=1,\dots,M \tag{3-38}$$

where the slack variables $\boldsymbol{\xi}$ are introduced to deal with the presence of outliers in the training set as generally done in SVM methods. The parameter $\nu\in(0,1]$ allows tuning the trade-off between having a small $\|\mathbf{w}\|$ for controlling the complexity of the model and the number of training samples categorised as belonging to the targeted class of interest ω_{int} according to the decision rule:

$$f(\mathbf{x})=\text{sgn}(\mathbf{w}\cdot\phi(\mathbf{x})-\rho) \tag{3-39}$$

In particular, if $f(\mathbf{x})$ is positive, then $\mathbf{x}$ is associated with ω_{int}; otherwise, $\mathbf{x}$ is labelled as ω_{unk}.

It is possible to demonstrate that, by means of the Lagrange multipliers α_i, solving (3-38) is equal to find a solution to:

$$\min_{\boldsymbol{\alpha}}\left(\frac{1}{2}\sum_{i=1}^{M}\sum_{j=1}^{M}\alpha_i\alpha_j K(\bar{\mathbf{x}}_i,\bar{\mathbf{x}}_j)\right)$$
$$\text{s.t. } \textstyle\sum_{i=1}^{M}\alpha_i,\ \ 0\leq\alpha_i\leq\frac{1}{\nu M}\ \ \forall i=1,\dots,M \tag{3-40}$$

where $K(\cdot,\cdot)$ is a kernel function defined as $K(\boldsymbol{a}_i,\boldsymbol{a}_j)=\phi(\boldsymbol{a}_i)\cdot\phi(\boldsymbol{a}_j)$ which avoids a direct computation of the nonlinear mapping $\phi(\cdot)$ (Schölkopf *et al.*, 2001).

Kernel functions must be continuous, symmetric (i.e., $K(\boldsymbol{a}_i,\boldsymbol{a}_j)=K(\boldsymbol{a}_j,\boldsymbol{a}_i)$) and positive semidefinite (i.e., $\sum_{i,j=1}^{N}K(\boldsymbol{a}_i,\boldsymbol{a}_j)c_ic_j\geq 0$ for any $\{\boldsymbol{a}_i\}_{i=1}^{N}$ and $\{c_i\in\mathbb{R}\}_{i=1}^{N}$) (Mercer, 1909). In this framework, the most commonly used are:

- the linear kernel

$$K(\boldsymbol{a}_i,\boldsymbol{a}_j)=\boldsymbol{a}_i\cdot\boldsymbol{a}_j+c \tag{3-41}$$

- the polynomial kernel

$$K(\boldsymbol{a}_i,\boldsymbol{a}_j)=(\gamma\boldsymbol{a}_i\cdot\boldsymbol{a}_j+c)^d \tag{3-42}$$

- the Radial Basis Function (RBF) Gaussian kernel

$$K(\boldsymbol{a}_i,\boldsymbol{a}_j)=\exp\left(-\frac{\|\boldsymbol{a}_i-\boldsymbol{a}_j\|^2}{2\sigma^2}\right) \tag{3-43}$$

- the inverse multi-quadratic kernel

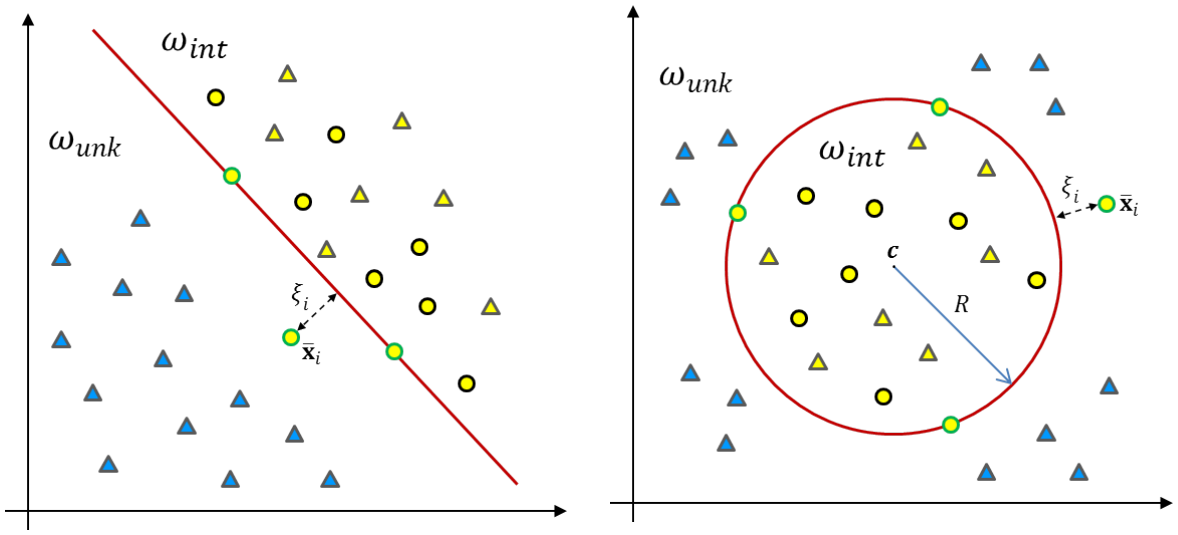

Figure 3-6: 2D example where yellow circles denote the training samples available for ω_{int} (among these support vectors are those with green outline), while triangles denote test samples which are associated to ω_{int} (yellow) or ω_{unk} (blue) according to the OC-SVM separation hyperplane (a) or the SVDD separation hypersphere (b) depicted in red.

$$K(\boldsymbol{a}_i, \boldsymbol{a}_j) = \frac{1}{\sqrt{\|\boldsymbol{a}_i - \boldsymbol{a}_j\|^2 + c^2}} \tag{3-44}$$

where c, γ, d and σ are free parameters.

Once determined the value of the coefficients α_i in (3-40), the final decision function becomes:

$$f(\mathbf{x}) = \text{sgn}\left(\sum_{i=1}^{M} \alpha_i \, K(\bar{\mathbf{x}}_i, \mathbf{x}) - \rho\right) \tag{3-45}$$

in which $\rho = \sum_{j=1}^{M} \alpha_j K(\bar{\mathbf{x}}_i, \bar{\mathbf{x}}_j)$ for any $\bar{\mathbf{x}}_i$ such that $0 < \alpha_i < \frac{1}{\nu M}$. All training samples $\{\bar{\mathbf{x}}_i | \bar{\mathbf{x}}_i \in \mathcal{T}, \alpha_i > 0\}$ are defined as Support Vectors (SV) and are the only ones affecting the position of the hyperplane.

In the literature, an alternative but similar OC-SVM formulation has also been proposed which is known as support vector domain description (SVDD) (Tax and Duin, 1999). Specifically, rather than determining the hyperplane with maximum margin separation from the origin, the SVDD technique aims at identifying the hypersphere with minimum volume solely enclosing the samples of the class of interest ω_{int}. All the samples outside the hypersphere are instead considered as outliers and associated with the unknown class ω_{unk}. The corresponding minimisation problem corresponds to:

$$\min_{R,\mathbf{c},\xi} \left(R^2 + \frac{1}{\nu M} \sum_{i=1}^{M} \xi_i\right) \tag{3-46}$$

$$\text{s.t. } \|\phi(\bar{\mathbf{x}}_i) - \mathbf{c}\|^2 \leq R^2 + \xi_i, \;\; \xi_i \geq 0 \;\; \forall i = 1, \ldots, M$$

where R and $\mathbf{c}$ represent the radius and the center of the hypersphere, respectively. In the case normalised data and isotropic kernels are used (e.g., the RBF Gaussian kernel), then the OC-SVM and SVDD formulations lead to the same solution (Schölkopf *et al.*, 2001). A schematic example highlighting the main principles of the OC-SVM and SVDD classifiers is given in Figure 3-6.

3.3.2. Multi-class classification

So far, hundreds of algorithms have been presented in the literature for addressing supervised classification. In this framework, a thorough comparison has been recently carried out by Fernández-Delgado *et al.* (2014), where 179 of them have been tested on 121 datasets from the UCI repository (Lichman, 2013), which is a reference for the machine learning community. From this analysis, the two methods exhibiting the best accuracies proved to be the Random Forest classifier (Breiman, 2001) and the Support Vector Machines (SVM) (Vapnik, 1998; Cristianini and Shawe-Taylor, 2000) with RBF Gaussian Kernel. Between these two techniques, the SVM have been more largely used for addressing remote-sensing applications since they exhibit very good generalisation capabilities even in cases where few training samples are available (Mountrakis *et al.*, 2011). Moreover, the convexity of the objective function used in the learning phase results in a unique solution (hence avoiding to sub-optimal solutions associated with local minima). Accordingly, in the light of their proven effectiveness, SVM have been chosen to be employed in the multi-class classification module of the proposed hierarchical system.

Support Vector Machines (SVM)

SVM have been originally defined for addressing binary classification problems; however, several methods have been proposed to extend them to multi-class classification (Hsu and Lin, 2002). In the following, the basic theory of binary SVM is briefly recalled along with an overview of the most common multi-class strategies.

Let $\mathcal{T} = \{\bar{\mathbf{x}}_i\}_{i=1}^{M}$ be the set of M available training samples for the two classes ω_1 and ω_2, and let $\mathcal{Y} = \{\bar{y}_i\}_{i=1}^{M}$, $\bar{y}_i \in \{+1, -1\}$ be the set of corresponding labels (where $+1$ is associated with class ω_1, and -1 is associated with class ω_2). The goal of SVM is to linearly separate the data in the input space by means of the hyperplane $H: \mathbf{w} \cdot \mathbf{x} + b = 0$, where, as yet discussed when introducing the OC-SVM algorithm in the previous section, $\mathbf{x}$ represents a generic sample, $\mathbf{w}$ is a vector normal to the hyperplane, and b is a constant such that $b/\|\mathbf{w}\|^2$ represents the distance of the hyperplane from the origin. In particular, H is determined such that it maximises the margin M defined as the distance between $H^-: \mathbf{w} \cdot \mathbf{x} + b = -1$ and $H^+: \mathbf{w} \cdot \mathbf{x} + b = +1$ intersecting the training samples available for ω_1 and ω_2 closest to H, respectively. In the example reported in Figure 3-7, the two separating hyperplanes depicted in orange in Figure 3-7 (a) do not maximise the margin, contrarily to that represented in yellow in Figure 3-7 (b). The predicted label for $\mathbf{x}$ is then computed as $\hat{y} = \text{sgn}\big(f(\mathbf{x})\big) = \text{sgn}(\mathbf{w} \cdot \mathbf{x} + b)$, where the argument of the sign function is denoted as *decision function*.

Since $M = 2/\|\mathbf{w}\|$, the objective of the SVM is to solve the following constrained optimisation problem:

$$\begin{aligned} &\min_{\mathrm{w},\rho,\xi} \left(\frac{1}{2}\|\mathrm{w}\|^2\right) \\ &\text{s.t.} \quad \bar{y}_i(\mathrm{w} \cdot \bar{\mathrm{x}}_i + b) \geq 1, \quad \forall i = 1, \dots, M \end{aligned} \tag{3-47}$$

Nonetheless, since it often occurs that training samples are not linearly separable, the constraints are softened by introducing the slack variables $\boldsymbol{\xi}$ which allow for (permitted) errors and the associated *penalisation parameter C* (also called *regularisation parameter*) which tunes

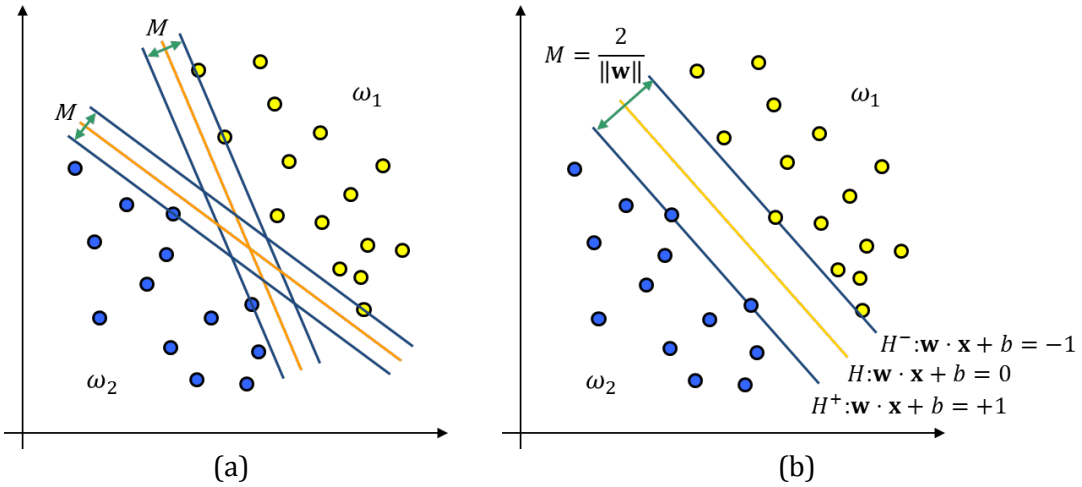

Figure 3-7: 2D example where yellow and blue circles denote the training samples available for ω_1 and ω_2, respectively. (a) separation hyperplanes (orange) not maximising the margin; (b) , separation hyperplane (yellow) maximising the margin.

the generalisation capability of the classifier. In particular, ξ corresponds to the distance from the margin bound for those samples falling into the margin (for which $0 < \xi_i \leq 1$) or on the wrong side with respect to the separation hyperplane (for which $\xi_i > 1$). An example is reported in Figure 3-8. The goal becomes then solving:

$$\min_{\mathrm{w},\rho,\xi} \left(\frac{1}{2}\|\mathrm{w}\|^2 + C \sum_{i=1}^{M} \xi_i \right)$$
$$\text{s.t. } \bar{y}_i(\mathrm{w} \cdot \bar{\mathrm{x}}_i + b) \geq 1 - \xi_i, \quad \xi_i \geq 0 \quad \forall i = 1, \dots, M \tag{3-48}$$

In this case, the optimisation problem is referred to as *soft margin* SVMs, contrarily to that reported in (3-47) denoted as *hard margin* SVM. To avoid direct handling of the inequality constraints, Lagrange theory is employed for deriving the corresponding equivalent dual representation:

$$\max_{\alpha} \left(\sum_{i=1}^{M} \alpha_i - \frac{1}{2} \sum_{i=1}^{M} \sum_{j=1}^{M} \bar{y}_i \bar{y}_j \alpha_i \alpha_j \bar{\mathrm{x}}_i \cdot \bar{\mathrm{x}}_j \right)$$
$$\text{s.t. } \sum_{i=1}^{M} \bar{y}_i \alpha_i = 0, \quad 0 \leq \alpha_i \leq C \quad \forall i = 1, \dots, M \tag{3-49}$$

where the coefficients $\alpha_{i=1}^{M}$ represent the Lagrange multipliers. It is possible to demonstrate that according to the Karush–Kuhn–Tucker conditions (Cristianini and Shawe-Taylor, 2000), also in this case the solution is a linear combination of the only training patterns associated with nonzero Lagrange multipliers (namely mislabelled training samples or correctly labelled samples falling between H^- and H^+), denoted as *support vectors*.

However, it is worth noting that, despite the use of the slack variables, when addressing operational problems ω_1 and ω_2 can be seldom accurately separated in the input space $\mathbb{R}^D$. Thus, as described for the OC-SVM, training samples are projected using the non-linear

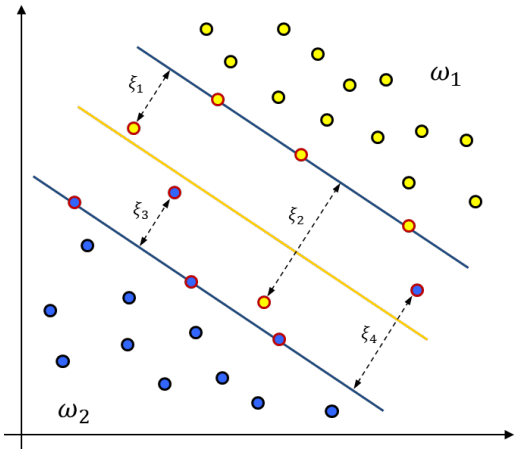

Figure 3-8: 2D example where training samples available for ω_1 and ω_2 (denoted as yellow and blue circles, respectively) are not linearly separable. Soft margin SVM penalise samples falling into the margin or on the wrong side with respect to the separation hyperplane by means of the slack variables ξ_i representing the corresponding distance from the margin bound. Support vectors are outlined in red.

transformation $\phi(\cdot)$ [defined in accordance with Cover's theorem (Cover, 1965)] into a high-dimensional Hilbert space where the chance is higher that they can be linearly separated.

The inner product between $\bar{\mathbf{x}}_i$ and $\bar{\mathbf{x}}_j$ in (3-49) becomes then $\phi(\bar{\mathbf{x}}_i) \cdot \phi(\bar{\mathbf{x}}_j)$. Nevertheless, to avoid considering explicitly $\phi(\cdot)$, according with the Mercer's theorem (Mercer, 1909), also here it is possible to use the kernel function $K(\bar{\mathbf{x}}_i, \bar{\mathbf{x}}_j) = \phi(\bar{\mathbf{x}}_i) \cdot \phi(\bar{\mathbf{x}}_j)$, which ensures the convexity of the objective function (and hence a unique solution). In particular, the same kernels listed in section 3.3.1 are also commonly employed in the literature.

By solving the resulting constrained maximisation problem (e.g., employing quadratic optimisation techniques) with respect to $\alpha_{i=1}^{M}$, for any given sample $\mathbf{x}$, its predicted label $\hat{y}$ is finally computed as:

$$\hat{y} = \text{sgn}(f(\text{x})) = \text{sgn}(\text{w} \cdot \phi(\text{x}) + b) = \text{sgn}\left(\sum_{i=1}^{M} \bar{y}_i \alpha_i K(\bar{\text{x}}_i, \text{x}) + b\right) \tag{3-50}$$

with $b = 1 - \sum_{i=1}^{M} \bar{y}_i \alpha_i K(\bar{\text{x}}_i, \text{x}^+)$, where x^+ is any support vector lying on H^+.

Among the different approaches proposed so far for extending the SVM to multiclass classification, two are the ones most commonly employed in the literature, namely the one-against-all (OAA) and the one-against-one (OAO). Given a classification problem with L different classes $\omega_{i=1}^{L}$, with the OAA strategy L different binary SVM are used. In particular, the l-th SVM is trained associating the training samples available for ω_l to the positive class and all the other to the negative class, hence resulting in the decision function $f_l(\mathbf{x})$. The generic sample $\mathbf{x}$ is then associated with the class whose corresponding decision function exhibits the highest value, i.e. $\omega_{\bar{l}} = \text{argmax}_{l=1,\dots,N}(f_l(\mathbf{x}))$.

With the OAO method, overall $L(L-1)/2$ binary SVM classifiers are employed, where each one is trained by using the labelled samples available from any two classes ω_i and ω_l, resulting in the decision function $f_{il}(\mathbf{x})$. Next, a voting scheme is applied: if, according to $\text{sgn}(f_{il}(\mathbf{x}))$, $\mathbf{x}$ is

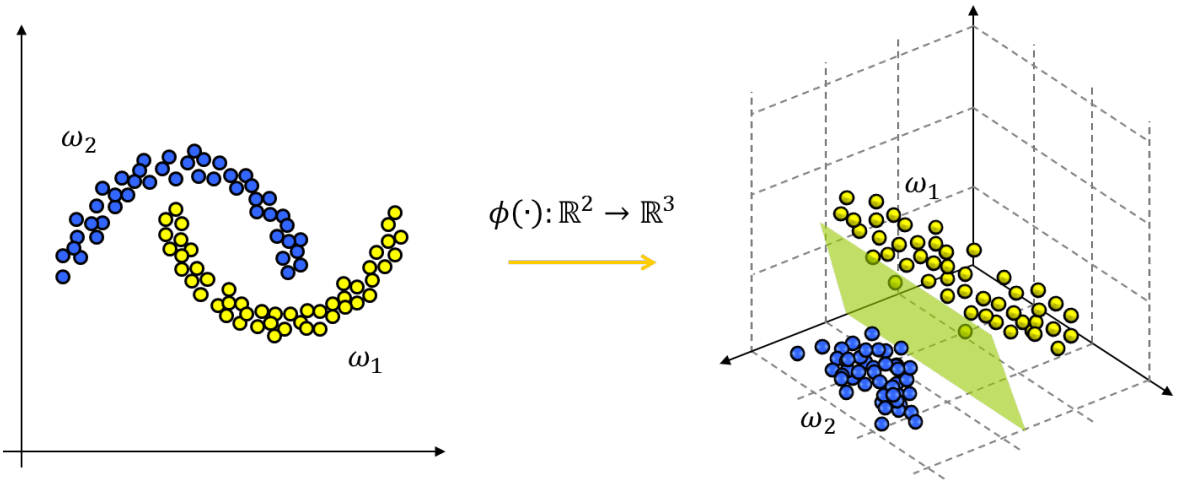

Figure 3-9: Example of non-linear transformation. When a set of samples cannot be linearly separated in the original input space (left), they are mapped by means of a non-linear transformation into a higher dimensional space (right) where they can be correctly discriminated by means of a hyperplane.

associated with ω_i, then the number of votes for ω_i is increased by one; otherwise, a vote is added to ω_j. Finally, $\mathbf{x}$ is categorised as belonging to the class $\omega_{\bar{l}}$ to which it is associated with the highest occurrence (in case two classes have identical votes, different heuristics are commonly employed as selecting the class for which more training samples are available, or, more simply, the one with the smaller/higher index).

Proposed multi-class MaxEnt

One-class classifiers can be also employed to tackle targeted-classification problems. In particular, as discussed previously, this can be carried out by considering an ensemble of one-class classifiers each one associated to a specific class and then properly combining their outputs. Nevertheless, despite its general effectiveness when addressing one-class problems, this strategy mostly results in poor performances when employing the MaxEnt classifier (as also documented in the experimental analysis presented in chapter 5). In particular, this is due to the challenge of identifying a suitable threshold θ_i for each i-th member of the ensemble, which allows to reliable discriminate the corresponding class ω_i both from all the other targeted classes, as well as from ω_{unk}.

Nevertheless, in the framework of the proposed hierarchical system, it is worth noting that if the ensemble is solely applied in the only areas marked as positive in the first phase, then no threshold θ_i has to be tuned since no remaining sample is supposed to belong to ω_{unk}. Rather, each pixel can be directly associated with the class for which the corresponding MaxEnt provides the highest estimated conditional probability. Such an approach, which has the great advantage of being fully automatic (i.e., no free parameter must be tuned) has been also tested alternatively to the multi-class SVM classifier.

4. DATASET DESCRIPTION

To evaluate the capabilities of the proposed classification scheme described in chapter 3, several experimental trials have been carried out over two test sites located in: i) Southern Bavaria (Germany) between the Lake "Starnberger See" and the foothills of the Bavarian Alps; and ii) the lake district "Mecklenburger Seenplatte" in Mecklenburg Western-Pomerania (Germany). In this chapter, a description of the two study regions is given, along with details about the selected targeted classes of interest and the corresponding *in situ* ground truth retrieved during intensive field campaigns. Moreover, information is also provided about the multitemporal and multi-polarisation TerraSAR-X (TSX) and Radarsat-2 (RS2) satellite data employed in this work, as well as the dedicated pre-processing activities.

4.1. Study sites and targeted classes

4.1.1. Test areas

The two selected test areas are located in Central Europe and have been chosen in the framework of the MSAVE project (www.msave.de) under the assumptions that: i) they host similar habitats with a great variety in terms of species composition and structure; and ii) they both experience a great variation in the phenological processes. In particular, the boundaries of the areas of interest (AOI) correspond to the outlines of the TSX and RS2 data employed for which details are given in chapter 4.2.1. Specifically, the Bavarian study site (see Figure 4-1) is located in a top moraine area with strong phenological gradient and great variety of HNV grasslands as well as Natura2000 habitat types which are similar to those characterising the upper moraine region of the Mecklenburg test area (see Figure 4-2).

Both study sites are part of the continental biogeographic region, despite the mountainous areas within the one in Bavaria already belong to the alpine biogeographic region. In general, biogeographic regions have been defined by the European Commission and the Council of Europe for evaluating and assessing the nature conservation and, within Europe, they represent geographical reference units inside which habitats and species exist under comparable circumstances (Condé *et al.*, 2002). As shown in green in Figure 4-3, the continental region stretches West-East from Central France to the Ural Mountains and North-South from Denmark to Italy and the Balkans (Condé *et al.*, 2002). Main habitat types are agriculture (52%), grasslands (14%), and forests (27%), while heathland, shrubs (less than 2%), and wetlands are seldom (Condé *et al.*, 2002). As regards wetlands, although the corresponding extent is limited, numerous and valuable different types are present, such as peat bogs, freshwater marshes, or

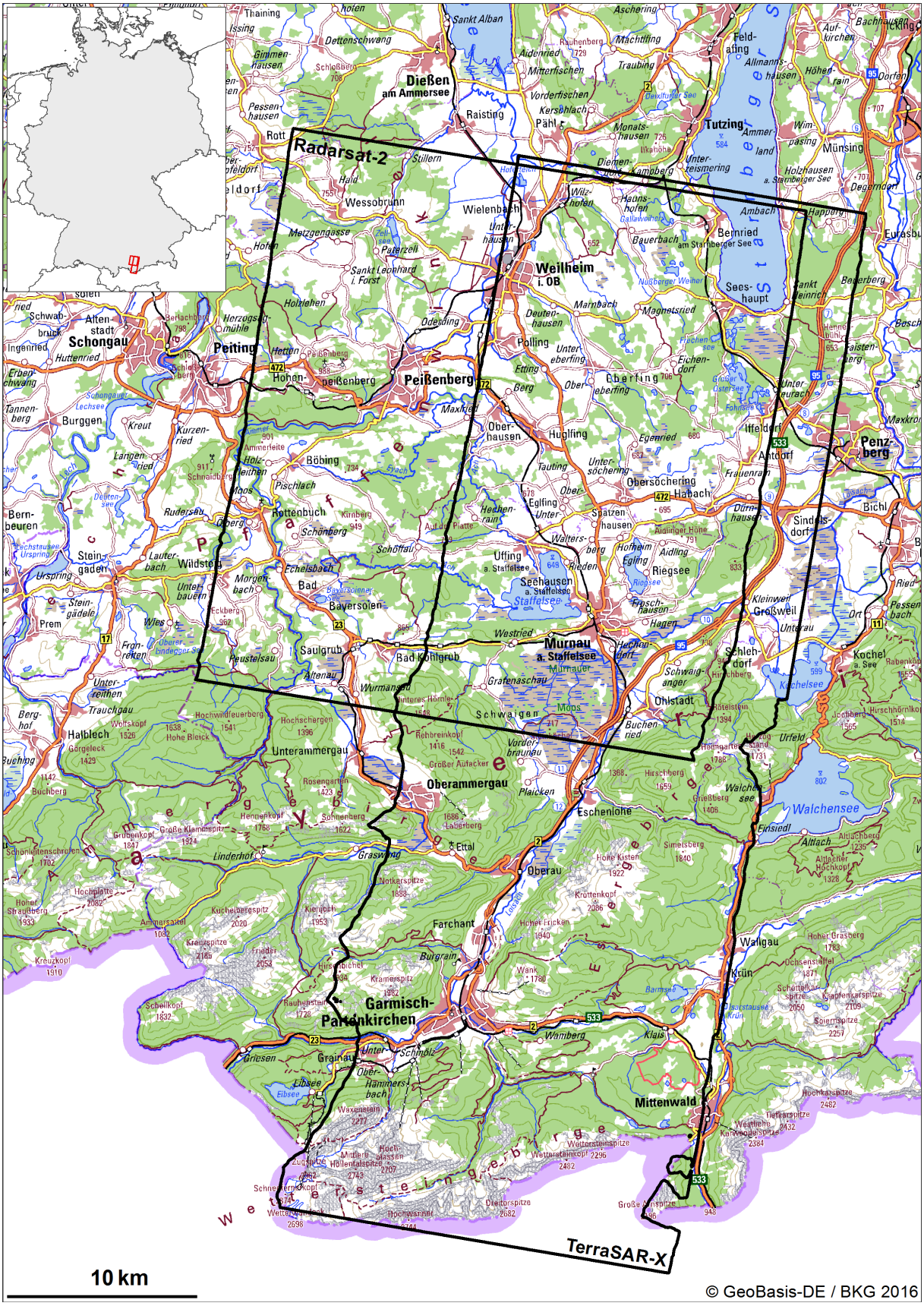

Figure 4-1: Bavaria test site – Outlines of the TSX and RS2 AOIs used in the study [background: Digital Topographic Map 1:250.000 (DTK250); © GeoBasis-DE / BKG 2016].

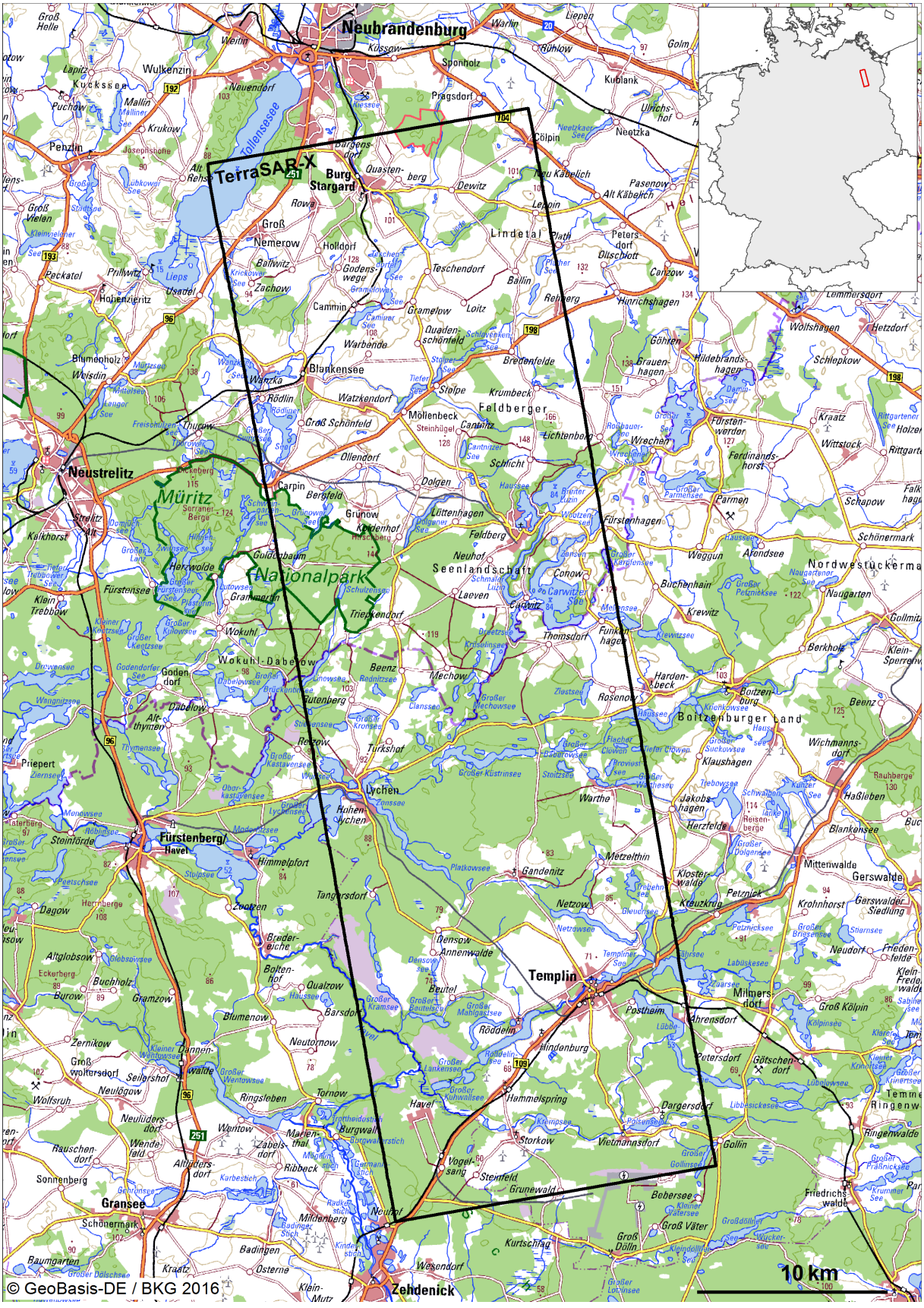

Figure 4-2: Mecklenburg test site – Outlines of the TSX AOI used in the study [background: Digital Topographic Map 1:250.000 (DTK250); © GeoBasis-DE / BKG 2016].

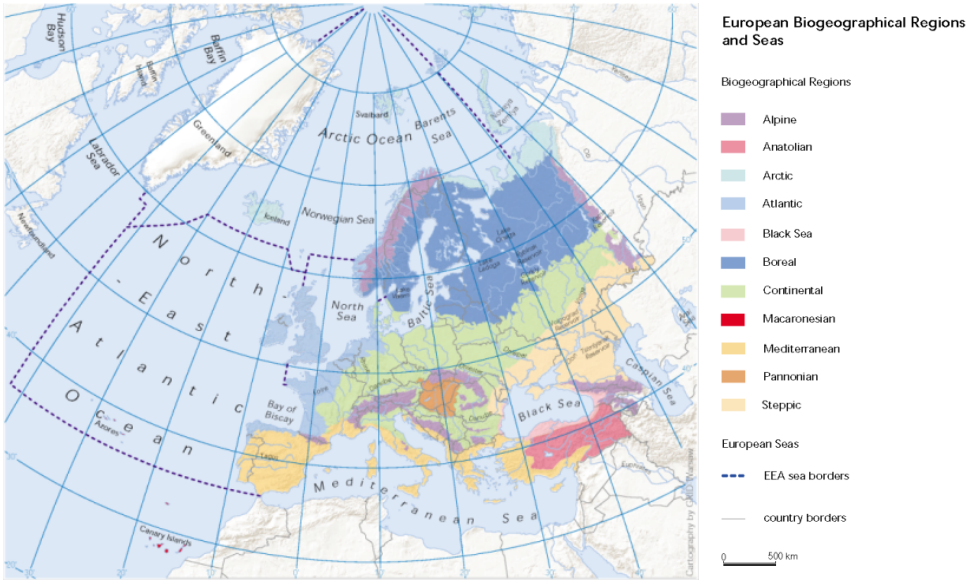

Figure 4-3: European biogeographical regions and seas [source: European Environment Agency (2012), figure processed].

wet meadows (Condé *et al.*, 2002). Instead, concerning grasslands, it is worth highlighting that in the last years they have experienced a shrinkage of ~14% both due to intensification of agriculture as well as afforestation (Condé *et al.*, 2002).

According to the updated global map of the Köppen-Geiger climate classification by Kottek *et al.* (2006), both test sites are within the fully humid, warm temperate climate zone, which has minimum temperatures between -3° C and +18°C and warm summers with an average temperature of more than 10° C in at least four months. To this aim, from the graphics reported in Figure 4-4, one can notice that the two areas show rather similar temperature trends; however, Bavaria is subject to higher precipitation than Mecklenburg (more than twice as much), mostly due to its landscape smoothly inclining towards the Alps.

Bavaria test site

The selected study area is located in the *Oberbayern* administrative district as part of the Bavarian Federal State (BY). It belongs to the geological region *foothills of the Alps*, whose German side represent its Southern border, and it is spans North up to the Lakes *Starnberger See* and *Ammersee* close to the city of Munich. The region has been mainly formed during the Pleistocene, where cold and dry periods (the so called glacials) alternated several times with warm and humid periods (the so called interglacials) (Glaser *et al.*, 2008). In particular, it is characterised by top moraine zones of the *Würm* glacial period, with Molasse areas in the South and a border zone of lower moraines of the glacial periods *Günz, Mindel* and *Riß* in the North. During the interglacials, due to temperatures higher than today deep residual soils and widespread forests developed and peats accumulated (Glaser *et al.*, 2008). During the glacials, heavy ice masses ran through the main valleys towards the North and stretched out into the foothill area, where they formed deep basins of which some are nowadays still hosting lakes (Glaser *et al.*, 2008). Furthermore, the glaciers skimmed deep and wide u-shaped valleys and denuded the resulting stones into the foothills (Glaser *et al.*, 2008).

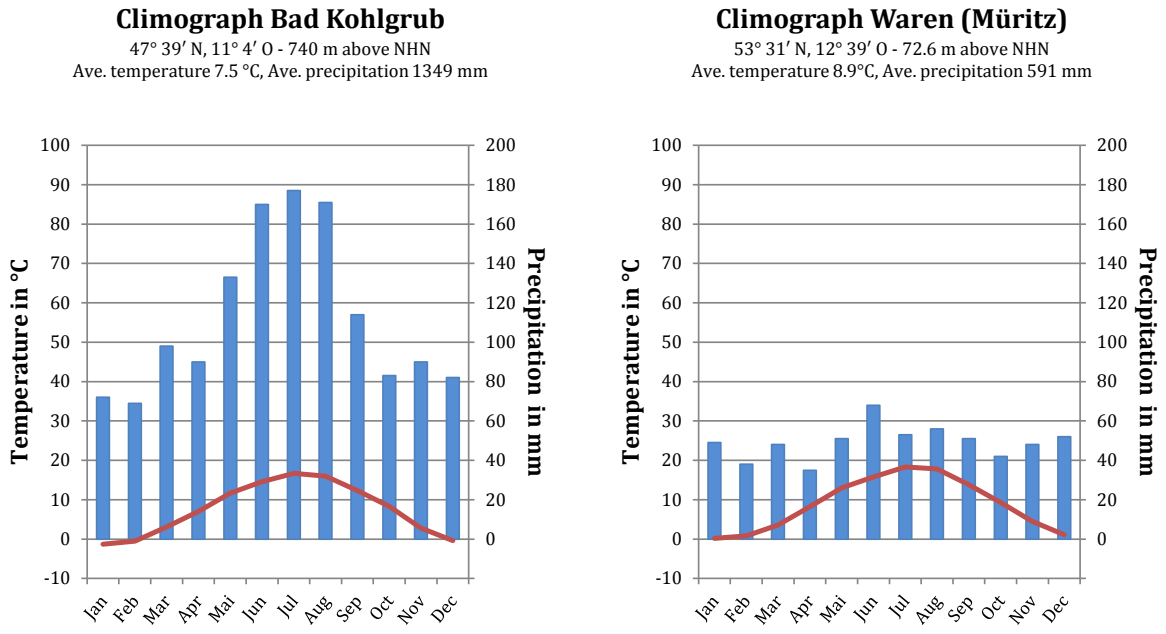

Figure 4-4: Average temperature and precipitation for the years 1981-2010 of the observation stations Bad Kohlgrub in the test area Bavaria and Waren (Müritz) in the test area Mecklenburg; source: based on data from Deutscher Wetterdienst, figures processed.

Today, Bavaria is mainly covered by agricultural areas (46.99%), forests (36.43%) and urban and transportation areas (11.78%) (Statistisches Bundesamt Wiesbaden, 2015). According to the Bayerisches Staatsministerium für Umwelt und Verbraucherschutz (2015) 645404.89 ha representing 9.15 % of its land area (covering overall 7055011.44 ha) are protected areas according to the FFH directive.

Mecklenburg test site

The chosen study area is almost entirely comprised in the Mecklenburg Western Pomerania (MV) Federal State located in the North-East of Germany, which has borders to Poland in the East (78 km), and the Federal States of Brandenburg in the South (448 km), Niedersachsen in the South-West (79 km), as well as Schleswig-Holstein in the West (137 km). Instead, the Baltic Sea forms the natural border in the North (Statistisches Amt Mecklenburg-Vorpommern, 2015) with a highly structured coastline which has an outer border length of 377 km and 1568 km of indentation and backwater coastline. Furthermore, it also comprises 62 offshore islands (Weiss, 1996).

The present landscape of the region has been formed in the *Saale* and *Weichsel* glacial periods (Ratzke and Mohr, 2005). At the beginning of the Holocene (~10.000 years ago) the permafrost soils began to dissolve and the typical glacial shapes (i.e., clay plates, flat and wide sandy areas, flat ground waves, deep domes, small depressions, etc.) began to develop (Ratzke and Mohr, 2005). As a result of the improving climatic conditions, a closed soil and vegetation cover started to develop leading to a complete afforestation (Ratzke and Mohr, 2005).

Due to the upsurge of the Baltic Sea approximately 5000 years ago, the groundwater level began to rise; accordingly, fens and bogs started to develop in the lowlands and river valleys (e.g.,

Warnow, Recknitz, Trebel, Peene, Tollense, etc.) (Ratzke and Mohr, 2005). Next, the landscape was majorly influenced by human activity, which grew with the development of agriculture and cattle breeding occurring due to the increasing settled down living (Ministerium für Landwirtschaft, Umwelt und Verbraucherschutz Mecklenburg-Vorpommern *et al.*, 2012). While human activity like forest clearance, grazing or drainage was limited to small areas until the middle of the 19th century, it majorly changed afterwards due to new agricultural techniques such as mechanising of the agriculture, large area drainage and use of mineral fertiliser (Ministerium für Landwirtschaft, Umwelt und Verbraucherschutz Mecklenburg-Vorpommern *et al.*, 2012). Consequently, species which had adapted to these nutrient-poor conditions vanished and the quality of habitats and biodiversity decreased (Ministerium für Landwirtschaft, Umwelt und Verbraucherschutz Mecklenburg-Vorpommern *et al.*, 2012).

Today, the region is embossed by agricultural areas (62.4%), forests (21.9%) and numerous lakes connected through rivers and channels (6.1%) (Statistisches Amt Mecklenburg-Vorpommern, 2014), while the extent of urban and transportation areas is rather small (8.1%) (Statistisches Amt Mecklenburg-Vorpommern, 2014). Moreover, 573,500 ha representing 18.5% of the whole land and coastal area of Mecklenburg Western Pomerania (overall 3,098,600 ha also including territorial waters) are protected areas according to the FFH directive (Landesamt für Umwelt, Naturschutz und Geologie (LUNG) Mecklenburg-Vorpommern (2015)).

4.1.2. Targeted classes

Four different Natura 2000 habitats of the FFH directive as well as the HNV grasslands subdivided into two groups have been defined as targeted classes of interest for this study. Details are provided below.

Natura 2000 habitat types

The four chosen Natura 2000 habitat types (HT) are:

- 6410 Molina meadows on calcareous, peaty or clayey-silt-laden soils;
- 7120 Degraded raised bogs still capable of natural regeneration;
- 7140 Transition mires and quaking bogs;
- 7230 Alkaline fens.

Type 6410 belongs to the Natura 2000 category "6 - Natural and semi-natural grassland formations" and its subcategory "64 - Semi-natural tall-herb humid meadows" (Council of the European Union, 1992) and includes planar to montane Molina meadows. These are nutrient-poor to semi nutrient-rich and not fertilized grasslands and occur on base-rich to calcareous and acidic humid to wet soils (Bundesamt für Naturschutz, 2011d). In particular, they have mainly evolved due to extensive late mowing regimes (Bundesamt für Naturschutz, 2011c) and can be mainly found in the East and South of Germany, especially in the areas of the Mecklenburg Lake District (*Mecklenburger Seenplatte*) and the Brandenburg lowlands (*Brandenburgische Niederungen*), as well as in the Bavarian alpine upland. However, they are currently mainly at risk due to drainage, shrub encroachment (as a result of missing use), nutrient contamination (e.g. through fertilization), intensive mowing or grazing as well as ploughing (Bundesamt für Naturschutz, 2011d). For the protection of this HT, a sufficient groundwater level as well as a minimum of one mowing every three to five years is necessary, although a yearly mowing in autumn is recommended. Examples of type 6410 are shown in Figure 4-5.

The remaining three selected HT types belong to the Natura 2000 category "7 - Raised bogs and mires and fens". While classes 7120 and 7140 are members of the subcategory "71 - Sphagnum acid bogs", class 7230 is part of the "72 - Calcareous fens" (Council of the European Union, 1992).

Figure 4-5: Examples of Natura 2000 HT type 6410. Pictures taken in the Bavaria (left) and Mecklenburg (right) test sites; credits: Stenzel, Metz.

Figure 4-6: Examples of Natura 2000 HT type 7120. Pictures taken in the Bavaria (left) and Mecklenburg (right) test sites; credits: Stenzel, Metz.

Type 7120 (see Figure 4-6) includes degraded raised bogs, whose hydrology has been negatively influenced or which have partly been cut, but may still be capable of natural regeneration (Bundesamt für Naturschutz, 2012b). Plants characteristic are the main vegetation and its stages of degeneration are characterised by migrating Molinia and dwarf shrubs (Bundesamt für Naturschutz, 2012c). Within Germany, they can be mainly found in Atlantic areas (Lower Saxony and Schleswig-Holstein) as well as in the Alpine uplands (Bundesamt für Naturschutz, 2011a). Type 7120 is mainly at risk due to past peat digging (which has mainly caused the destruction of this habitat type), drainage and conversion into grassland, afforestation, use for leisure as well as nutrient and pollutant contamination, which hinder the natural regeneration of the bogs (Bundesamt für Naturschutz, 2012c). This HT can be protected by i) preserving living cores for the regeneration of damaged parts, ii) restoring the natural water and nutrient level; and iii) grazing parts with sheep that are influenced by shrub encroachment (Bundesamt für Naturschutz, 2012c).

Type 7140 includes transition mires and quaking bogs which are located on peaty soils and have a water level that is either close to the surface or standing (Bundesamt für Naturschutz, 2012e). These are usually of dystrophic nature, meaning they are of brown color, because of dissolved topsoil, and are of poor to medium nutrient content (oligotrophic to mesotrophic) (Bundesamt für Naturschutz, 2012f). Type 7140 includes lagg zones and also silted-up oligotrophic to

Figure 4-7: Examples of Natura 2000 HT type 7140. Pictures taken in the Bavaria (left) and Mecklenburg (right) test sites; credits: Stenzel, Metz.

Figure 4-8: Examples of Natura 2000 HT type 7230. Pictures taken in the Bavaria (left) and Mecklenburg (right) test sites; credits: Stenzel, Metz.

mesotrophic water zones with Carex rostrate at the border (Bundesamt für Naturschutz, 2012e). In Germany, this HT is largely present in a good status throughout the entire alpine uplands despite it can be also found in other regions of the country (Bundesamt für Naturschutz, 2012f). Currently, it is mainly at risk due to drainage, change for agricultural or forestry use, use for leisure as well as nutrient contamination from bordering agricultural fields (Bundesamt für Naturschutz, 2012f). According to Bundesamt für Naturschutz (2012f), this HT can be protected by i) preserving the natural water and nutrient level through removing drainage systems, and ii) grazing parts with sheep that are influenced by shrub encroachment. Examples of type 7140 are shown in Figure 4-7.

Type 7230 (see Figure 4-8) includes alkaline fens with mainly low-growing sedge and rush communities and helophilous mosses, which include Carex davalliana fens and Schoenus fens as well as stands of Alpine rush and of Blunt-flowered rush (Bundesamt für Naturschutz, 2012a). In Germany, this HT is mostly located in the low mountain range (*Mittelgebirge*), North-East German lowlands and the alpine uplands, but it can be found in a good status especially throughout the alpine uplands as well as the Mecklenburg and Brandenburg Lake Districts (Bundesamt für Naturschutz, 2012d). Type 7230 is mainly at risk due to drainage or lowering of water level, change of use including conversion, afforestation, and fertilization and can only be protected by preserving or re-establishing the typical water regime and by extensive maintenance (Bundesamt für Naturschutz, 2012d).

High nature value grassland

The HNV grasslands are divided into five classes depending on the occurrence of indicator species (Bundesamt für Naturschutz, 2011b). In particular, lists with these indicator species have been established for seven landscapes in Germany (i.e., North-West Germany, North-East Germany, Western Central-Germany, Hesse, Eastern Central-Germany, Saxony, and Southern Germany) each with different species since they have regional differing occurrences (Bundesamt für Naturschutz, 2011b). Specifically, their latest version is available at Bundesamt für Naturschutz (2014), while different levels are rated according to the general rules specified in Table 4-1 (Bundesamt für Naturschutz (2011b)).

Table 4-1: HNV classes list, along with their corresponding level, nature value and number of indicator species (Bundesamt für Naturschutz (2011b)).

Class	Explanation	HNV level	Nature Value	Number of indicator species
HVNe	Extensively used HNV	HVN-1	Extreme high	≥ 8
		HNV-2	Very high	6 - 7
		HNV-3	High	4 - 5
HNVi	Intensively used HNV	HNV-4	Non	3
		HNV-5	Non	≤ 2

HVN-4 and HNV-5 are areas usually intensively managed with low ecological value and are thus not considered of high nature value (see for instance Figure 4-9).

HNV-3, HNV-2, and HNV-1 are considered as high nature value, very high nature value, and extreme high nature value, respectively (Bundesamt für Naturschutz, 2011b). They have high species richness and are extensively managed, which allows this floristic variation. Thus, these areas provide a high biodiversity and conservation contribution at German and European level.

Figure 4-9: Examples of HNVi levels HNV-4 (top) and HNV-5 (bottom); fields are shown on the left, whereas the corresponding plots are displayed on the right. Pictures taken in the Bavaria test site; credits: Stenzel, Metz.

Examples are shown in Figure 4-10.

Moreover, the Bundesamt für Naturschutz (2011b) also defines a number of habitat types of the FFH directive which can be classified at minimum into level HNV-3, but based on their indicator species and overall status also into the levels HNV-1 and HNV-2. These include among others also the Natura 2000 HT 6410, 7140, and 7230.

Figure 4-10: Examples of HNVe levels HNV-1 (top), HNV-2 (center), and HNV-3 (bottom); fields are shown on the left, whereas the corresponding plots are displayed on the right. Pictures taken in the Bavaria test site; credits: Stenzel, Metz.

These classes are very similar in their appearance and mainly vary in their management procedure. Accordingly, by assuming that this can be characterised by means of multitemporal satellite data if acquired over the different mowing times, the five levels have been subdivided into two groups, namely HNVe, comprising levels HNV-1, HNV-2, and HNV-3, and HNVi comprising levels HNV-4 and HNV-5 (see Table 4-1).

4.2. Available data

4.2.1. Satellite data

In the framework of this study, data of the two synthetic aperture radar (SAR) satellites TSX and RS2 have been acquired through the proposal 5073/LAN0996 accepted in response to the joint call "AO for Radarsat-2/TerraSAR-X Initiative (CSA-DLR-2010)" of the German Aerospace Centre (DLR) and the Canadian Space Agency (CSA). Their specifications as well as details on the investigated scenes are provided in the following. In particular, dualpol TSX data have been used for both test sites, whereas dual- and quadpol RS2 imagery only for the Bavaria study area (see Figure 4-11).

TerraSAR-X

TSX and its twin TanDEM-X (TDX) are German X-band SAR satellites launched in 2007 and 2010, respectively, built in a public-private partnership between DLR, who "owns and operates the satellites and the payload ground segment and holds the rights for the scientific exploitation of the TerraSAR-X mission data" (DLR, 2013), and the industry partner Astrium, who "holds the exclusive rights for the commercial exploitation of the TerraSAR-X mission data products" (DLR, 2013). The satellites fly in a close formation in a sun-synchronous 11 days repeat pass orbit with an altitude of 514 km at the equator (DLR, 2013). A schematic view of TSX is given in Figure 4-12 and a detailed overview of the satellites specifications is reported in Table 4-2.

In general, X-band refers to a frequency range between 8 and 12 GHz (Woodhouse, 2006) hence corresponding to a rather short wavelength capable to solely penetrate the canopy of the land

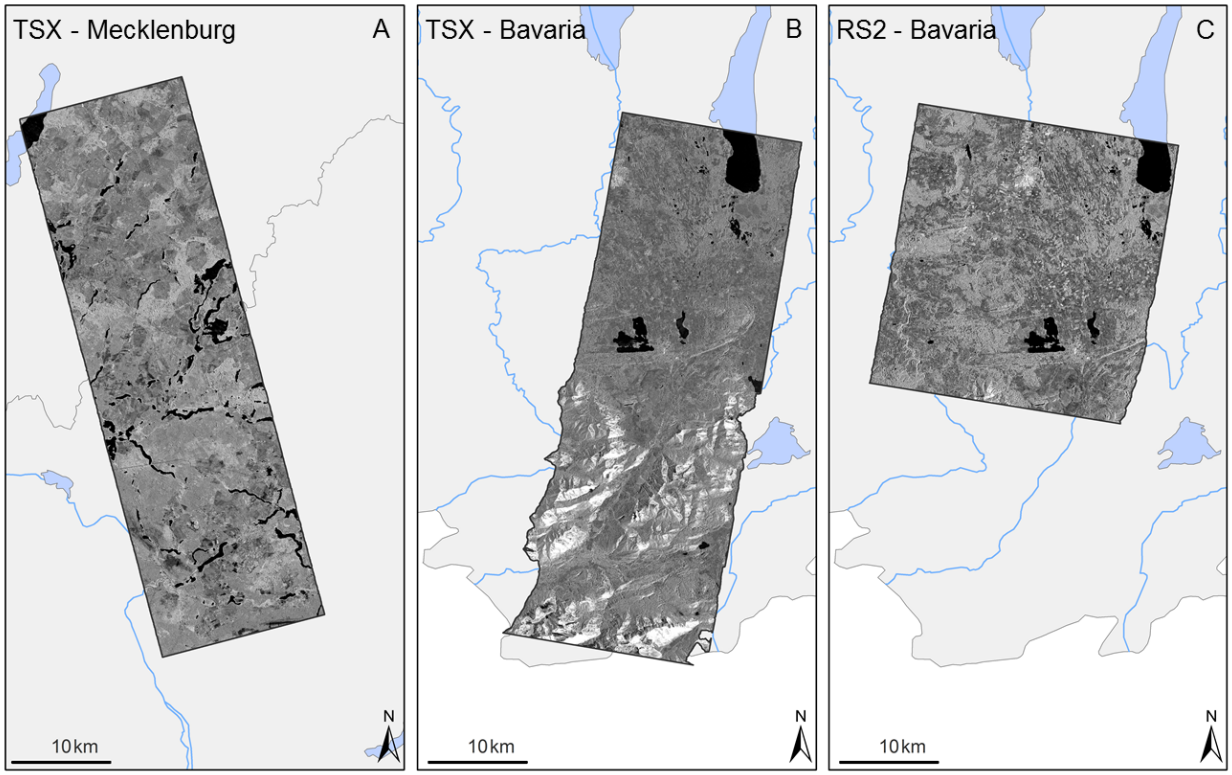

Figure 4-11: Sample quicklooks of the TSX imagery available for the Mecklenburg and Bavaria test sites (A and B, respectively), and of the RS2 imagery available for the Bavaria test site (C).

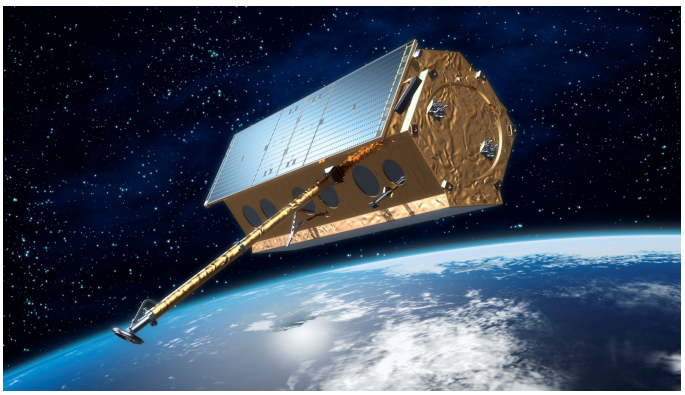

Figure 4-12: TerraSAR-X (source: EADS Astrium via DLR, 2010).

cover. Specifically, TSX/TDX operate at a frequency of 9.65 GHz, resulting in a wavelength of 3 cm (DLR, 2013).

As stated in DLR (2013), TSX/TDX have the following five standard imaging modes:

- Stripmap mode (SM) in single or dual polarisation,
- High Resolution Spotlight mode (HS) in single or dual polarisation,
- Spotlight mode (SL) in single or dual polarisation,
- Staring Spotlight mode (ST) in single polarisation, and
- ScanSAR mode (SC) in single polarisation.

An overview of the parameters of the single modes is given in Table 4-4, whereas a detailed description can be found in DLR (2013).

In the light of the high spatial detail necessary to characterise the small-extent targeted grassland types, as well as the greater spatial coverage needed for a large-scale (e.g., European) operational employment of the proposed methodology, the Stripmap mode has been selected. In particular, in dualpol mode it allows to cover an area of 15 x 50 km with azimuth resolution (i.e., the one referring to the along-track dimension parallel to the satellite flight direction) of 6.6 m and ground range resolution (i.e., the one referring to the across-track dimension perpendicular

Table 4-2: TSX/TDX orbit and system parameters, source: DLR, 2013.

Date of launch	TerraSAR-X: 15 June 2007 TanDEM-X: 21 June 2010
Orbit Height	514 km at equator
Orbit per day	15 2/11
Orbit Repeat Cycle	11 days
Inclination	97.44 degree
Ascending node / equatorial crossing time	18:00 ± 0.25h (local)
Radar Carrier frequency	9.65 GHz
Polarizations	HH, VH, HV, VV
Antenna length	4.8 m
Nominal look direction	right
Antenna width	0.7 m
Range Bandwidth	150 MHz (experimental: 300 Mhz)
Onboard sensors provided under TPM	X-Band Radar
Number of stripmap beams	12 (full performance range)

Table 4-4: Parameters for the different TSX modes (source: DLR, 2013)

Parameter	SM	HS	SL	ST	SC (four beam)	SC (six beam)
Swath width (ground range)	30 km single 15 km dual	10 km	10 km	6 to 3.8 km - worst case 7.5 to 4.6 km - typical case	100 km	266 – 194 km (wide_001 to wide_005)
Nom. L1b product length	50 km	5 km (azimuth)	10 km (azimuth)	2.5 to 2.8 km	150 km	200 km
Full performance incidence angle range	20° - 45°	20° - 55°	20° - 55°	20° - 45°	20° - 45°	15.6° - 49°
Data access incidence angle range	15° - 60°	15° - 60°	15° - 60°	15° - 60°	15° - 60°	15.6° - 49°
Number of elevation beams	12 (full performance) 27 (data access)	91 (full performance) 122 (data access)	91(full performance) 122 (data access)	58(full performance) 122 (data access)	27 (9 x 4 stripmap beam combinations in full perf. range)	10 specific wide beams (5 x 6 - beam combinations)
Azimuth resolution	3.3 m (single) 6.6 m (dual)	1.1 m (single) 2.2 m (dual)	1.7 m (single) 3.4 m (dual)	0.24 m (single)	18.5 m	40 m
Ground range resolution	1.70 m - 3.49 m	1.48 m - 3.49 m 0.74 m – 1.77 m (with 300 MHz bandwidth option and reduced swath extent in range)	1.48 m - 3.49 m	0.85 m – 1.77 m	1.70 m - 3.49 m	< 7 m

to the satellite flight direction) between 1.7 m - 3.49 m.

In the context of this study, two multitemporal series of dualpol (VV/VH) Stripmap TSX scenes have been acquired for the years 2011 and 2012 between March and October over both test areas; the corresponding lists are given in Table 4-3. It is worth noting that, originally, acquisitions had been planned every 11 days in the considered time frames; nevertheless, due to conflicts with requests from other users or with the higher-priority acquisitions for the production of the WorldDEM™ (the digital elevation model derived from TSX/TDX data for the

Table 4-3: List of 2011 and 2012 TSX/TDX acquisitions taken for the Bavaria and Mecklenburg test sites.

Bavaria				Mecklenburg			
2011	2012	Orbit / Beam	Mode	2011	2012	Orbit / Beam	Mode
26.03.	14.04.	78 / stripFAR_005R	Dualpol VV/VH	10.04.	10.05.	146 / stripFAR_007R	Dualpol VV/VH
06.04.	28.05.			21.04.	21.05.		
17.04.	08.06.			13.05.	12.06.		
09.05.	19.06.			24.05.	23.06.		
20.05.	30.06.			26.06.	15.07.		
31.05.	11.07.			20.08.	28.08.		
11.06.	22.07.			31.08.	19.09.		
05.08.	13.08.			22.09.			
16.08.	24.08.			03.10.			
27.08.	15.09.						
07.09.	26.09.						
18.09.							
29.09.							

Table 4-5: Parameters for the RS2 single beam modes available as SLC products [single co or cross refers to HH or VV or HV or VH; dual refers to HH+HV or VV+VH; quad refers to: HH+VV+HV+VH, source: MacDonald, Dettwiler and Associates Ltd. (2015)].

BEAM MODE	Nominal Pixel Spacing [Rng × Az] (m)	Nominal Resolution [Rng x Az] (m)	Nominal Scene Size [Rng x Az] (km)	Nominal Incidence Angle Range [deg]	Polarization Option
Spotlight	1.3 x 0.4	1.6 x 0.8	18 x 8	20 to 54	Single Co or Cross
Ultra-fine	1.3 x 2.1	1.6 x 2.8	20 x 20	20 to 54	Single Co or Cross
Wide Ultra-fine	1.3 x 2.1	1.6 x 2.8	50 x 50	29 to 50	Single Co or Cross
Multi-Look Fine	2.7 x 2.9	3.1 x 4.6	50 x 50	30 to 50	Single Co or Cross
Wide Multi-Look Fine	2.7 x 2.9	3.1 x 4.6	90 x 50	29 to 50	Single Co or Cross
Extra-Fine (Full Res)	2.7 x 2.9	3.1 x 4.6	125 x 125	22 to 49	Single Co or Cross
Extra-Fine (Fine Res)	4.3 x 5.8	5.2 x 7.6			
Extra-Fine (Std Res)	7.1 x 5.8	8.9 x 7.6			
Extra-Fine (Wide Res)	10.6 x 5.8	13.3 x 7.6			
Fine	4.7 x 5.1	5.2 x 7.7	50 x 50	30 to 50	Single Co or Cross or Dual
Wide Fine	4.7 x 5.1	5.2 x 7.7	150 x 150	20 to 45	Single Co or Cross or Dual
Standard	8 or 11.8 x 5.1	9.0 or 13.5 x 7.7	100 x 100	20 to 52	Single Co or Cross or Dual
Wide	11.8 x 5.1	13.5 x 7.7	150 x 150	20 to 45	Single Co or Cross or Dual
Extended High	11.8 x 5.1	13.5 x 7.7	75 x 75	49 to 60	Single (HH only)
Extended Low	8.0 x 5.1	9.0 x 7.7	170 x 170	10 to 23	Single (HH only)
Fine Quad-Pol	4.7 x 5.1	5.2 x 7.6	25 x 25	18 to 49	Quad
Wide Fine Quad-Pol	4.7 x 5.1	5.2 x 7.6	50 x 25	18 to 42	Quad
Standard Quad-Pol	8 or 11.8 x 5.1	9.0 or 13.5 x 7.6	25 x 25	18 to 49	Quad
Wide Standard Quad-Pol	8 or 11.8 x 5.1	9.0 or 13.5 x 7.6	50 x 25	18 to 42	Quad

world (Airbus Defence and Space / Infoterra GmbH and DLR, 2014) only a subset could be finally taken.

The data for the Bavaria test area refer to the descending-pass orbit 78 and have been acquired with the stripFAR_005R beam, whose incidence angle is ~27°. Instead, the images for the Mecklenburg study region refer to the ascending-pass orbit 146 and have been taken with the stripFAR_007R beam, with an incidence angle of ~31.6°. The two datasets have been collected with both either TSX or TDX, depending on the available acquisition capacity; nevertheless, for simplicity, TSX will be solely used when referring to them in the following. All scenes have been delivered as Single Look Slant Range Complex (SSC) Level 1B data, which is the basic single look product of the focused radar signal in azimuth-slant range geometric projection including the full bandwidth and the phase information (DLR, 2013).

Radarsat-2

RS2 is a Canadian C-band SAR satellite co-funded in a public-private partnership of the Canadian Space Agency (CSA) and the MacDonald, Dettwiler and Associates Ltd. of Richmond, BC (MDA), which was launched on 14th December 2007 from Baikonur, Kazakhstan (ESA, 2015a). It flies in a sun-synchronous polar orbit at an altitude of 798 km with a repeat cycle of 24 days. RS2 has over 20 different beam modes with a spatial resolution range between 3 and 100m (ESA, 2015a). Among these, in Table 4-5 the 19 are reported which provide Single Look Complex (SLC) products, i.e. the basic single look product of the focused radar signal in azimuth-slant range

Table 4-6: RS2 orbit and system parameters, source: ESA (2015).

Date of launch	14 December 2007
Orbit Height	798 km at equator
Orbits per day	14 7/24
Orbit Repeat Cycle	24 days
Inclination	98.6 degree
Ascending node / equatorial crossing time	18:00 ± 0.25h (local)
Radar Carrier frequency	5.405 GHz (C-band, 5.6cm wavelength)
Polarizations	HH, VH, HV, VV
Antenna length	15 m
Nominal look direction	right or left
Antenna width	1.37 m
Range Bandwidth	100 MHz
Onboard sensors provided under TPM	C-Band Radar

geometric projection (MacDonald, Dettwiler and Associates Ltd., 2015). A detailed overview of the RS2 orbit and system parameters is given in Table 4-6.

According to MacDonald, Dettwiler and Associates Ltd. (2015), RS-2 products can be taken in three main beam modes, namely:

- *Single Beam* including Ultra-fine, Wide Ultra-fine, Multi-Look Fine, Wide Multi-Look Fine, Extra-Fine (Full Res, Fine Res, Std Res, Wide Res), Fine, Wide Fine, Standard, Wide, Extended High, Extended Low, Fine Quad-Pol, Wide Fine Quad-Pol, Standard Quad-Pol, Wide Standard Quad-Pol;
- *ScanSAR* including ScanSAR Narrow, ScanSAR Wide, Ocean Surveillance, Ship Detection; *Spotlight*.

For this study, a time series for the Bavaria test site has been acquired in fine quadpol mode (HH + HV + VV + VH) between April and September 2011 with a scene size of ~25 x 25 km. The complete list of eight scenes is given in Table 4-7. In particular, they have been collected in descending pass orbits with beam FQ12 (with near range incidence angle of 31.36°) and delivered as SLC data.

Table 4-7: List of 2011 RS2 acquisitions taken for the Bavaria test site.

Bavaria			
2011	**Orbit**	**Beam**	**Mode**
05.04	17259 Descending	FQ12	Fine Quadpol HH,VV, HV,VH
29.04	17602 Descending		
23.05	17945 Descending		
16.06	18288 Descending		
10.07	18631 Descending		
03.08	18974 Descending		
27.08	19317 Descending		
20.09	19660 Descending		

4.2.2. Reference data

In the framework of the MSAVE project, reference data for the selected targeted classes of interest have been acquired during two intensive field campaigns which took place for both test sites and investigated years between May and June. In particular, in 2011 ground truth information has been gathered for a first set of point locations; then, in 2012 they have been revisited to check the actual status and in situ information has been collected for additional sites within the AOI.

Concerning the four Natura 2000 HT of interest, a dedicated sampling strategy has been defined by the group of Prof. Sebastian Schmidtlein (KIT, Germany) taking into account their spatial distribution within both test areas. In particular, reference points along with the corresponding class membership have been collected for the selected habitats using a hybrid approach which combines the preferential sampling (i.e., the standard for ecological analysis), with the statistically more meaningful stratified sampling design (Roleček *et al.*, 2007). According to Roleček *et al.* (2007), by means of the preferential sampling all vegetation types within a given landscape (whose vegetation variability has been preliminary analysed by the researcher) are recorded subjectively "either without intentional emphasis on some species combinations or in what some phytosociologists call 'typical' stands." Despite this method is highly influenced by the subjective selection of the researcher, it has the great advantage of recording nearly the complete vegetation variation of the area of interest including rare species (Roleček *et al.*, 2007). On the contrary, using the stratified design, sampling plots are placed randomly within a priori selected strata (e.g., vegetation or habitat types) by means of a Geographic Information System (GIS) or, during a field campaign, using a Global Positioning System (GPS) device (Roleček *et al.*, 2007). While thereby the data are recorded with a reasonable representation even in rare types, the resulting sampling data are mainly influenced by the quality and criteria of the stratification (Roleček *et al.*, 2007). In such context, first an up-to-date database of the FFH directive (EEA, 2010) has been obtained. However, although it specifies the size of each habitat within the single Natura 2000 sites, it does not provide any information about their location (see Figure 4-13); moreover, an exact classification of the habitats was not available during the entire lifetime of the project. Accordingly, the plots were then sampled in the field within the predefined areas derived from the Natura 2000 database using a GPS receiver Magellan™ Mobile Mapper 6 (error < 2 m) (Stenzel *et al.*, 2014). As all satellite imagery employed in the project (i.e., RapidEye, TSX and RS2) has been resampled to 5 m spatial resolution, finally plots with size greater than 15 m x 15 m were considered in order to prevent mixed pixels.

The ground truth data for the defined HNVi and HNVe grassland classes have been obtained by properly merging reference points collected for the five HNV classes separately using the same sampling design adopted for the Natura 2000 HT. In particular, grasslands have been evaluated according to the survey instructions of the German Federal Agency for Nature Conservation (Bundesamt für Naturschutz, 2011b) which take into account the occurrence of indicator species defined by the German Federal States (Bundesamt für Naturschutz, 2014). Therefore, a given field was initially surveyed excluding a buffer of 3 m within its border. If at least three indicator species occurred, then it was further analysed concerning the level of HNV (HNV Level 1, 2, or 3)

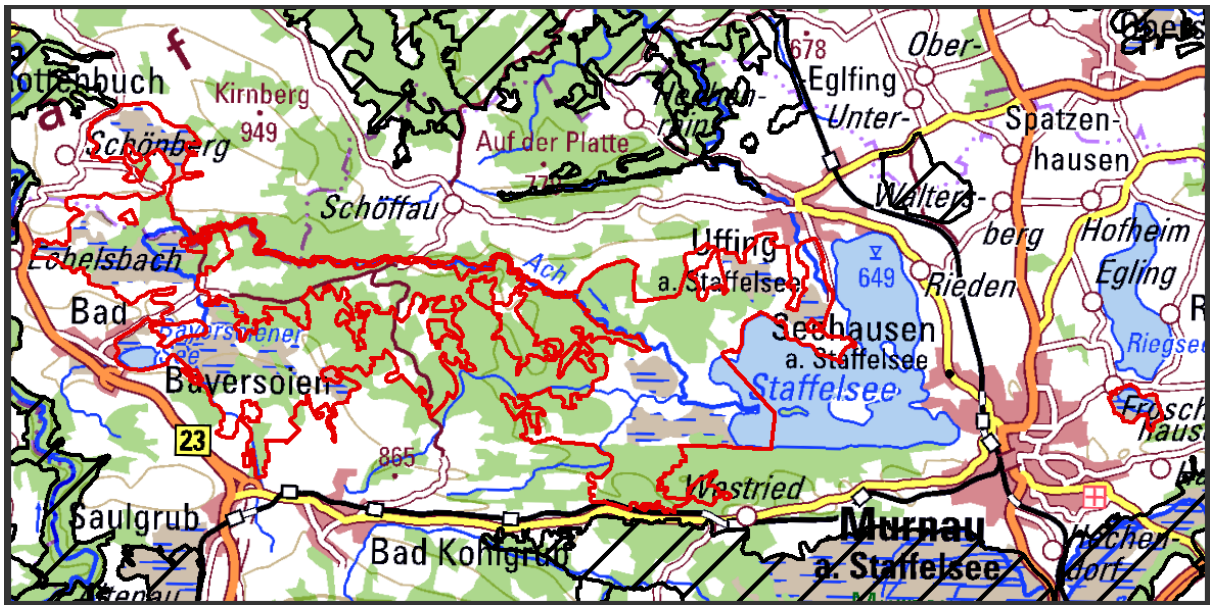

DE8332372 Amtsblatt der Europäischen Gemeinschaften Nr. L 107/6

3. ÖKOLOGISCHE ANGABEN

3.1. Im Gebiet vorhandene Lebensräume und ihre Beurteilung

Anhang I - Lebensräume

Kennziffer	Anteil (%)	Repräsentativität	Relative Fläche	Erhaltungszustand	Gesamtbeurteilung
3140	< 1	B	C	B	C
3150	2	A	C	A	A
3260	< 1	A	C	B	B
6210	< 1	C	C	B	C
6230	< 1	B	C	B	B
6410	1 5	A	B	A	A
6430	< 1	B	C	B	B
6510	< 1	B	C	B	C
7110	1 2	A	B	A	A
7120	1 9	B	B	B	B
7140	1	B	C	B	B
7150	< 1	B	C	B	B
7210	< 1	B	C		C
7220	< 1	B	C	A	B
7230	1 2	A	B	B	A
9130	6	B	C	B	B
9180	8	A	C	A	A
91D0	8	A	C	B	B
91E0	2	B	C	A	B
91F0	< 1	C	C	A	C

Figure 4-13: Example taken from the database of the FFH directive available for the Bavaria test site (ID: DE8332-372) - top: outline (in red) of the area for which information is available about the presence of Natura 2000 HT as well as other land-cover classes; bottom: corresponding data sheet listing the occurring HT and their percentage within the considered area [Natura 2000 shapefile data source: Bayerisches Landesamt für Umwelt, www.lfu.bayern.de, background: Digital Topographic Map 1:250.000 (DTK250); © GeoBasis-DE / BKG 2016].

by counting the indicator species present in a 30 x 2 m transect. Instead, HNV level 4 and 5 were defined based on the first check of the field.

For each plot of both HT and HNV classes, the following additional information and characteristics were collected in a field sheet:

- General information (including observer, plot number, date, time, location, GPS coordinates, slope, and exposition);
- Homogeneity;
- Photographs and measurements taken;
- Dominant species (species, cover);
- Vegetation and structure parameters;
    - HT / HNV type;
    - Fraction (%) and height (m) of shrub layer, tall grass, short grass;
    - Fraction (%) of soil, litter, water, and cryptogam;
    - Type and intensity of usage (nominal);
    - Humidity (nominal);
    - Rare species (types).

These field sheets were then transferred to MS Excel and transformed to the geospatial vector data format point-shapefiles, separated for HT and HNV by test area.

Due to the one-year interval between the two field campaigns, the selected HT types did not experience any change (this generally takes a number years); hence, all points collected over both 2011 and 2012 have been then merged into a single reference dataset. On the contrary, this is not true for the HNV classes, which are generally more variable and subject even to short-time changes. However, since the Natura 2000 HT 6410, 7140, and 7230 are also considered as grasslands with extreme high nature value, the corresponding reference points have been merged to those collected for the HNVe class.

For the experimental analysis, both for HT and HNV classes, labelled samples have been evenly split into training and validation sets. Nevertheless, it is worth highlighting that taking a single point as reference for a certain plot might result in poor performances of the proposed system since SAR data are affected by speckle (see chapter 3.2.1). Indeed, if the point whose class membership has been gathered during the field campaign is severely affected by granular noise, then it is not at all representative of the plot to which it belongs. To overcome this issue, a strategy has been implemented which takes into account the geometrical relationship between a reference point and its neighbours in order to increase the size of both training and validation sets. In particular, for each year and test site, segmentation is first applied to the multitemporal series of the MEA texture feature (see chapter 3.2.2) (where homogeneous structures tend to appear more clearly) derived from both TSX and RS2 imagery. Specifically, the two-phase algorithm available within the eCognition Developer software version 8.64.1 is used, where multiresolution segmentation is followed by spectral difference segmentation. The former merges neighbouring pixels based on homogeneity features (Trimble, 2011a) and requires the tuning of three free parameters which influence the size and homogeneity of the resulting objects, namely shape, compactness, and scale (Trimble, 2011b). Shape describes the textural homogeneity of the resulting segments, compactness tunes their spatial solidity, whereas scale

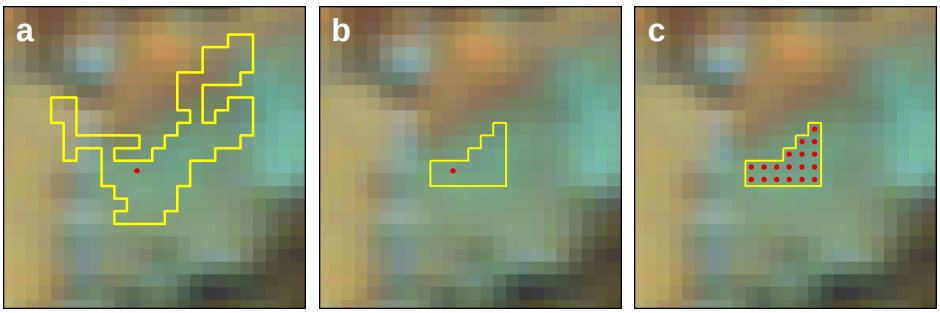

Figure 4-14: Example of the implemented strategy for extending the original reference dataset. Given the reference point depicted in red, the associated segment resulting from the two-step segmentation is reported in (a). Pixels not likely to belong to the same class/landscape element are manually pruned (b). Finally, all remaining pixels are associated with the same information class of the original reference point (c). [Background: RGB false color composite of RapidEye optical imagery available for the 9th May 2011 for the Bavaria test site from the MSAVE project].

influences their size (Trimble, 2011a, 2011b). The goal was to determine objects enclosing the available reference points, which are finally relatively small and compact in order to reasonably capture neighbour pixels solely belonging to the same information class. Accordingly, after intensive empirical analysis, the most suitable values proved to be: scale 200, shape 0.001 and compactness 0.9. The subsequent spectral difference segmentation merges adjoined objects depending on their mean intensity and a maximum spectral difference value to be defined by the user (Trimble, 2011b). Again based on empirical analysis this was set to 30. A visual inspection

Table 4-8: Number of original and final extended training (T) and validation (V) HT reference points for the TSX Bavaria and Mecklenburg AOIs.

HT	TSX Bavaria AOI		TSX Mecklenburg AOI	
	Original	Extended	Original	Extended
6410	T: 17 V: 16	T: 1397 V: 1260	0	0
7120	T: 12 V: 12	T: 1385 V: 1634	T: 6 V: 3	T: 1160 V: 744
7140	T: 3 V: 3	T: 291 V: 207	T: 1 V: 1	T: 48 V: 52
7230	T: 8 V: 8	T: 614 V: 547	0	0

Table 4-9: Number of original and final extended training (T) and validation (V) HT reference points for the RS2 Bavaria AOI.

HT	RS2 AOI Bavaria	
	Original	Extended
6410	T: 23 V: 19	T: 1572 V: 1322
7120	T: 19 V: 18	T: 1543 V: 1896
7140	T: 5 V: 5	T: 340 V: 283
7230	T: 11 V: 10	T: 697 V: 682

Table 4-10: Number of original and final extended training (T) and validation (V) HNV reference points for the TSX Bavaria and Mecklenburg AOIs.

Year	Class	HNV	TSX Bavaria AOI				TSX Mecklenburg AOI			
			Original	Combined	Original Extended	Combined Extended	Original	Combined	Original Extended	Combined Extended
2011	HNVi	5	10 T: 5, V: 5	T: 6 V: 6	T: 332 V: 450	**T: 542 V: 564**	4 T: 2, V: 2	T: 4 V: 3	T: 66 V: 123	**T: 263 V: 259**
		4	2 T: 1, V: 1		T: 210 V: 114		3 T: 2, V: 1		T: 197 V: 136	
	HNVe	3	3 T: 2, V: 1	T: 6 V: 4	T: 133 V: 76	**T: 1699 V: 1498**	2 T: 1, V: 1	T: 2 V: 2	T: 31 V: 76	**T: 95 V: 134**
		2	4 T: 2, V: 2		T: 64 V: 89		2 T: 1, V: 1		T: 64 V: 58	
		1	3 T: 2, V: 1		T: 1502 V: 1333		0		T: 0 V: 0	
2012	HNVi	5	19 T: 9, V: 10	T: 12 V: 12	T: 2139 V: 2353	**T: 2442 V: 2656**	4 T: 2, V: 2	T: 3 V: 3	T: 131 V: 123	**T: 213 V: 178**
		4	5 T: 3, V: 2		T: 303 V: 303		2 T: 1, V: 1		T: 82 V: 55	
	HNVe	3	6 T: 3, V: 3	T: 7 V: 6	T: 517 V: 256	**T: 2083 V: 1678**	8 T: 4, V: 4	T: 5 V: 6	T: 228 V: 544	**T: 292 V: 737**
		2	4 T: 2, V: 2		T: 64 V: 89		2 T: 1, V: 1		T: 64 V: 135	
		1	3 T: 2, V: 1		T: 1502 V: 1333		1 T: 0, V: 1		T: 0 V: 58	

Table 4-11: Number of original and final extended training (T) and validation (V) HNV reference points for the RS2 Bavaria AOI.

Year	Class	HNV	RS2 Bavaria AOI			
			Original	Combined	Original Extended	Combined Extended
2011	HNVi	5	19 T: 9, V:10	T: 9 V: 11	T: 2152 V: 1923	**T: 2152 V: 2037**
		4	1 T: 0, V:1		T: 0 V: 114	
	HNVe	3	6 T: 3, V: 3	T: 30 V: 26	T: 302 V: 256	**T: 3102 V: 2020**
		2	7 T: 3 , V: 4		T: 274 V: 460	
		1	43 T: 24, V: 19		T: 2526 V: 1304	

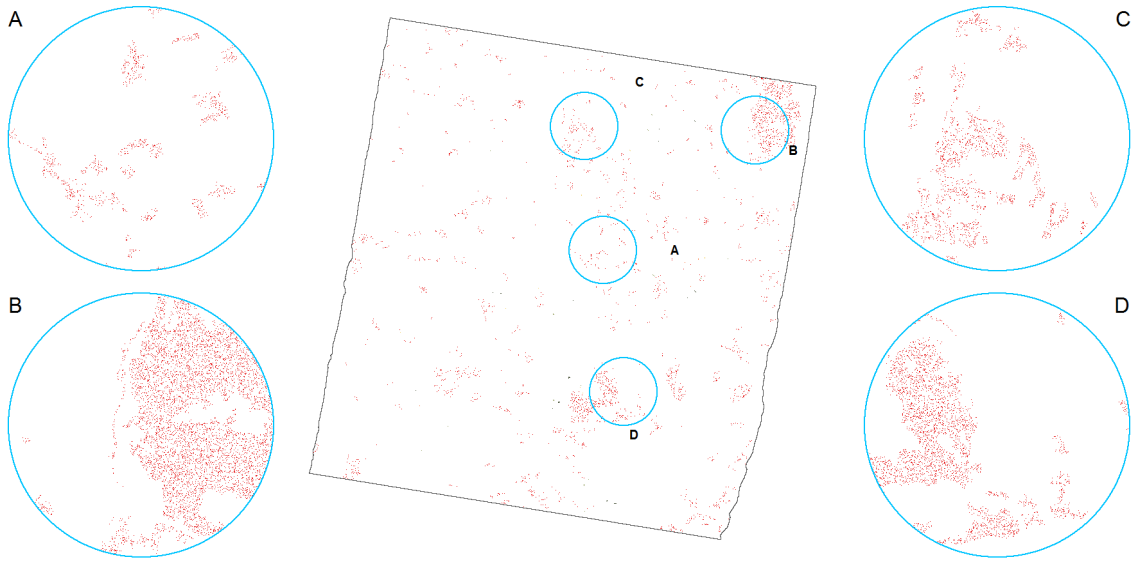

Figure 4-15: NGL validation points derived for the RS2 AOI.

has been then performed to reasonably exclude pixels which do not belong to the same landscape element and/or show a completely different behaviour over time with respect to the original reference point associated with the object. Finally, all pixels belonging to the refined segments are associated with the information class of the corresponding reference sample. An example of the procedure is given in Figure 4-14, while the list of original and extended reference points for the TSX and RS2 datasets are given in Table 4-8, Table 4-9, Table 4-10 and Table 4-11.

Within the MSAVE project, field campaign activities were foreseen to gather in situ data for the only defined classes of interest. Nevertheless, to evaluate the performances of the proposed targeted classification system, validation points were also necessary for the remaining land-cover types present in the study areas. To this aim, additional labelled samples for the non-grassland (NGL) classes (mainly forest, urban, water and agricultural areas) have been derived by intensive photointerpretation exploiting: i) multitemporal RapidEye optical imagery at 5 m spatial resolution available for the year 2011 from the MSAVE project (3 scenes for the Bavaria test site acquired on 9th May, 28th June, and 21st August, as well as 3 scenes for the Mecklenburg test site acquired on 9th May, 28th June and 25th September); and ii) reference data from the Land Use and Cover Area frame Survey (LUCAS) 2012 (EUROSTAT, 2013) as well as the CORINE Land Use/Land Cover layer (Büttner *et al.*, 2014). Specifically: i) NGL CORINE objects have been checked against both the LUCAS points and the RapidEye images, and then manually refined accordingly (e.g., areas for which it was not possible to reliably asses the corresponding

Table 4-12: Amount of final validation points derived for the NGL class.

Targeted Classification Problem	Bavaria		Mecklenburg
	TSX AOI	RS2 AOI	TSX AOI
HT	288039	181012	349195
HNV	288046	181012	350076

information class have been all excluded); or ii) NGL objects have been manually drawn by visual inspection of the satellite optical data (especially in the case of small landscape elements as agricultural fields). This resulted in a huge amount of NGL samples (i.e., greater than one-two millions), thus 10% was randomly subset and employed for assessing the effectiveness of the presented method. Their final amount is reported for each AOI in Table 4-12; moreover, the NGL validation points derived for the RS2 AOI are shown in Figure 4-15.

4.3. Dataset generation

4.3.1. Preprocessing

As specified before in this chapter, the available multitemporal TSX data have been acquired in VV/VH dual polarisation Stripmap mode between March and October of both 2011 and 2012 for the two test areas. Instead, the available RS2 time series has been acquired in fine quadpol mode (HH + HV + VV + VH) between April and September 2011 for the only Bavaria study region. However, in the latter case a simulated RS2 dualpol multitemporal series has also been generated by solely considering the VV/VH information from the quadpol data. The resulting six dataset will be referred to in the following as:

- BY-TSX-2011 [VV/VH];
- BY-TSX-2012 [VV/VH];
- MV-TSX-2011 [VV/VH];
- MV-TSX-2012 [VV/VH];
- BY-RS2-2011 [VV/VH];
- BY-RS2-2011 [QUAD].

where BY and MV denote the Bavaria and Mecklenburg study area, respectively.

According to the description of the proposed hierarchical approach provided in chapter 3.1, first a preprocessing is carried out by applying the automatic chain implemented by Schmitt (2012). In particular, all six datasets have been individually calibrated, orthorectified, and coregistered. Next, from the subsequent Kennaugh decomposition, four elements (K_0, K_1, K_5, and K_8) have been derived for the dualpol datasets (see equations (3-13), (3-14), (3-15), (3-16) in chapter 3.1) and ten elements ($K_0 - K_9$) for the quadpol dataset (see equations (3-3) to (3-12) in chapter 3.1). Quicklooks of the Kennaugh elements derived for the scene acquired on 20th May 2011 belonging to the BY-TSX-2011 [VV/VH] dataset are provided in Figure 4-16.

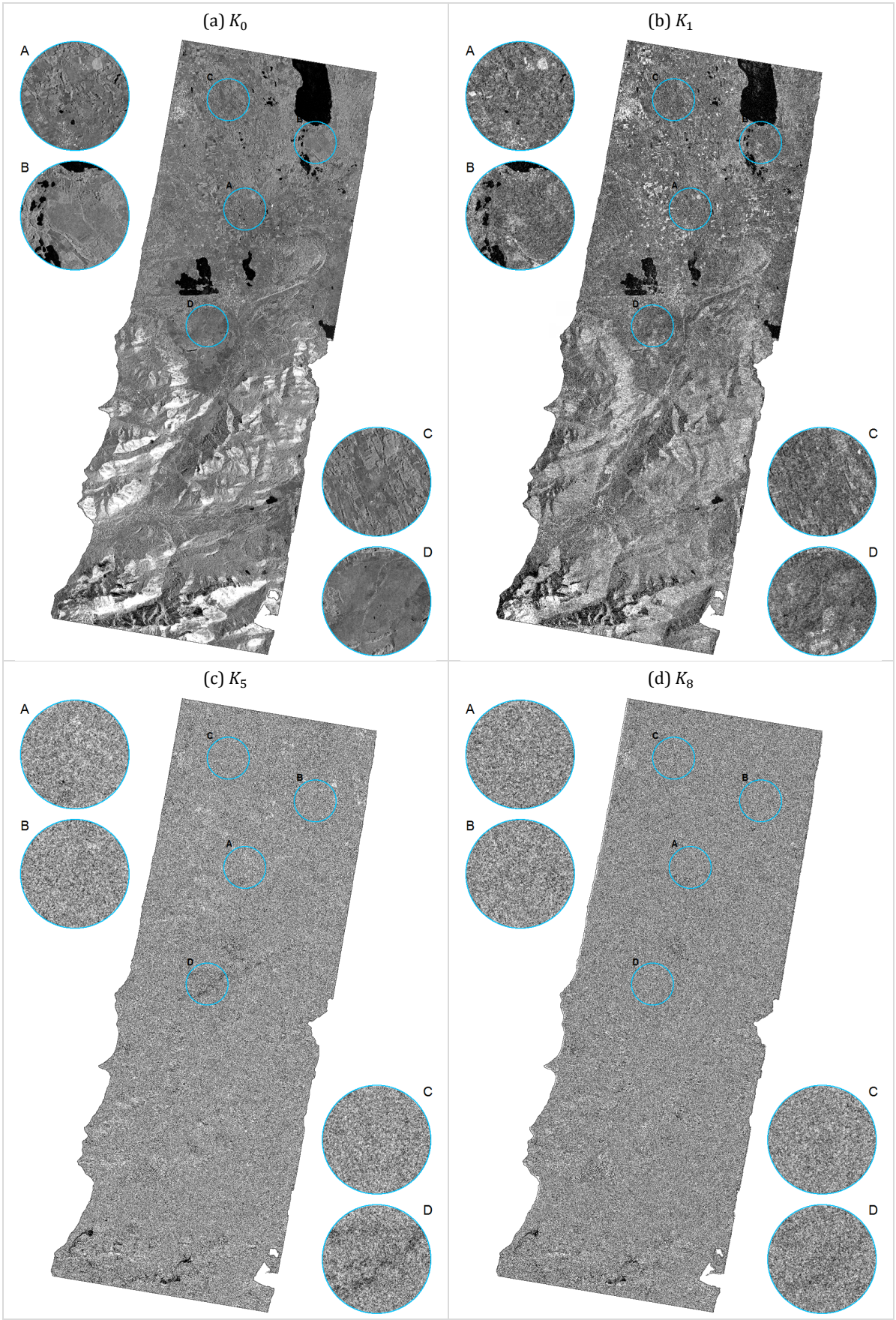

Figure 4-16: Quicklooks of the Kennaugh elements derived for the scene acquired on 20th May 2011 belonging to the BY-TSX-2011 [VV/VH] dataset.

4.3.2. Feature extraction

After preprocessing, the multitemporal filtering has been applied; in particular, the corresponding tool implemented in the Next ESA SAR Toolbox (NEST) Version 4C-1.1 has been used. To derive the optimal processing window, a preliminary analysis has been carried out on the BY-TSX-2011 [VV/VH] dataset, for which the ENL (see equation (3-17)) of K_0 has been computed, along with that derived after filtering it using any of the window sizes supported by NEST, namely 3x3, 5x5, 7x7, 9x9, and 11x11 pixels.

The results in Table 4-13 show that the ENL has low values for images more affected by the speckle, while it increases with the size of the processing window; this is also qualitatively confirmed by the example reported in Figure 4-17. Accordingly, a processing window of 11x11 pixels has been applied to all datasets since it provided the best performances in terms of speckle reduction while preserving both spatial and radiometric resolution.

Moreover, the obtained temporally-filtered Kennaugh elements are finally converted to dB in order to obtain a Gaussian distribution of the data.

Table 4-13: BY-TSX-2011 [VV/VH] dataset - ENL computed for the original K_0 as well as for that obtained after applying the multitemporal filter using different processing window sizes (i.e., 3x3, 5x5, 7x7, 9x9 and 11x11 pixels).

ACQUISITION DATE	**ENL**					
	K_0	**3x3**	**5x5**	**7x7**	**9x9**	**11x11**
26.03.2011	0.6624	0.7093	0.7372	0.7525	0.7600	0.7644
06.04.2011	0.7222	0.7747	0.8105	0.8301	0.8398	0.8457
17.04.2011	0.5604	0.6023	0.6242	0.6380	0.6455	0.6504
09.05.2011	0.5916	0.6328	0.6571	0.6717	0.6791	0.6836
20.05.2011	0.7742	0.8315	0.8719	0.8929	0.9025	0.9078
31.05.2011	0.6632	0.7122	0.7425	0.7597	0.7680	0.7728
11.06.2011	0.7835	0.8485	0.8867	0.9065	0.9150	0.9192
05.08.2011	0.7574	0.8223	0.8599	0.8796	0.8882	0.8924
16.08.2011	0.8167	0.8830	0.9217	0.9409	0.9486	0.9520
27.08.2011	0.7703	0.8332	0.8693	0.8880	0.8959	0.8997
07.09.2011	0.7608	0.8253	0.8595	0.8777	0.8856	0.8894
18.09.2011	0.8198	0.8908	0.9309	0.9512	0.9595	0.9633
29.09.2011	0.7376	0.7989	0.8355	0.8549	0.8636	0.8681

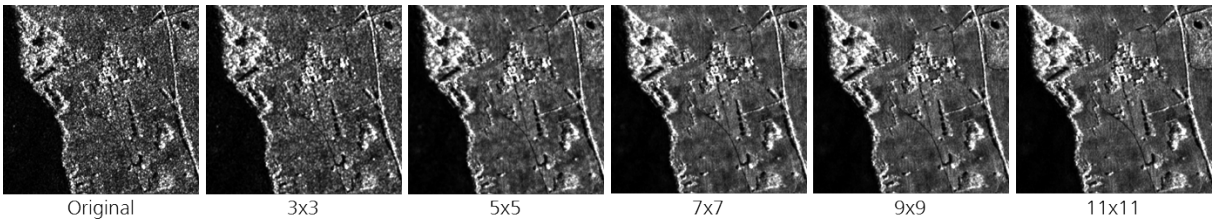

Figure 4-17: Example showing the results of the multitemporal filtering applied to K_0 for different sizes of the processing window (i.e., 3x3, 5x5, 7x7, 9x9 and 11x11 pixels).

Table 4-14: Overview of the final number of features for each dataset.

Dataset	Temporal acquisitions	Kennaugh elements per acquisition (total amount)	Texture features per acquisition (total amount)	Total number of features
BY-TSX-2011 [VV/VH]	13	4 (52)	4 (52)	104
BY-TSX-2012 [VV/VH]	11	4 (44)	4 (44)	88
MV-TSX-2011 [VV/VH]	9	4 (36)	4 (36)	72
MV-TSX-2012 [VV/VH]	7	4 (28)	4 (28)	56
BY-RS2-2011 [VV/VH]	8	4 (32)	4 (32)	64
BY-RS2-2011 [QUAD]	8	10 (80)	4 (32)	112

Four texture features, i.e., DRG, MEA, SKE and VAR, have been then derived from the multitemporal series of K_0 elements of each dataset by using the image processing software ENVI 4.8 tool *Texture Filters – Occurrence Measures*. Again, after analysing the effects of the selected processing window size (i.e., several values have been tested, namely 3x3, 5x5, 7x7, 9x9, 11x11 pixels), the 7x7 pixel one has been chosen since, by qualitative assessment, it better allowed to characterise the landscape of both study regions. Texture features derived for the K_0 element of the TSX scene acquired on 24th May 2011 belonging to the MV-TSX-2011 [VV/VH] dataset are shown in Figure 4-18.

The final datasets, which serve as input for the subsequent hierarchical targeted classification, consist of four Kennaugh elements in the case of dual-polarisation data or ten elements in the case of quad-polarisation data, as well as four texture features computed for K_0 for each image of the given time series. Table 4-14 provides an overview of the final number of features for each of the 6 considered dataset.

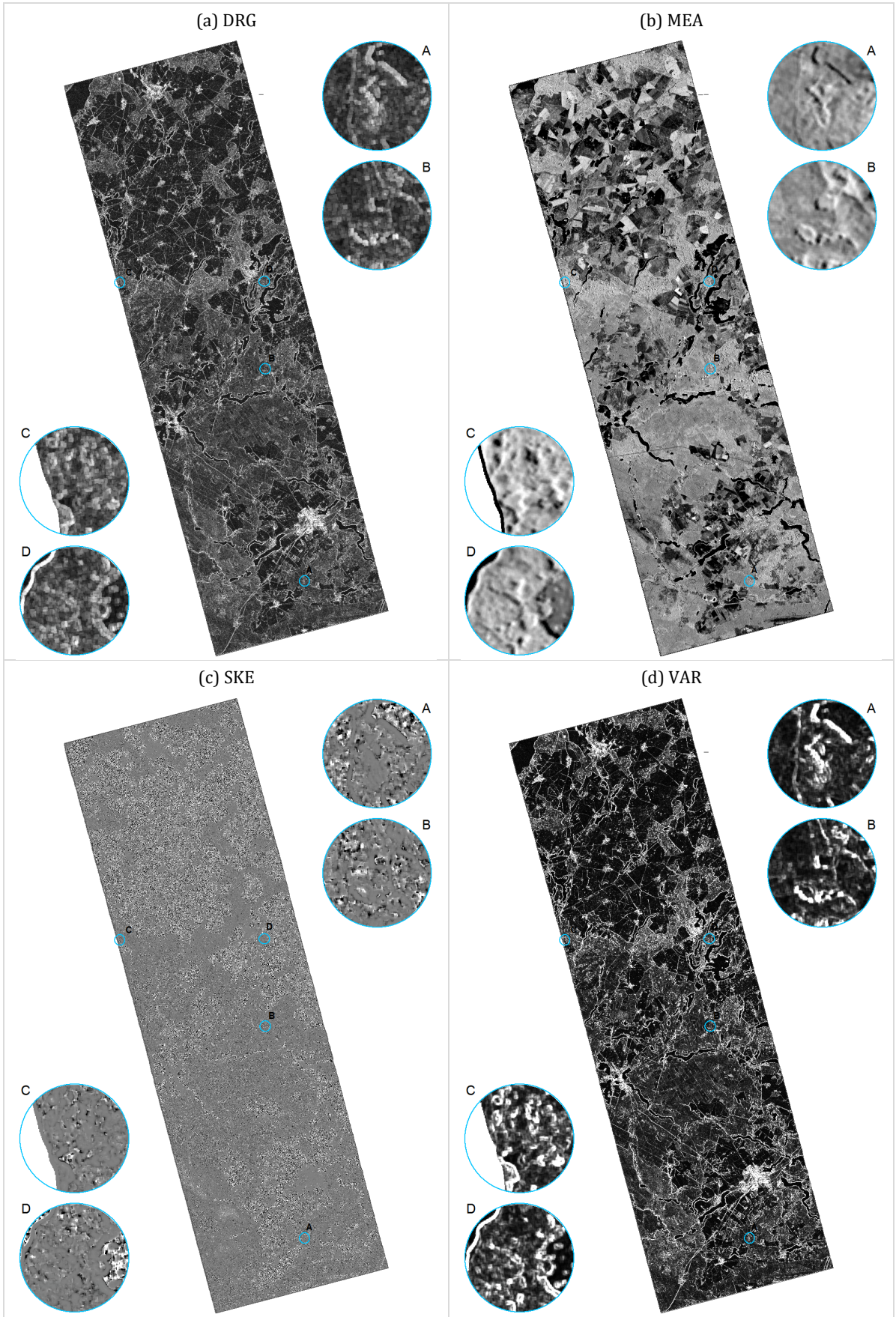

Figure 4-18: Texture features derived for the K_0 element of the TSX scene acquired on 24th May 2011 belonging to the MV-TSX-2011 [VV/VH] dataset.

5. EXPERIMENTAL ANALYSIS

In the following, the experimental analysis performed to address the targeted classification of the selected Natura 2000 habitats and HNV grassland types using TSX and RS2 multitemporal imagery is presented in detail. In particular, this is done under the main hypothesis that training samples are exclusively available for the considered classes of interest.

The proposed two-phase hierarchical classification approach has been applied where:

i) A one-class classifier is first employed to outline the merger of all the grassland types of interest considered as a single information class;
ii) A multi-class classifier is then used for discriminating the specific targeted classes within the areas identified as positive by the one-class classifier.

In the framework of phase I, both the MaxEnt and OC-SVM techniques have been tested and compared.

As concerns the MaxEnt, the IDL based wrapper for the dedicated software by Phillips *et al.* (2004) available at https://www.cs.princeton.edu/~schapire/maxent/ has been used (Oldenburg *et al.*, 2012), which has been implemented within the EnMAP-Box (i.e., a freely available, platform-independent software originally designed to process hyperspectral remote sensing data (van der Linden *et al.*, 2015)). The convergence threshold κ and the maximum number of iterations φ (see chapter 3.3.1) have been set to the recommended default values, namely 0.00001 and 500, respectively. Regarding the number of background samples to consider for a reliable estimation of the term $Z_{\boldsymbol{\lambda}}$, different trials have been carried out when classifying the Natura 2000 habitats in the Bavaria datasets for the year 2011. Specifically, five different runs with random point selection have been performed both with 10.000 and 100.000 samples. The mean improvement of using more points resulted in negligible increase of the classification accuracy (~0.1%) against a sensible rise of the processing time (several hours vs. few minutes), thus confirming the conclusions by Elith *et al.* (2011) and Yates *et al.* (2010). Accordingly, the number of background samples has been set to 10.000 for all the experiments (being it also the recommended default value of the employed MaxEnt tool). When dealing with the MaxEnt classifier, the most critical parameter to set proved to be the threshold θ based on which input samples are finally associated with the class of interest ω_{int} or to the unknown class ω_{unk}. As stated in chapter 3, a common approach in the literature is to fix a significance level ρ and compute θ such that the omission error calculated over the training points available for ω_{int} is not greater than ρ (Jeon and Landgrebe, 1999; Engler *et al.*, 2004; Phillips *et al.*, 2006). To this purpose a simple strategy has been defined. In particular, a first classification map is derived fixing $\rho = 0.15$ (for which underestimation of ω_{int} was always experienced). Afterwards, a new

map is iteratively generated lowering the threshold to 0.125, and so on to 0.1, 0.075, 0.05, 0.025, 0.015, 0.01, 0.005 and 0.001. Each time, a qualitative visual inspection is performed. As soon as landscape elements which are obviously not belonging to any of the considered grassland types (e.g., urban areas, forests, lakes) start being wrongly misclassified as ω_{int}, then the procedure is stopped and the previous value for ρ (for which such kind of overestimation did not occur) is selected (as an example, if this is experienced for $\rho = 0.015$, then $\rho = 0.025$ is chosen). As it will emerge from the results presented in the following pages, this scheme proved to be particularly effective and, above all, it can be easily employed also by non-trained operators thus making it suitable for an operative usage.

Regarding the OC-SVM classifier, the corresponding software available within the LibSVM library has been employed (Chang and Lin, 2011; Software available at http://www.csie.ntu.edu.tw/cjlin/libsvm). In particular, LibSVM is very popular and extensively used by the machine learning community; it has been developed at the National Taiwan University and for solving constrained quadratic minimization it implements the modified and faster version of the Sequential Minimal Optimization (SMO) algorithm proposed by Fan *et al.* (2005). As recommended by its developer, for each input feature data have been normalized between -1 and $+1$. The RBF Gaussian kernel has been chosen as commonly done in the literature for addressing remote-sensing classification problems. Indeed, it tends to provide good performances under the assumption that the optimal discrimination function is smooth (i.e., it has derivatives of all orders everywhere in its domain) or if no additional knowledge of the data is available (Smola *et al.*, 1998). Accordingly, a grid search strategy has been used to identify the most suitable values for $\gamma = 1/2\sigma^2$ (where σ is the free parameter ruling the RBF kernel as specified in section 3.3.1) as well as $\nu \in (0,1]$ (i.e., the parameter tuning the trade-off between the complexity of the model and the number of training samples categorized as belonging to ω_{int}). In particular, γ has been varied between 0.1 and 1 with step 0.05, between 1 and 10 with step 0.5 and between 10 and 100 with step 5, whereas ν has been varied between 0.01 and 0.1 with step 0.01, and between 0.1 and 1 with step 0.1. For each of the resulting 1045 possible (γ, ν) combinations an SVM has been trained; among these, the criterion $\text{argmax}_{\gamma,\nu}(OA\%/\#SV)$ has been chosen for identifying the most suitable one for solving the investigated one-class problem (Muñoz-Marí *et al.*, 2010), where $OA\%$ denotes the overall accuracy computed over the training set (i.e., the percentage of training samples correctly classified as belonging to the class of interest), while $\#SV$ represents the number of support vectors. In particular, this allows selecting the SVM providing the best trade-off between accuracy and model complexity, which is expected to result in the highest generalisation capability (Banerjee *et al.*, 2006).

From preliminary experimental trials with both the MaxEnt and OC-SVM methods, it emerged that, despite multi-temporal filtering has been applied to the considered multi-temporal SAR data, a non-negligible amount of pixels was still partly affected by the speckle noise. This made the corresponding one-class classification maps appearing generally rather scattered. Hence, to overcome this issue, the same two-step segmentation approach employed for extending the original labeled samples (see section 4.2.2) has been first used considering that grasslands generally occur as compact landscape elements (rather than small patches), within which different sub-types might be present. Specifically, it has been applied to the multitemporal series of the MEA texture feature, where homogeneous structures tend to appear more clearly. Based

on visual interpretation, the best fitting parameters proved to be: scale 9, shape 0.0001, compactness 0.9 and maximum spectral difference 0.4 (i.e., they differ from those used in section 4.2.2 which were more stringent to avoid including any error in the extended training set). Afterwards, the three following rulesets have been defined (and compared) to determine whether, based on the given original one-class classification map, each resulting segment should be categorized as ω_{int} or ω_{unk}. In particular, one segment is associated with the grassland class if:

Rule I. the percentage of pixels labeled as grasslands within the segment is greater or equal to 30;

Rule II. the percentage of pixels labeled as grasslands within the segment is greater or equal to 30 and the size of the segment is greater than 0.5 ha, or the percentage of pixels labeled as grasslands within the segment is greater or equal to 50;

Rule III. the percentage of pixels labeled as grasslands within the segment is greater or equal to 30 and the size of the segment is greater than 1 ha, or the percentage of pixels labeled as grasslands within the segment is greater or equal to 50.

Compared to Rule I, in the hypothesis that they are more challenging to be correctly classified, Rules II and III are stricter for smaller segments (i.e., considered as those with area lower than 0.5 and 1 ha, respectively), while for all the remaining segments yet a consistent presence (i.e., 30%) of grassland pixels is considered sufficient. Here, it is worth noting that a dedicated model selection of the parameters for both the MaxEnt and OC-SVM has been carried out for each of the three rulesets.

In phase II of the proposed hierarchical system, SVM have been employed being them currently the reference state-of-the-art technique when addressing the multi-class categorisation of remote-sensing imagery (as discussed in chapter 3.3.2). Similarly to what done for the above-mentioned OC-SVM, the corresponding software available in the LibSVM library has been used (which supports the one-against-one multi-class approach). Also in this case, the RBF Gaussian kernel has been employed; therefore, the set of free parameters to tune included γ and C (which regulates the generalization capability of the classifier). In particular, a grid search strategy has been applied with a 5-fold cross validation. k-fold cross validation is a largely accepted and widely employed model selection criterion (especially in the machine learning community) where the training set is split in k (commonly five) disjoint groups: $k-1$ sets are employed for training, while the remaining is used for validation (Duda *et al.*, 2000). The procedure is repeated k times and, finally, the best combination of free parameters is chosen by minimising an average error measurement computed with the predictions on the k different validation sets. In this context, the Kappa coefficient of accuracy has been chosen as commonly done in the literature, since, with respect to the OA%, it also takes into consideration omission and commission errors (Richards and Jia, 2006). Specifically, Kappa is defined as $(p_0 - p_e)/(1 - p_e)$, where p_0 is given by the ratio between the overall number of samples correctly classified and the total number of samples $\#TS$, while p_e denotes the probability of random agreement (i.e., given the $N \times N$ confusion matrix it is computed as $\left(\sum_{i=1}^{N} \bar{C}_i \cdot \bar{R}_i\right)/\#TS^2$ being $\bar{C}_i$ and $\bar{R}_i$ the sum over all the elements in the i-th column and row, respectively) (Smeeton, 1985). γ has been varied as done for the OC-SVM, while C has been varied between 1 and 10 with step 1, between 10 and 100 with step 10, and between 100 and 1000 with step 100, thus resulting in 1540 different

combinations. Finally, a SVM is trained on the complete training set using the resulting best parameters.

Alternatively to the SVM, the proposed multi-class approach based on multiple MaxEnt classifiers has also been employed. In particular, for each targeted class a dedicated MaxEnt is trained. However, being all of them finally applied in the only areas marked as positive in the first phase of the hierarchical approach, no threshold θ has to be tuned. Rather, each pixel is directly associated with the class for which the corresponding MaxEnt provides the highest estimated conditional probability.

As it will be clarified in the following pages, the MaxEnt classifier proved generally more effective than the OC-SVM when addressing the one-class classification task. Hence, it has been finally adopted in phase I of the presented hierarchical system in all experimental trials. The hierarchical classifier resulting from the combination of the MaxEnt in the first phase and the SVM in the second phase is then referred to as *hierarchical MaxEnt + SVM*, while that obtained combining the MaxEnt in the first phase and the multiple MaxEnt classifiers in the second phase is referred to as *hierarchical MaxEnt + MaxEnt*.

So far, targeted classification has been generally addressed by using an ensemble of multiple one-class classifiers each one trained on a specific class of interest. A winner-takes-all rule is then applied on the outputs accounting for some heuristics to avoid potential conflicts if more than one classifier categorises a given pixel as belonging to its corresponding targeted class. Accordingly, for comparison purposes, in all sets of performed experiments also an ensemble of MaxEnt classifiers has been tested (referred to as *standard MaxEnt*); in particular, the MaxEnt has been chosen based on the highest performances exhibited on the single one-class classification problem mentioned above. However, concerning the selection of the threshold θ_i for each *i*-th item of the ensemble, it proved to be not feasible to determine an optimal value following the same strategy considered in the hierarchical system. Indeed, in the case of a single grassland class given by the merger of all classes of interest, this task can be effectively accomplished by visually analysing when misclassification of non-grassland areas occurs. Contrarily, when accounting for each *i*-th targeted class ω_i separately: i) the corresponding conditional probability density $\hat{p}(\mathbf{x}|\omega_i)$ is modelled using a lower amount of samples (thus resulting in less reliable estimates especially when few training samples are available); and ii) it is not possible to determine by photointerpretation if, for a certain threshold θ_i, grasslands belonging to the other targeted classes are misclassified as ω_i. To overcome this issue, similarly to what done in Stenzel *et al.* (2014), for each MaxEnt classifier eight thresholds are computed according to as many dedicated strategies implemented in the Species Distribution Modelling Tools (SDMT) (VanDerWal *et al.*, 2012) and finally the median value is taken (which is generally robust to the presence of outliers). When generating the final targeted classification maps, in case of conflicts for a given pixel the class with the highest estimated conditional probability is chosen.

In the next sections, results are presented first for the dualpol TSX and then for the dual- and quadpol RS2 datasets. Classification results have been evaluated in terms of: OA%, Kappa coefficient, percentage producer's accuracy PA% (denoting for each class the corresponding percentage of samples categorized correctly) and, for the one-class problems, also average accuracy AA% (given by the average PA% of the grassland and non-grassland class).

5.1. Experimental Results with TerraSAR-X data

In this section, experimental trials performed with dualpol TSX datasets are discussed. The attention is focused first on the Bavaria and then on the Mecklenburg test site. In both cases, results are presented both for the Natura 2000 and the HNV targeted classification problems.

5.1.1. Bavaria test site: Natura 2000

All four Natura 2000 classes of interest, namely 6410, 7120, 7140 and 7230, are present in the Bavaria test site. These specific grassland types are not expected to change significantly – especially in their extent – within few months, but this generally takes up to several years. Accordingly, as described in section 4.2.2 labelled samples collected in 2011 and 2012 have been merged together to define single training and validation sets. Nevertheless, separate experimental analyses have been carried out for 2011 and 2012 for two main reasons.

On the one hand, combining all scenes available for the two years would have resulted in a dataset composed of 190 features, thus making the targeted classification problem actually even more challenging due to the lower ratio between the available number of training samples (especially for class 7140 and 7230) and the total number of features. Indeed, according to Hughes (1968), for a given number of training samples, the predictive power reduces as the dimensionality increases (in the machine learning community this well-known issue is referred to as Hughes phenomenon or “curse of dimensionality”).

On the other hand, scenes available for 2011 and 2012 cover different time frames; hence, by investigating the two years separately, it was possible to assess the benefits/disadvantages given by the presence/lacking of acquisitions in certain periods.

Initially, all the available training points for the different classes have been merged together in a single grassland (GL) class and used to train the MaxEnt and OC-SVM one-class classifiers for both years according to the strategies described at the beginning of the chapter. As concerns the former, in Figure 5-1 to Figure 5-3 examples are given to show how the value for the significance level ρ has been determined. In particular, Figure 5-1 depicts the nine one-class classification maps derived for the BY-TSX-2011 [VV/VH] dataset with $\rho = 0.05$, $\rho = 0.025$, and $\rho = 0.015$ and applying the three rulesets defined to account for local spatial homogeneity. By visual inspection, it was possible to easily recognize the overestimation occurring when setting $\rho = 0.015$; indeed, forested and urban areas located in the north-western side of the investigated AOI are wrongly categorized as belonging to the GL class. Instead, this does not happen for $\rho = 0.025$, which has been finally selected as optimal significance level. Such a choice is also confirmed by the underestimation of several grasslands fields for which training samples were actually available when fixing $\rho = 0.05$. Moreover, by also analysing the behaviour over grasslands where training points have been drawn, the map generated by employing Rule II has been finally chosen as it appeared the most reliable. Larger pictures are provided in Figure 5-2 of the maps derived with Rule II for $\rho = 0.05$, $\rho = 0.025$, and $\rho = 0.015$, and in Figure 5-3 of the maps obtained with $\rho = 0.025$ for the three rulesets.

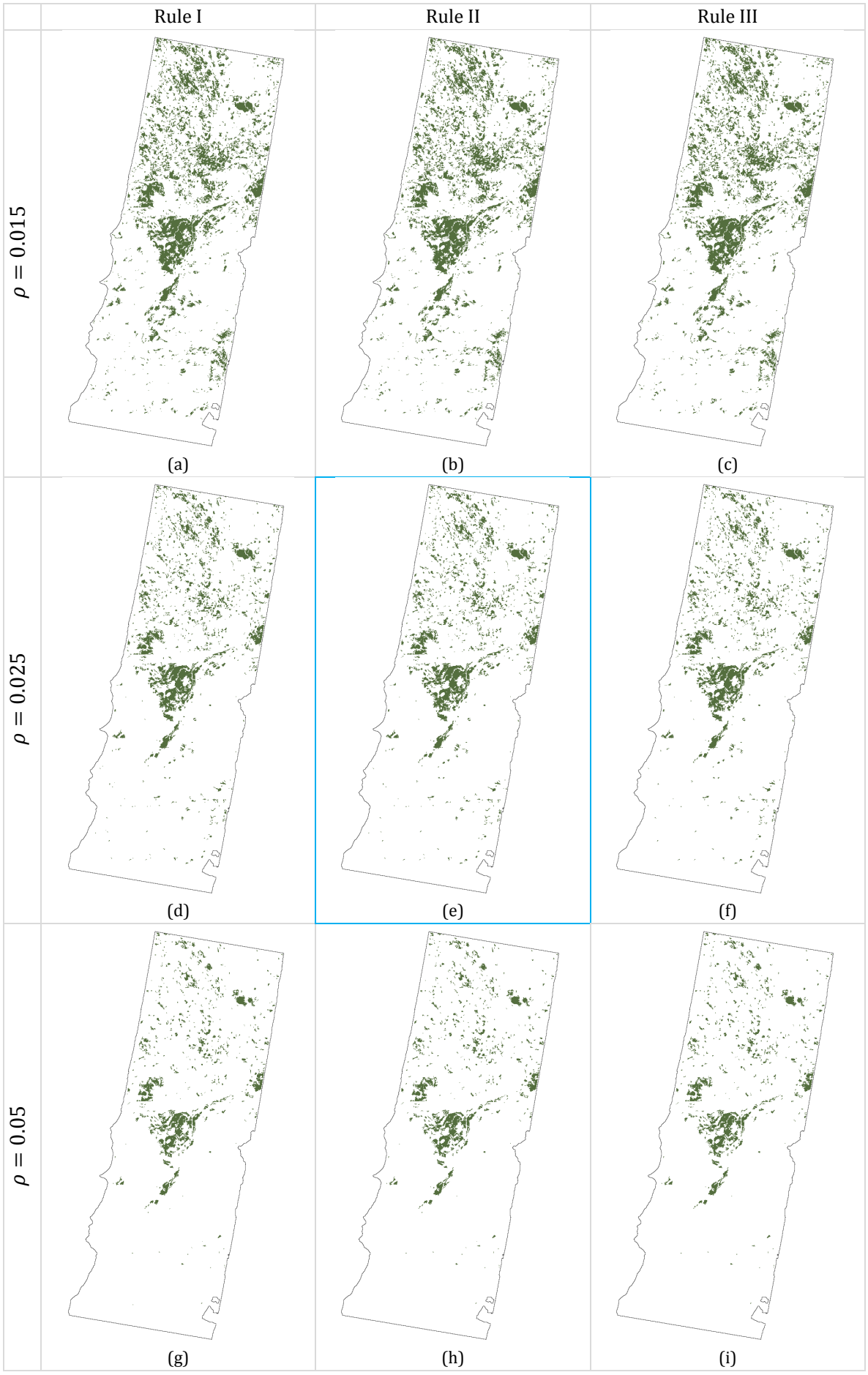

Figure 5-1: BY-TSX-2011 [VV/VH] dataset - HT one-class classification maps obtained using the MaxEnt for $\rho = 0.05$, $\rho = 0.025$, and $\rho = 0.015$ in combination with the three defined spatial homogeneity rulesets.

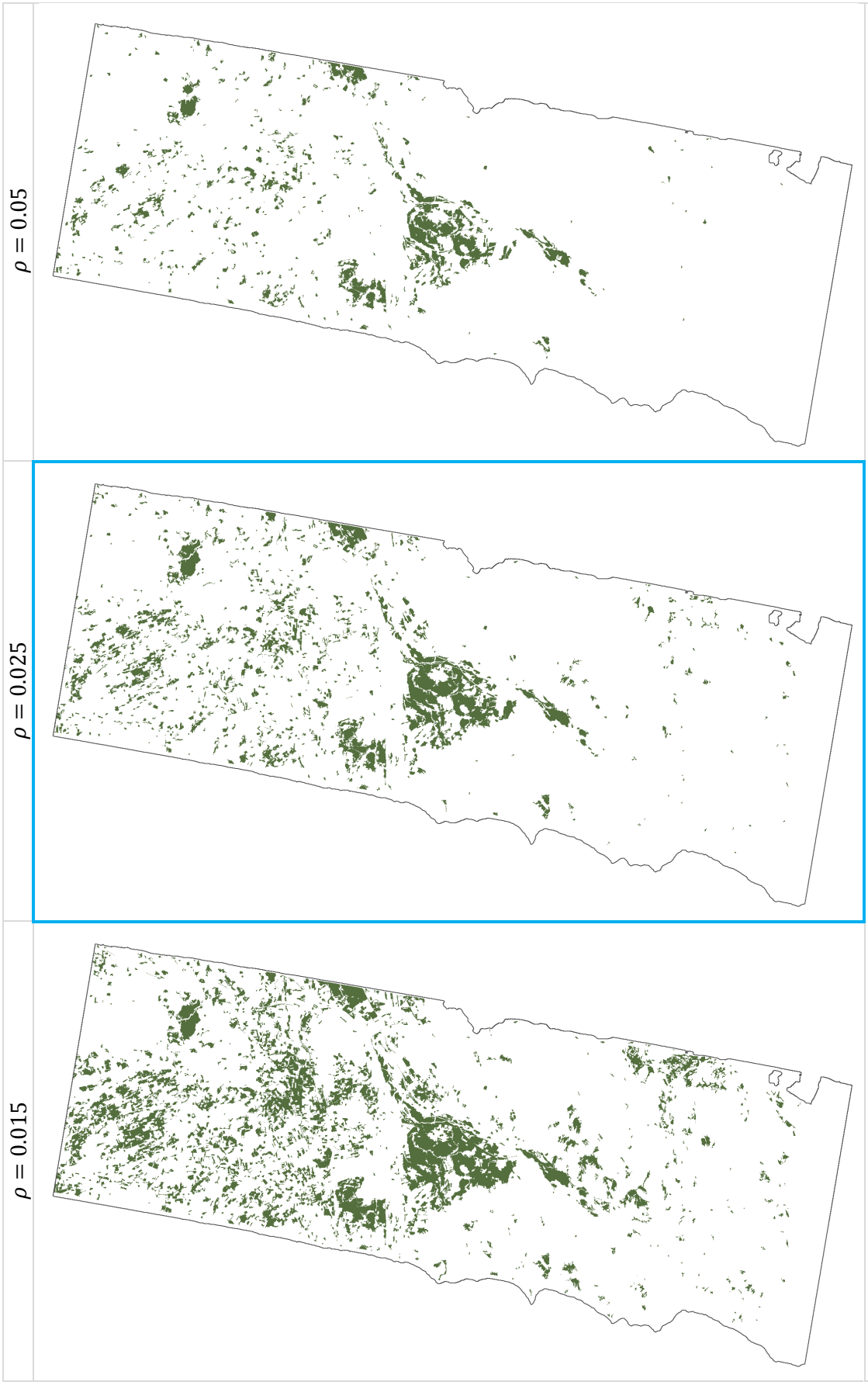

Figure 5-2: BY-TSX-2011 [VV/VH] dataset - HT one-class classification maps obtained using the MaxEnt for $\rho = 0.05$, $\rho = 0.025$, and $\rho = 0.015$ in combination with Rule II.

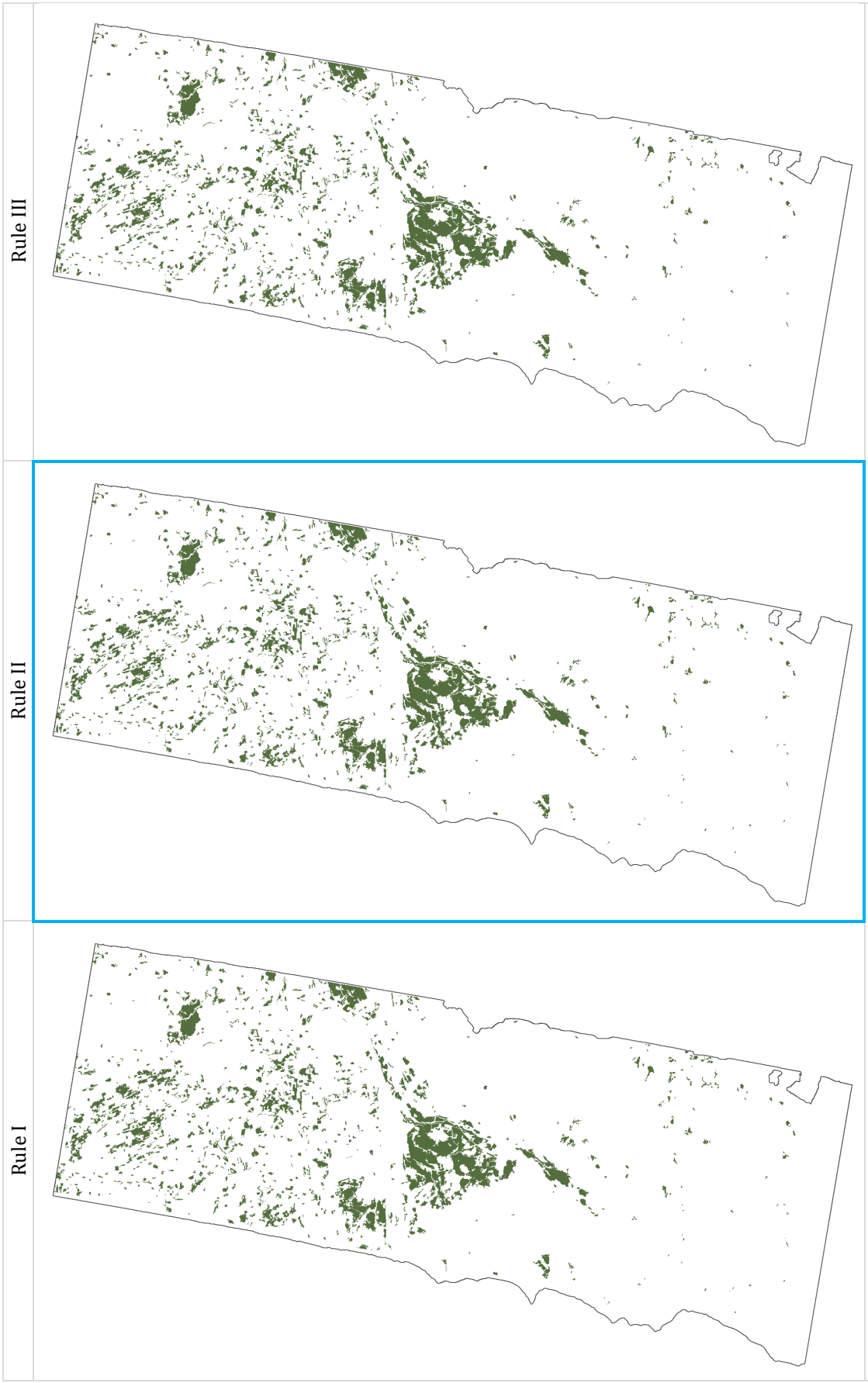

Figure 5-3: BY-TSX-2011 [VV/VH] dataset - HT one-class classification maps obtained using the MaxEnt for $\rho = 0.025$ in combination with the three defined spatial homogeneity rulesets.

Table 5-1: HT one-class classification – Validation accuracies computed for the maps obtained applying the OC-SVM and MaxEnt (for different values of ρ) to the BY-TSX-2011 [VV/VH] and BY-TSX-2012 [VV/VH] datasets using the three defined spatial homogeneity rulesets. Results for the maps selected by qualitative assessment as most reliable for the OC-SVM and MaxEnt are highlighted in yellow and blue, respectively. At the bottom, accuracies are also provided for the maps derived combining the ones selected for 2011 and 2012 for each classifier [GL training samples: 3687; GL validation samples: 3648; NGL validation samples: 288039].

		Rule I					Rule II					Rule III				
		OA%	Kappa	GL PA%	NGL PA%	AA%	OA%	Kappa	GL PA%	NGL PA%	AA%	OA%	Kappa	GL PA%	NGL PA%	AA%
BY-TSX-2011 [VV/VH]	OC-SVM	99.35	0.6681	52.96	99.94	76.45	99.35	0.6681	52.96	99.94	76.45	99.35	0.6681	52.96	99.94	76.45
	MaxEnt ρ = 0.015	98.07	0.5295	98.18	89.53	93.86	98.08	0.5298	98.19	89.53	93.86	98.04	0.5113	98.20	84.98	91.59
	MaxEnt ρ = 0.025	99.44	0.7894	85.01	99.63	92.32	99.44	0.7894	85.01	99.63	92.32	99.40	0.7676	80.46	90.05	90.05
	MaxEnt ρ = 0.05	99.57	0.7953	68.04	99.97	84.00	99.57	0.7953	68.04	99.97	84.00	99.54	0.7803	65.84	82.91	82.91
	MaxEnt ρ = 0.075	99.49	0.7480	60.96	99.98	80.47	99.49	0.7480	60.96	99.98	80.47	99.49	0.7480	60.96	80.47	80.47
	MaxEnt ρ = 0.1	99.47	0.7311	58.50	99.99	79.24	99.47	0.7311	58.50	99.99	79.24	99.47	0.7311	58.50	79.24	79.24
	MaxEnt ρ = 0.125	99.47	0.7321	58.50	99.99	79.24	99.47	0.7321	58.50	99.99	79.24	99.47	0.7321	58.50	79.24	79.24
	MaxEnt ρ = 0.15	99.45	0.7184	56.66	99.99	78.33	99.45	0.7184	56.66	99.99	78.33	99.45	0.7184	56.66	78.33	78.33
BY-TSX-2012 [VV/VH]	OC-SVM	98.98	0.6320	71.88	99.32	85.60	98.98	0.6320	71.88	99.32	85.60	98.98	0.6320	71.88	99.32	85.60
	MaxEnt ρ = 0.015	96.46	0.3805	96.52	91.50	94.01	96.46	0.3808	96.53	91.50	94.01	96.46	0.3748	96.55	89.31	92.93
	MaxEnt ρ = 0.025	99.03	0.6856	86.54	99.19	92.86	99.03	0.6858	86.54	99.19	92.86	98.98	0.6623	81.99	90.59	90.59
	MaxEnt ρ = 0.05	99.37	0.7463	75.11	99.68	87.39	99.37	0.7466	75.11	99.68	87.39	99.35	0.7334	72.75	86.22	86.22
	MaxEnt ρ = 0.075	99.44	0.7536	69.08	99.83	84.45	99.44	0.7536	69.08	99.83	84.45	99.45	0.7550	69.08	84.46	84.46
	MaxEnt ρ = 0.1	99.41	0.7310	65.35	99.84	82.59	99.41	0.7310	65.35	99.84	82.59	99.41	0.7320	65.35	82.60	82.60
	MaxEnt ρ = 0.125	99.40	0.7243	63.65	99.86	81.75	99.40	0.7243	63.65	99.86	81.75	99.41	0.7252	63.65	81.75	81.75
	MaxEnt ρ = 0.15	99.38	0.6929	56.44	99.93	78.18	99.38	0.6935	56.44	99.93	78.19	99.39	0.6937	56.44	78.19	78.19
OC-SVM 2011-2012							99.38	0.6780	52.96	99.97	76.46					
MaxEnt 2011-2012							99.68	0.8682	85.01	99.87	92.44					

The quantitative accuracy assessment performed using the available validation set (where again the samples for the four specific targeted classes have been merged into a single GL class) are reported in Table 5-1. In particular, as clarified in section 4.2.2, these samples have been drawn from different grassland fields than those from which training points have been extracted and have not been considered at any stage in the learning phase of both the MaxEnt and OC-SVM classifiers.

As regards the BY-TSX-2011 [VV/VH] dataset, the choice discussed above of selecting $\rho = 0.025$ for the MaxEnt proves effective also in the light of the corresponding classification accuracies, resulting in a good trade-off between high OA% (greater than 99) and Kappa (close to 0.8), without consistent under-/overestimation (i.e., the PA% of both GL and NGL is greater than 85, with an AA% higher than 92). Instead, for $\rho = 0.05$ the OA% and Kappa show slightly higher values (+0.13 and 0.0059, respectively), but the PA% of the GL class and the AA% are sensibly lower (-15.97 and -8.32, respectively); whereas, the opposite occurs for $\rho = 0.15$, where the PA% for the GL class and the AA% are higher due to the overestimation of the grassland areas (+13.18 and +1.54, respectively) at the price of lower OA% and PA% for the NGL (-1.36 and -10.1, respectively), and, especially, a drop in terms of Kappa (-0.2596). In general, results are the same when using Rule I or Rule II, while they differ with Rule III only for low values of ρ. Concerning the OC-SVM, the couple of optimal parameters proved to be $(\gamma = 4, \nu = 0.1)$ for all three rulesets with no difference among the corresponding classification maps. However, by

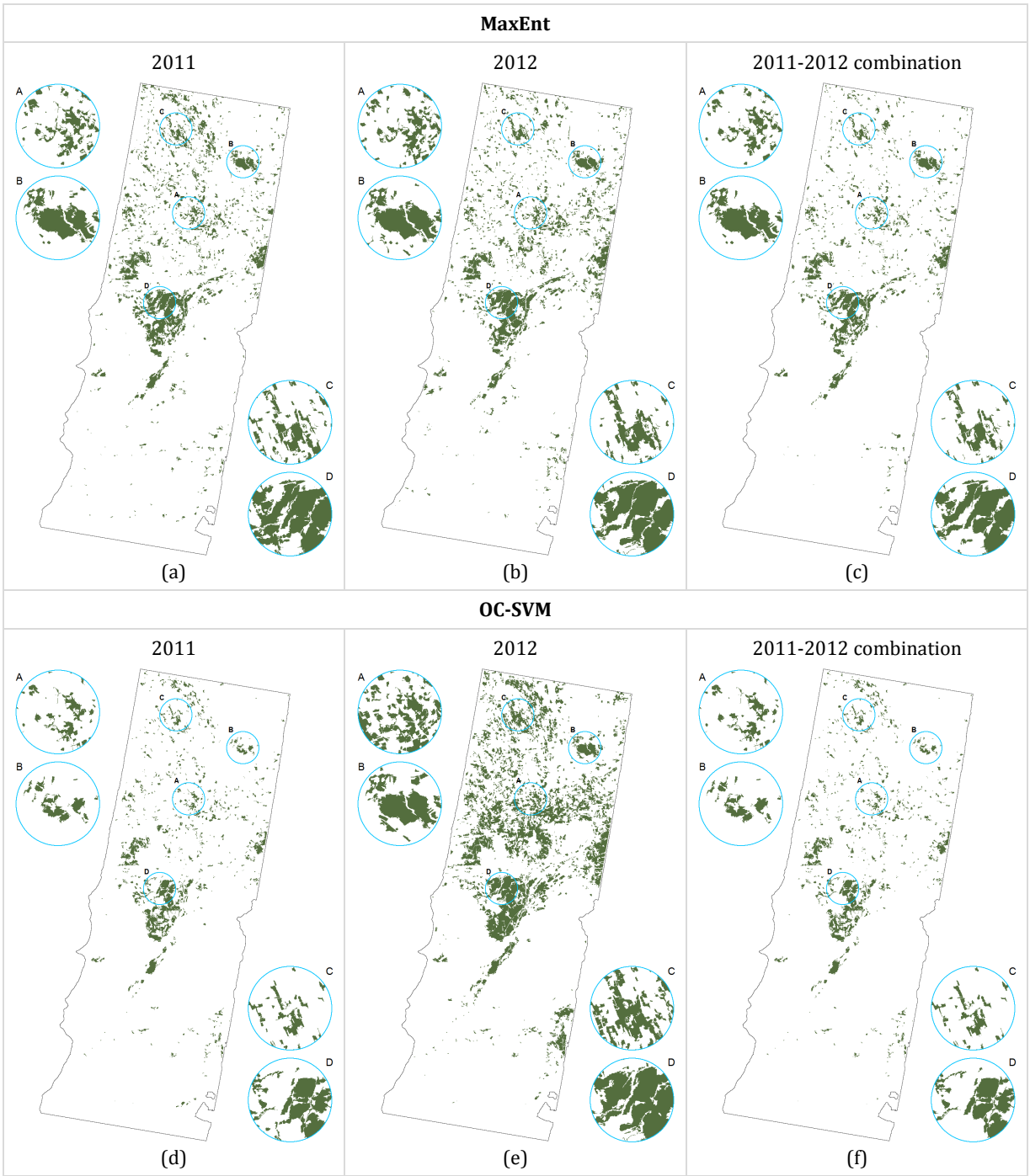

Figure 5-4: HT one-class classification maps selected using the MaxEnt and OC-SVM for the BY-TSX-2011 [VV/VH] (a and d, respectively) and BY-TSX-2012 [VV/VH] (b and e, respectively) datasets, along with their combinations (c and f, respectively).

comparing the one derived with Rule II to that obtained with the MaxEnt reported in Figure 5-4 (a) and (d), the underestimation of the GL class is evident, which is reflected especially in the sensibly lower values for both PA% (52.96) and Kappa (0.6681).

The same behaviour occurs for the BY-TSX-2012 [VV/VH] dataset, where again the map generated for $\rho = 0.025$ and Rule II has been chosen for the MaxEnt, while for the OC-SVM the couple $(\gamma = 8, \nu = 0.1)$ was selected without any appreciable difference between the three spatial homogeneity rulesets (see Figure 5-4 (b) and (e)). With respect to the 2011 dataset,

accuracies are lower due to a general overestimation of the GL class. This is most likely due to the lower number of scenes available in 2012, together with the higher amount of spring acquisitions in 2011 which seem allowing a better discrimination of the targeted classes with respect to other land-cover types. However, again the MaxEnt exhibited better performances with respect to the OC-SVM which wrongly associated several NGL areas with the GL class but also vice-versa, as highlighted by the lower Kappa (0.6320 against 0.6858) and lower PA% for the GL class (71.88 against 84.54).

To take anyhow into account that the extent of the areas where the grasslands classes of interest are present does not vary in a single-year time frame, both for the MaxEnt and OC-SVM the corresponding one-class classification maps derived for 2011 and 2012 have been finally combined. In particular, the only samples associated in both years with the GL class are preserved (see Figure 5-4 (c) and (f)). Such a strategy proved rather effective, as confirmed by the resulting accuracies reported at the bottom of Table 5-1. In particular, with the MaxEnt the final Kappa and AA% are equal to 0.8682 and 92.44, respectively (+0.1902 and +15.98 with respect to the OC-SVM). As this clearly emerges also by qualitative visual assessment, as already anticipated in the previous section, the corresponding map has been chosen to be employed in the multi-class phase of the proposed hierarchical system.

The targeted classification maps obtained with the hierarchical MaxEnt + SVM and hierarchical MaxEnt + MaxEnt approaches, along with those generated with the standard MaxEnt are shown in Figure 5-5 for 2011 and in Figure 5-6 for 2012. However, to take into consideration the above-mentioned temporal stability of the classes of interest also when applying the standard MaxEnt, an additional combined MaxEnt method has been tested, which excludes pixels categorised by the standard MaxEnt as one of the four considered grassland types in just one of the two investigated years. The quantitative assessment performed to evaluate the effectiveness of the different classifiers is presented in Table 5-2. Primarily, it can be seen that for all of them the results are similar between the two years, despite different number and dates of acquisitions were available. However, by applying the proposed hierarchical concept the accuracies are sensibly improved; indeed, the hierarchical MaxEnt + SVM and the hierarchical MaxEnt + MaxEnt outperform the standard MaxEnt as well as the combined MaxEnt approach exhibiting Kappa values ~0.15 to 0.18 higher. Furthermore, the proposed hierarchical MaxEnt + SVM approach results in the best OA% and Kappa both for 2011 and 2012 (where the optimal SVM parameters based on the employed 5-fold cross validation were $(\gamma = 20, C = 1)$ and $(\gamma = 2.5, C = 1)$ respectively). This behaviour is also confirmed by visually comparing the maps reported in Figure 5-5 and Figure 5-6. Especially, the hierarchical approaches well characterise the considered targeted classes throughout the entire study area (Figure 5-5 (a) and (b) and Figure 5-6 (a) and (b)), while by using the *standard MaxEnt* the extent of the grassland areas is consistently underestimated. By applying the *combined MaxEnt* method false alarms are reduced, but the resulting improvement in the classification accuracies is minor (~ 0.02 in terms of Kappa).

Generally, the locations of the raised bogs (class 7120) are well defined within the test area by all classifiers. In particular, these can be mainly found close to the “Osterseen” in the north of the test area (zoom B), within the large bog influenced landscape “Murnauer Moos” in the centre of the image (zoom D), within the area west of the “Staffelsee” (upper-left of zoom D), and within

an area in the north-eastern part of the test site. However, the final delineation of the single bogs differs majorly with the different classification approaches. For instance, this can be clearly noticed in zoom B, where the hierarchical approaches properly define the area of the raised bogs (class 7120) while the results of the *standard MaxEnt* and *combined MaxEnt* (Figure 5-5 (c) and (d) and Figure 5-6 (c) and (d)) appear more scattered due to the many missed alarms. The intra field variability of the various grassland classes can be well seen in zoom D, despite there is a big difference between the *hierarchical MaxEnt + SVM* and the *hierarchical MaxEnt + MaxEnt* in the distribution and classification of the single classes. For the *standard MaxEnt* and *combined MaxEnt* approaches this variability gets lost due to the consistent underestimation of the targeted classes and the corresponding scattered classification maps.

It is worth noting that, despite the standard techniques tend to underestimate the targeted classes, the OA% results anyhow in high values due to the extremely high number of validation samples for the NGL (288039) compared to that available for the targeted classes (overall 3648). In Table 5-2 also the percentage of samples misclassified as NGL (% unclassified) per class is reported. For the hierarchical approaches it is relatively low for the classes 6410 (120 over 1260), 7120 (272 over 1634) and 7140 (0 over 207). Only for the class 7230 it is slightly higher (28.34%), but actually this corresponds to only 155 samples. Instead, for the *standard MaxEnt*

Table 5-2: HT targeted classification – Validation accuracies computed for the maps obtained applying the four considered methods to the BY-TSX-2011 [VV/VH] and BY-TSX-2012 [VV/VH] datasets using 1397 training samples for class 6410, 1385 for class 7120, 291 for class 7140 and 614 for class 7230 [NGL validation samples: 288039].

		OA%	Kappa	PA%					% unclassified				# validation points			
				NGL	6410	7120	7140	7230	6410	7120	7140	7230	6410	7120	7140	7230
BY-TSX-2011	*hierarchical MaxEnt + SVM*	99.47	0.7810	99.87	85.87	82.93	0.00	6.58	9.52	16.65	0.00	28.34	1260	1634	207	547
	hierarchical MaxEnt + MaxEnt	99.42	0.7598	99.87	60.95	82.68	1.93	36.56	9.52	16.65	0.00	28.34				
	standard MaxEnt	99.07	0.5964	99.71	36.83	73.81	1.93	15.36	42.94	26.19	31.40	53.38				
	combined MaxEnt	99.22	0.6118	99.94	31.90	65.42	1.93	14.26	49.84	34.58	38.65	56.67				
BY-TSX-2012	*hierarchical MaxEnt + SVM*	99.44	0.7693	99.87	81.35	83.05	0.48	1.28	9.52	16.65	0.00	28.34	1260	1634	207	547
	hierarchical MaxEnt + MaxEnt	99.42	0.7611	99.87	71.90	83.05	0.48	12.43	9.52	16.65	0.00	28.34				
	standard MaxEnt	98.93	0.6106	99.45	66.59	73.26	0.00	17.92	17.06	26.74	21.74	25.05				
	combined MaxEnt	99.24	0.6233	99.94	40.56	65.42	0.00	7.31	49.84	34.58	38.65	56.67				

Table 5-3: Intra-class classification accuracies (computed without considering the NGL validation points) for the HT targeted classification maps obtained applying the four considered methods to the BY-TSX-2011 [VV/VH] and BY-TSX-2012 [VV/VH] datasets using 1397 training samples for class 6410, 1385 for class 7120, 291 for class 7140 and 614 for class 7230.

		OA%	Kappa	PA%				# validation points			
				6410	7120	7140	7230	6410	7120	7140	7230
BY-TSX-2011	*hierarchical MaxEnt + SVM*	79.75	0.6667	94.91	99.49	0.00	9.18	1140	1362	207	392
	hierarchical MaxEnt + MaxEnt	74.91	0.6121	67.37	99.19	1.93	51.02	1140	1362	207	392
	standard MaxEnt	75.71	0.6030	64.53	100.0	2.82	32.94	719	1206	142	255
	combined MaxEnt	75.21	0.5967	63.61	100.0	3.15	32.91	632	1069	127	237
BY-TSX-2012	*hierarchical MaxEnt + SVM*	77.07	0.6272	89.91	99.63	0.48	1.79	1140	1362	207	392
	hierarchical MaxEnt + MaxEnt	75.20	0.6037	79.47	99.63	0.48	17.35	1140	1362	207	392
	standard MaxEnt	75.84	0.6180	80.29	100.0	0.00	23.90	1045	1197	162	410
	combined MaxEnt	78.45	0.6415	80.85	100.0	0.00	16.88	632	1069	127	237

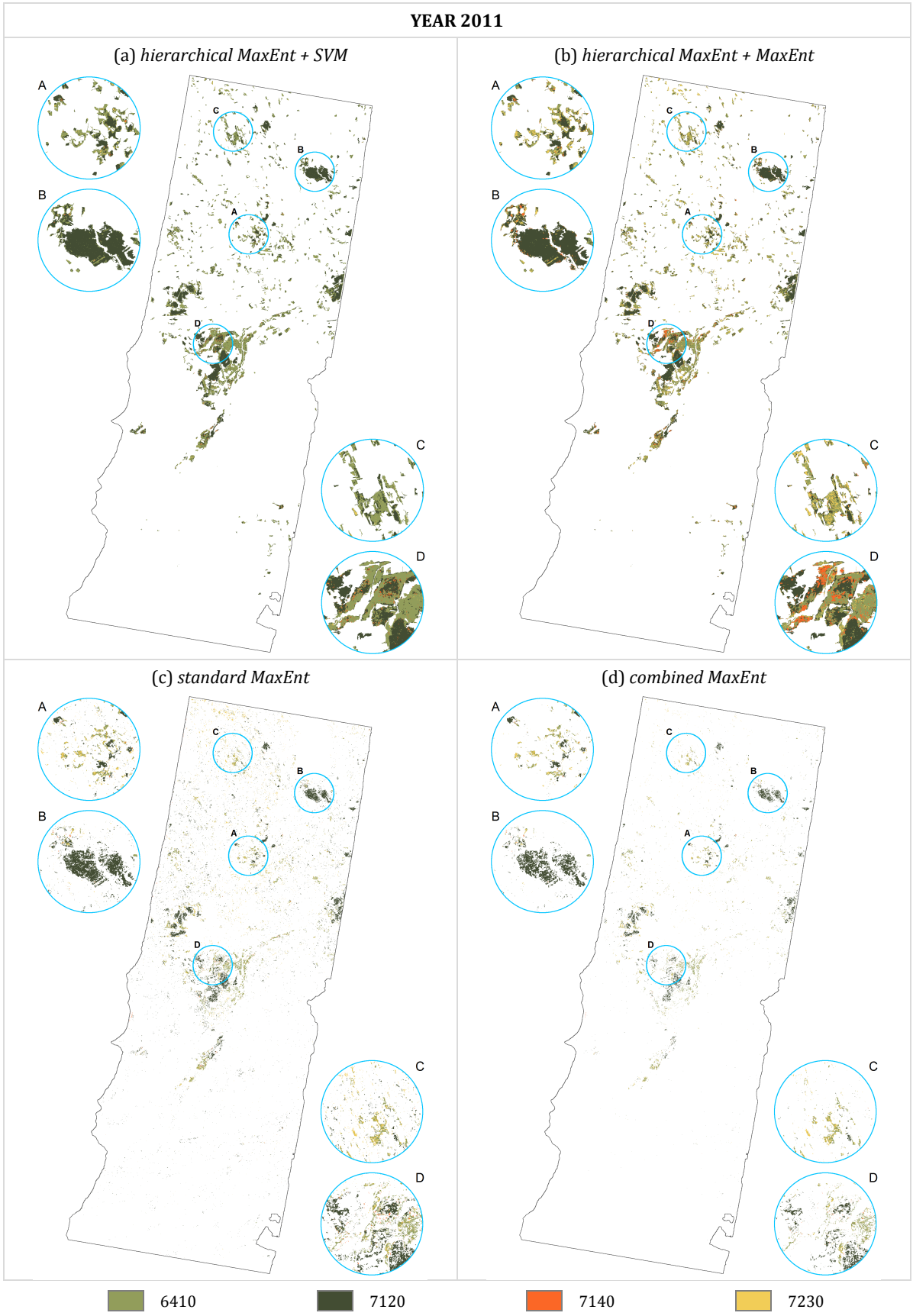

Figure 5-5: BY-TSX-2011 [VV/VH] dataset - HT targeted classification maps obtained using: (a) the *hierarchical MaxEnt + SVM*, (b) the *hierarchical MaxEnt + MaxEnt*, (c) the *standard MaxEnt*, and (d) the *combined MaxEnt* approaches.

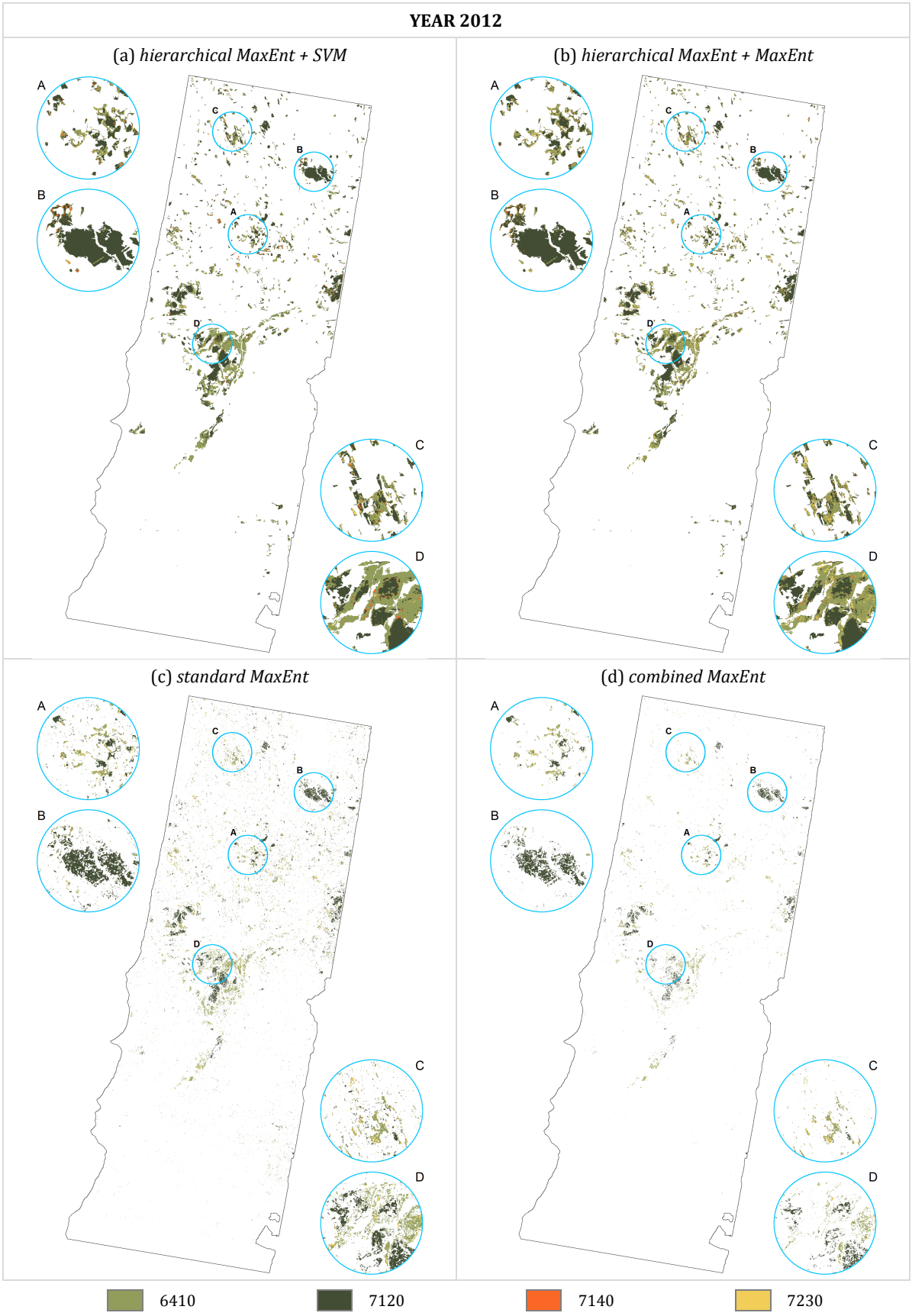

Figure 5-6: BY-TSX-2012 [VV/VH] dataset - HT targeted classification maps obtained using: (a) the *hierarchical MaxEnt + SVM*, (b) the *hierarchical MaxEnt + MaxEnt*, (c) the *standard MaxEnt*, and (d) the *combined MaxEnt* approaches.

and *combined MaxEnt* the corresponding values are always significantly higher with peaks over 56%. The class 7120 is the one exhibiting the highest PA% with all classification approaches and for both datasets with respect to the other classes. With the *hierarchical MaxEnt + SVM*, class 6410 has a higher PA% (85.87) while it is very low for 7140 (0.00) and 7230 (6.58). With the *hierarchical MaxEnt + MaxEnt*, the PA% is lower for class 6410 (60.95), but it slightly increases for classes 7140 (1.93) and 7230 (36.56). This behaviour allows inferring that the classes 6410, 7140 and 7230 are extremely similar in the analysed feature space. Accordingly, the intra-class accuracy for the four classification methods (i.e., computed without considering the NGL validation points) is given in Table 5-3 as a means for assessing how well they can discriminate the classes of interest among each other. Here, the number of considered validation points varies depending on whether the hierarchical or any of the standard approaches is considered (indeed, in the former case only those not wrongly categorised as NGL are preserved). Again, one can notice that either when the SVM or an ensemble of MaxEnt is applied, class 7120 exhibits very high PA% (> 99). Instead when the class 6410 shows higher PA% values those of classes 7140 and 7230 are lower or vice-versa. As for the results reported in Table 5-2, also here the *hierarchical MaxEnt + SVM* results in the best OA% and Kappa.

Based on this analysis, a further set of experimental trials has been performed by merging the classes 6410, 7140 and 7230 into a single "wet grasslands" class since they are all characterised by the presence of surface water compared to class 7120 where this does not occur. A new run of the four classification approaches has been then carried out accordingly performing, where applicable, a new model selection for the specific free parameters.

The resulting maps are shown in Figure 5-7 for 2011 and Figure 5-8 for 2012. The corresponding accuracy assessment is presented in Table 5-4. Generally, it can be seen that also in the two-class case each method provides similar results over the two years. Here, the hierarchical approaches result in Kappa higher than 0.85, hence again outperforming the standard ones which exhibit values ~0.15 to 0.2 lower. Specifically, the *hierarchical MaxEnt + MaxEnt* performs marginally better with OA% and Kappa equal to 99.66 and 0.8607 for 2011 and 99.67 and 0.8631 for 2012, respectively compared to 99.64 and 0.8530 for 2011 and 99.66 and 0.8575 for 2012 of the *hierarchical MaxEnt + SVM.* However, with both methods, the two targeted classes (i.e., wet grasslands and 7120) have PA% higher than 80, hence confirming the choice of merging the three classes 6410, 7140, and 7230 together. One can notice that the PA% of the wet grassland class is slightly higher in 2012 probably due to the availability of summer scenes which can have an influence on the classification since these classes are mowed or grazed by sheep at least once per year to prevent shrub encroachment.

As it can be seen in Figure 5-7 and Figure 5-8 the location and outline of the raised bogs (class 7120) are similar to the four-class case (Figure 5-5 and Figure 5-6). Indeed, the hierarchical approaches correctly define the areas of the class 7120 (Figure 5-7 (a) and (b) and Figure 5-8 (a) and (b)), while the results of the standard approaches again appear scattered due to the many missed alarms (Figure 5-7 (c) and (d) and Figure 5-8 (c) and (d)). This underestimation is also reflected in the percentage of unclassified samples (see Table 5-4), where the values of the *standard MaxEnt* and *combined MaxEnt* are considerably higher ranging from ~20% up to ~50%. Instead, both hierarchical methods always exhibit lower values (i.e., 13.65% for the wet grassland class and 16.65% for class 7120 in both years).

Table 5-4: HT 2-class targeted classification – Validation accuracies computed for the maps obtained applying the four considered methods to the BY-TSX-2011 [VV/VH] and BY-TSX-2012 [VV/VH] datasets using 1385 training samples for class 7120 and 2302 for the merger of the classes 6410, 7140 and 7230 [NGL validation samples: 288039].

		OA%	Kappa	PA%			% unclassified		# validation points		
				NGL	6410, 7140, 7230	7120	6410, 7140, 7230	7120	NGL	6410, 7140, 7230	7120
BY-TSX-2011	*hierarchical MaxEnt + SVM*	99.64	0.8530	99.87	80.64	83.11	13.65	16.65	288039	2014	1634
	hierarchical MaxEnt + MaxEnt	99.66	0.8607	99.87	83.66	82.71	13.65	16.65			
	standard MaxEnt	99.71	0.6783	99.71	54.92	73.81	44.59	26.19			
	combined MaxEnt	99.40	0.6987	99.94	49.30	65.42	50.55	34.58			
BY-TSX-2012	*hierarchical MaxEnt + SVM*	99.66	0.8575	99.87	82.37	82.93	13.65	16.65	288039	2014	1634
	hierarchical MaxEnt + MaxEnt	99.67	0.8631	99.87	84.21	83.05	13.65	16.65			
	standard MaxEnt	99.17	0.6948	99.45	79.99	73.26	19.71	26.74			
	combined MaxEnt	99.40	0.6990	99.94	49.40	65.42	50.55	34.58			

Table 5-5: Intra-class classification accuracies (computed without considering the NGL validation points) for the HT 2-class targeted classification maps obtained applying the four considered methods to the BY-TSX-2011 [VV/VH] and BY-TSX-2012 [VV/VH] datasets using 1385 training samples for class 7120 and 2302 for the merger of the classes 6410, 7140 and 7230.

		OA%	Kappa	PA%		# validation points	
				6410, 7140, 7230	7120	6410, 7140, 7230	7120
BY-TSX-2011	*hierarchical MaxEnt + SVM*	96.16	0.9228	93.39	99.71	1739	1362
	hierarchical MaxEnt + MaxEnt	97.90	0.9576	96.89	99.19	1739	1362
	standard MaxEnt	99.57	0.9914	99.10	100.00	1116	1206
	combined MaxEnt	99.85	0.9971	99.70	100.00	996	1069
BY-TSX-2012	*hierarchical MaxEnt + SVM*	97.19	0.9434	95.40	99.49	1739	1362
	hierarchical MaxEnt + MaxEnt	98.45	0.9687	97.53	99.63	1739	1362
	standard MaxEnt	99.79	0.9956	99.63	100.00	1617	1197
	combined MaxEnt	99.95	0.9990	99.90	100.00	996	1069

Comparing the intra-class accuracies presented in Table 5-5 (obtained by disregarding all samples categorised as NGL), all four approaches reach similar OA% and Kappa values (greater than 96.1 and 0.92, respectively). Highest values have been obtained with the *standard MaxEnt* and *combined MaxEnt*, thus confirming the effectiveness of the MaxEnt classifier in discriminating these two specific targeted classes.

By analysing the final maps of 2011 and 2012 (especially when using the hierarchical approaches), no significant differences can be appreciated - as expected - due to the limited temporal gap. As pointed out for the four-class case, considering that different numbers and dates of acquisitions have been analysed, this confirms the robustness of the proposed hierarchical system.

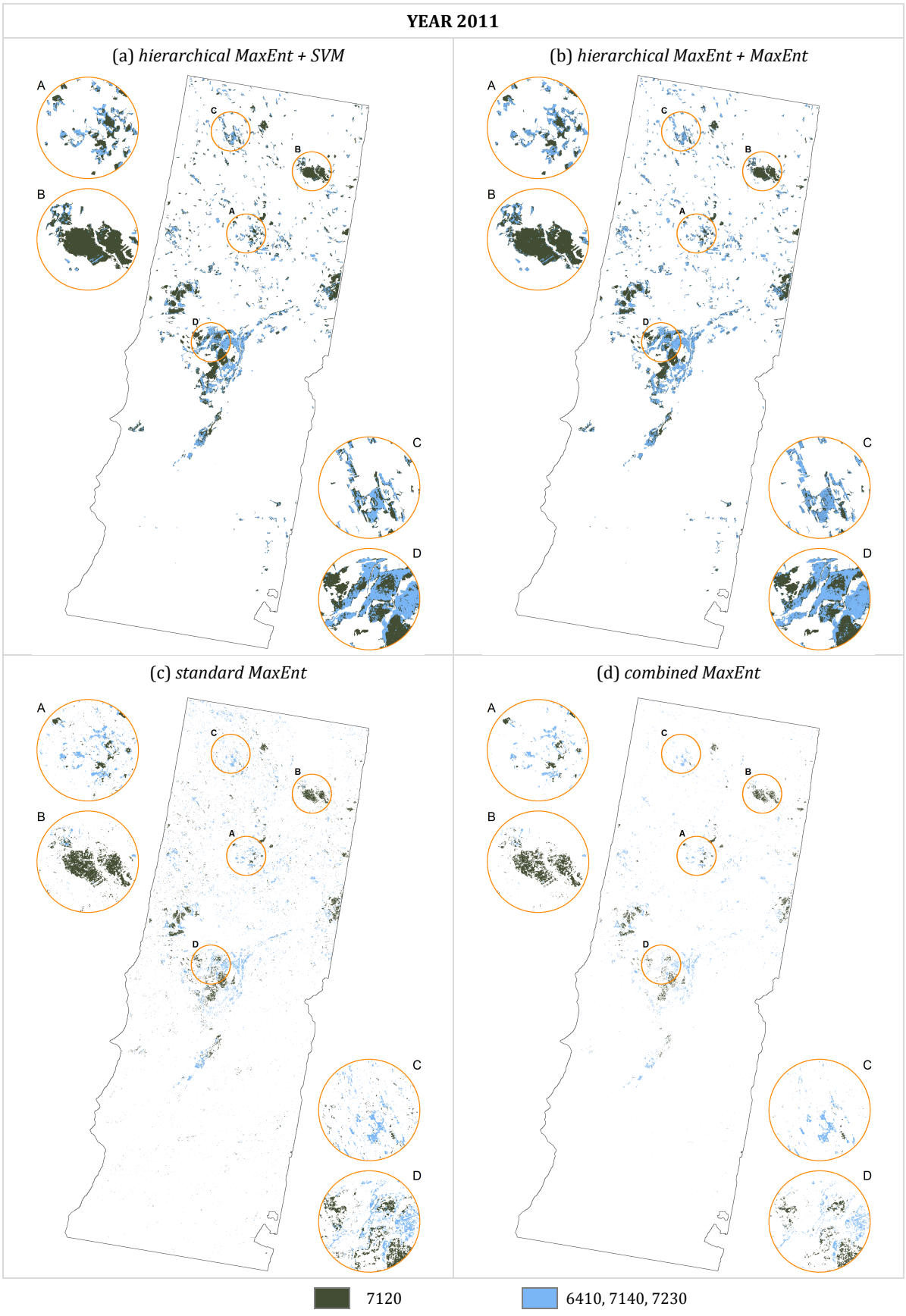

Figure 5-7: BY-TSX-2011 [VV/VH] dataset - HT two-class targeted classification maps obtained using: (a) the *hierarchical MaxEnt + SVM*, (b) the *hierarchical MaxEnt + MaxEnt*, (c) the *standard MaxEnt*, and (d) the *combined MaxEnt* approaches.

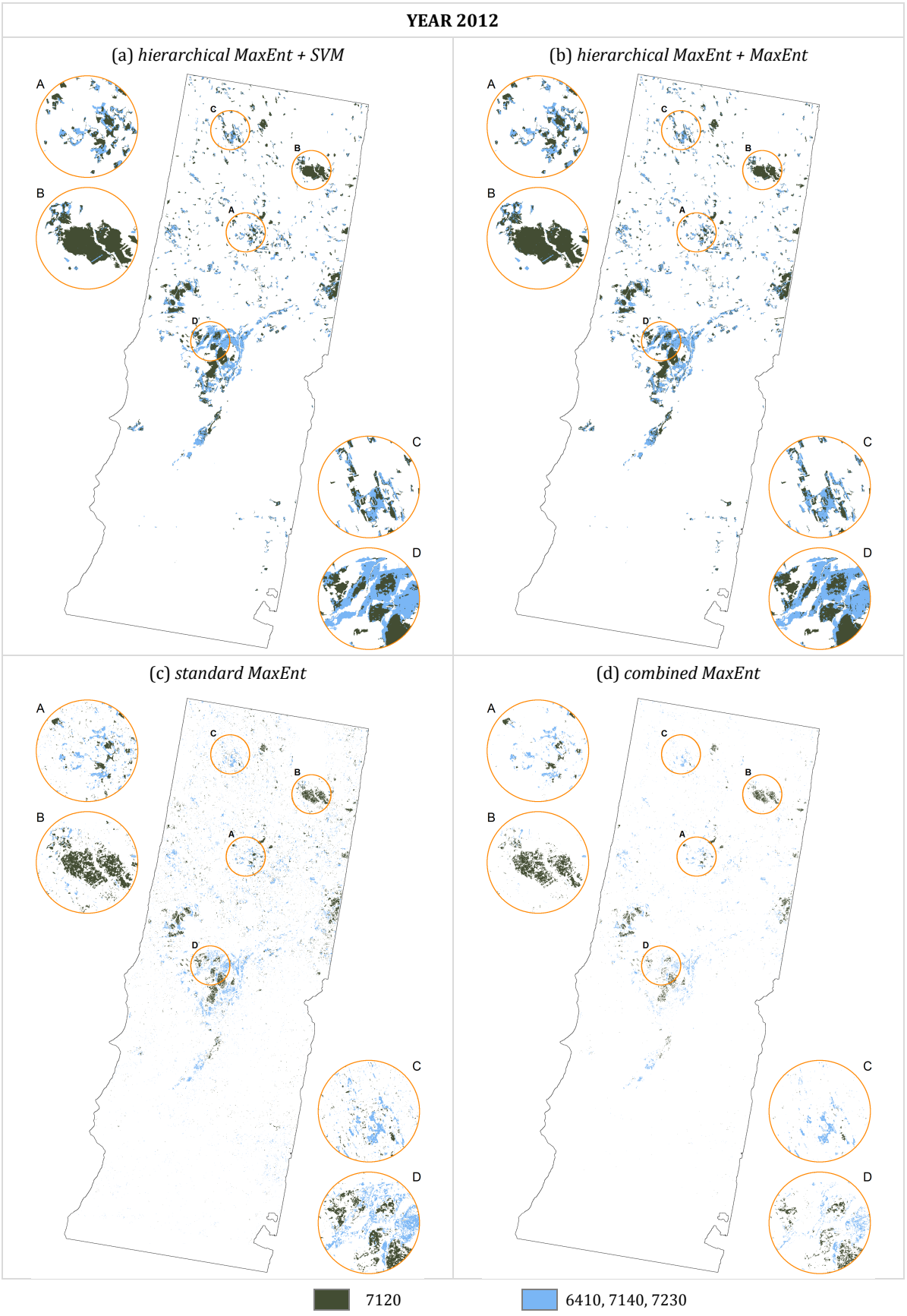

Figure 5-8: BY-TSX-2012 [VV/VH] dataset - HT two-class targeted classification maps obtained using: (a) the *hierarchical MaxEnt + SVM*, (b) the *hierarchical MaxEnt + MaxEnt*, (c) the *standard MaxEnt*, and (d) the *combined MaxEnt* approaches.

5.1.2. Bavaria test site: High Nature Value Grasslands

Two classes of interests were taken into consideration when addressing the targeted classification of HNV grasslands, namely HNVi and HNVe. However, contrarily to the Natura 2000 types discussed in the previous section, here their extent and type might vary from one year to another. As expected, the investigated problem proved to be particularly challenging due to the fact that the selected classes (especially the HNVi) exhibit a behaviour over time rather similar to that of several crops present in the study area.

In Table 5-6 and Table 5-7 the accuracies in outlining the grasslands of interest as a whole

Table 5-6: HNV one-class classification – Validation accuracies computed for the maps obtained applying the OC-SVM and MaxEnt (for different values of ρ) to the BY-TSX-2011 [VV/VH] datasets using the three defined spatial homogeneity rulesets. Results for the maps selected by qualitative assessment as most reliable for the OC-SVM and MaxEnt are highlighted in yellow and blue, respectively [GL training samples: 2241; GL validation samples: 2062; NGL validation samples: 287882].

		Rule I					Rule II					Rule III				
		OA%	Kappa	GL PA%	NGL PA%	AA%	OA%	Kappa	GL PA%	NGL PA%	AA%	OA%	Kappa	GL PA%	NGL PA%	AA%
BY-TSX-2011 [VV/VH]	OC-SVM	99.53	0.6603	64.94	99.78	82.36	99.53	0.6603	64.94	99.78	82.36	99.53	0.6603	64.94	99.78	82.36
	MaxEnt ρ = 0.001	80.54	0.0925	100.00	80.29	90.15	80.56	0.0926	100.00	80.32	90.16	80.62	0.0929	100.00	80.38	90.19
	MaxEnt ρ = 0.005	98.47	0.5407	74.23	98.78	86.50	98.47	0.5409	77.52	95.49	86.50	98.44	0.5199	69.68	98.80	84.24
	MaxEnt ρ = 0.01	98.82	0.5816	67.19	99.22	83.20	98.82	0.5817	67.19	99.22	83.20	98.83	0.5755	64.99	99.26	82.13
	MaxEnt ρ = 0.015	98.93	0.5929	63.60	99.38	81.49	98.93	0.5931	63.60	99.38	81.49	98.92	0.5826	61.40	99.40	80.40
	MaxEnt ρ = 0.025	98.95	0.5094	44.60	99.64	72.12	98.95	0.5098	72.01	72.23	72.12	98.94	0.4942	42.41	99.65	71.03
	MaxEnt ρ = 0.05	99.10	0.5151	38.87	99.86	69.37	99.10	0.5156	38.87	99.86	69.37	99.08	0.4946	36.68	99.87	68.27
	MaxEnt ρ = 0.075	99.12	0.4969	35.25	99.93	67.59	99.12	0.4974	35.25	99.93	67.59	99.10	0.4742	33.06	99.93	66.50
	MaxEnt ρ = 0.1	99.02	0.3918	25.71	99.95	62.83	99.02	0.3918	25.71	99.95	62.83	99.03	0.3939	25.71	99.95	62.83
	MaxEnt ρ = 0.125	98.96	0.3209	19.98	99.96	59.97	98.96	0.3209	19.98	99.96	59.97	98.97	0.3227	19.98	99.97	59.97
	MaxEnt ρ = 0.15	98.96	0.3220	19.98	99.96	59.97	98.96	0.3220	19.98	99.96	59.97	98.97	0.3238	19.98	99.97	59.98

Table 5-7: HNV one-class classification – Validation accuracies computed for the maps obtained applying the OC-SVM and MaxEnt (for different values of ρ) to the BY-TSX-2012 [VV/VH] datasets using the three defined spatial homogeneity rulesets. Results for the maps selected by qualitative assessment as most reliable for the OC-SVM and MaxEnt are highlighted in yellow and blue, respectively [GL training samples: 4525; GL validation samples: 4334; NGL validation samples: 287882].

		Rule I					Rule II					Rule III				
		OA%	Kappa	GL PA%	NGL PA%	AA%	OA%	Kappa	GL PA%	NGL PA%	AA%	OA%	Kappa	GL PA%	NGL PA%	AA%
BY-TSX-2012 [VV/VH]	OC-SVM	98.74	0.6459	79.33	99.04	89.18	98.74	0.6459	79.33	99.04	89.18	98.74	0.6459	79.33	99.04	89.18
	MaxEnt ρ = 0.001	91.88	0.2044	92.54	91.88	92.21	91.90	0.2047	92.54	91.89	92.22	91.94	0.2015	90.35	91.96	91.16
	MaxEnt ρ = 0.005	95.42	0.2963	82.48	95.58	89.03	95.43	0.2968	82.48	96.60	89.54	95.42	0.2906	80.29	95.61	87.95
	MaxEnt ρ = 0.01	96.77	0.3715	80.29	96.98	88.64	96.78	0.3718	80.29	96.98	88.64	96.73	0.3543	75.74	96.99	86.37
	MaxEnt ρ = 0.015	97.86	0.4723	79.28	98.10	88.69	97.87	0.4725	79.28	98.10	88.69	97.82	0.4519	74.73	98.11	86.42
	MaxEnt ρ = 0.025	98.08	0.4652	69.00	98.45	83.73	98.08	0.4652	69.00	98.45	83.73	98.03	0.4416	64.45	98.46	81.45
	MaxEnt ρ = 0.05	98.31	0.3905	44.76	98.99	71.88	98.31	0.3907	44.76	98.99	71.88	98.31	0.3773	42.41	99.02	70.71
	MaxEnt ρ = 0.075	98.63	0.4046	38.29	99.39	68.84	98.63	0.4049	38.29	99.40	68.85	98.65	0.4091	38.29	99.42	68.86
	MaxEnt ρ = 0.1	98.73	0.4032	35.14	99.54	67.34	98.73	0.4035	35.14	99.54	67.34	98.76	0.4084	35.14	99.56	67.35
	MaxEnt ρ = 0.125	98.87	0.4320	35.14	99.68	67.41	98.87	0.4323	35.14	99.68	67.41	98.90	0.4388	35.14	99.71	67.42
	MaxEnt ρ = 0.15	98.89	0.4369	35.14	99.70	67.42	98.89	0.4373	35.14	99.70	67.42	98.92	0.4427	35.14	99.72	67.43

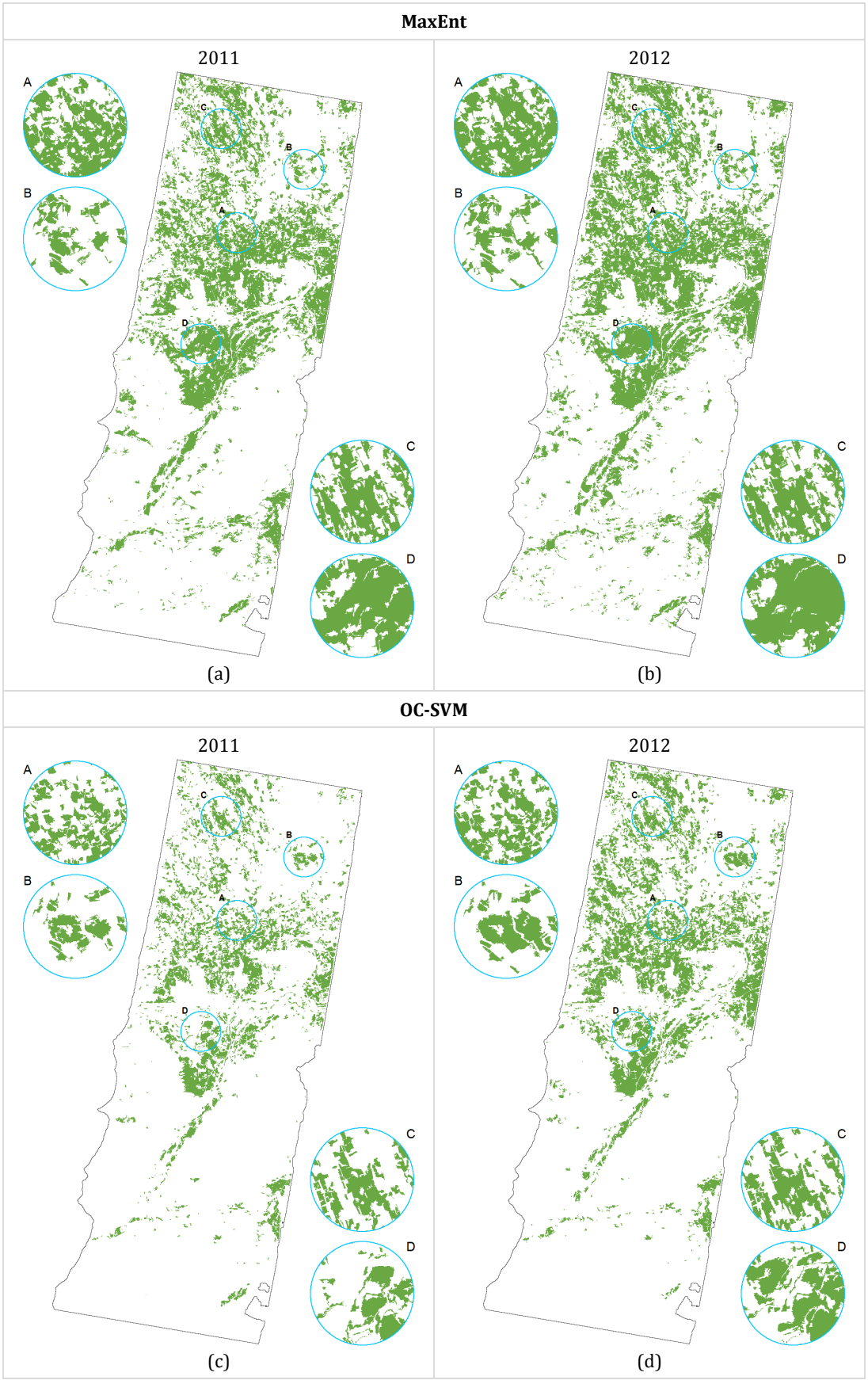

Figure 5-9: HNV one-class classification maps selected using the MaxEnt and OC-SVM for the BY-TSX-2011 [VV/VH] (a and c, respectively) and BY-TSX-2012 [VV/VH] (b and d, respectively) datasets.

obtained by both the MaxEnt and OC-SVM are given for 2011 and 2012, respectively, while the corresponding one-class classification maps are shown in Figure 5-9. According to the proposed strategy to determine the most suitable MaxEnt significance level, for both years $\rho = 0.005$ was selected in combination with Rule II. Again, such a strategy proved to guarantee a good trade-off between high PA% values for both the GL and NGL classes and relatively high OA%. Especially, it is possible to notice that, instead, for $\rho = 0.001$ a consistent decrease for both OA% and Kappa occurs due to the extreme overestimation of the GL class. However, in this case the MaxEnt did not provide in general very high values of Kappa compared to the Natura 2000 problem (i.e., ~0.54 and ~0.3 with $\rho = 0.005$ for 2011 and 2012, respectively), due to the fact that, given the high similarity between the targeted classes and other land-cover types in the study site, to obtain a good characterisation of the GL class costs some underestimation of the NGL areas.

Regarding the OC-SVM, the optimal values for the free parameters chosen using the employed grid-search-based strategy proved to be $(\gamma = 10, \nu = 0.1)$ for 2011 and $(\gamma = 20, \nu = 0.1)$ for 2012. Again, no differences occurred in the classification maps derived with the three considered rulesets as the OC-SVM tends itself yet to entirely associate homogenous areas with the same class (either GL or NGL). By analysing the corresponding accuracies, one can see that the performances in terms of OA% and Kappa are better compared to the MaxEnt, especially for 2012. However, this is mainly due to the underestimation of the GL class for which a lower PA%,

Table 5-8: HNV targeted classification – Validation accuracies computed for the maps obtained applying the three considered methods to the BY-TSX-2011 [VV/VH] dataset (using 657 training samples for class HNVi and 1566 for class HNVe) and the BY-TSX-2012 [VV/VH] dataset (using 3077 training samples for class HNVi and 1448 for class HNVe).

		OA%	Kappa	PA%			% unclassified		# validation points		
				NGL	HNVi	HNVe	HNVi	HNVe	NGL	HNVi	HNVe
BY-TSX-2011	*hierarchical MaxEnt + SVM*	98.66	0.4814	95.49	64.18	88.52	0.00	0.05	287993	564	1498
	hierarchical MaxEnt + MaxEnt	98.82	0.5164	95.49	64.54	89.85	0.00	0.05			
	standard MaxEnt	74.16	0.0245	74.51	90.96	0.00	1.24	0.00			
BY-TSX-2012	*hierarchical MaxEnt + SVM*	95.48	0.3665	96.60	96.99	72.53	0.01	0.04	287993	2656	1678
	hierarchical MaxEnt + MaxEnt	95.86	0.3848	96.60	93.86	71.22	0.01	0.04			
	standard MaxEnt	56.90	0.0208	57.28	42.24	15.55	0.19	0.06			

Table 5-9: Intra-class classification accuracies (computed without considering the NGL validation points) for the HNV targeted classification maps obtained applying the three considered methods to the BY-TSX-2011 [VV/VH] dataset (using 657 training samples for class HNVi and 1566 for class HNVe) and the BY-TSX-2012 [VV/VH] dataset (using 3077 training samples for class HNVi and 1448 for class HNVe).

		OA%	Kappa	PA%		# validation points	
				HNVi	HNVe	HNVi	HNVe
BY-TSX-2011	*hierarchical MaxEnt + SVM*	84.82	0.6048	64.18	92.99	564	1426
	hierarchical MaxEnt + MaxEnt	85.93	0.6298	64.54	94.39	564	1426
	standard MaxEnt	24.96	-0.0434	92.10	0.00	557	1498
BY-TSX-2012	*hierarchical MaxEnt + SVM*	89.33	0.7638	97.58	75.78	2640	1606
	hierarchical MaxEnt + MaxEnt	86.86	0.7113	94.43	74.41	2640	1606
	standard MaxEnt	31.95	-0.4160	42.32	15.56	2651	1677

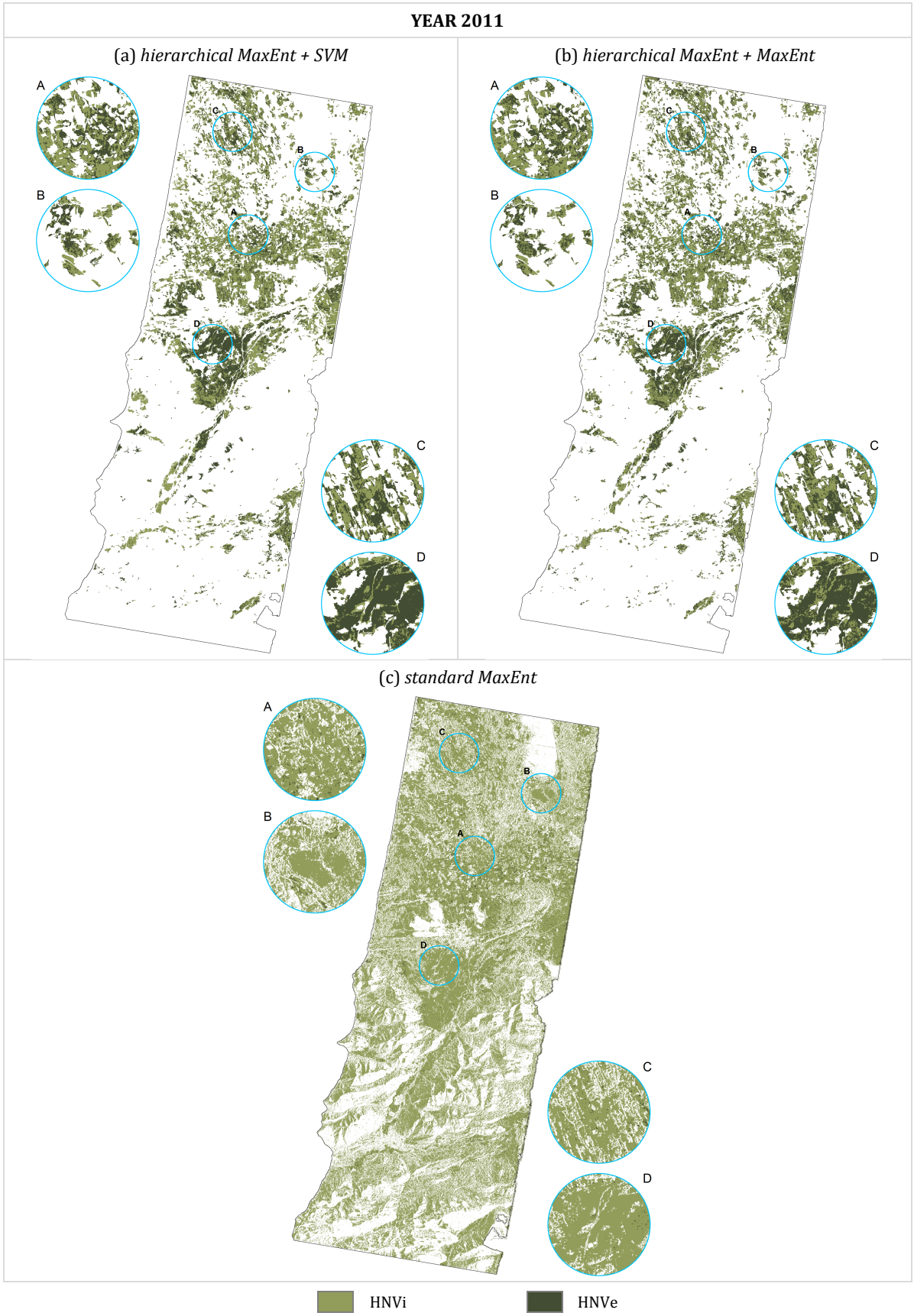

Figure 5-10: BY-TSX-2011 [VV/VH] dataset - HNV targeted classification maps obtained using: (a) the *hierarchical MaxEnt + SVM*, (b) the *hierarchical MaxEnt + MaxEnt*, and (c) the *standard MaxEnt* approaches.

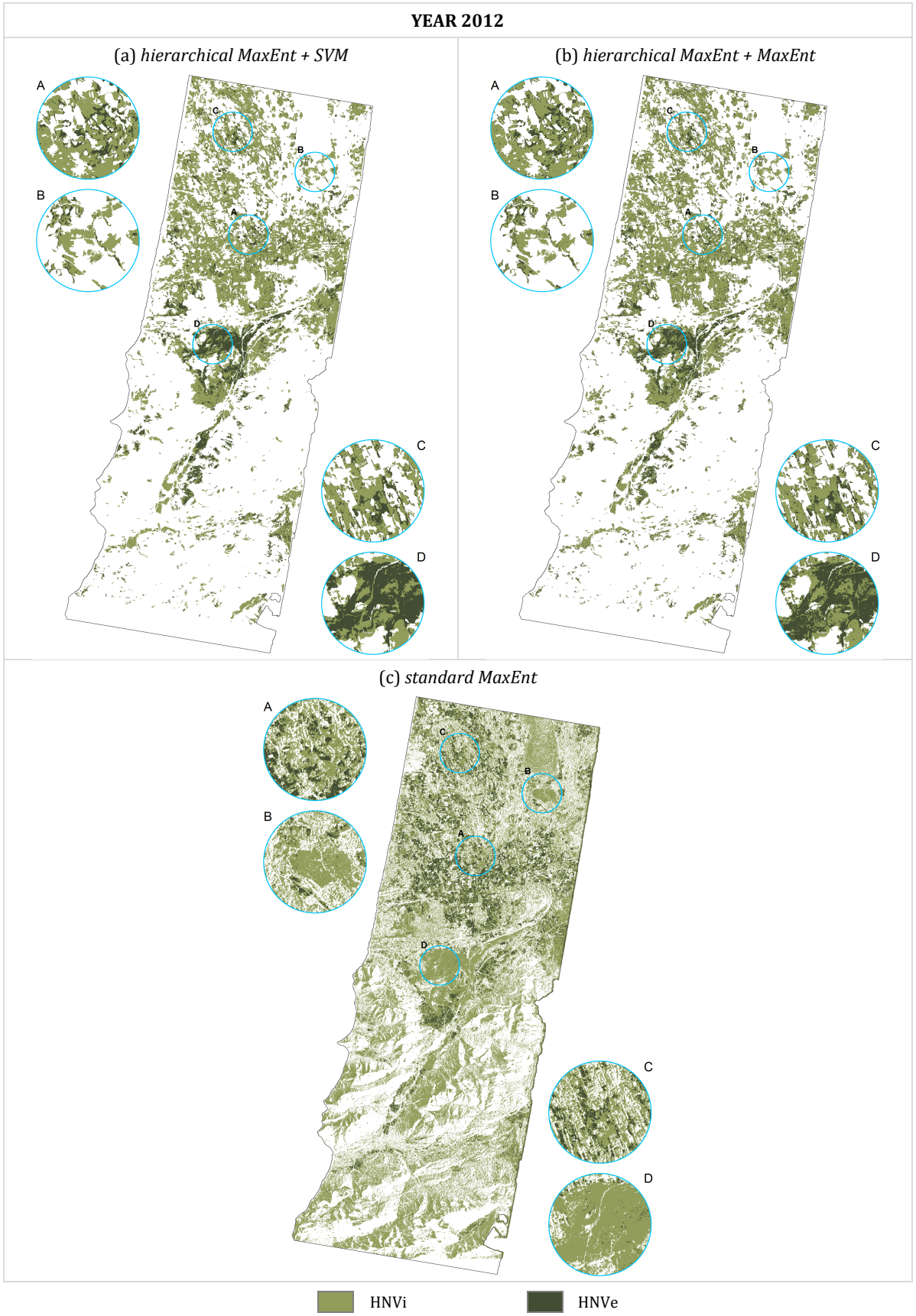

Figure 5-11: BY-TSX-2012 [VV/VH] dataset - HNV targeted classification maps obtained using: (a) the *hierarchical MaxEnt + SVM*, (b) the *hierarchical MaxEnt + MaxEnt*, and (c) the *standard MaxEnt* approaches.

(and hence lower AA%) is obtained. Since this also occurs for several grasslands from which training samples were taken (e.g., zoom D in Figure 5-9), by qualitative assessment the MaxEnt map was preferred.

The final targeted classification maps derived with the *hierarchical MaxEnt + SVM*, *hierarchical MaxEnt + MaxEnt* and *standard MaxEnt* approaches are shown in Figure 5-10 and Figure 5-11. Moreover, the results of the corresponding accuracy assessment are presented in Table 5-8, from which one can notice that all classifiers performed better on the BY-TSX-2011 [VV/VH] dataset. In particular, the hierarchical approaches show OA% greater than 98 and Kappa greater than 0.48 (i.e., about +3 and +0.1 compared to the BY-TSX-2012 [VV/VH] dataset, respectively). Specifically, the *hierarchical MaxEnt + MaxEnt* provided values ~0.02 to ~0.03 higher in terms of Kappa with respect to the *hierarchical MaxEnt + SVM* (for which the optimal parameters proved to be ($\gamma = 0.01, C = 5$) for 2011 and ($\gamma = 0.5, C = 1$) for 2012). In both cases, while the PA% is higher in 2011 for the HNVe compared to the HNVi class (~89 against ~64, respectively), the opposite occurs for 2012 (slightly higher than 70 and greater than 93, respectively); instead, the NGL PA% is between 95.60 and 98.94, hence confirming the slight overestimation of the one-class GL map, which resulted in very low percentages of samples being classified as NGL by all classifiers (i.e., between 0.00 and 1.24).

On the contrary, the *standard MaxEnt* exhibited very poor performances, with OA% and Kappa equal to 74.16 and 0.0245 for 2011 and 50.89 and 0.0208 for 2012, respectively. This can also be qualitatively assessed by analysing the classification maps in Figure 5-10 (c) and Figure 5-11 (c), where a consistent overestimation in agricultural fields, forest, water and mountainous regions is clearly visible. Here, protected areas (which are also part of this study) are classified as HNVi in 2012 (see zoom B and D), while they should rather be categorised as HNVe since they represent grasslands with extremely high nature value as described in section 4.2.2. Such behaviour resulted in low PA% values for the HNVe (i.e., 0.00 for 2011 and 15.55 for 2012), as well as for the NGL class (i.e., 74.51 for 2011 and 57.28 for 2012), whereas for the HNVi class they are high only for 2011 (i.e., 90.96 compared to 42.24 in 2012).

Analysing the intra-class quantitative assessment reported in Table 5-9, it can be seen that all three approaches provided better results for 2012 in terms of OA% and Kappa with respect to those obtained for 2011. Here, again the hierarchical approaches performed better in discriminating the two targeted classes between each other with OA% over ~85 and Kappa values between ~0.6 and ~0.76, showing greater PA% values for HNVe in 2011 (≥92.99) and for HNVi in 2012 (≥94.43). Instead, the *standard MaxEnt* exhibited poor performances with OA% below ~32 and Kappa below 0.00, as well as rather low PA% values (only in 2011 it results higher than 92 simply due to the consistent overestimation).

As mentioned above, despite fewer training data were available (especially for the HNVi class), performances were generally better in 2011. However, it is worth noting that the corresponding dataset contains acquisitions in early spring (i.e., March and beginning of April) as well as between mid-April and the end of May, which are missing in the BY-TSX-2012 [VV/VH] dataset. These seem to be rather important for discriminating the targeted classes from agricultural fields, such as maize or root crops. Nonetheless, the classification maps derived from the 2012 data had on average marginally higher intra-class accuracies. This is due on the one hand to the higher amount of training points available for the HNVi class and on the other hand to the higher

amount of summer scenes in 2012, especially in July, compared to the BY-TSX-2011 [VV/VH] dataset (where no scenes were available between 12th June and 4th August).

5.1.3. Mecklenburg test site: Natura 2000

As discussed in section 4.2.2, the AOIs of this work have been defined by thoroughly examining the Natura 2000 database of the FFH directive (EEA, 2010) with respect to the availability and extent of the four considered classes of interest in both Bavaria and Mecklenburg. However, in the latter case the expected size of the selected targeted classes did not correspond to that observed during the field campaign, proving a potential overestimation by the database. In this framework, within the Mecklenburg AOI it was possible to solely collect reference data for the targeted classes 7120 and 7140. Nevertheless, while for the former overall 1160 training and 744 validation samples have been derived after the extension procedure described in section 4.2.2, for the latter only 48 training and 52 validation samples were finally defined, hence making the resulting targeted classification problem particularly complex. However, it is worth noting that this represented an interesting benchmark for the proposed hierarchical approaches under extreme conditions.

As explained in section 5.1.1 for the Bavaria Natura 2000 experimental analysis, despite the temporal stability of the addressed targeted classes, also here different one-class classification maps have been separately derived for 2011 and 2012 with both the MaxEnt and OC-SVM classifiers and, afterwards, combined by excluding pixels associated with the GL class in only one of them (see Figure 5-12). The corresponding quantitative assessment is given in Table 5-10.

The optimal parameters obtained after the model selection for the OC-SVM were $(\gamma = 4, \nu = 0.1)$ for 2011 and $(\gamma = 8, \nu = 0.1)$ for 2012, without any appreciable difference between the three

Table 5-10: HT one-class classification – Validation accuracies computed for the maps obtained applying the OC-SVM and MaxEnt (for different values of ρ) to the MV-TSX-2011 [VV/VH] and MV-TSX-2012 [VV/VH] datasets using the three defined spatial homogeneity rulesets. Results for the maps selected by qualitative assessment as most reliable for the OC-SVM and MaxEnt are highlighted in yellow and blue, respectively. At the bottom, accuracies are also provided for the maps derived combining the ones selected for 2011 and 2012 for each classifier [GL training samples: 1208; GL validation samples: 796; NGL validation samples: 349195].

		Rule I					Rule II					Rule III				
		OA%	Kappa	GL PA%	NGL PA%	AA%	OA%	Kappa	GL PA%	NGL PA%	AA%	OA%	Kappa	GL PA%	NGL PA%	AA%
MV-TSX-2011 [VV/VH]	OC-SVM	92.76	0.0120	25.26	92.93	59.09	92.76	0.0120	25.26	92.93	59.09	92.76	0.0120	25.26	92.93	59.09
	MaxEnt ρ = 0.025	99.61	0.5183	87.43	99.64	93.53	99.61	0.5186	87.43	99.64	93.53	99.62	0.5257	87.43	93.54	90.05
	MaxEnt ρ = 0.05	99.85	0.7381	87.43	99.88	93.65	99.85	0.7385	87.43	99.88	93.65	99.86	0.7470	87.43	93.66	82.91
	MaxEnt ρ = 0.075	99.87	0.6441	49.47	99.99	74.73	99.87	0.6446	49.47	99.99	74.73	99.87	0.6446	49.47	74.73	80.47
	MaxEnt ρ = 0.1	99.81	0.3712	23.62	99.99	61.81	99.79	0.3715	23.62	99.99	61.81	99.81	0.3726	23.62	61.81	79.24
	MaxEnt ρ = 0.125	99.81	0.3719	23.62	99.99	61.81	99.81	0.3723	23.62	99.99	61.81	99.81	0.3733	23.62	61.81	79.24
	MaxEnt ρ = 0.15	99.81	0.3719	23.62	99.99	61.81	99.81	0.3723	23.62	99.99	61.81	99.81	0.3733	23.62	61.81	78.33
MV-TSX-2012 [VV/VH]	OC-SVM	98.50	0.0717	25.26	98.67	61.97	98.50	0.0717	25.29	98.67	61.97	98.50	0.0717	25.26	98.67	61.97
	MaxEnt ρ = 0.025	85.44	0.0248	91.07	85.42	88.25	85.44	0.0248	91.07	85.42	88.25	85.48	0.0249	91.07	88.27	90.59
	MaxEnt ρ = 0.05	94.53	0.0690	89.07	94.54	91.81	94.53	0.0690	89.07	94.54	91.81	94.56	0.0694	89.07	91.82	86.22
	MaxEnt ρ = 0.075	97.44	0.1407	89.07	97.46	93.26	97.44	0.1408	89.07	97.46	93.26	97.46	0.1417	89.07	93.27	84.46
	MaxEnt ρ = 0.1	98.99	0.2264	61.57	99.09	80.33	99.00	0.2270	61.57	99.09	80.33	99.00	0.2280	61.57	80.33	82.60
	MaxEnt ρ = 0.125	99.71	0.5049	61.57	99.80	80.69	99.71	0.5068	61.57	99.80	80.69	99.66	0.3475	37.96	68.88	81.75
	MaxEnt ρ = 0.15	99.75	0.5395	61.57	99.84	80.71	99.75	0.5412	61.57	99.84	80.71	99.69	0.3734	37.96	68.90	78.19
OC-SVM 2011-2012							98.68	0.0816	25.26	98.86	62.06					
MaxEnt 2011-2012							99.92	0.8456	93.47	96.70	95.08					

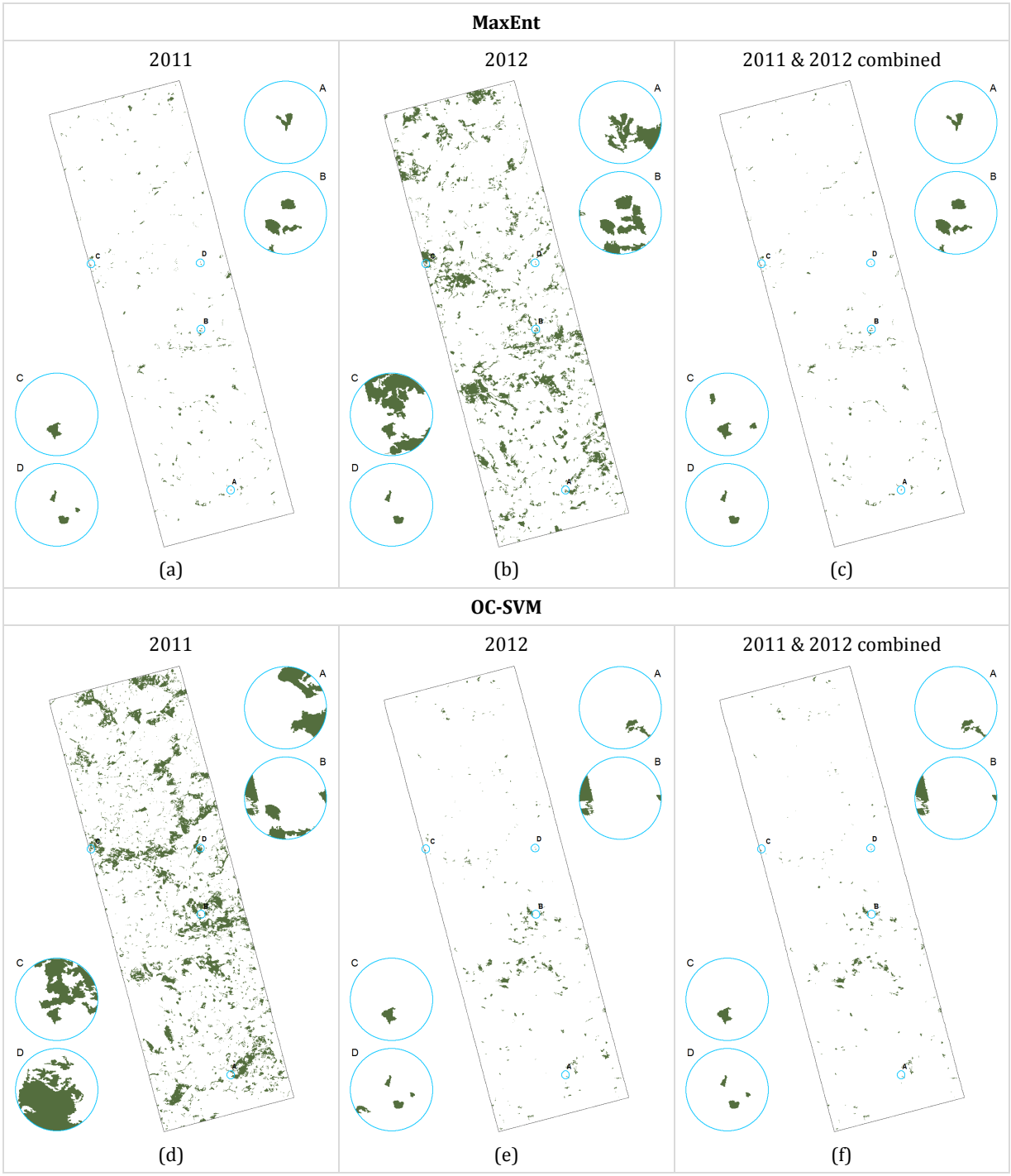

Figure 5-12: HT one-class classification maps selected using the MaxEnt and OC-SVM for the MV-TSX-2011 [VV/VH] (a and d, respectively) and MV-TSX-2012 [VV/VH] (b and e, respectively) datasets, along with their combinations (c and f, respectively).

spatial homogeneity rulesets. With respect to the Bavaria datasets, in this case it is evident that for both years the OC-SVM provided poor performances with Kappa and AA% close to 0 and 60, respectively, due to consistent misclassification of both GL areas as NGL and vice-versa (see Figure 5-12 (d) and (e)).

This phenomenon is significantly more pronounced in the 2011 classification map (where large forested areas have been wrongly categorized as GL throughout the entire study site), despite accuracies are almost identical in 2012 due to the limited number of available validation

samples. When combining the two maps, the areas solely overestimated in 2011 disappear; nevertheless, the final accuracies do not vary (Kappa is equal to 0.0816 and still many NGL areas located in the middle of the AOI remain wrongly classified) but rather only a negligible improvement in the PA% of the NGL class occurs.

The MaxEnt, for which $\rho = 0.05$ in combination with Rule II was chosen for both years, proved instead particularly effective when applied to the MV-TSX-2011 [VV/VH] dataset, exhibiting very good discrimination capabilities (with Kappa and AA% equal to 0.7385 and 93.65, respectively). This is also confirmed by the extent of the grassland areas outlined in Figure 5-12 (a), which is compatible to that assessed during the field campaigns. On the contrary, strong overestimation of the GL class occurred for the MV-TSX-2012 [VV/VH] dataset, as highlighted by the rather high corresponding PA% (89.07), and, especially, the low Kappa (only 0.069). However, this can be reasonably attributed to the fact that only seven scenes were available and not even equally distributed over time, since four of them have been acquired between mid-May and June, while the remaining three between July and September. This prevented a reliable modelling of the GL probability conditional density due to the very similar behaviour of different crops at such stages of the growing season. Nonetheless, by combining the 2011 and 2012 maps it was possible to obtain very good results especially in terms of Kappa (0.8456) and AA% (95.08),

Table 5-11: HT targeted classification – Validation accuracies computed for the maps obtained applying the four considered methods to the MV-TSX-2011 [VV/VH] and MV-TSX-2012 [VV/VH] datasets using 1160 training samples for class 7120 and 48 for class 7140.

		OA%	Kappa	PA%			% unclassified		# validation points		
				NGL	7120	7140	7120	7140	NGL	7120	7140
MV-TSX-2011	*hierarchical MaxEnt + SVM*	99.89	0.8076	96.70	98.92	5.61	0.00	28.97	349195	744	107
	hierarchical MaxEnt + MaxEnt	99.91	0.8387	96.70	99.87	55.14	0.00	28.97			
	standard MaxEnt	97.34	0.0788	97.46	54.97	0.00	45.03	81.31			
	combined MaxEnt	98.99	0.1450	99.15	41.13	0.00	58.87	99.07			
MV-TSX-2012	*hierarchical MaxEnt + SVM*	99.89	0.8086	96.70	100.00	0.00	0.00	28.97	349195	744	107
	hierarchical MaxEnt + MaxEnt	99.89	0.8086	96.70	100.00	0.00	0.00	28.97			
	standard MaxEnt	91.69	0.0304	91.76	69.89	0.00	30.11	94.39			
	combined MaxEnt	98.99	0.1450	99.15	41.13	0.00	58.87	99.07			

Table 5-12: Intra-class classification accuracies (computed without considering the NGL validation points) for the HT targeted classification maps obtained applying the four considered methods to the MV-TSX-2011 [VV/VH] and MV-TSX-2012 [VV/VH] datasets using 1160 training samples for class 7120 and 48 for class 7140.

		OA%	Kappa	PA%		# validation points	
				7120	7140	7120	7140
MV-TSX-2011	*hierarchical MaxEnt + SVM*	90.49	0.1076	98.92	7.89	744	76
	hierarchical MaxEnt + MaxEnt	97.80	0.8559	99.87	77.63	744	76
	standard MaxEnt	95.34	0.0000	100.00	0.00	409	20
	combined MaxEnt	99.67	0.0000	100.00	0.00	306	1
MV-TSX-2012	*hierarchical MaxEnt + SVM*	90.73	0.0000	100.00	0.00	744	76
	hierarchical MaxEnt + MaxEnt	90.73	0.0000	100.00	0.00	744	76
	standard MaxEnt	98.86	0.0000	100.00	0.00	520	6
	combined MaxEnt	99.67	0.0000	100.00	0.00	306	1

even better than those obtained for 2011 alone. This supports the choice of selecting the MaxEnt to be applied in the first phase of the developed hierarchical system.

The classification maps obtained with the *hierarchical MaxEnt + SVM*, *hierarchical MaxEnt + MaxEnt*, *standard MaxEnt* and *combined MaxEnt* (where pixels only associated with any of the targeted classes by the *standard MaxEnt* in both years are kept) are depicted in Figure 5-13 for 2011 and in Figure 5-14 for 2012, while the results of the corresponding accuracy assessment are reported in Table 5-11. At first glance, one can immediately notice that although the OA% are relatively similar for each classifier over the two years, the Kappa values differ consistently. Indeed, the hierarchical approaches reach values greater than 0.8 for both datasets, whereas those obtained with the standard methods drop below 0.15. Specifically, the *hierarchical MaxEnt + MaxEnt* performs slightly better with a Kappa of 0.8387 and an OA% of 99.91 compared to the *hierarchical MaxEnt + SVM* (whose Kappa and OA% are equal to 0.8076 and 99.89, respectively), for which the optimal parameters were $(\gamma = 0.08, C = 75)$ for 2011 and $(\gamma = 0.1, C = 1)$ for 2012.

Despite the lower number of training samples compared to the Bavarian case, class 7120 is anyhow effectively outlined in the maps generated using the hierarchical approaches (see Figure 5-13 (a) and (b) and Figure 5-14 (a) and (b)). This is also reflected by the fact that none of the corresponding validation samples was wrongly classified as NGL either by the *hierarchical MaxEnt + SVM* or *hierarchical MaxEnt + MaxEnt* in both years. On the contrary, the *standard MaxEnt* often misclassified forested areas as class 7120 (see Figure 5-13 (c) and Figure 5-14 (c)); however, such phenomenon could be only slightly reduced with the *combined MaxEnt* approach (see Figure 5-13 (d) and Figure 5-14 (d)). The corresponding PA% reflects this behaviour with values ranging from 41.14 to 69.89. Furthermore, between 30.11% and 58.87% of the samples of class 7120 have been wrongly classified as NGL (see Table 5-11) with the standard approaches.

As concerns class 7140, solely the *hierarchical MaxEnt + MaxEnt* approach was capable of correctly identifying the corresponding validation reference areas in the MV-TSX-2011 [VV/VH] dataset (see for instance zoom C), despite 28.97% of the samples have been anyhow categorized as NGL. Instead, the other approaches resulted in poor performances, with PA% lower than 6 (even the *hierarchical MaxEnt + SVM* correctly identified just few pixels). Besides, in 2012 none of the classifiers could associate with class 7140 any of the grassland fields from which validation points have been drawn. Nevertheless, such behaviour is actually not completely unexpected. Indeed, it can be again related to the reduced number of available TSX data already discussed when describing the one-class classification above; in particular, it emerges that the limited amount of summer scenes does not probably allow to effectively discriminate class 7140 from 7120. In this context, when analysing the intra-class accuracies reported in Table 5-12, it can be noticed that only the *hierarchical MaxEnt + MaxEnt* approach was able to properly differentiate the two considered classes of interest in the 2011 dataset, exhibiting an OA% and Kappa equal to 97.80 and 0.8559, respectively. For the remaining classifiers and the complete set of 2012 experiments, class 7140 was entirely misclassified as 7120, hence, resulting in very poor Kappa values between 0.00 and 0.1076. Nevertheless, it is worth pointing out again that these low accuracies are reasonably mostly due both to the few training data and, for 2012, the few scenes available rather than intrinsic limitations of the presented methodology.

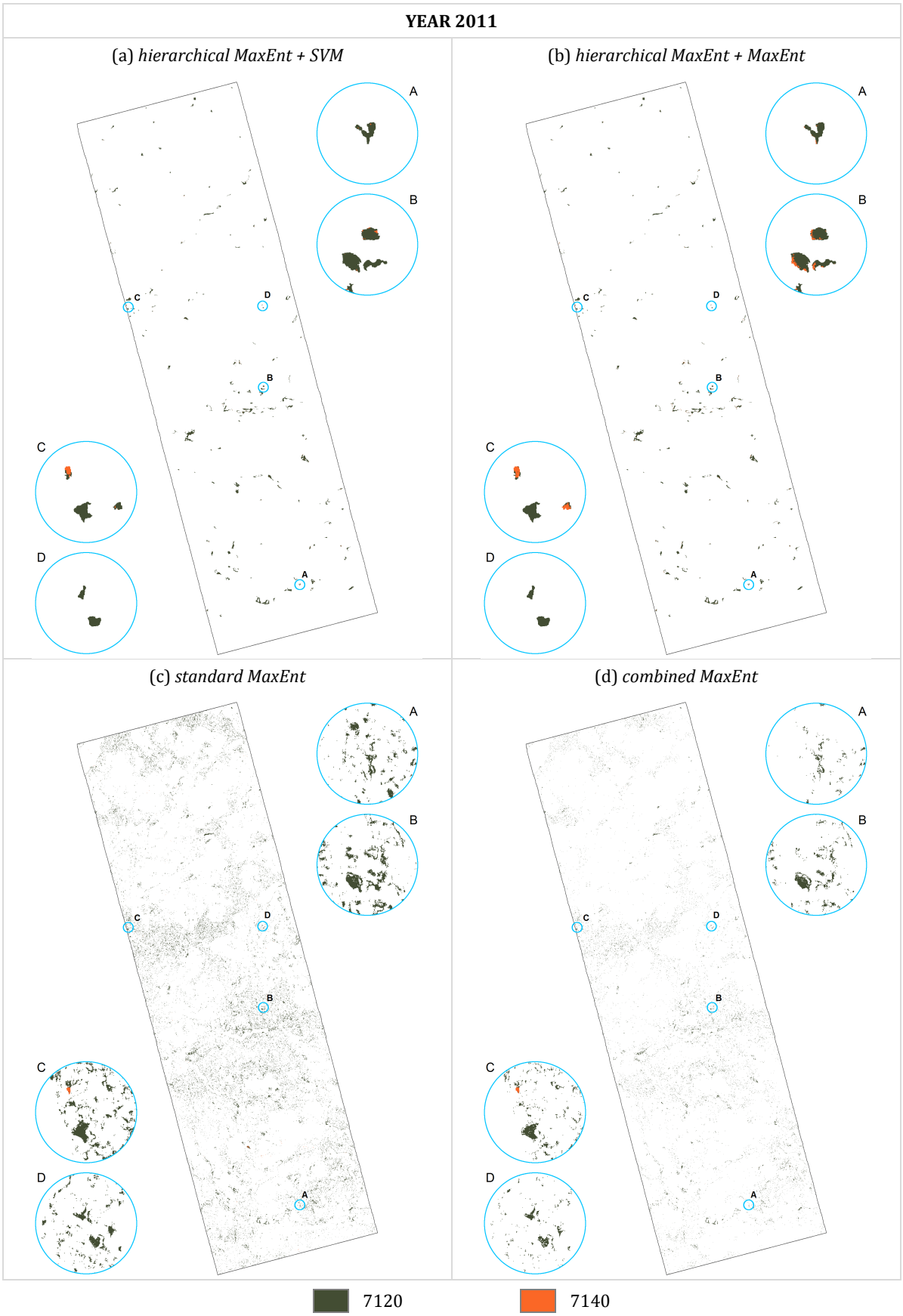

Figure 5-13: MV-TSX-2011 [VV/VH] dataset - HT targeted classification maps obtained using: (a) the *hierarchical MaxEnt + SVM*, (b) the *hierarchical MaxEnt + MaxEnt*, (c) the *standard MaxEnt*, and (d) the *combined MaxEnt* approaches.

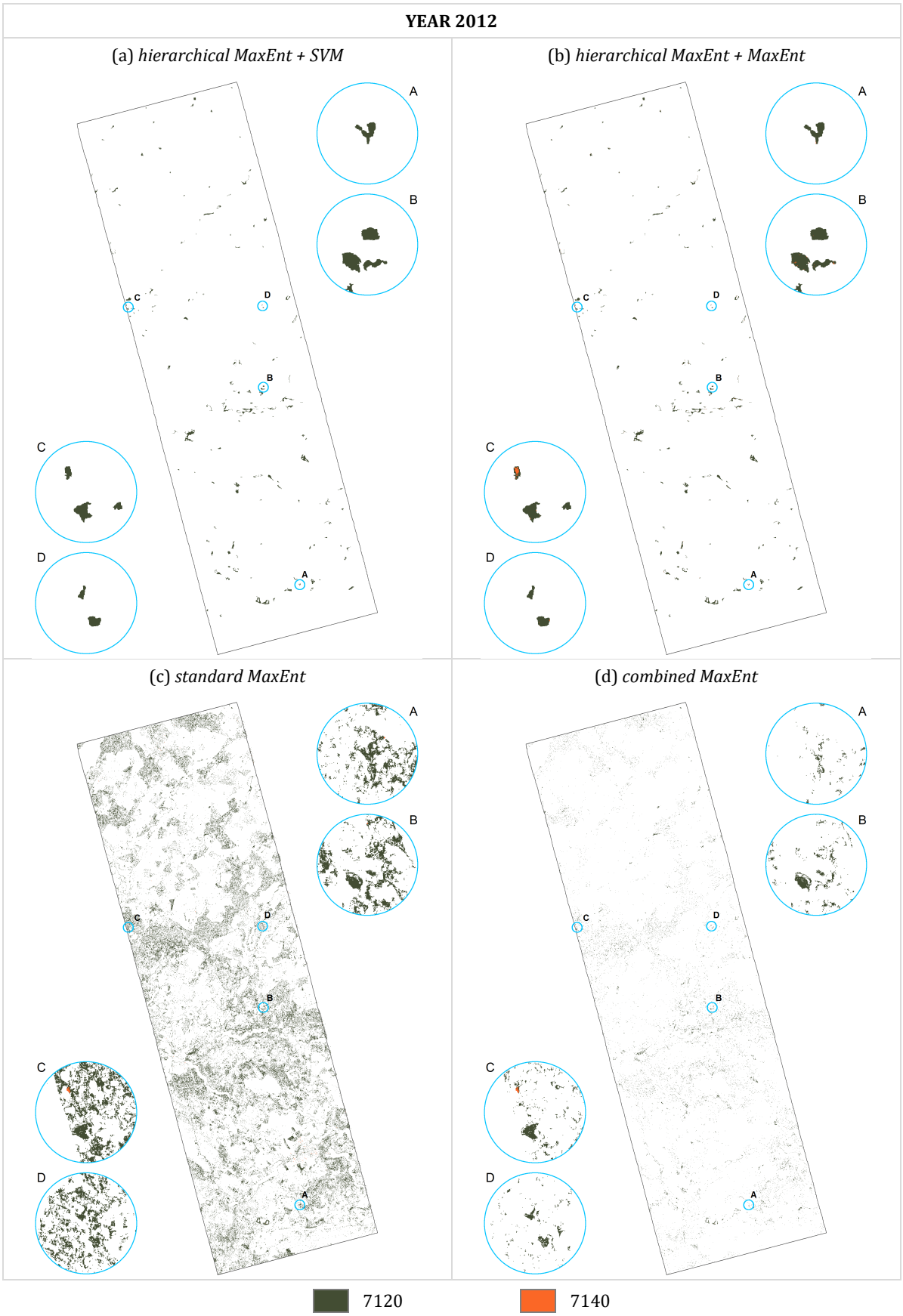

Figure 5-14: MV-TSX-2012 [VV/VH] dataset - HT targeted classification maps obtained using: (a) the *hierarchical MaxEnt + SVM*, (b) the *hierarchical MaxEnt + MaxEnt*, (c) the *standard MaxEnt*, and (d) the *combined MaxEnt* approaches.

5.1.4. Mecklenburg test site: High Nature Value Grasslands

Similarly to the Natura 2000 case, also when addressing the targeted classification of high nature value grasslands, few labelled samples could be defined in the Mecklenburg test site. Nevertheless, while previously at least for one class the amount of training points was consistent (i.e., 1160 for class 7120), here overall just 358 (i.e., 263 for the HNVi and 95 for the HNVe class) were available for 2011 and 505 (i.e., 213 for the HNVi and 292 for the HNVe class) for 2012, hence resulting in an extremely challenging problem. Again, due to the potentially high variability of the two targeted classes even between successive growing seasons, the years 2011 and 2012 have been analysed independently from each other.

Results for the one-class classification aimed at outlining the GL of interest as a whole are given

Table 5-13: HNV one-class classification – Validation accuracies computed for the maps obtained applying the OC-SVM and MaxEnt (for different values of ρ) to the MV-TSX-2011 [VV/VH] dataset using the three defined spatial homogeneity rulesets. Results for the maps selected by qualitative assessment as most reliable for the OC-SVM and MaxEnt are highlighted in yellow and blue, respectively [GL training samples: 358; GL validation samples: 393; NGL validation samples: 349867].

		Rule I					Rule II					Rule III				
		OA%	Kappa	GL PA%	NGL PA%	AA%	OA%	Kappa	GL PA%	NGL PA%	AA%	OA%	Kappa	GL PA%	NGL PA%	AA%
MV-TSX-2011 [VV/VH]	OC-SVM	99.09	0.1013	46.56	99.15	72.86	99.09	0.1013	46.56	99.15	72.86	99.09	0.1013	46.56	99.15	72.86
	MaxEnt ρ = 0.001	99.41	0.1484	46.56	99.47	73.02	99.41	0.1484	46.56	99.47	73.02	99.41	0.1485	46.56	99.47	73.02
	MaxEnt ρ = 0.005	99.72	0.2695	46.56	99.78	73.17	99.72	0.2695	46.56	99.78	73.17	99.70	0.1664	27.23	99.78	63.50
	MaxEnt ρ = 0.01	99.79	0.2505	31.81	99.86	65.84	99.79	0.2505	31.81	99.86	65.84	99.77	0.1056	12.47	99.86	56.17
	MaxEnt ρ = 0.015	99.89	0.0000	0.00	100.00	50.00	99.89	0.0000	0.00	100.00	50.00	99.89	0.0000	0.00	100.00	50.00
	MaxEnt ρ = 0.025	99.89	0.0000	0.00	100.00	50.00	99.89	0.0000	0.00	100.00	50.00	99.89	0.0000	0.00	100.00	50.00
	MaxEnt ρ = 0.05	99.89	0.0000	0.00	100.00	50.00	99.89	0.0000	0.00	100.00	50.00	99.89	0.0000	0.00	100.00	50.00
	MaxEnt ρ = 0.075	99.89	0.0000	0.00	100.00	50.00	99.89	0.0000	0.00	100.00	50.00	99.89	0.0000	0.00	100.00	50.00
	MaxEnt ρ = 0.1	99.89	0.0000	0.00	100.00	50.00	99.89	0.0000	0.00	100.00	50.00	99.89	0.0000	0.00	100.00	50.00
	MaxEnt ρ = 0.125	99.89	0.0000	0.00	100.00	50.00	99.89	0.0000	0.00	100.00	50.00	99.89	0.0000	0.00	100.00	50.00
	MaxEnt ρ = 0.15	99.89	0.0000	0.00	100.00	50.00	99.89	0.0000	0.00	100.00	50.00	99.89	0.0000	0.00	100.00	50.00

Table 5-14: HNV one-class classification – Validation accuracies computed for the maps obtained applying the OC-SVM and MaxEnt (for different values of ρ) to the MV-TSX-2012 [VV/VH] dataset using the three defined spatial homogeneity rulesets. Results for the maps selected by qualitative assessment as most reliable for the OC-SVM and MaxEnt are highlighted in yellow and blue, respectively [GL training samples: 505; GL validation samples: 915; NGL validation samples: 349867].

		Rule I					Rule II					Rule III				
		OA%	Kappa	GL PA%	NGL PA%	AA%	OA%	Kappa	GL PA%	NGL PA%	AA%	OA%	Kappa	GL PA%	NGL PA%	AA%
MV-TSX-2012 [VV/VH]	OC-SVM	99.62	0.1008	8.42	99.85	54.14	99.62	0.1008	8.42	99.85	54.14	99.62	0.1008	8.42	99.85	54.14
	MaxEnt ρ = 0.01	96.73	0.0735	53.11	96.84	74.98	96.73	0.0735	53.11	96.84	74.98	96.73	0.0735	53.11	96.84	74.98
	MaxEnt ρ = 0.015	98.41	0.1195	42.84	98.56	70.70	98.41	0.1195	42.84	98.56	70.70	98.41	0.1195	42.84	98.56	70.70
	MaxEnt ρ = 0.025	98.46	0.0694	23.39	98.66	61.02	98.46	0.0694	23.39	98.66	61.02	98.44	0.0438	15.08	98.66	56.87
	MaxEnt ρ = 0.05	99.74	0.0000	0.00	100.00	50.00	99.74	0.0000	0.00	100.00	50.00	99.74	0.0000	0.00	100.00	50.00
	MaxEnt ρ = 0.075	99.74	0.0000	0.00	99.74	49.87	99.74	0.0000	0.00	99.74	49.87	99.74	0.0000	0.00	100.00	50.00
	MaxEnt ρ = 0.1	99.74	0.0000	0.00	100.00	50.00	99.74	0.0000	0.00	100.00	50.00	99.74	0.0000	0.00	100.00	50.00
	MaxEnt ρ = 0.125	99.74	0.0000	0.00	100.00	50.00	99.74	0.0000	0.00	100.00	50.00	99.74	0.0000	0.00	100.00	50.00
	MaxEnt ρ = 0.15	99.74	0.0000	0.00	100.00	50.00	99.74	0.0000	0.00	100.00	50.00	99.74	0.0000	0.00	100.00	50.00

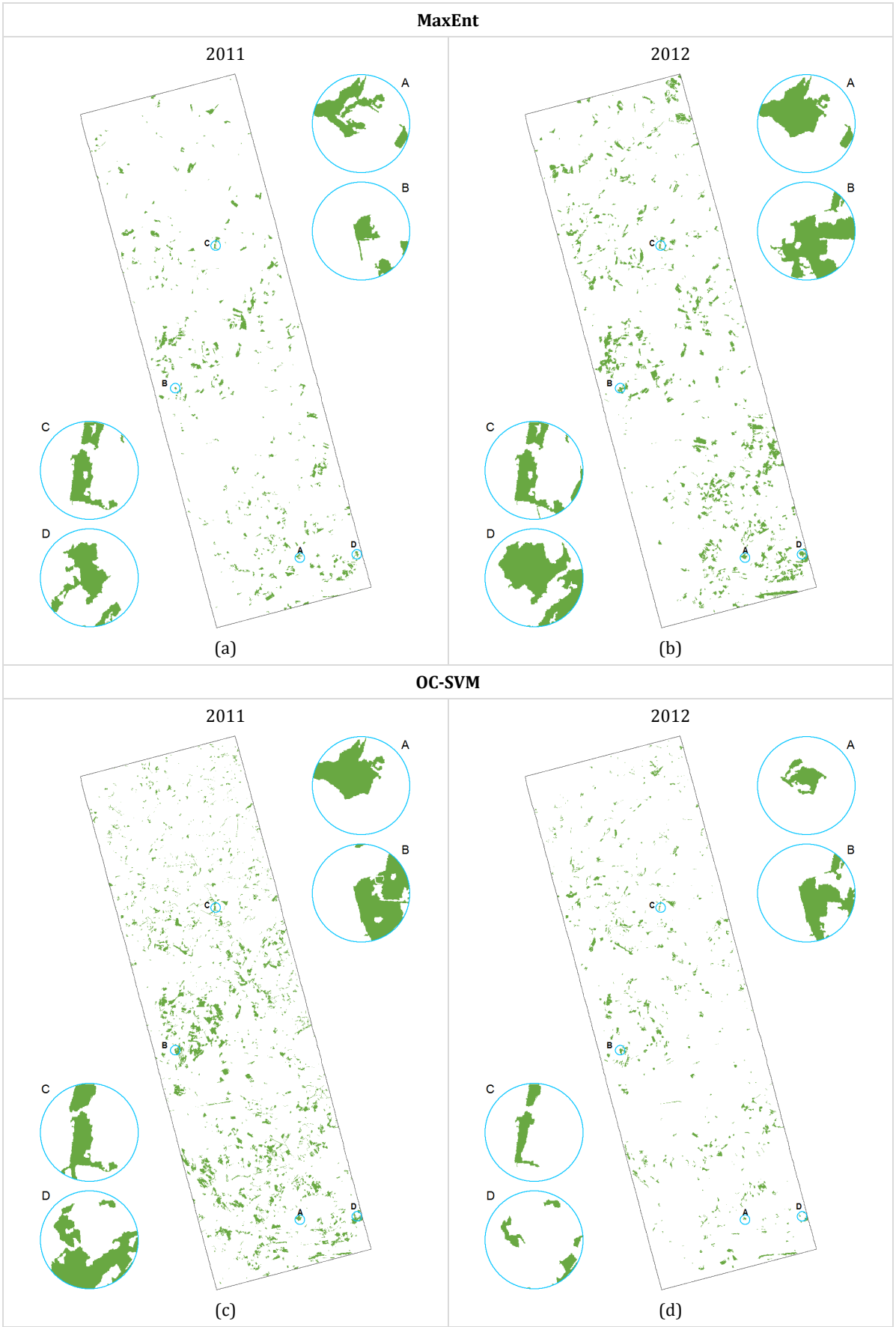

Figure 5-15: HNV one-class classification maps selected using the MaxEnt and OC-SVM for the MV-TSX-2011 [VV/VH] (a and b, respectively) and MV-TSX-2012 [VV/VH] (b and d, respectively) datasets.

in Table 5-13 and Table 5-14, while the corresponding maps are depicted in Figure 5-15. As one can notice by analysing the accuracies, with the OC-SVM no differences occurred when using the different spatial homogeneity rulesets ($(\gamma = 2, \nu = 0.1)$ for 2011 and $(\gamma = 4, \nu = 0.1)$ for 2012 always proved to be the most suitable values for the free parameters). However, in 2011 some NGL areas mostly located in the southern and western part of the AOI are wrongly classified as GL (see Figure 5-15 (c)), whereas only about 46% of GL areas are detected correctly, thus resulting in quite low Kappa (0.1013) and AA% (72.86). In 2012, the underestimation of the NGL areas is lower (see Figure 5-15 (d)), but this occurs at the price of a very low PA% of the GL class (8.42) with final similar Kappa (0.1008).

Concerning the MaxEnt, $\rho = 0.005$ and $\rho = 0.015$ have been chosen in combination with Rule II for 2011 and 2012, respectively. However, compared to the experiments discussed in the previous pages, it is possible to notice that, for higher values of the confidence level, in both years the PA% of the GL class is 0. This is due to the consistent overlapping between the conditional probability density estimated for the GL class and the true one of the NGL class, which occurs due to the similarity between the GL and some NGL areas (i.e., mostly agricultural fields), but also to the limited number of training samples available. Results for 2011 are in line with those derived with the OC-SVM (i.e., the GL PA% is equal to 46.56), despite by examining the map reported in Figure 5-15 (a), the lower overestimation of the GL class is clear, hence resulting in slightly higher Kappa (0.2695). For the MV-TSX-2012 [VV/VH] dataset, where only 7 TSX scenes were available, some NGL areas mostly located in the lower right and upper left part

Table 5-15: HNV targeted classification – Validation accuracies computed for the maps obtained applying the three considered methods to the MV-TSX-2011 [VV/VH] dataset (using 263 training samples for class HNVi and 95 for class HNVe) and the MV-TSX-2012 [VV/VH] dataset (using 213 training samples for class HNVi and 292 for class HNVe).

		OA%	Kappa	PA%			% unclassified		# validation points		
				NGL	HNVi	HNVe	HNVi	HNVe	NGL	HNVi	HNVe
MV-TSX-2011	*hierarchical MaxEnt + SVM*	99.70	0.2547	99.78	18.15	94.78	81.08	0.00	349991	259	134
	hierarchical MaxEnt + MaxEnt	99.69	0.1846	99.78	6.56	38.06	81.08	0.00			
	standard MaxEnt	25.82	0.0006	25.78	99.61	0.00	0.39	0.00			
MV-TSX-2012	*hierarchical MaxEnt + SVM*	98.37	0.1126	98.56	67.98	31.61	30.90	63.50	349991	178	737
	hierarchical MaxEnt + MaxEnt	98.34	0.0802	98.56	0.00	19.00	30.90	63.50			
	standard MaxEnt	31.12	0.0009	31.09	29.73	100.00	7.34	0.00			

Table 5-16: Intra-class classification accuracies (computed without considering the NGL validation points) for the HNV targeted classification maps obtained applying the three considered methods to the MV-TSX-2011 [VV/VH] dataset (using 263 training samples for class HNVi and 95 for class HNVe) and the MV-TSX-2012 [VV/VH] dataset (using 213 training samples for class HNVi and 292 for class HNVe).

		OA%	Kappa	PA%		# validation points	
				HNVi	HNVe	HNVi	HNVe
MV-TSX-2011	*hierarchical MaxEnt + SVM*	95.08	0.8785	95.92	94.78	49	134
	hierarchical MaxEnt + MaxEnt	37.16	-0.2048	34.69	38.06	49	134
	standard MaxEnt	65.82	0.0000	100.00	0.00	258	134
MV-TSX-2012	*hierarchical MaxEnt + SVM*	90.31	0.7906	98.37	86.62	123	269
	hierarchical MaxEnt + MaxEnt	35.71	-0.4733	0.00	52.04	123	269
	standard MaxEnt	56.42	0.2529	32.08	100.00	165	737

of the AOI are instead classified as GL (see Figure 5-15 (b)), hence leading to an AA% of about 70. Overall, by qualitative assessment the MaxEnt anew proved more effective than the OC-SVM, being then selected to be employed in the final hierarchical system.

The classification maps obtained with the *hierarchical MaxEnt + SVM*, *hierarchical MaxEnt + MaxEnt* and *standard MaxEnt* are shown in Figure 5-16 and Figure 5-17, whereas the corresponding accuracy assessment is reported in Table 5-15. As stressed above when discussing the performances of the one-class classifiers, results confirm how challenging the addressed targeted classification problem is for the investigated datasets. The *hierarchical MaxEnt + SVM* approach (for which the optimal parameters proved to be ($\gamma = 0.4, C = 1$) for the 2011 and ($\gamma = 0.08,\ C = 1$) for the 2012 dataset) allowed a good categorisation of the HNVe areas in 2011 with PA% equal to 94.78. On the contrary, the corresponding value for the HNVi class is lower than 20. However, such a result is mainly due to the strong underestimation ensued from the first phase of the hierarchical approach where 81.08% of the validation samples of class HNVi have been wrongly categorised as NGL. Indeed, the SVM proved capable of very good discrimination between the two targeted classes, as it emerges from the intra-class accuracies given in Table 5-16 with Kappa higher than 0.87 and PA% values greater than 94. A similar behaviour occurs for 2012, where again the underestimation of the one-class MaxEnt in the first phase results in quite low PA% of both classes of interest (67.98 for the HNVi and 31.61 for the HNVe class) despite the multi-class SVM showed good intra-class discrimination capabilities with PA% greater than 86 as it can be seen from Table 5-16.

The final performances exhibited by the *hierarchical MaxEnt + MaxEnt* are poorer in this case, since for both 2011 and 2012 the few available training samples did not allow a reliable estimate of the conditional probability density of the two targeted classes, hence resulting in consistent misclassification and very low intra-class accuracies.

The *standard MaxEnt* approach, as one can notice from Figure 5-16 (c) and Figure 5-17 (c), resulted in extremely high overestimation of the HNVi class for the year 2011 and of the HNVe class for the year 2012. In particular, almost the entire study area is categorised as the targeted class for which it occurs. This is reflected in the corresponding classification accuracies (with OA% lower 32 and Kappa close to 0) and confirms the complexities arising in the presence of a limited number of training samples. However, even in such a critical situation, the proposed hierarchical concept yet resulted in a consistent improvement with respect to the current approach commonly employed for this type of problems.

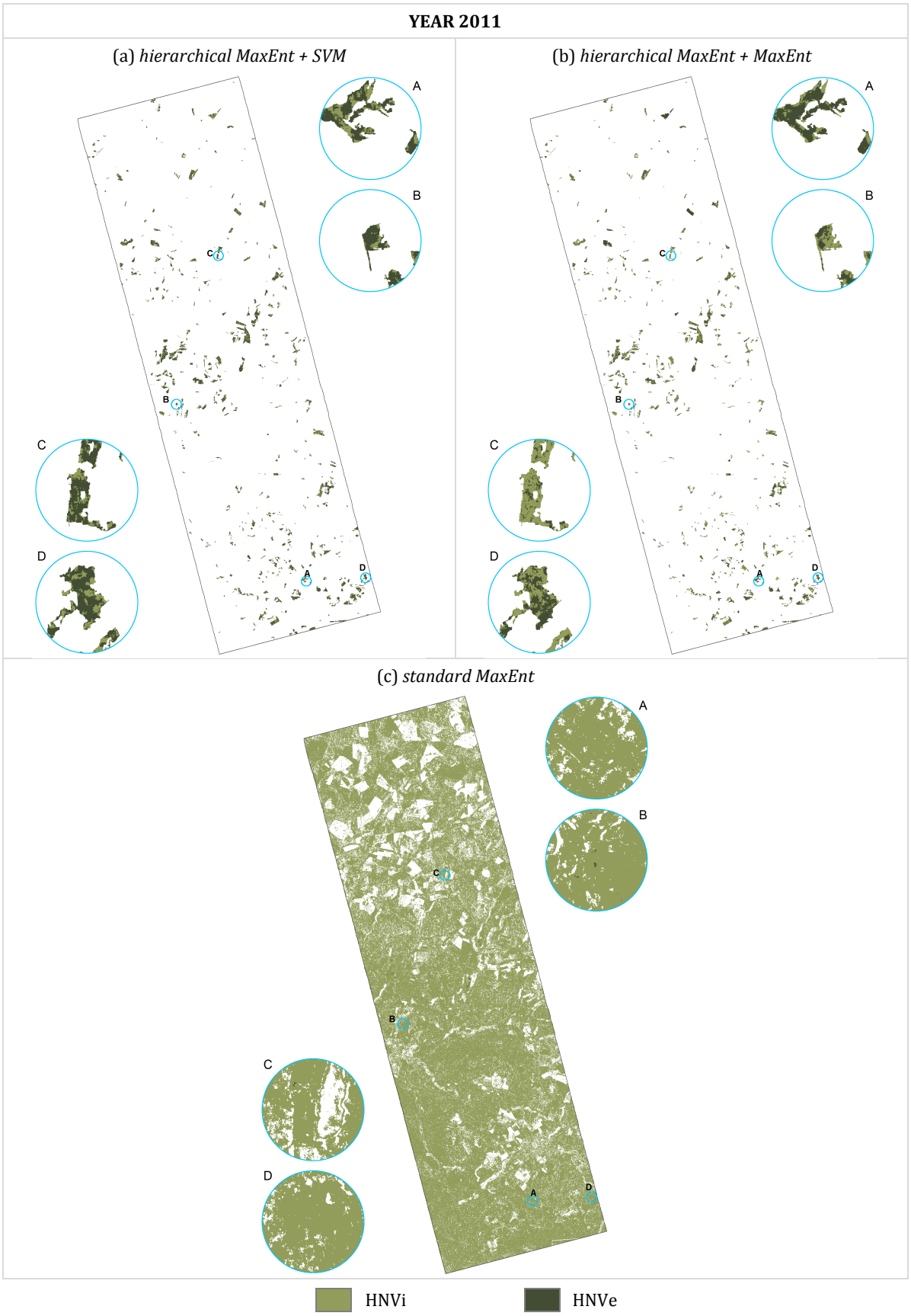

Figure 5-16: MV-TSX-2011 [VV/VH] dataset - HNV targeted classification maps obtained using: (a) the *hierarchical MaxEnt + SVM*, (b) the *hierarchical MaxEnt + MaxEnt*, and (c) the *standard MaxEnt* approaches.

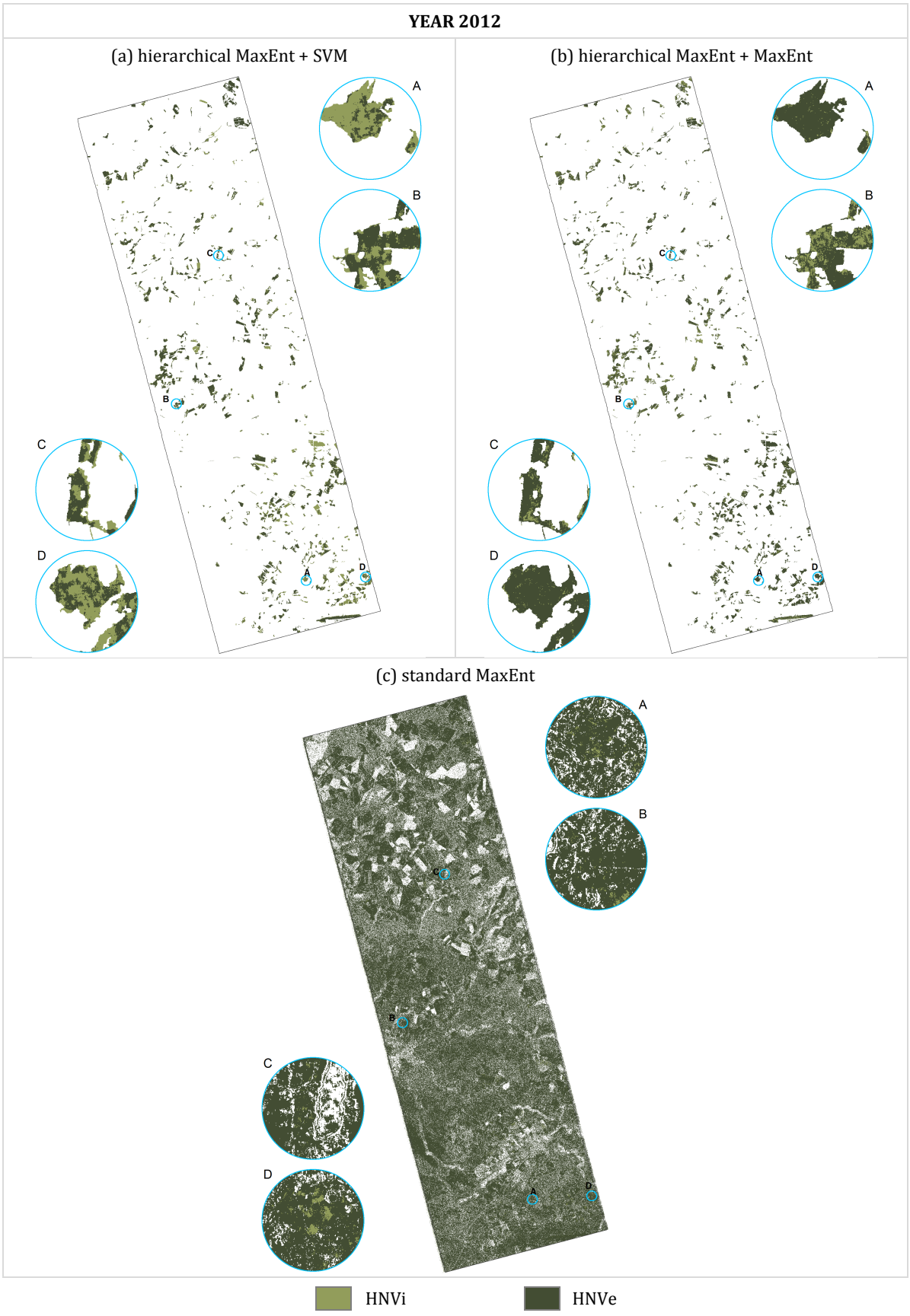

Figure 5-17: MV-TSX-2012 [VV/VH] dataset - HNV targeted classification maps obtained using: (a) the *hierarchical MaxEnt + SVM*, (b) the *hierarchical MaxEnt + MaxEnt*, and (c) the *standard MaxEnt* approaches.

5.2. Experimental Results with Radarsat-2 data

In this section, results obtained for the Bavaria test site using RS2 data are discussed. In particular, this set of experiments allows to assess the effectiveness of using dual- and quadpol data, as well as to compare the performances exhibited by C-band data compared to X-band TSX data.

5.2.1. Bavaria test site: Natura 2000

For the RS2 study area in Bavaria (whose extent and location are slightly different from the TSX one) overall 4152 training and 4183 validation samples were available when addressing the Natura 2000 targeted classification problem after applying the extension strategy described in section 4.2.2. In this context, the results obtained using the MaxEnt and the OC-SVM for the one-class GL classification are shown in Table 5-17, while the final maps are given in Figure 5-18 and Figure 5-19, respectively.

When using the MaxEnt, $\rho = 0.075$ in combination with Rule II was chosen for both datasets. In terms of Kappa, this resulted in better performances of the quadpol with respect to the dualpol data (0.8826 against 0.8032) due to the lower misclassification of NGL areas (99.87 against 99.23, corresponding to a difference of ~65000 more validation points classified correctly). Instead, with dualpol data the GL PA% is ~6 higher (90.32 vs. 84.01), resulting in a greater AA% (94.78 vs. 91.94). However, when comparing the two maps in Figure 5-18, it is worth noting that the one derived with quadpol data looks qualitatively more reliable based on the knowledge of the AOI gathered during the field campaigns, especially in the upper and lower-left side.

The OC-SVM, whose selected free parameter values were $(\gamma = 3.5, \nu = 0.01)$ for the dualpol and $(\gamma = 3.5, \nu = 0.1)$ for the quadpol dataset, exhibited poorer performances compared to the MaxEnt especially in terms of Kappa (-0.1401 in the dual and -0.2102 in the quadpol case).

Table 5-17: HT one-class classification – Validation accuracies computed for the maps obtained applying the OC-SVM and MaxEnt (for different values of ρ) to the dualpol BY-RS2-2011 [VV/VH] and quadpol BY-RS2-2011 [QUAD] dataset using the three defined spatial homogeneity rulesets. Results for the maps selected by qualitative assessment as most reliable for the OC-SVM and MaxEnt are highlighted in yellow and blue, respectively [GL training samples: 4152; GL validation samples: 4183; NGL validation samples: 181012].

		Rule I					Rule II					Rule III				
		OA%	Kappa	GL PA%	NGL PA%	AA%	OA%	Kappa	GL PA%	NGL PA%	AA%	OA%	Kappa	GL PA%	NGL PA%	AA%
dualpol	OC-SVM	98.34	0.6631	75.23	98.87	87.05	98.34	0.6631	75.23	98.87	87.05	98.34	0.6631	75.23	98.87	87.05
	MaxEnt ρ = 0.05	98.76	0.7614	90.41	98.96	94.69	98.80	0.7663	90.41	98.99	94.70	98.76	0.7496	85.30	99.07	92.18
	MaxEnt ρ = 0.075	99.00	0.7984	90.32	99.20	94.76	99.03	0.8032	90.32	99.23	94.78	98.99	0.7866	85.20	99.31	92.25
	MaxEnt ρ = 0.1	99.16	0.8102	81.31	99.58	90.44	99.17	0.8118	81.31	99.59	90.45	99.12	0.7934	77.29	99.62	88.45
	MaxEnt ρ = 0.125	99.18	0.8111	80.18	99.62	89.90	99.18	0.8118	80.18	99.62	89.90	99.16	0.8017	77.27	99.67	88.47
	MaxEnt ρ = 0.15	99.30	0.8311	78.51	99.78	89.14	99.30	0.8317	75.59	99.70	87.64	99.28	0.8218	75.59	99.83	87.71
quadpol	OC-SVM	98.21	0.6724	84.68	98.52	91.60	98.21	0.6724	84.68	98.52	91.60	98.21	0.6724	84.68	98.52	91.60
	MaxEnt ρ = 0.05	99.55	0.8970	88.60	99.80	94.20	99.56	0.8979	88.60	99.81	94.20	99.56	0.8953	85.46	99.89	92.68
	MaxEnt ρ = 0.075	99.53	0.8878	85.01	99.86	92.44	99.51	0.8826	84.01	99.87	91.94	99.48	0.8736	80.92	99.91	90.42
	MaxEnt ρ = 0.1	99.51	0.8828	83.67	99.88	91.77	99.50	0.8786	82.67	99.89	91.28	99.49	0.8753	80.68	99.93	90.31
	MaxEnt ρ = 0.125	99.47	0.8694	80.09	99.92	90.00	99.45	0.8645	79.08	99.92	89.50	99.48	0.8694	79.01	99.95	89.48
	MaxEnt ρ = 0.15	99.40	0.8488	76.60	99.92	88.26	99.40	0.8499	76.60	99.93	88.26	99.42	0.8539	76.38	99.96	88.17

Specifically, as evident from the analysis of the corresponding classification maps, this arises from the severe misclassification of many agricultural and forested areas scattered throughout the entire study site wrongly categorised as belonging to the GL class. For this reason, also in this set of experiments the MaxEnt classifier has been chosen to be included in the final hierarchical system.

The results obtained with the *hierarchical MaxEnt + SVM*, *hierarchical MaxEnt + MaxEnt*, and *standard MaxEnt* are presented in Figure 5-20 for the dualpol case and in Figure 5-21 for the quadpol case, while the corresponding classification maps are reported in Table 5-18. Overall, the hierarchical methods provide similar results for both datasets with accuracies only slightly higher in the presence of quadpol data. In particular, the *hierarchical MaxEnt + SVM* exhibits the

Figure 5-18: HT one-class classification map obtained for the dualpol BY-RS2-2011 [VV/VH] (a) and quadpol BY-RS2-2011 [QUAD] (b) datasets using the MaxEnt.

best performances in terms of OA% and Kappa in the dualpol (i.e., 98.49 and 0.6928, respectively, obtained with ($\gamma = 2.5, C = 1000$)) as well as in the quadpol case (i.e., 98.98 and 0.7158, respectively, obtained with ($\gamma = 3.5, C = 1000$),). Nevertheless, the *hierarchical MaxEnt + MaxEnt* resulted in values only marginally lower. Instead, the *standard MaxEnt* method showed poorer accuracies for both datasets with Kappa between ~0.09 to 0.15 lower than the hierarchical approaches. This behaviour is also confirmed by analysing the classification maps presented in Figure 5-20 and Figure 5-21. Notably, the hierarchical classifiers properly describe the considered targeted classes over the whole study area (Figure 5-20 (a) and (b) and Figure 5-21 (a) and (b)); while the results of the *standard MaxEnt* are constantly underestimating the natural extent of the targeted grassland areas.

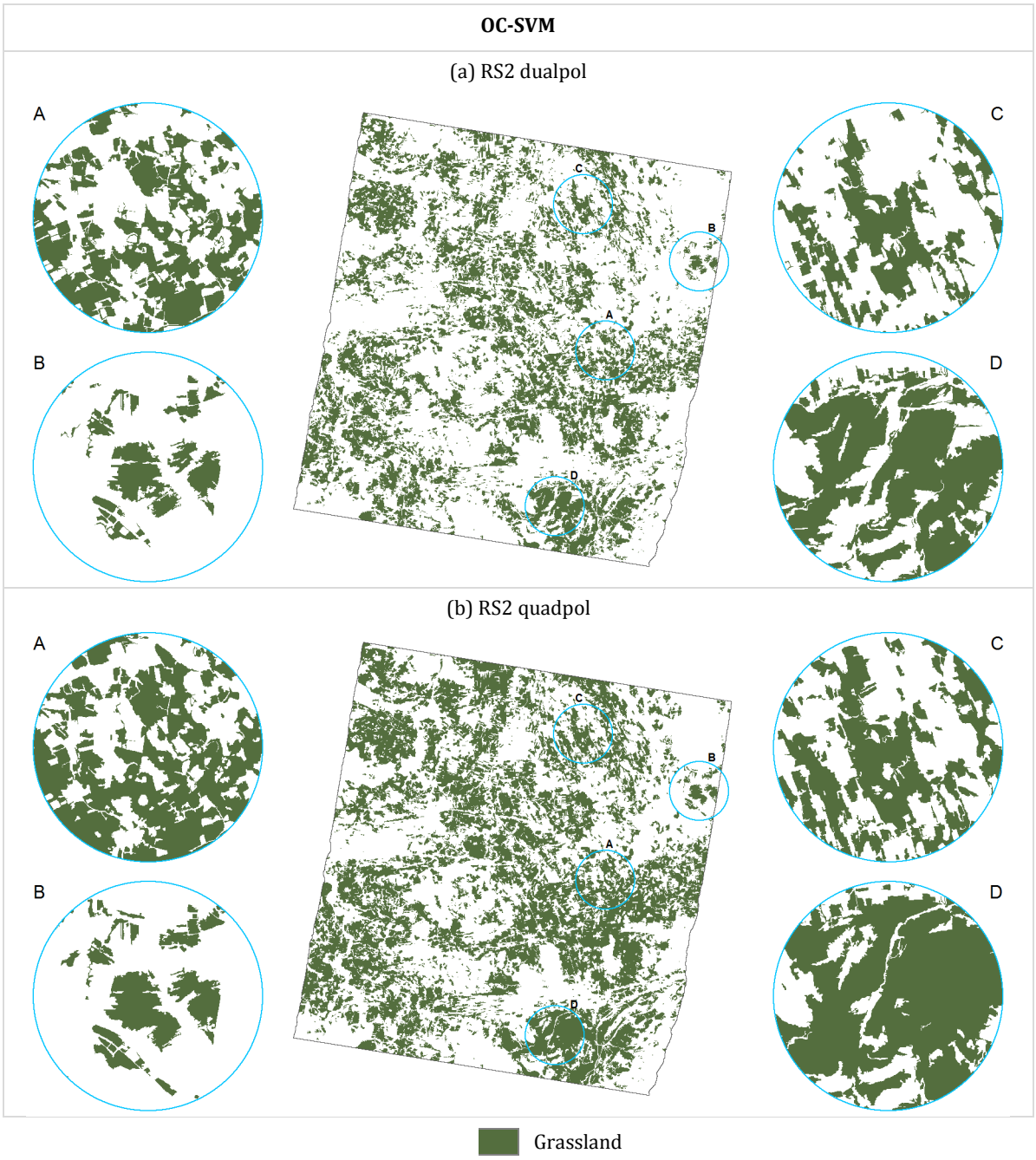

Figure 5-19: HT one-class classification map obtained for the dualpol BY-RS2-2011 [VV/VH] (a) and quadpol BY-RS2-2011 [QUAD] (b) datasets using the OC-SVM.

Similar to the results obtained with TSX data for the Bavarian test site, the location of the raised bogs (class 7120) is generally correctly identified within the test area in all three maps. In particular, these are located close to the "Osterseen" in the north of the test area (zoom B), within the large bog influenced landscape "Murnauer Moos" in the centre of the image (zoom D), and within the area at the western site of the "Staffelsee" (northwest of zoom D). However, while the final delineation of the single bogs is quite similar between the *hierarchical MaxEnt + SVM* and the *hierarchical MaxEnt + MaxEnt* for both datasets, it differs considerably with the *standard MaxEnt* as they appear more dispersed (see Figure 5-20 (c) and Figure 5-21 (c)). Furthermore, comparing the classification maps obtained with the hierarchical approaches for the dual- and quadpol case separately, the resulting distribution and size of the three remaining targeted classes are reasonably similar, despite there are greater differences in the intra-class variability between the two datasets. When using the *standard MaxEnt* approach this variability gets lost due to the consistent underestimation of the targeted classes and the corresponding scattered classification maps.

Also here, although the *standard MaxEnt* method tends to consistently underestimate the targeted classes, it still results in high OA% values due to the large number of validation samples considered for the NGL (181004) compared to that available for the targeted classes (overall 4183). Additionally, in Table 5-18 the percentage of unclassified samples per class is listed. No significant differences occur for the classes 6410, 7140, and 7230 for all three classifiers (ranging from 12.71% to 29.18%), while for class 7120 they are ~15% to 18% higher for the

Table 5-18: HT targeted classification – Validation accuracies computed for the maps obtained applying the three considered methods to the dualpol BY-RS2-2011 [VV/VH] and quadpol BY-RS2-2011 [QUAD] datasets using 1572 training samples for class 6410, 1543 for class 7120, 340 for class 7140 and 697 for class 7230 [NGL validation samples: 181004].

		OA%	Kappa	PA%					% unclassified				# validation points			
				NGL	6410	7120	7140	7230	6410	7120	7140	7230	6410	7120	7140	7230
dualpol	*hierarchical MaxEnt + SVM*	98.49	0.6928	99.23	67.78	92.09	1.77	8.06	12.71	0.26	24.03	24.05	1322	1896	283	682
	hierarchical MaxEnt + MaxEnt	98.44	0.6860	99.23	67.40	92.62	2.12	5.13	12.71	0.26	24.03	24.05				
	standard MaxEnt	97.29	0.5302	98.20	63.31	80.54	4.95	6.01	15.51	15.93	20.49	23.17				
quadpol	*hierarchical MaxEnt + SVM*	98.98	0.7158	99.87	63.24	94.39	0.35	4.99	17.55	10.76	24.03	24.19	1322	1896	283	682
	hierarchical MaxEnt + MaxEnt	98.41	0.6796	99.87	68.31	87.34	1.41	9.38	17.55	10.76	24.03	24.19				
	standard MaxEnt	98.04	0.5809	99.14	59.15	66.14	1.06	12.32	26.10	28.59	19.08	29.18				

Table 5-19: Intra-class classification accuracies (computed without considering the NGL validation points) for the HT targeted classification maps obtained applying the three considered methods to the dualpol BY-RS2-2011 [VV/VH] and quadpol BY-RS2-2012 [QUAD] datasets using 1572 training samples for class 6410, 1543 for class 7120, 340 for class 7140 and 697 for class 7230.

		OA%	Kappa	PA%				# validation points			
				6410	7120	7140	7230	6410	7120	7140	7230
dualpol	*hierarchical MaxEnt + SVM*	71.52	0.5406	77.64	92.33	2.33	10.62	1154	1891	215	518
	hierarchical MaxEnt + MaxEnt	71.15	0.5353	77.21	92.86	2.79	6.76	1154	1891	215	518
	standard MaxEnt	69.91	0.5281	74.93	95.80	6.22	7.82	1117	1594	225	524
quadpol	*hierarchical MaxEnt + SVM*	70.32	0.5216	76.70	94.56	0.47	6.58	1090	1692	215	517
	hierarchical MaxEnt + MaxEnt	69.53	0.5080	78.25	87.57	1.86	12.36	1090	1692	215	517
	standard MaxEnt	69.77	0.5285	80.04	92.61	1.31	17.39	977	1354	229	483

Figure 5-20: BY-RS2 2011 [VV/VH] dataset - HT targeted classification maps obtained using: (a) the *hierarchical MaxEnt + SVM*, (b) the *hierarchical MaxEnt + MaxEnt*, and (c) the *standard MaxEnt* approaches.

Figure 5-21: BY-RS2 2011 [QUAD] dataset - HT targeted classification maps obtained using: (a) the *hierarchical MaxEnt + SVM*, (b) the *hierarchical MaxEnt + MaxEnt*, and (c) the *standard MaxEnt* approaches.

standard MaxEnt compared to the hierarchical approaches.

By analysing Table 5-18, it emerges that class 7120 always exhibits highest PA% over all classifiers and for both datasets with respect to the other targeted classes. However, the values derived with the proposed hierarchical classifiers are ~15 - 28% higher than those obtained by the *standard MaxEnt*. Instead, the results for the remaining classes are poorer and relatively similar among all classifiers, namely 60 to 68 for class 6410, 5 to 12 for class 7230, and 0.35 to 5 for class 7140. Again, as experienced with the TSX data for the Bavaria dataset, such behaviour allows assuming that the classes 6410, 7140, and 7230 are quite similar in the analysed feature space also when C-band RS2 data are used. This is also supported by the intra-class accuracy reported in Table 5-19. Here, all classifiers have similar OA% (between 69 and 71) and Kappa (between 0.50 and 0.54). The PA% of all targeted classes have no significant differences among all three methods, with class 7120 still showing the highest PA% (95.80 in the dual- and 87.57 in the quadpol case). Class 6410 exhibits higher values (i.e., between 74.93% and 80.04%). Nevertheless, this results in very low PA% for both classes 7140 and 7230 due to the high confusion among the three classes.

Analogously to what was done in section 5.1.1, a further set of experimental trials has been then performed by merging the classes 6410, 7140 and 7230 into a single "wet grasslands" class. The resulting maps obtained with the three considered approaches are shown in Figure 5-22 for the dualpol and in Figure 5-23 for the quadpol case, whereas the corresponding accuracy assessment is presented in Table 5-20.

Table 5-20: HT two-class targeted classification – Validation accuracies computed for the maps obtained applying the three considered methods to the dualpol BY-RS2-2011 [VV/VH] and quadpol BY-RS2-2012 [QUAD] datasets using 1543 training samples for class 7120 and 2609 for the merger of the classes 6410, 7140 and 7230.

		OA%	Kappa	PA%			% unclassified		# validation points		
				NGL	6410, 7140, 7230	7120	6410, 7140, 7230	7120	NGL	6410, 7140, 7230	7120
dualpol	*hierarchical MaxEnt + SVM*	98.96	0.7877	99.23	77.39	95.04	17.49	0.26	181004	2287	1896
	hierarchical MaxEnt + MaxEnt	98.91	0.7805	99.23	78.79	92.66	17.49	0.26			
	standard MaxEnt	97.78	0.6146	98.20	78.90	80.54	18.41	15.93			
quadpol	*hierarchical MaxEnt + SVM*	99.40	0.8074	99.87	72.37	92.76	20.33	10.76	181004	2287	1896
	hierarchical MaxEnt + MaxEnt	98.82	0.7615	99.87	75.57	87.37	20.33	10.76			
	standard MaxEnt	98.42	0.6605	99.14	68.45	66.14	26.15	28.59			

Table 5-21: Intra-class classification accuracies (computed without considering the NGL validation points) for the HT 2-class targeted classification maps obtained applying the three considered methods to the BY-RS2-2011 [VV/VH] and BY-RS2-2012 [QUAD] datasets using 1543 training samples for class 7120 and 2609 for the merger of the classes 6410, 7140 and 7230.

		OA%	Kappa	PA%		# validation points	
				6410, 7140, 7230	7120	6410, 7140, 7230	7120
dual	*hierarchical MaxEnt + SVM*	94.55	0.8909	93.40	95.29	1887	1891
	hierarchical MaxEnt + MaxEnt	94.18	0.8835	95.50	92.86	1887	1891
	standard MaxEnt	96.32	0.9260	96.77	95.80	1866	1594
quad	*hierarchical MaxEnt + SVM*	92.83	0.8566	96.33	94.98	1822	1692
	hierarchical MaxEnt + MaxEnt	89.59	0.7918	91.61	87.57	1822	1692
	standard MaxEnt	92.74	0.8534	92.85	92.61	1689	1354

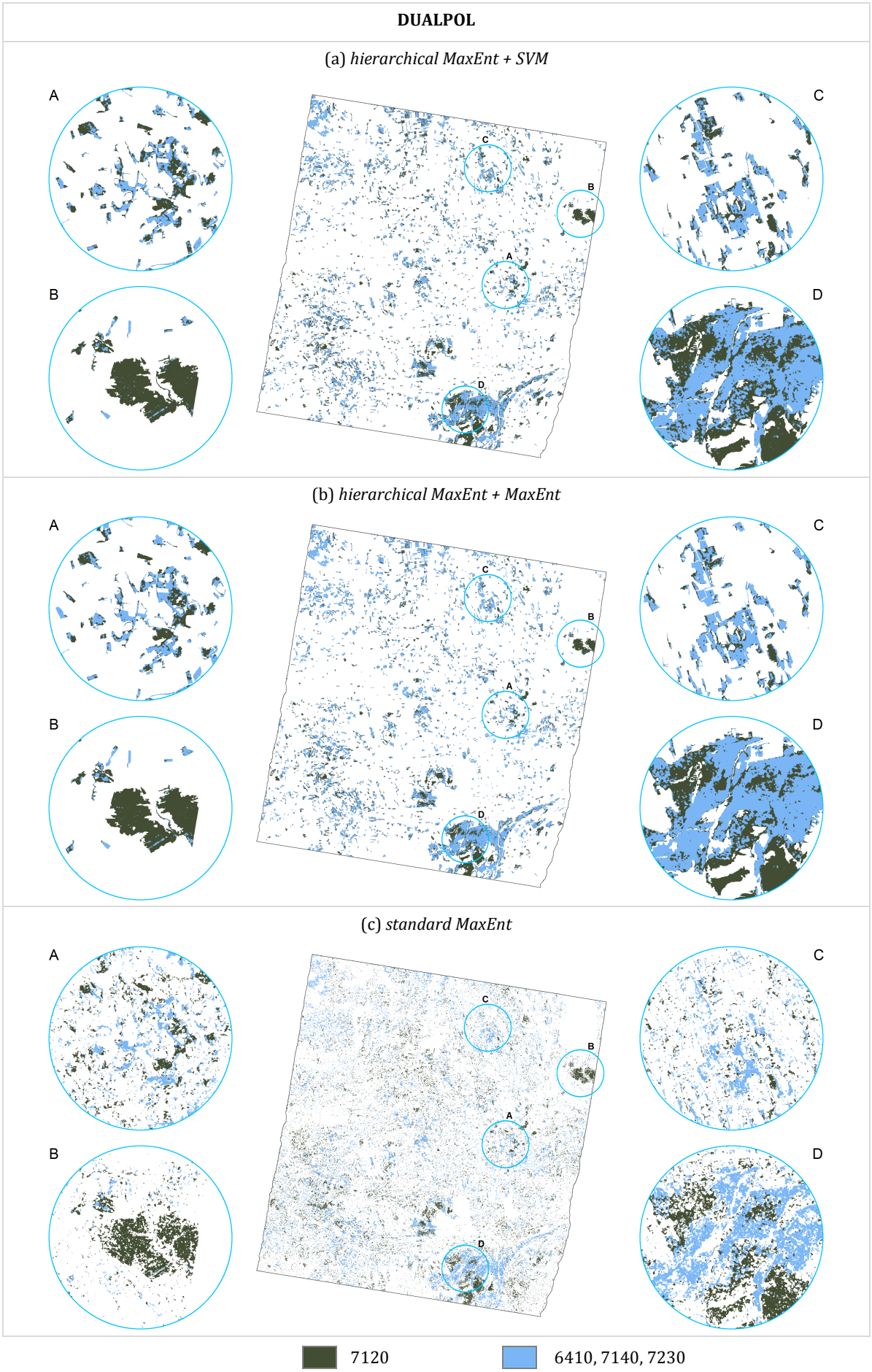

Figure 5-22: BY-RS2 2011 [VV/VH] dataset - HT two-class targeted classification maps obtained using: (a) the *hierarchical MaxEnt + SVM*, (b) the *hierarchical MaxEnt + MaxEnt*, and (c) the *standard MaxEnt* approaches.

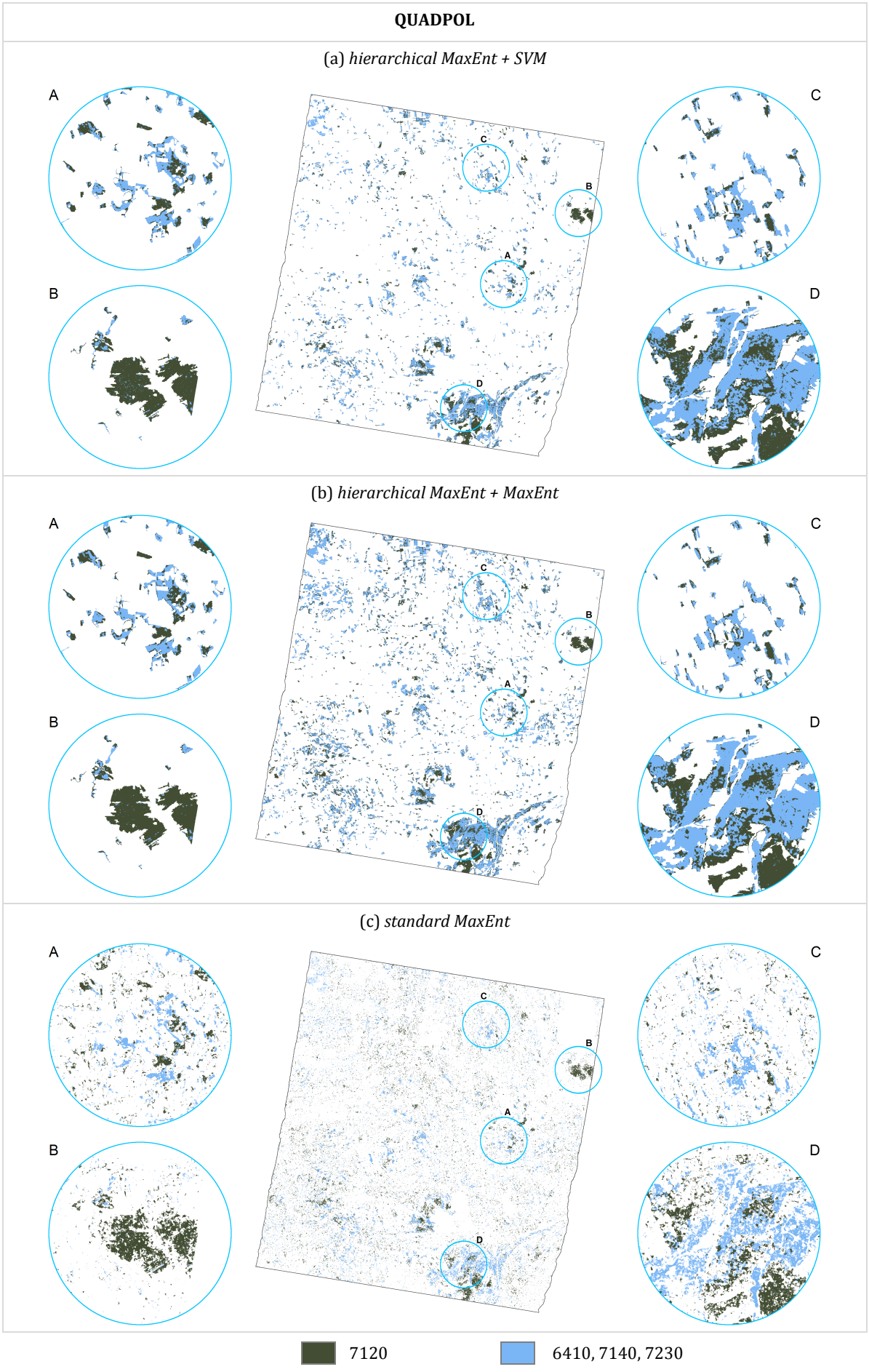

Figure 5-23: BY-RS2 2011 [QUAD] dataset - HT two-class targeted classification maps obtained using: (a) the *hierarchical MaxEnt + SVM*, (b) the *hierarchical MaxEnt + MaxEnt*, and (c) the *standard MaxEnt* approaches.

As it can be seen in Table 5-20 the hierarchical classifiers show also in this case consistently better performances compared to the *standard MaxEnt* (the difference in terms of Kappa between ~0.15 and 0.19). In particular, the *hierarchical MaxEnt + SVM* approach provides the highest OA% and Kappa values for the dualpol (98.96 and 0.7877, respectively) and for the quadpol case (99.40 and 0.8074, respectively) obtained with $\gamma = 8$, $C = 1000$ and $\gamma = 10$, $C = 1$, respectively. However, the *hierarchical MaxEnt + MaxEnt* exhibits OA% and Kappa values only negligibly lower.

By analysing the PA%, it can be noticed that results for class 7120 are comparable to those obtained when addressing the four-class problem for all three classifiers and in both datasets. Instead, the values for the wet grassland class are sensibly higher compared to the ones derived for the single targeted classes separately. This, as highlighted in section 5.1.1, confirms the usefulness of merging the three classes 6410, 7140 and 7230 together. In particular, the PA% for the wet grassland class is similar for all three classifiers in the dualpol case (between 77.39 and 78.90), but differs in the quadpol case, where the hierarchical approaches exhibit greater values than the *standard MaxEnt* (between ~4 and 8). Furthermore, for both classes the PA% is slightly higher for all three classifiers in the dualpol compared to the quadpol classifications.

In the maps presented in Figure 5-22 and Figure 5-23 the areas marked as class 7120 are almost identical to those obtained for the four-class problem (Figure 5-20 and Figure 5-21). In particular, while the hierarchical approaches tend to correctly characterise their extent and location (Figure 5-22 (a) and (b) and Figure 5-23 (a) and (b)), the results of the *standard MaxEnt* again appear scattered due to the many missed alarms (Figure 5-22 (c) and Figure 5-23 (c)). This underestimation is also reflected in the percentage of samples wrongly classified as NGL (see Table 5-20), which are ~1 to 6 % higher for the wet grassland class and ~15 to 18% higher for class 7120 when the *standard MaxEnt* is used compared to the hierarchical approaches.

Analysing the intra-class accuracies presented in Table 5-21 (i.e., computed disregarding all samples categorised as NGL), all three approaches show very high values, hence proving the effectiveness of both the MaxEnt and SVM classifiers to reliably discriminate the two considered classes. However, it is worth pointing out that accuracies derived using the dualpol data are almost always higher than those obtained with quadpol data for all methods (i.e., between ~0.035 and ~0.08 in terms of Kappa and between 2 and 5 in terms of OA%). This aspect is particularly interesting; indeed from the performed analysis it emerges that the quadpol data performs slightly better in discriminating the targeted classes from the remaining land cover classes present in the test area. Nonetheless, while on the one hand dualpol data allow obtaining similar performances when addressing the considered targeted classification problem, on the other hand they resulted in higher intra-class separability between the targeted classes.

5.2.2. Bavaria test site: High Nature Value Grasslands

The last set of experiments carried out in this work addressed the RS2 targeted classification of the high nature value grasslands, which, using TSX data, proved to be a complex task even in the presence of a large training set due to the high similarity between the two classes of interest in the analysed feature space. Even in the case of RS2 several training points have been defined, i.e. overall 5254 (namely 2152 for the HNVi and 3102 for the HNVe class as described in section 4.2.2).

Regarding the one-class classification task, the final selected maps were those derived with Rule II choosing ($\gamma = 1, \nu = 0.1$) for the OC-SVM and $\rho = 0.005$ for the MaxEnt in the dualpol case and ($\gamma = 3, \nu = 0.1$) for the OC-SVM and $\rho = 0.015$ for the MaxEnt in the quadpol case (see Figure

Table 5-22: HNV one-class classification – Validation accuracies computed for the maps obtained applying the OC-SVM and MaxEnt (for different values of ρ) to the dualpol BY-RS2-2011 [VV/VH] datasets using the three defined spatial homogeneity rulesets. Results for the maps selected by qualitative assessment as most reliable for the OC-SVM and MaxEnt are highlighted in yellow and blue, respectively [GL training samples: 5254; GL validation samples: 4057; NGL validation samples: 181004].

			Rule I					Rule II					Rule III				
			OA%	Kappa	GL PA%	NGL PA%	AA%	OA%	Kappa	GL PA%	NGL PA%	AA%	OA%	Kappa	GL PA%	NGL PA%	AA%
dualpol	OC-SVM		97.83	0.6446	93.71	97.93	95.82	97.83	0.6446	93.71	97.93	95.82	97.83	0.6446	93.71	97.93	95.82
	MaxEnt	ρ = 0.001	91.91	0.3272	100.00	91.73	95.86	92.13	0.3339	100.00	91.96	95.98	92.58	0.3482	100.00	92.42	96.21
		ρ = 0.005	96.44	0.5342	98.89	96.38	97.64	96.56	0.5430	98.89	96.51	97.70	96.79	0.5582	97.71	96.77	97.24
		ρ = 0.01	97.22	0.5957	98.42	97.19	97.81	97.31	0.6038	98.42	97.28	97.85	97.45	0.6099	95.51	97.49	96.50
		ρ = 0.015	97.72	0.6441	98.42	97.71	98.06	97.80	0.6525	98.42	97.79	98.11	97.89	0.6547	95.51	97.94	96.73
		ρ = 0.025	98.03	0.6779	98.42	98.03	98.22	98.09	0.6846	98.42	98.09	98.25	98.11	0.6731	92.70	98.23	95.47
		ρ = 0.05	98.17	0.6611	84.59	98.48	91.54	98.21	0.6658	84.59	98.52	91.56	98.26	0.6644	81.69	98.63	90.16
		ρ = 0.075	98.40	0.6827	81.46	98.78	90.12	98.42	0.6857	81.46	98.80	90.13	98.44	0.6835	79.74	98.86	89.30
		ρ = 0.1	98.42	0.6727	76.58	98.91	87.75	98.43	0.6734	76.58	98.92	87.75	98.44	0.6713	75.35	98.96	87.15
		ρ = 0.125	98.53	0.6734	71.46	99.14	85.30	98.54	0.6752	71.46	99.15	85.30	98.57	0.6752	70.22	99.20	84.71
		ρ = 0.15	98.34	0.5974	58.17	99.24	78.71	98.35	0.5985	58.17	99.25	78.71	98.37	0.5967	56.94	99.30	78.12

Table 5-23: HNV one-class classification – Validation accuracies computed for the maps obtained applying the OC-SVM and MaxEnt (for different values of ρ) to the quadpol BY-RS2-2011 [QUAD] datasets using the three defined spatial homogeneity rulesets. Results for the maps selected by qualitative assessment as most reliable for the OC-SVM and MaxEnt are highlighted in yellow and blue, respectively [GL training samples: 5254; GL validation samples: 4057; NGL validation samples: 181004].

			Rule I					Rule II					Rule III				
			OA%	Kappa	GL PA%	NGL PA%	AA%	OA%	Kappa	GL PA%	NGL PA%	AA%	OA%	Kappa	GL PA%	NGL PA%	AA%
quadpol	OC-SVM		98.50	0.7173	90.21	98.68	94.45	98.50	0.7173	90.21	98.68	94.45	98.50	0.7173	90.21	98.68	94.45
	MaxEnt	ρ = 0.01	97.85	0.6525	96.08	97.89	96.99	97.91	0.6589	96.08	97.95	97.02	98.02	0.6639	93.17	98.13	95.65
		ρ = 0.015	97.96	0.6621	95.02	98.03	96.53	98.01	0.6678	95.02	98.08	96.55	98.11	0.6721	92.11	98.24	95.18
		ρ = 0.025	98.01	0.6435	85.46	98.29	91.87	98.03	0.6459	85.46	98.31	91.89	98.07	0.6427	82.55	98.42	90.48
		ρ = 0.05	98.30	0.6717	82.35	98.66	90.51	98.32	0.6744	82.35	98.68	90.52	98.27	0.6522	77.13	98.74	87.93
		ρ = 0.075	98.46	0.6665	72.81	99.03	85.92	98.37	0.6381	68.15	99.04	83.60	98.37	0.6328	66.48	99.08	82.78
		ρ = 0.1	98.47	0.6590	70.00	99.10	84.55	98.37	0.6295	65.34	99.11	82.23	98.38	0.6252	63.96	99.15	81.56
		ρ = 0.125	98.64	0.6767	67.29	99.34	83.31	98.54	0.6447	62.63	99.34	80.99	98.56	0.6468	62.16	99.37	80.77
		ρ = 0.15	98.38	0.5775	52.18	99.42	75.80	98.28	0.5392	47.52	99.42	73.47	98.31	0.5419	47.30	99.45	73.37

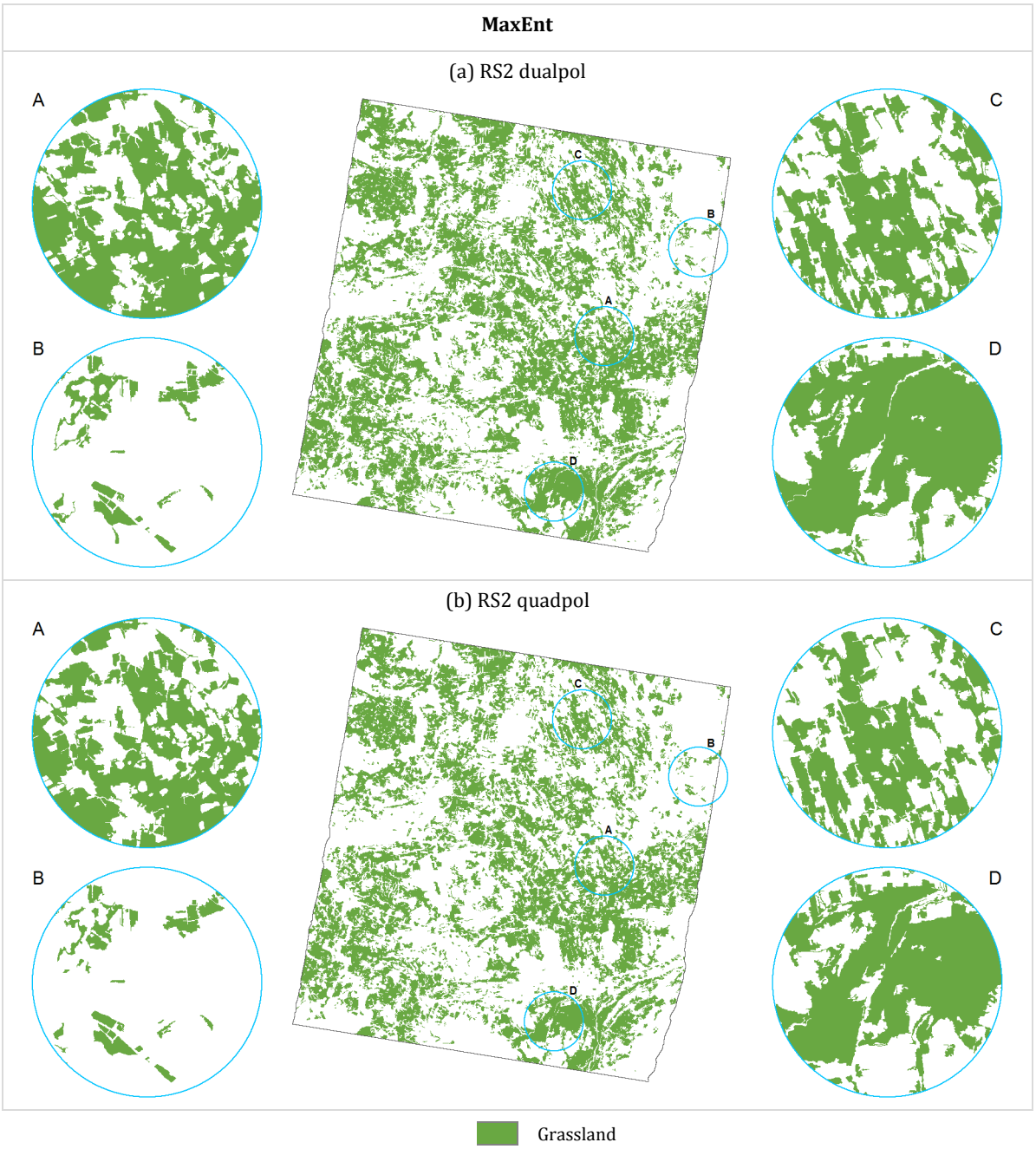

Figure 5-24: HNV one-class classification map obtained for the dualpol BY-RS2-2011 [VV/VH] (a) and quadpol BY-RS2-2011 [QUAD] (b) datasets using the MaxEnt.

5-24 and Figure 5-25). By visually comparing them it is clear that they are qualitatively very similar with just minor differences among the two classifiers and datasets, exhibiting an AA% always higher than 94 as reported in Table 5-22 and Table 5-23. Accordingly, for consistency with the other experimental trials, the MaxEnt was employed again in the final hierarchical system, despite when analysing the accuracies, the OC-SVM actually resulted in higher values of Kappa due to the higher PA% for the NGL class (for which more validation samples were available), despite the MaxEnt provides higher PA% for the GL class. In general, it is worth noting that even exploiting C-band data, performances are in line with those obtained with TSX dualpol imagery (despite less scenes were available); furthermore, also here some smaller agricultural areas tend to be misclassified as belonging to the GL class.

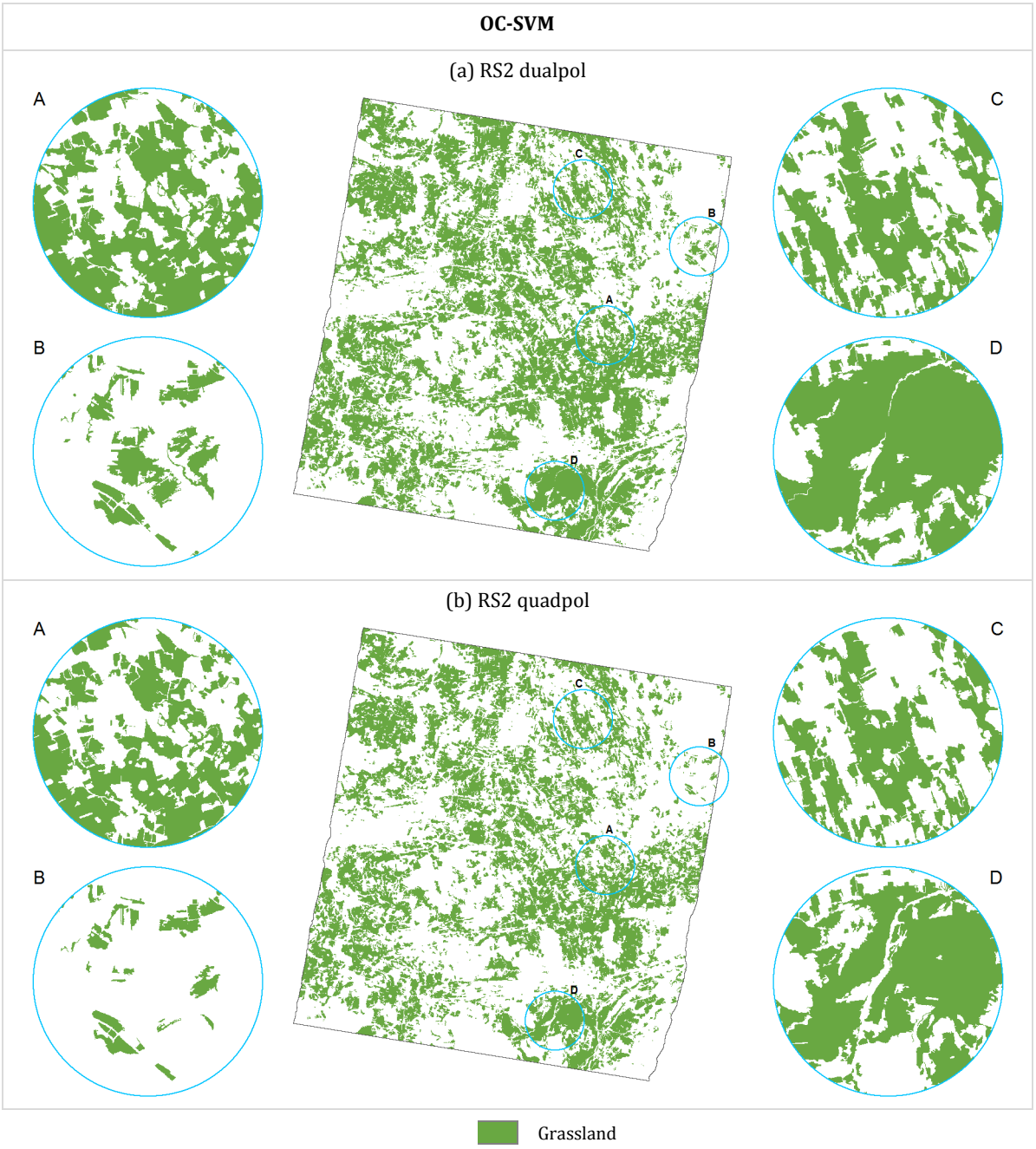

Figure 5-25: HNV one-class classification map obtained for the dualpol BY-RS2-2011 [VV/VH] (a) and quadpol BY-RS2-2011 [QUAD] (b) datasets using the OC-SVM.

The final targeted classification maps derived with the *hierarchical MaxEnt + SVM*, *hierarchical MaxEnt + MaxEnt* and *standard MaxEnt* are shown in Figure 5-26 and Figure 5-27, whereas the results of the corresponding accuracy assessment are presented in Table 5-24. It can be directly noticed that each method shows similar OA% and Kappa values for the two datasets BY-RS2-2011 [VV/VH] and BY-RS2-2011 [QUAD], but they both strongly vary among the different classifiers. Indeed, while the hierarchical approaches exhibit OA% greater than 97 and Kappa values greater 0.55, the *standard MaxEnt* exhibits an OA% of 50.20 and Kappa of 0.0443 for the dualpol case and an OA% of 50.89 and Kappa of 0.0391 for the quadpol case due to consistent overestimation of the targeted classes in the NGL areas. In particular, the *hierarchical MaxEnt + SVM* (for which the optimal parameters proved to be ($\gamma = 0.004, C = 1000$) for the dualpol and

Table 5-24: HNV targeted classification – Validation accuracies computed for the maps obtained applying the three considered methods to the BY-RS2-2011 [VV/VH] and BY-RS2-2011 [QUAD] datasets using 2152 training samples for class HNVi and 3102 for class HNVe.

		OA%	Kappa	PA%			% unclassified		# validation points		
				NGL	HNVi	HNVe	HNVi	HNVe	NGL	HNVi	HNVe
dualpol	*hierarchical MaxEnt + SVM*	97.70	0.6210	96.51	79.58	79.46	0.00	3.17	181004	2037	2020
	hierarchical MaxEnt + MaxEnt	97.18	0.5570	96.51	58.37	81.58	0.00	3.17			
	standard MaxEnt	53.20	0.0443	52.79	58.42	84.60	0.00	0.00			
quadpol	*hierarchical MaxEnt + SVM*	97.81	0.6200	98.08	76.83	70.15	0.00	10.00	181004	2037	2020
	hierarchical MaxEnt + MaxEnt	97.30	0.5524	98.08	52.77	72.62	0.00	10.00			
	standard MaxEnt	50.89	0.0391	50.52	53.02	81.63	0.34	0.00			

Table 5-25: Intra-class classification accuracies (computed without considering the NGL validation points) for the HNV targeted classification maps obtained applying the four considered methods to the BY-RS2-2011 [VV/VH] and BY-RS2-2011 [QUAD] datasets using 2152 training samples for class HNVi and 3102 for class HNVe.

		OA%	Kappa	PA%		# validation points	
				HNVi	HNVe	HNVi	HNVe
dualpol	*hierarchical MaxEnt + SVM*	80.79	0.6159	79.58	82.06	2037	1956
	hierarchical MaxEnt + MaxEnt	71.05	0.4239	58.37	84.25	2037	1956
	standard MaxEnt	71.46	0.4298	58.42	84.60	2037	2020
quadpol	*hierarchical MaxEnt + SVM*	77.35	0.5466	76.83	77.94	2037	1818
	hierarchical MaxEnt + MaxEnt	65.94	0.3287	52.77	80.69	2037	1818
	standard MaxEnt	67.38	0.3481	53.20	81.63	2030	2020

($\gamma = 0.01, C = 1$) for the quadpol case) performed best, with Kappa ~0.07 higher than the *hierarchical MaxEnt + MaxEnt.*

The poor performances of the *standard MaxEnt* are also evident in the classification maps reported in Figure 5-26 (c) and Figure 5-27 (c), where forested areas and water bodies are wrongly classified as any of the targeted HNV classes. For instance, this occurs for both the "Staffelsee" (north of zoom D) as well as the "Starnberger See" (north of zoom B) and emerges when analysing the PA% (see Table 5-24), where the *standard MaxEnt* achieved good results for the class HNVe (84.60 for the dual- and 81.63 for the quadpol data), but was not able to reliably categorise class HNVi (obtaining solely 58.42 for the dual- and 53.02 for the quadpol case) as well as the NGL class with 52.79 for the dual- and 50.52 for the quadpol dataset). A slight overestimation of the targeted classes also occurred with the hierarchical classifiers (as confirmed by the extremely low percentage of unclassified samples given in Table 5-24 and the relatively lower PA% of the NGL compared to the HT problem). Nevertheless, as yet pointed out before when analysing the one-class classification maps, this is linked to the fact that, especially for the HNVi class, the behaviour over time is rather similar to that of some crops with relatively small extent present in the study area.

From the intra-class accuracies reported in Table 5-25, one can notice that the *hierarchical MaxEnt + SVM* was able to better differentiate the two targeted classes for the dual- and quadpol case achieving OA% of 80.79 and 77.35 as well as Kappa of 0.6159 and 0.5466, respectively; moreover, this is reflected in the obtained PA% (79.58 and 76.83 for HNVi and 82.06 and 77.94 for the HNVe class). With the other two classifiers, HNVi areas are often incorrectly classified as

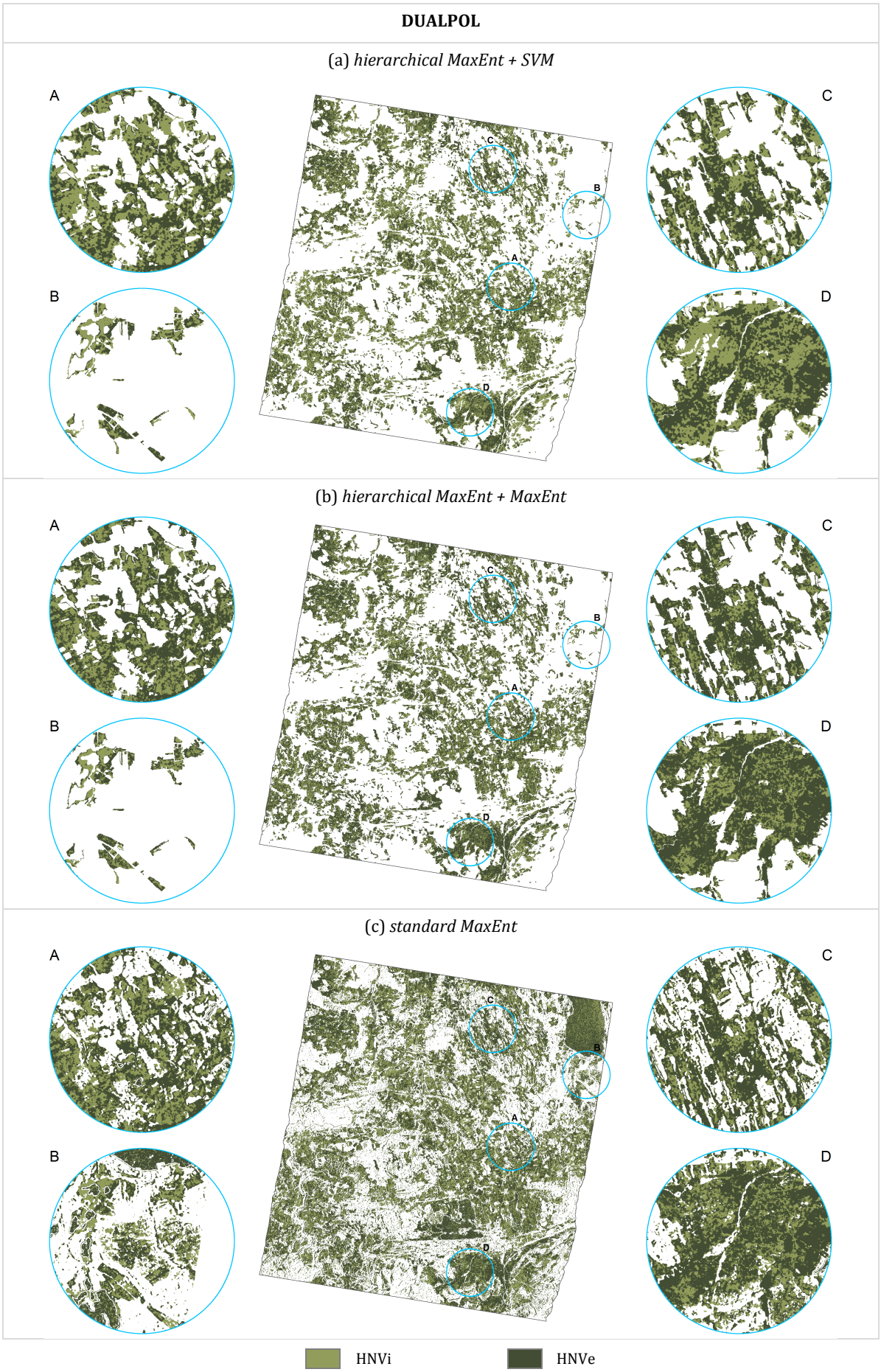

Figure 5-26: BY-RS2 2011 [VV/VH] dataset - HNV targeted classification maps obtained using: (a) the *hierarchical MaxEnt + SVM*, (b) the *hierarchical MaxEnt + MaxEnt*, and (c) the *standard MaxEnt* approaches.

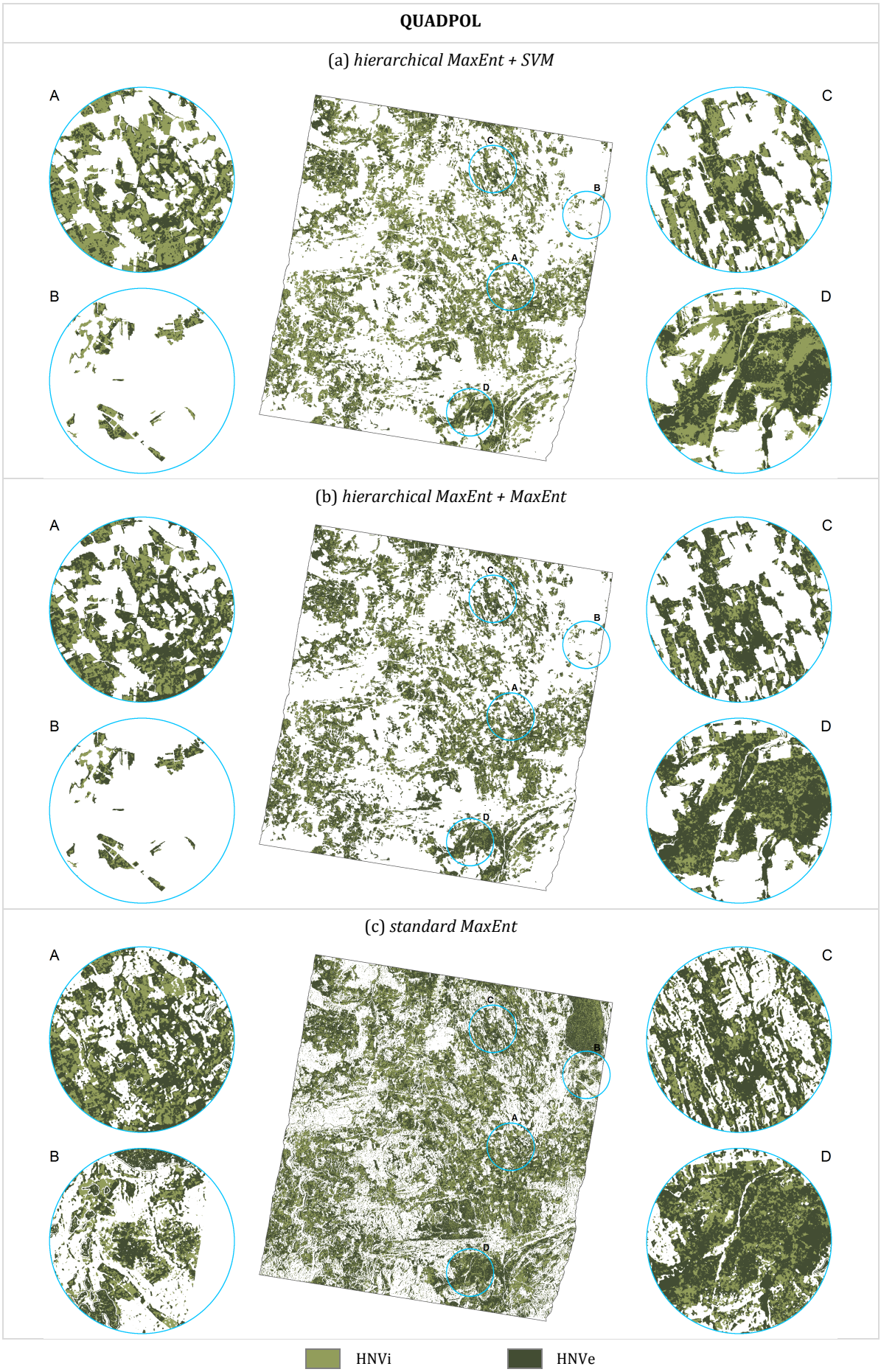

Figure 5-27: BY-RS2-2011 [QUAD] dataset - HNV targeted classification maps obtained using: (a) the *hierarchical MaxEnt + SVM*, (b) the *hierarchical MaxEnt + MaxEnt*, and (c) the *standard MaxEnt* approaches.

HNVe resulting in a poorer PA% for HNVi (i.e., between 52.77 and 58.42) compared to the one for HNVe (i.e., between 80.69 and 84.60).

However, it is worth pointing out that Kappa and OA% for all methods derived using the dualpol data were always ~0.06 to ~0.1 and ~3 to 5 higher than those obtained with quadpol data. This supports what has been discussed in section 5.2.1 for the HT based classifications. Indeed, it appears that the quadpol data allow better discrimination of the targeted classes from the remaining land cover types present in the test area. Nevertheless, the dualpol data resulted in higher intra-class separability between the targeted classes while obtaining similar performances in differentiating them from the NGL areas.

6. SUMMARY AND CONCLUSIONS

The presented work aimed at developing a novel targeted classification system for the automatic identification of grassland types by means of multi-temporal and multi-polarised SAR data.

In the light of the ongoing loss of biodiversity at the global scale, monitoring grasslands is nowadays of utmost importance considering their functional relevance in terms of the ecosystem services that they provide. Here, guidelines of the European Union like the FFH directive and the EAFRD regulation with its HNV indicators are crucial. Indeed, they form the legal framework for nature conservation and define grasslands as one of their conservation targets, whose status needs to be assessed and reported by all member states on a regular basis. However, costly and time consuming field surveys or photointerpretation are still the most common practices for mapping their habitat distribution.

To this purpose, a cost-effective solution is offered by EO data for which specific grassland monitoring methodologies shall be then implemented which are capable of processing multitemporal acquisitions collected throughout the entire growing season. Although optical data are most suited for characterising vegetation in terms of spectral information content, they are actually subject to weather conditions (especially cloud coverage), which hinder the possibility of collecting enough information over the full phenological cycle. To overcome this limitation, SAR systems can be employed which provide imagery independent from weather or daytime conditions, hence enabling vegetation analysis by means of complete time series. However, in this context presently only very few techniques have been implemented, which are anyhow not suitable to be employed in an operational framework.

Furthermore, to address the classification task, supervised approaches (which require in situ information for all the land-cover classes present in the study area) represent the most accurate methodological solution; nevertheless, collecting an exhaustive ground truth is generally expensive both in terms of time and economic costs and is not even feasible when the test site is remote (Fernández-Delgado *et al.*, 2014). However, in many applications the end-users are generally only interested in very few specific targeted land-cover classes which, for instance, have high ecological value or are associated with support actions, subsidies or benefits from national or international institutions (Mack *et al.*, 2014). The categorisation of specific grasslands and habitat types as those addressed in this thesis falls within such category of problems, which is defined in the literature as targeted land-cover classification (Marconcini *et al.*, 2014).

In this framework, the main objective of this work was to develop a robust and effective approach for the targeted classification of the considered grasslands of interest (i.e., four Natura

2000 HT as well as intensive and extensive HNV grasslands), capable of handling either dual- or quadpol VHR multi-temporal SAR imagery. The proposed hierarchical classification approach consist of two phases where first a one-class classifier is employed to outline the merger of all the grassland types of interest considered as a single information class and then a multi-class classifier is applied for discriminating the specific targeted classes within the areas identified as positive by the one-class classifier. To evaluate the capabilities of the proposed methodology, several experimental trials have been carried out over two test sites located in Southern Bavaria (Germany) and Mecklenburg Western-Pomerania (Germany) for which six diverse datasets have been derived from multitemporal series of dualpol TSX as well as dual-/quadpol RS2 images (i.e., BY-TSX-2011 [VV/VH], BY-TSX-2012 [VV/VH], MV-TSX-2011 [VV/VH], MV-TSX-2012 [VV/VH], BY-RS2-2011 [VV/VH], and BY-RS2-2011 [QUAD]).

In the first phase of the proposed system, the two currently most largely employed one class-classifiers (i.e., the MaxEnt and the OC-SVM) have been tested and compared. The MaxEnt classifier proved generally more effective than the OC-SVM, thus it has been finally adopted in the first phase of the presented hierarchical system in all experimental trials. In the second phase, SVM have been used due to their proven effectiveness when dealing with remote-sensing supervised classification problems. However, also an alternative multi-class approach based on an ensemble of different MaxEnt classifiers has been tested, which does not require any free parameter to be tuned by the user. The performances of the two approaches (i.e., referred to as *hierarchical MaxEnt + SVM* and *hierarchical MaxEnt + MaxEnt*) have been also compared to those of a standard ensemble of MaxEnt classifiers (*standard MaxEnt*) each one applied to discriminate a specific targeted class from the others.

Concerning the classification of the Natura 2000 HT, when employing the proposed hierarchical system, the pixels not categorised as grassland by the MaxEnt during the first phase in both years were discarded since the considered targeted classes experience changes only over several years. To account for this also when using the standard approach, an additional *combined MaxEnt* has been defined where, similarly, only pixels associated with any of the targeted classes both in 2011 and 2012 were kept. The hierarchical classifiers always outperformed the standard ones in terms of OA% and Kappa with the *hierarchical MaxEnt + SVM* having mostly marginally higher OA% and Kappa values. However, the classification accuracies of the *hierarchical MaxEnt + MaxEnt* are similar (even slightly higher for the Mecklenburg datasets). Performances were always very satisfactory for class 7120 (as also confirmed by the qualitative assessment of the final targeted classification maps); instead, accuracies for classes 6410, 7140, and 7230 in Bavaria as well as for class 7140 in Mecklenburg were rather low. For the three classes in Bavaria this was mainly due to their similar characteristics among each other in the analysed feature space. Thus, a further set of experimental trails has been performed merging the three classes into a single “wet grasslands” class. The obtained results confirmed the usefulness of joining them together; indeed, the PA% of the wet grasslands class were sensibly higher for both hierarchical approaches with values greater than 80 and 77 for the TSX and RS2 datasets, respectively. The poor performances for class 7140 in Mecklenburg were mainly due to the very few training data available and the reduced number of scenes lacking crucial temporal coverages during the phenological phase for discriminating the targeted class from agricultural areas. However, the experiments carried out on the Mecklenburg dataset represented an extreme test

case and, despite the lower accuracies in some experiments, the obtained maps were qualitatively good especially compared to those obtained with the standard approaches that proved to be completely unreliable. Indeed, these resulted in a consistent underestimation of the targeted classes, as well as severe misclassification of the NGL areas such as forests for all six datasets. Also, it is worth noting that despite different numbers and dates of image acquisitions have been analysed, the results did not show any significant differences among the six experimental trials, thus, proving the robustness of the proposed hierarchical approach.

The targeted classification for the HNV problem proved to be rather challenging based on the few training data and the diverse number and dates of image acquisitions that were available. In general, the hierarchical classification approaches outperformed the standard one in all six experimental analyses. For the Bavarian TSX datasets (BY-TSX-2011 [VV/VH] and BY-TSX-2012 [VV/VH]), the hierarchical approaches reached similar classification results with a higher PA% for HNVe in 2011 and for HNVi in 2012, where the *hierarchical MaxEnt + MaxEnt* performed slightly better than the *hierarchical MaxEnt + SVM*. For the Mecklenburg test case (MV-TSX-2011 [VV/VH], MV-TSX-2012 [VV/VH]) only the *hierarchical MaxEnt + SVM* was capable of properly discriminating the two targeted classes. The few available training samples did not allow for a reliable estimation of the conditional probability density when using the MaxEnt in the second phase of the presented method, thus resulting in significant misclassifications and poor performances of the *hierarchical MaxEnt + MaxEnt*. For the Bavaria RS2 datasets (BY-RS2-2011 [VV/VH], and BY-RS2-2011 [QUAD]) the *hierarchical MaxEnt + SVM* performed slightly better than the *hierarchical MaxEnt + MaxEnt,* despite that Kappa and OA% values derived using the dualpol data were always higher than those obtained with quadpol data. In particular, it emerged that the quadpol data allowed better discrimination of the targeted classes from the remaining land cover types present in the test area. Nevertheless, the dualpol data allowed to obtain higher intra-class separability between the targeted classes and similar performances in differentiating them from the NGL areas. On the contrary, the classification results of the *standard MaxEnt* for all six datasets were rather poor showing a consistent overestimation of either HNVi or HNVe in the NGL areas in the corresponding classification maps. However, even in such a critical situation, the proposed hierarchical concept resulted in a consistent improvement with respect to the standard approach. Again, also when addressing the HNV problem, the results of the *hierarchical MaxEnt + MaxEnt* were in line with those obtained by the *hierarchical MaxEnt + SVM*, exhibiting even better performances in some of the experiments. However, it is worth recalling that the *hierarchical MaxEnt + MaxEnt* requires only a single parameter to be tuned by the user (i.e. the threshold for the MaxEnt used in the first phase); instead, when employing the SVM an additional model selection (despite fully automatic) of the corresponding free parameters has to be done.

6.1. Potentials and limitations

The results obtained over of the six considered datasets clearly show the potential of the proposed methodology and demonstrate that an automatic targeted classification of SAR imagery is well suited for defining specific types of grasslands with distinct characteristics, as well as determining different degrees of farming practices (i.e., intensively, extensively). Indeed, the addressed classification problems were quite challenging in terms of similarity of the

targeted classes, availability of reference data and sufficient temporal coverage during the phenological cycle of the classes of interest. In particular, it could be demonstrated that the proposed hierarchical targeted classification approach outperforms the available state-of-the-art methods and has a clear advantage with respect to the standard approaches in terms of robustness, reliability and transferability.

The most crucial points proved to be the availability of a consistent set of training points for the targeted classes and the number and frequency of the SAR acquisitions throughout the whole growing season. The former aspect proved of key importance especially for discriminating the classes of interest among each other (the more the training samples, the higher the accuracies), while the latter seems crucial for a proper discrimination of the targeted classes with respect to some types of crops exhibiting similar spectral and temporal behaviour which can only be effectively separated if scenes acquired in certain time frames are available. This emerged especially for the HNV classes which in some cases were misclassified as agricultural fields. Nevertheless, it is worth noting that for solving this issue the integration of information from optical (e.g., Landsat-8, Sentinel-2 (S2)) or even hyperspectral data (e.g., from the future EnMAP mission) might be of great support.

The results obtained with X-band TSX and C-band RS2 data showed comparable accuracies, although the classifications based on TSX data had slightly better results due to a significant higher number of training samples available. Thus, both frequency bands prove to be suitable for the discrimination of grasslands and enable the operational application in the light of new SAR missions as Sentinel-1.

Concerning the RS2 polarisation, the quadpol data only allowed a slightly better separation of the targeted classes from the NGL areas with respect to the dualpol data when addressing the initial one-class classification problem with the presented hierarchical approaches; instead, dualpol data resulted in marginally higher intra-class separability among the targeted classes. Accordingly, in the light of their wider swath covering larger areas, and the corresponding lower number of features, dualpol data seem more suitable for a potential operational employment of the methodology.

Furthermore, the *Kennaugh elements* form an easy to use basis for the considered analyses. In particular, they enable exploiting the full capacity of dualpol as well as quadpol information independently from the type of polarisation (i.e., cross-pol, co-pol). This is particularly interesting, as previous decomposition methods have been established for quadpol data or very few specific dualpol cases only, but multi-polarisation data are nowadays most commonly acquired in dualpol mode as for instance in the case of Sentinel-1 or TerraSAR-X (see section 3.1).

6.2. Future Research Potential

Overall, the proposed system proved to be robust and confirmed the effectiveness of employing multitemporal and multi-polarisation VHR SAR data for discriminating HT and HNV grassland types, exhibiting high potential for future employment even at larger scales. In this context, new SAR missions like the C-band Sentinel-1 (S1) offer an ideal framework. Indeed, already the first satellite of the constellation (i.e., S1A) is providing a massive amount of data over Europe,

whereas the second (i.e., S1B) has been launched recently and is foreseen to be operative in few months. With both of them fully operating, tens of thousands of dualpol acquisitions mostly in VV/VH mode will be available every year over Europe since the S1 mission is serving the European Earth observation programme Copernicus (www.copernicus.eu). In particular, S1 imagery is regularly acquired without the need of any acquisition planning by the researchers, thus providing continuous times series of data and preventing the interference with priority acquisitions (e.g., for disaster management and emergency relief). This fosters the applicability of the proposed methodology to the extent of a whole continent and even other regions of the world, especially in the light of the good performance that it exhibited based on the C-band RS2 data.

Regarding future developments from the thesis, the presented classification system will be tested also with other habitat types. Despite it was not possible to gather existing reference data on the Natura 2000 habitats from local or governmental authorities during the lifetime of the MSAVE project, this information should already be available as the first reporting had to be performed and knowledge about the classes, their location and extent exists. Indeed, these reference datasets could be employed for evaluating the applicability of the proposed system to further habitat types for monitoring purposes and updating existing databases. Furthermore, the presented system should be tested in another context, i.e., other land cover classes for which exhaustive ground truth data is available, different input data such as optical data from S2 or Landsat 8, or the characterisation of the status of the habitats like soil moisture or shrub encroachment.

REFERENCES

Airbus Defence and Space / Infoterra GmbH and DLR (2014), *WorldDEM™: Reaching new heights* No. GEO/022/0514, available at: http://www2.geo-airbusds.com/files/pmedia/public/r5434_9_geo_022_worlddem_en_low.pdf (accessed 8 May 2016).

Alberga, V. (2004), "Volume Decorrelation Effects in Polarimetric SAR Interferometry", *Geoscience and Remote Sensing, IEEE Transactions on*, Vol. 42 No. 11, pp. 2467–2477.

Andersen, E., Baldock, D., Bennett, H., Beaufoy, G., Bignal, E., Brouwer, F., Elbersen, B., Eiden, G., Godeschalk, F., Jones, G., McCracken, D., Nieuwenhuizen, W., van Eupen, M., Hennekens, S. and Zervas, G. (2003), *Developing a High Nature Value Farming area indicator - final report: Internal report for the European Environment Agency*.

Anys, H., Bannari, A., He, D.-C. and Morin, D. (Eds.) (1994), *Texture analysis for the mapping of urban areas using airborne MEIS-II images*, Vol. 3.

Banerjee, A., Burlina, P. and Diehl, C. (2006), "A support vector method for anomaly detection in hyperspectral imagery", *IEEE Transactions on Geoscience and Remote Sensing*, Vol. 44 No. 8, pp. 2282–2291.

Bayerisches Staatsministerium für Umwelt und Verbraucherschutz (2015), "Europäischer Biotopverbund Natura 2000: Allgemeine Informationen zur Umsetzung in Bayern", available at: http://www.stmuv.bayern.de/umwelt/naturschutz/natura2000/index.htm (accessed 30 December 2015).

Bennett, J. (2003), "The economic value of biodiversity: a scoping paper", available at: http://www.environment.gov.au/resource/economic-value-biodiversity-scoping-paper (accessed 30 April 2016).

Betbeder, J., Rapinel, S., Corgne, S., Pottier, E. and Hubert-Moy, L. (2015), "TerraSAR-X dual-pol time-series for mapping of wetland vegetation", *ISPRS Journal of Photogrammetry and Remote Sensing*, No. 0, pp. -.

Bishop, C.M. (1994), "Novelty detection and neural network validation", *Vision, Image and Signal Processing, IEE Proceedings* -, Vol. 141 No. 4, pp. 217–222.

Blaes, X. and Defourny, P. (2003), "Retrieving crop parameters based on tandem 5ERS6 1/2 interferometric coherence images", *Remote Sensing of Environment*, Vol. 88 No. 4, pp. 374–385.

Blaes, X., Vanhalle, L. and Defourny, P. (2005), "Efficiency of crop identification based on optical and SAR image time series", *Remote Sensing of Environment*, Vol. 96 No. 3-4, pp. 352–365.

Bock, M. and Lessing, R. (2000), "Remote sensing, formation of objects and determination of quality", in Cremers, A.B. and Greve, K. (Eds.), *EnviroInfo 2000: Umweltinformatik '00 Umweltinformation für Planung, Politik und Öffentlichkeit, Bonn*, Metropolis Verlag, Marburg.

Bock, M., Rossner, G., Wissen, M., Remm, K., Langanke, T., Lang, S., Klug, H., Blaschke, T. and Vrščaj, B. (2005a), "Spatial indicators for nature conservation from European to local scale", *Ecological Indicators*, Vol. 5 No. 4, pp. 322–338.

Bock, M., Xofis, P., Mitchley, J., Rossner, G. and Wissen, M. (2005b), "Object-oriented methods for habitat mapping at multiple scales – Case studies from Northern Germany and Wye Downs, 5UK6", *Journal for Nature Conservation*, Vol. 13 No. 2–3, pp. 75–89.

Breiman, L. (2001), "Random Forests", *Machine Learning*, Vol. 45 No. 1, pp. 5–32.

Brisco, B. and Brown, R.J. (1995), "Multidate SAR/TM Synergism for Crop Classification in Western Canada", *Photogrammetric Engineering & Remote Sensing*, Vol. 91 No. 8, pp. 1009–1014.

Buck, O., Garcia Millán, Virginia E., Klink, A. and Pakzad, K. (2015), "Using information layers for mapping grassland habitat distribution at local to regional scales", *International Journal of Applied Earth Observation and Geoinformation*, Vol. 37, pp. 83–89.

Buck, O., Klink, A., Elena García Millán, Virginia, Pakzad, K. and Müterthies, A. (2013), "Image Analysis Methods to Monitor Natura 2000 Habitats at Regional Scales – the MS. MONINA State Service Example in Schleswig-Holstein, Germany", *Photogrammetrie - Fernerkundung - Geoinformation*, Vol. 2013 No. 5, pp. 415–426.

Bundesamt für Naturschutz (BfN) (2011a), "* Naturnahe lebende Hochmoore. NATURA 2000-Code: *7110", available at: https://www.bfn.de/0316_typ7110.html (accessed 11 December 2015).

Bundesamt für Naturschutz (BfN) (2011b), *Erfassungsanleitung für den HNV-Farmland-Indikator,* 3rd ed.

Bundesamt für Naturschutz (BfN) (2011c), "Molinia meadows on calcareous, peaty or clayey-silt-laden soils (Eu-Molinion). NATURA 2000 Code: 6410", available at: https://www.bfn.de/0316_typ6410+M5054de7a952.html (accessed 11 December 2015).

Bundesamt für Naturschutz (BfN) (2011d), "Pfeifengraswiesen auf kalkreichem Boden und Lehmboden (Eu-Molinion). NATURA 2000-Code: 6410", available at: https://www.bfn.de/0316_typ6410.html (accessed 11 December 2015).

Bundesamt für Naturschutz (BfN) (2012a), "Alkaline fens. NATURA 2000 Code: 7230", available at: https://www.bfn.de/0316_typ7230+M52087573ab0.html (accessed 12 December 2015).

Bundesamt für Naturschutz (BfN) (2012b), "Degraded raised bogs (which may still be capable of natural regeneration). NATURA 2000 Code: 7120", available at: https://www.bfn.de/0316_typ7120+M5054de7a952.html (accessed 11 December 2015).

Bundesamt für Naturschutz (BfN) (2012c), "Geschädigte Hochmoore (die möglicherweise noch auf natürlichem Wege regenerierbar sind). NATURA 2000-Code: 7120", available at: https://www.bfn.de/0316_typ7120.html (accessed 11 December 2015).

Bundesamt für Naturschutz (BfN) (2012d), "Kalkreiche Niedermoore. NATURA 2000-Code: 7230", available at: https://www.bfn.de/0316_typ7230.html (accessed 12 December 2015).

Bundesamt für Naturschutz (BfN) (2012e), "Transition mires and quaking bogs. NATURA 2000 Code: 7140", available at: https://www.bfn.de/0316_typ7140+M52087573ab0.html (accessed 12 December 2015).

Bundesamt für Naturschutz (BfN) (2012f), "Übergangs- und Schwingrasenmoore. NATURA 2000-Code: 7140", available at: https://www.bfn.de/0316_typ7140.html (accessed 12 December 2015).

Bundesamt für Naturschutz (BfN) (2014), "Character taxa for a regional classification of grassland for the High Nature Value Farmland (HNV Farmland) indicator in Germany", available at: https://www.bfn.de/fileadmin/MDB/documents/themen/monitoring/14_02_26_Kennartenliste_HNV_barrfrei_Englisch.pdf (accessed 8 December 2015).

Büttner, G., Soukop, T. and Kosztra, B. (2014), *CLC2012 Addendum to CLC2006 Technical Guidelines*.

Capraro, R.M. (2007), "Significance Level", in Salkind, N.J. (Ed.), *Encyclopedia of Measurement and Statistics*, 0th ed., SAGE Publications, Inc, pp. 890–893.

Chang, C.-C. and Lin, C.-J. (2011), "LIBSVM: A library for support vector machines", *ACM Transactions on Intelligent Systems and Technology*, Vol. 2 No. 3, pp. 27:1-27:27.

Cloude, S.R. (2007), "The dual polarisation entropy/alpha decompositon: A palsar case study".

Cloude, S.R. and Pottier, E. (1996), "A review of target decomposition theorems in radar polarimetry", *Geoscience and Remote Sensing, IEEE Transactions on*, Vol. 34 No. 2, pp. 498–518.

Condé, S., Richard, D., Liamine, N., Leclère, A.-S., Mitlacher, G., Hansen, H.-O., Merzliakova, I., Pinborg, U., Larsson, T.-B., Svensson, L. and Andersson, G. (2002), *Europe's biodiversity: biogeographical regions and seas*.

Conner, R., Seidl, A., VanTassell, L. and Wilkins, N. (2001), "United States Grasslands and Related Resources: An Economic and Biological Trends Assessment", available at: http://twri.tamu.edu/media/256592/unitedstatesgrasslands.pdf (accessed 31 October 2013).

Corbane, C., Alleaume, S. and Deshayes, M. (2013), "Mapping natural habitats using remote sensing and sparse partial least square discriminant analysis", *International Journal of Remote Sensing*, Vol. 34 No. 21, pp. 7625–7647.

Corbane, C., Lang, S., Pipkins, K., Alleaume, S., Deshayes, M., García Millán, Virginia Elena, Strasser, T., Vanden Borre, J., Toon, S. and Förster, M. (2015), "Remote sensing for mapping natural habitats and their conservation status – New opportunities and challenges", *International Journal of Applied Earth Observation and Geoinformation*, Vol. 37, pp. 7–16.

Council of the European Union (Council of the European Union) (1992), *Council Directive 92/43/EEC of 21 May 1992 on the conservation of natural habitats and of wild fauna and flora: FFH directive*, available at: http://eur-lex.europa.eu/legal-content/EN/TXT/?uri=CELEX:31992L0043 (accessed 25 January 2015).

Cover, T.M. (1965), "Geometrical and Statistical Properties of Systems of Linear Inequalities with Applications in Pattern Recognition", *IEEE Transactions on Electronic Computers*, EC-14 No. 3, pp. 326–334.

Cristianini, N. and Shawe-Taylor, J. (2000), *An Introduction to Support Vector Machines and Other Kernel-based Learning Methods*, Cambridge University Press, Cambridge, United Kingdom.

Darroch, J. N. and Ratcliff, D. (1972), "Generalized Iterative Scaling for Log-Linear Models", *The Annals of Mathematical Statistics*, Vol. 43 No. 5, pp. 1470–1480.

Della Pietra, S., Della Pietra, V. and Lafferty, J. (1997), "Inducing features of random fields", *Pattern Analysis and Machine Intelligence, IEEE Transactions on*, Vol. 19 No. 4, pp. 380–393.

Díaz Varela, R., Ramil Rego, P., Calvo Iglesias, S. and Muñoz Sobrino, C. (2008), "Automatic habitat classification methods based on satellite images: A practical assessment in the NW Iberia coastal mountains", *Environmental Monitoring and Assessment*, Vol. 144 No. 1, pp. 229–250.

Dieudonné, J. (1960), *Foundations of Modern Analysis*, Academic Press Inc., New York.

DLR (2013), *TerraSAR-X Ground Segment Basic Product Specification Document*, Oberpfaffenhofen, Germany.

Duda, R.O., Hart, P.E. and Stork, D.G. (2000), *Pattern Classification*, Wiley-Interscience, New York, NY, USA.

Dudík, M., Phillips, S.J. and Schapire, R.E. (2004), "Performance Guarantees for Regularized Maximum Entropy Density Estimation", in John Shawe-Taylor and Yoram Singer (Eds.), *Learning Theory, Proceedings of the 17th Annual Conference on Learning Theory (COLT) 2004, Banff, Canada, July 1-4, 2004*, Springer, pp. 472–486.

EEA (2010), "Natura 2000 data - the European network of protected sites. Public data mid 2010", available at: http://www.eea.europa.eu/data-and-maps/data/natura (accessed 8 December 2015).

Elith, J., Phillips, S.J., Hastie, T., Dudík, M., Chee, Y.E. and Yates, C.J. (2011), "A statistical explanation of MaxEnt for ecologists", *Diversity and Distributions*, Vol. 17 No. 1, pp. 43–57.

Engler, R., Guisan, A. and Rechsteiner, L. (2004), "An improved approach for predicting the distribution of rare and endangered species from occurrence and pseudo-absence data", *Journal of Applied Ecology*, Vol. 41 No. 2, pp. 263–274.

Erasmi, S. (2013), "Habitat Mapping from Optical and SAR Satellite Data: Implications of Synergy and Uncertainty for Landscape Analysis", *PFG Photogrammetrie, Fernerkundung, Geoinformation*, Vol. 2013 No. 3, pp. 139–148.

ESA (2015a), "eoPortal - Satellite Missions Radarsat-2", available at: https://directory.eoportal.org/web/eoportal/satellite-missions/r/radarsat-2 (accessed 6 December 2015).

ESA (2015b), "Sentinel-1 Oberservation Scenario", available at: https://sentinel.esa.int/web/sentinel/missions/sentinel-1/observation-scenario (accessed 14 September 2015).

Esch, T., Metz, A., Marconcini, M. and Keil, M. (2014a), "Combined use of multi-seasonal high and medium resolution satellite imagery for parcel-related mapping of cropland and grassland", *International Journal of Applied Earth Observation and Geoinformation*, Vol. 28 No. 0, pp. 230–237.

Esch, T., Metz, A., Marconcini, M. and Keil, M. (2014b), "Differentiation of crop types and grassland by multi-scale analysis of seasonal satellite data", in Manakos, I. and Braun, M. (Eds.), *Land Use and Land Cover Mapping in Europe: Practices & Trends*, *Remote Sensing and Digital Image Processing*, 1st ed., Springer, Dordrecht, pp. 329–339.

European Commission (EC) (2006), *Commission Regulation (EC) No 1974/2006 of 15 December 2006 laying down detailed rules for the application of Council Regulation (EC) No 1698/2005 on support for rural development by the European Agricultural Fund for Rural Development: EAFRD*.

EUROSTAT (2013), *LUCAS 2012 (Land Use / Cover Area Frame Survey): Technical Reference Document: C-1 Instructions for Surveyors*.

Evangelista, P., Stohlgren, T., Morisette, J. and Kumar, S. (2009), "Mapping Invasive Tamarisk (Tamarix): A Comparison of Single-Scene and Time-Series Analyses of Remotely Sensed Data", *Remote Sensing*, Vol. 1 No. 3, pp. 519–533.

Fan, R.-E., Chen, P.-H. and Lin, C.-J. (2005), "Working Set Selection Using Second Order Information for Training SVM", *Journal of Machine Learning Research*, Vol. 6, pp. 1889–1918.

FAO (Food and Agriculture Organization of the United Nations) (Ed.) (2005), *Grasslands of the World: F*, Rome.

FAOSTAT ((Statistics Division of FAO)) (2013), "Composition of agricultural areas 2010 - 2013 within the European Union", available at: http://faostat3.fao.org/browse/R/RL/E (accessed 30 April 2016).

Feilhauer, H., Stenzel, S., Kübert, C., Metz, A., Conrad, C., Ehlers, M., Esch, T., Klein, D., Oldenburg, C., Reinartz, P. and Schmidtlein, S. (2012), "RapidEye im Projekt MSAVE - Multisaisonale Fernerkundung für das Vegetationsmonitoring", paper presented at 4. RESA Workshop, Neustrelitz.

Feilhauer, H., Thonfeld, F., Faude, U., He, K.S., Rocchini, D. and Schmidtlein, S. (2013), "Assessing floristic composition with multispectral sensors—A comparison based on monotemporal and multiseasonal field spectra", *International Journal of Applied Earth Observation and Geoinformation*, Vol. 21, pp. 218–229.

Fernández-Delgado, M., Cernadas, E., Barro, S. and Amorim, D. (2014), "Do We Need Hundreds of Classifiers to Solve Real World Classification Problems?", *Journal of Machine Learning Research*, Vol. 15 No. 1, pp. 3133–3181.

Ferrazzoli, P., Paloscia, S., Pampaloni, S., Schiavon, G., Sigismondi, S. and Solimini, D. (1997), "The Potential of Multifrequency Polarimetric SAR in Assessing Agricultural and Arboreous Biomass", *Geoscience and Remote Sensing, IEEE Transactions on*, Vol. 35 No. 1, pp. 5–17.

Foody, G.M., Mathur, A., Sanchez-Hernandez, C. and Boyd, D.S. (2006), "Training set size requirements for the classification of a specific class", *Remote Sensing of Environment*, Vol. 104 No. 1, pp. 1–14.

Förster, M., Schmidt, T., Schuster, C. and Kleinschmit, B. (2012), "Multi-temporal detection of grassland vegetation with RapidEye imagery and a spectral-temporal library", in *IEEE International Geoscience and Remote Sensing Symposium 2012 (IGARSS)*.

Franke, J., Keuck, V. and Siegert, F. (2012), "Assessment of grassland use intensity by remote sensing to support conservation schemes", *Journal for Nature Conservation*, Vol. 20 No. 3, pp. 125–134.

Freeman, A. and Durden, S.L. (1998), "A three-component scattering model for polarimetric SAR data", *Geoscience and Remote Sensing, IEEE Transactions on*, Vol. 36 No. 3, pp. 963–973.

Glaser, S., Lagally, U., Loth, G., Schmid, H. and Schwerd, K. (2008), *Geotope in Oberbayern, Erdwissenschaftliche Beiträge zum Naturschutz*, Vol. 6, Bayerisches Landesamt für Umwelt, Augsburg.

Gödeke, I. and Sukopp, U. (2010), *Der Indikatorenbericht 2010 zur Nationalen Strategie zur biologischen Vielfalt*, Berlin.

Gross, J.E., Goetz, S.J. and Cihlar, J. (2009), "Application of remote sensing to parks and protected area monitoring: Introduction to the special issue", *Monitoring Protected Areas*, Vol. 113 No. 7, pp. 1343–1345.

Gu, Y., Brown, J.F., Verdin, J.P. and Wardlow, B. (2007), "A five-year analysis of MODIS NDVI and NDWI for grassland drought assessment over the central Great Plains of the United States", *Geophysical Research Letters*, Vol. 34 No. 6, pp. n/a.

Hamming, R. W. (1991), *The art of probability for scientists and engineers*, Addison-Wesley, Redwood City, Calif.

Haralick, R.M., Shanmugam, K. and Dinstein, I. (1973), "Textural Features for Image Classification", *IEEE Transactions on Systems, Man, and Cybernetics*, SMC-3 No. 6, pp. 610–621.

Henle, K., Alard, D., Clitherow, J., Cobb, P., Firbank, L., Kull, T., McCracken, D., Moritz, R.F., Niemelä, J., Rebane, M., Wascher, D., Watt, A. and Young, J. (2008), "Identifying and managing the conflicts between agriculture and biodiversity conservation in Europe-A review", *Agriculture, Ecosystems & Environment*, Vol. 124 No. 1-2, pp. 60–71.

Hill, M.J., Smith, A.M. and Foster, T.C. (2000), "Remote Sensing of Grassland with RADARSAT; Case Studies from Australia and Canada", *Canadian Journal of Remote Sensing*, Vol. 26 No. 4, pp. 285–296.

Hill, M.J., Ticehurst, C.J., Lee, J.-S., Grunes, M.R., Donald, G.E. and Henry, D. (2005), "Integration of Optical and Radar Classifications for Mapping Pasture Type in Western Australia", *IEEE Transactions on Geoscience and Remote Sensing*, Vol. 43 No. 7, pp. 1665–1681.

Hill, M.J., Vickery, P.J., Furnival, E.P. and Donald, G.E. (1999), "Pasture Land Cover in Eastern Australia from NOAA-AVHRR NDVI and Classified Landsat TM", *Remote Sensing of Environment*, Vol. 67 No. 1, pp. 32–50.

Hoffmann, A., Penner, J., Vohland, K., Cramer, W., Doubleday, R., Henle, K., Kõljalg, U., Kühn, I., Kunin, W., Negro, J.J., Penev, L., Rodríguez, C., Saarenmaa, H., Schmeller, D., Stoev, P., Sutherland, W., Ó Tuama, É., Wetzel, F. and Häuser, C.L. (2014), "The need for an integrated biodiversity policy support process – Building the European contribution to a global Biodiversity Observation Network (EU BON)", *Nature Conservation*, Vol. 6, pp. 49-65.

Hollaus, M., Mücke, W., Höfle, B., Dorigo, W., Pfeifer, N., Wagner, W., Bauerhansl, C. and Regner, B. (2009), "Tree species classification based on full-waveform airborne laser scanning data", Texas A & M University: College Station, Texas, USA.

Hsu, C.-W. and Lin, C.-J. (2002), "A comparison of methods for multiclass support vector machines", *IEEE Transactions on Neural Networks*, Vol. 13 No. 2, pp. 415–425.

Hufkens, K., Thoonen, G., Vanden Borre, J., Scheunders, P. and Ceulemans, R. (2010), "Habitat reporting of a heathland site: Classification probabilities as additional information, a case study", *Ecological Informatics*, Vol. 5 No. 4, pp. 248–255.

Hughes, G. (1968), "On the mean accuracy of statistical pattern recognizers", *IEEE Transactions on Information Theory*, Vol. 14 No. 1, pp. 55–63.

Ichter, J., Evans, D., Richard, D., Poncet, L., Spyropoulou, R. and Martins, I.P. (2014), *Terrestrial habitat mapping in Europe: an overview*, Publications Office.

Japkowicz, N. (1999), "Concept Learning in the Absence of Counter-Examples: An Autoassociation-Based Approach to Classification", The State University of New Jersey, 1999.

Jaynes, E.T. (1957), "Information Theory and Statistical Mechanics", *Phys. Rev.*, Vol. 106 No. 4, pp. 620–630.

Jensen, M.E., Dibenedetto, J.P., Barber, J.A., Montagne, C. and Bourgeron, P.S. (2001), "Spatial Modeling of Rangeland Potential Vegetation Environments", *Journal of Range Management*, Vol. 54 No. 5, pp. p 528-536.

Jeon, B. and Landgrebe, D.A. (1999), "Partially supervised classification using weighted unsupervised clustering", *Geoscience and Remote Sensing, IEEE Transactions on*, Vol. 37 No. 2, pp. 1073–1079.

Keramitsoglou, I., Kontoes, C., Sifakis, N., Mitchley, J. and Xofis, P. (2005), "Kernel based re-classification of Earth observation data for fine scale habitat mapping", *Journal for Nature Conservation*, Vol. 13 No. 2-3, pp. 91–99.

Khan, S.S. and Madden, M.G. (2014), "One-class classification: taxonomy of study and review of techniques", *The Knowledge Engineering Review*, Vol. 29 No. 03, pp. 345–374.

Kobler, A., Džeroski, S. and Keramitsoglou, I. (2006), "Habitat mapping using machine learning-extended kernel-based reclassification of an Ikonos satellite image", *Ecological Modelling*, Vol. 191 No. 1, pp. 83–95.

Kottek, M., Grieser, J., Beck, C., Rudolf, B. and Rubel, F. (2006), "World Map of the Köppen-Geiger climate classification updated", *Meteorologische Zeitschrift*, Vol. 15 No. 3, pp. 259–263.

Küchler-Krischun, J. and Walter, A.M. (2007), *Nationale Strategie zur biologischen Vielfalt,* 3. Auflage, Berlin.

Kumar, S., Spaulding, S.A., Stohlgren, T.J., Hermann, K.A., Schmidt, T.S. and Bahls, L.L. (2009), "Potential habitat distribution for the freshwater diatom Didymosphenia geminata in the continental US", *Frontiers in Ecology and the Environment*, Vol. 7 No. 8, pp. 415–420.

Landesamt für Umwelt, Naturschutz und Geologie (LUNG) Mecklenburg-Vorpommern (2015), "Statistik der europäischen Schutzgebiete (Stand: 05/2015)", available at: http://www.lung.mv-regierung.de/insite/cms/umwelt/natur/schutzgebiete_portal/schutzgebiete_listen.htm (accessed 29 December 2015).

Lang, S., Mairota, P., Pernkopf, L. and Padoa Schioppa, E. (2015), "Earth observation for habitat mapping and biodiversity monitoring", *International Journal of Applied Earth Observation and Geoinformation*, Vol. 37, pp. 1–6.

Li, W. and Guo, Q. (2010), "A maximum entropy approach to one-class classification of remote sensing imagery", *International Journal of Remote Sensing*, Vol. 31 No. 8, pp. 2227–2235.

Li, Z., Huffman, T., McConkey, B. and Townley-Smith, L. (2013), "Monitoring and modeling spatial and temporal patterns of grassland dynamics using time-series MODIS NDVI with climate and stocking data", *Remote Sensing of Environment*, Vol. 138, pp. 232–244.

Lichman, M. (2013), *UCI Machine Learning Repository*, University of California, School of Information and Computer Sciences, Irvine, California, available at: http://archive.ics.uci.edu/ml.

Lindberg, E., Eysn, L., Hollaus, M., Holmgren, J. and Pfeifer, N. (2014), "Delineation of Tree Crowns and Tree Species Classification From Full-Waveform Airborne Laser Scanning Data Using 3-D Ellipsoidal Clustering", *IEEE Journal of Selected Topics in Applied Earth Observations and Remote Sensing*, Vol. 7 No. 7, pp. 3174–3181.

Liu, Y., Zha, Y., Gao, J. and Ni, S. (2004), "Assessment of grassland degradation near Lake Qinghai, West China, using Landsat TM and in situ reflectance spectra data", *International Journal of Remote Sensing*, Vol. 25 No. 20, pp. 4177–4189.

Lopez-Sanchez, J.M., Ballester-Berman, J.D. and Hajnsek, I. (2011), "First Results of Rice Monitoring Practices in Spain by Means of Time Series of TerraSAR-X Dual-Pol Images", *Selected Topics in Applied Earth Observations and Remote Sensing, IEEE Journal of*, Vol. 4 No. 2, pp. 412–422.

Lopez-Sanchez, J.M., Cloude, S.R. and Ballester-Berman, J.D. (2012), "Rice Phenology Monitoring by Means of SAR Polarimetry at X-Band", *Geoscience and Remote Sensing, IEEE Transactions on*, Vol. 50 No. 7, pp. 2695–2709.

Lucas, R., Rowlands, A., Brown, A., Keyworth, S. and Bunting, P. (2007), "Rule-based classification of multi-temporal satellite imagery for habitat and agricultural land cover mapping", *ISPRS Journal of Photogrammetry and Remote Sensing*, Vol. 62 No. 3, pp. 165–185.

MacDonald, Dettwiler and Associates Ltd. (2015), *RADARSAT-2 product description*.

Mack, B., Roscher, R. and Waske, B. (2014), "Can I Trust My One-Class Classification?", *Remote Sensing*, Vol. 6 No. 9, pp. 8779–8802.

Malouf, R. (2002), "A comparison of algorithms for maximum entropy parameter estimation", in *Proceedings of the 6th conference on Natural language learning - Volume 20*, Association for Computational Linguistics, Stroudsburg, PA, USA, pp. 49–55.

Mander, Ü., Mitchley, J., Keramitsoglou, I., Bock, M. and Xofis, P. (2005), "Earth observation methods for habitat mapping and spatial indicators for nature conservation in Europe", *Journal for Nature Conservation*, Vol. 13 No. 2-3, pp. 69–73.

Marconcini, M., Fernandez-Prieto, D. and Buchholz, T. (2014), "Targeted Land-Cover Classification", *Geoscience and Remote Sensing, IEEE Transactions on*, Vol. 52 No. 7, pp. 4173–4193.

Mazhelis, O. (2006), "One-class classifiers. A review and analysis of suitability in the context of mobile-masquerader detection", *South African Computer Journal*, Vol. 36, pp. 29–48.

McNairn, H. and Brisco, B. (2004), "The application of C-band polarimetric SAR for agriculture: a review", *Canadian Journal of Remote Sensing*, Vol. 30 No. 3, pp. 525–542.

McNairn, H., Champagne, C., Shang, J., Holmstrom, D. and Reichert, G. (2009), "Integration of optical and Synthetic Aperture Radar (SAR) imagery for delivering operational annual crop inventories", *ISPRS Journal of Photogrammetry and Remote Sensing*, Vol. 64 No. 5, pp. 434–449.

Mercer, J. (1909), "Functions of Positive and Negative Type, and their Connection with the Theory of Integral Equations", *Philosophical Transactions of the Royal Society of London A: Mathematical, Physical and Engineering Sciences*, Vol. 209 No. 441-458, pp. 415–446.

Metz, A., Marconcini, M., Esch, T., Reinartz, P. and Ehlers, M. (2014), "Classification of grassland types by combining multi-seasonal TerraSAR-X and Radarsat-2 imagery", paper presented at IGARSS 2014 / 35th CSRS, 13-18. Jul. 2014, Québec, Canada.

Ministerium für Landwirtschaft, Umwelt und Verbraucherschutz Mecklenburg-Vorpommern, Landesamt für Umwelt, Naturschutz und Geologie (LUNG) Mecklenburg-Vorpommern and UmweltPlan GmbH Stralsund (2012), *Erhaltung und Entwicklung der Biologischen Vielfalt in Mecklenburg-Vorpommern*, Schwerin, Germany.

Möckel, T., Dalmayne, J., Prentice, H., Eklundh, L., Purschke, O., Schmidtlein, S. and Hall, K. (2014), "Classification of Grassland Successional Stages Using Airborne Hyperspectral Imagery", *Remote Sensing*, Vol. 6 No. 8, p. 7732.

Morán-Ordóñez, A., Suárez-Seoane, S., Elith, J., Calvo, L. and Luis, E. de (2012), "Satellite surface reflectance improves habitat distribution mapping: a case study on heath and shrub formations in the Cantabrian Mountains (NW Spain)", *Diversity and Distributions*, Vol. 18 No. 6, pp. 588–602.

Mountrakis, G., Im, J. and Ogole, C. (2011), "Support vector machines in remote sensing: A review", *ISPRS Journal of Photogrammetry and Remote Sensing*, Vol. 66 No. 3, pp. 247–259.

Muñoz-Marí, J., Bovolo, F., Gomez-Chova, L., Bruzzone, L. and Camp-Valls, G. (2010), "Semisupervised One-Class Support Vector Machines for Classification of Remote Sensing Data", *IEEE Transactions on Geoscience and Remote Sensing*, Vol. 48 No. 8, pp. 3188–3197.

Neumann, C., Weiss, G., Schmidtlein, S., Itzerott, S., Lausch, A., Doktor, D. and Brell, M. (2015), "Gradient-Based Assessment of Habitat Quality for Spectral Ecosystem Monitoring", *Remote Sensing*, Vol. 7 No. 3, p. 2871.

Numata, I., Roberts, D.A., Sawada, Y., Chadwick, O.A., Schimel, J.P. and Soares, J.V. (2007), "Regional Characterization of Pasture Changes through Time and Space in Rondônia, Brazil", *Earth Interact*, Vol. 11 No. 14, pp. 1–25.

Oldenburg, C., Stenzel, S. and Schmidtlein, S. (2012), *MaxEnt-Wrapper: Manual for Application: MaxEnt-Wrapper (1.4)*, Karlsruhe Institute of Technology, Germany.

Oliver, C.J. and Quegan, S. (1998), *Understanding Synthetic Aperture Radar Images*.

Ouchi, K. (2013), *Recent Trend and Advance of Synthetic Aperture Radar with Selected Topics, Remote Sensing*, Vol. 5.

Pearce, D. and Moran, D. (1994), *The economic value of biodiversity*, Earthscan Publications Limited, London, UK.

Peeters, A. (2009), "Importance, evolution, environmental impact and future challenges of grasslands and grassland-based systems in Europe", *Grassland Science*, Vol. 55 No. 3, pp. 113–125.

Petrou, Z.I., Kosmidou, V., Manakos, I., Stathaki, T., Adamo, M., Tarantino, C., Tomaselli, V., Blonda, P. and Petrou, M. (2014), "A rule-based classification methodology to handle uncertainty in habitat mapping employing evidential reasoning and fuzzy logic", *Pattern Recognition Letters*, Vol. 48, pp. 24–33.

Phillips, S.J., Anderson, R.P. and Schapire, R.E. (2006), "Maximum entropy modeling of species geographic distributions", *Ecological Modelling*, Vol. 190 No. 3–4, pp. 231–259.

Phillips, S.J. and Dudík, M. (2008), "Modeling of species distributions with Maxent: new extensions and a comprehensive evaluation", *Ecography*, Vol. 31 No. 2, pp. 161–175.

Phillips, S.J., Dudík, M. and Schapire, R.E. (2004), "A Maximum Entropy Approach to Species Distribution Modelling".

Price, K.P., Guo, X. and Stiles, J.M. (2002a), "Comparison of Landsat TM and ERS-2 SAR data for discriminating among grassland types and treatments in eastern Kansas", *Computers and Electronics in Agriculture*, Vol. 37 No. 1-3, pp. 157–171.

Price, K.P., Guo, X. and Stiles, J.M. (2002b), "Optimal Landsat TM band combinations and vegetation indices for discrimination of six grassland types in eastern Kansas", *International Journal of Remote Sensing*, Vol. 23 No. 23, pp. 5031–5042.

Quegan, S. and Yu, J.J. (2001), "Filtering of multichannel SAR images", *Geoscience and Remote Sensing, IEEE Transactions on*, Vol. 39 No. 11, pp. 2373–2379.

Rannow, S. and Neubert, M. (Eds.) (2014), *Managing Protected Areas in Central and Eastern Europe Under Climate Change, Advances in Global Change Research*, Springer Netherlands.

Ratzke, U. and Mohr, H.-J. (2005), *Böden in Mecklenburg-Vorpommern: Abriss ihrer Entstehung, Verbreitung, Beiträge zum Bodenschutz in Mecklenburg-Vorpommern,* 2. Auflage.

Richards, J.A. (2005), "Analysis of remotely sensed data: the formative decades and the future", *Geoscience and Remote Sensing, IEEE Transactions on*, Vol. 43 No. 3, pp. 422–432.

Richards, J.A. and Jia, X. (2006), *Remote Sensing Digital Image Analysis: An Introduction,* 4th ed., Springer-Verlag, Berlin Heidelberg.

Ritter, G. and Gallegos, M.T. (1997), "Outliers in statistical pattern recognition and an application to automatic chromosome classification", *Pattern Recognition Letters*, Vol. 18 No. 6, pp. 525–539.

Roleček, J., Chytrý, M., Hájek, M., Lvončík, S. and Tichý, L. (2007), "Sampling design in large-scale vegetation studies: Do not sacrifice ecological thinking to statistical purism!", *Folia Geobotanica*, Vol. 42 No. 2, pp. 199–208.

Roth, A., Braun, G., Schreier, G. and Werninghaus, R. (2004), "TerraSAR-X Science Plan", available at: http://sss.terrasar-x.dlr.de/pdfs/TSX-Science-Plan.pdf (accessed 14 September 2015).

Rufin, P., Müller, H., Pflugmacher, D. and Hostert, P. (2015), "Land use intensity trajectories on Amazonian pastures derived from Landsat time series", *International Journal of Applied Earth Observation and Geoinformation*, Vol. 41, pp. 1–10.

Salakhutdinov, R., Roweis, S. and Ghahramani, Z. (2003), "On the Convergence of Bound Optimization Algorithms", in *Proceedings of the Nineteenth Conference Annual Conference on Uncertainty in Artificial Intelligence (UAI-03)*, Morgan Kaufmann, San Francisco, CA, pp. 509–516.

Sanchez-Hernandez, C., Boyd, D.S. and Foody, G.M. (2007), "Mapping specific habitats from remotely sensed imagery: Support vector machine and support vector data description based classification of coastal saltmarsh habitats", *Ecological Informatics*, Vol. 2 No. 2, pp. 83–88.

Sankey, T.T. and Bond, P. (2011), "LiDAR-Based Classification of Sagebrush Community Types", *Rangeland Ecology & Management*, Vol. 64 No. 1, pp. 92–98.

SCBD (Secretariat of the Convention on Biological Diversity) (2016a), "About Agricultural Biodiversity - Why is it important?", available at: https://www.cbd.int/agro/Importance.shtml (accessed 30 April 2016).

SCBD (Secretariat of the Convention on Biological Diversity) (2016b), "About Forest Biodiversity - Why does it matter?", available at: https://www.cbd.int/forest/importance.shtml (accessed 30 April 2016).

SCBD (Secretariat of the Convention on Biological Diversity) (2016c), "History of the Convention", available at: https://www.cbd.int/history/default.shtml (accessed 30 April 2016).

Schlager, P., Krismann, A., Wiedmann, K., Hiltscher, H., Hochschild, V. and Schmieder, K. (2013), "Multisensoral, object- and GIS-based classification of grassland habitats in the Biosphere Reserve Schwäbische Alb", *Photogrammetrie - Fernerkundung - Geoinformation*, Vol. 2013 No. 3, pp. 163–172.

Schmidt, T., Schuster, C., Kleinschmit, B. and Förster, M. (2014), "Evaluating an Intra-Annual Time Series for Grassland Classification - How Many Acquisitions and What Seasonal Origin Are Optimal?", *Selected Topics in Applied Earth Observations and Remote Sensing, IEEE Journal of*, Vol. 7 No. 8, pp. 3428–3439.

Schmidtlein, S. and Sassin, J. (2004), "Mapping of continuous floristic gradients in grasslands using hyperspectral imagery", *Remote Sensing of Environment*, Vol. 92 No. 1, pp. 126–138.

Schmitt, A. (2012), *Änderungserkennung in multitemporalen und multipolarisierten Radaraufnahmen, Dissertation*, Institut für Photogrammetrie und Fernerkundung, Karlsruhe.

Schmitt, A., Wendleder, A. and Hinz, S. (2015), "The Kennaugh element framework for multi-scale, multi-polarized, multi-temporal and multi-frequency 5SAR6 image preparation", *ISPRS Journal of Photogrammetry and Remote Sensing*, Vol. 102 No. 0, pp. 122–139.

Schölkopf, B., Platt, J.C., Shawe-Taylor, J., Smola, A.J. and Williamson, R.C. (2001), "Estimating the Support of a High-Dimensional Distribution", *Neural Computation*, Vol. 13 No. 7, pp. 1443–1471.

Schuster, C., Ali, I., Lohmann, P., Frick, A., Förster, M. and Kleinschmit, B. (2011), "Towards Detecting Swath Events in TerraSAR-X Time Series to Establish NATURA 2000 Grassland Habitat Swath Management as Monitoring Parameter", *Remote Sensing*, Vol. 3 No. 7, pp. 1308–1322.

Schuster, C., Förster, M., Schmidt, T., Kolbe, M., Frick, A. and Kleinschmit, B. (2012), *CARE-X-Projekt Schlussbericht - Change Detection Analyse für das flächendeckende Biodiversitätsmonitoring zur Erfüllung der EU FFH-Richtlinie mit Hilfe von RapidEye und TerraSAR-X Satellitendaten*.

Schuster, C., Schmidt, T., Conrad, C., Kleinschmit, B. and Förster, M. (2015), "Grassland habitat mapping by intra-annual time series analysis - Comparison of RapidEye and TerraSAR-X satellite data", *International Journal of Applied Earth Observation and Geoinformation*, Vol. 34 No. 0, pp. 25–34.

Shan, Z., Wang, C., Zhang, H. and Chen, J. (2011), "H-α Decomposition and Alternative Parameters for Dual Polarization SAR Data", September 12-16, Suzhou, China.

Shannon, C. E. (1948), "A Mathematical Theory of Communication", *Bell System Technical Journal*, Vol. 27 No. 3, pp. 379–423.

Silva, J.P., Toland, J., Jones, W., Eldridge, J., Thorpe, E. and O'hara, E. (2008), *LIFE and Europe's grasslands: restoring a forgotten habitat*, Office for Official Publications of the European Communities.

Small, D., Miranda, N. and Meier, E. (2009), "A Revised Radiometric Normalisation Standard for SAR", available at: http://dx.doi.org/10.1109/IGARSS.2009.5417439.

Smeeton, N.C. (1985), "Early history of the kappa statistic", *Biometrics*, No. 41, p. 795.

Smith, A.M. and Buckley, J.R. (2011), "Investigating RADARSAT-2 as a tool for monitoring grassland in western Canada", *Canadian Journal of Remote Sensing*, Vol. 37 No. 1, pp. 93–102.

Smith, A.M., Major, D.J., McNeil, R.L., Willms, W.D., Brisco, B. and Brown, R.J. (1995), "Complementarity of radar and visible-infrared sensors in assessing rangeland condition", *Remote Sensing of Environment*, Vol. 52 No. 3, pp. 173–180.

Smola, A.J., Schölkopf, B. and Müller, K.-R. (1998), "The connection between regularization operators and support vector kernels", *Neural Networks*, Vol. 11 No. 4, pp. 637–649.

Statistisches Amt Mecklenburg-Vorpommern (2014), *Bodenfläche nach Art der tatsächlichen Nutzung in Mecklenburg-Vorpommern 2013: Ergebnisse der Flächenerhebung, Statistische Berichte*, Schwerin, Germany.

Statistisches Amt Mecklenburg-Vorpommern (2015), available at: www.statistik-mv.de (accessed 17 May 2015).

Statistisches Bundesamt Wiesbaden (2015), "GENESIS-Online, Datenlizenz by-2-0", available at: https://www-genesis.destatis.de/genesis/online (accessed 29 December 2015).

Stenzel, S., Feilhauer, H., Mack, B., Metz, A. and Schmidtlein, S. (2014), "Remote sensing of scattered Natura 2000 habitats using a one-class classifier", *International Journal of Applied Earth Observation and Geoinformation*, Vol. 33, pp. 211–217.

Svoray, T. and Shoshany, M. (2003), "Herbaceous biomass retrieval in habitats of complex composition: a model merging SAR images with unmixed landsat TM data", *Geoscience and Remote Sensing, IEEE Transactions on*, Vol. 41 No. 7, pp. 1592–1601.

Tasumi, M., Hirakawa, K., Hasegawa, N., Nishiwaki, A. and Kimura, R. (2014), "Application of MODIS Land Products to Assessment of Land Degradation of Alpine Rangeland in Northern India with Limited Ground-Based Information", *Remote Sensing*, Vol. 6 No. 10, p. 9260.

Tax, D.M.J. (2001), "One-class Classification", PhD thesis, Delft University of Technology, 2001.

Tax, D.M.J. and Duin, R.P.W. (1999), "Support vector domain description", *Pattern Recognition Letters*, Vol. 20 No. 11–13, pp. 1191–1199.

Thoonen, G., Spanhove, T., Haest, B., Borre, J.V. and Scheunders, P. (2010), "Habitat mapping and quality assessment of heathlands using a modified kernel-based reclassification technique".

Thoonen, G., Spanhove, T., Vanden Borre, J. and Scheunders, P. (2013), "Classification of heathland vegetation in a hierarchical contextual framework", *International Journal of Remote Sensing*, Vol. 34 No. 1, pp. 96–111.

Touzi, R., Boerner, W.-M., Lee, J.S. and Lueneburg, E. (2004), "A review of polarimetry in the context of synthetic aperture radar: concepts and information extraction.", *Canadian Journal of Remote Sensing*, No. 30 (3), pp. 380–407.

Trimble (2011a), *eCognition ® Developer 8.64.1: User Guide*.

Trimble (2011b), *eCognition Developer 8.64.1: Reference Book*, München, Germany.

Turner, W., Spector, S., Gardiner, N., Fladeland, M., Sterling, E. and Steininger, M. (2003), "Remote sensing for biodiversity science and conservation", *Trends in Ecology & Evolution*, Vol. 18 No. 6, pp. 306–314.

UN (United Nations) (1992), *Convention on biological diversity: CBD*.

van der Linden, S., Rabe, A., Held, M., Jakimow, B., Leitão, P., Okujeni, A., Schwieder, M., Suess, S. and Hostert, P. (2015), "The EnMAP-Box—A Toolbox and Application Programming Interface for EnMAP Data Processing", *Remote Sensing*, Vol. 7 No. 9, p. 11249.

Vanden Borre, J., Paelinckx, D., Mücher, C.A., Kooistra, L., Haest, B., Blust, G. de and Schmidt, A.M. (2011), "Integrating remote sensing in Natura 2000 habitat monitoring: Prospects on the way forward", *Journal for Nature Conservation*, Vol. 19 No. 2, pp. 116–125.

VanDerWal, J., Falconi, L., Januchowski, S., Shoo, L. and Storlie, C. (2012), "SDMTools: Species Distribution Modelling Tools: Tools for processing data associated with species distribution modelling exercises. R Package Version 1.1-13", available at: http://CRAN.R-project.org/package=SDMTools.

Vapnik, V.N. (1998), *Statistical Learning Theory,* 1st edition, John Wiley & Sons, Inc., New York.

Wan, Z., Wang, P. and Li, X. (2004), "Using MODIS Land Surface Temperature and Normalized Difference Vegetation Index products for monitoring drought in the southern Great Plains, USA", *International Journal of Remote Sensing*, Vol. 25 No. 1, pp. 61–72.

Wang, C., Hunt Jr. E. Raymond, Zhang, L. and Guo, H. (2013), "Phenology-assisted classification of C3 and C4 grasses in the U.S. Great Plains and their climate dependency with MODIS time series", *Remote Sensing of Environment*, Vol. 138, pp. 90–101.

Ward, G., Hastie, T., Barry, S., Elith, J. and Leathwick, J.R. (2009), "Presence-Only Data and the EM Algorithm", *Biometrics*, Vol. 65 No. 2, pp. 554–563.

Waske, B. and Benediktsson, J.A. (2007), "Fusion of Support Vector Machines for Classification of Multisensor Data", *Geoscience and Remote Sensing, IEEE Transactions on*, Vol. 45 No. 12, pp. 3858–3866.

Waske, B. and Braun, M. (2009), "Classifier ensembles for land cover mapping using multitemporal SAR imagery", *ISPRS Journal of Photogrammetry and Remote Sensing*, Vol. 64 No. 5, pp. 450–457.

Waske, B. and van der Linden, S. (2008), "Classifying Multilevel Imagery From SAR and Optical Sensors by Decision Fusion", *Geoscience and Remote Sensing, IEEE Transactions on*, Vol. 46 No. 5, pp. 1457–1466.

Wegmüller, U. and Werner, C. (1997), "Retrieval of Vegetation Parameters with SAR Interferometry", *Geoscience and Remote Sensing, IEEE Transactions on*, Vol. 35 No. 1, pp. 18–24.

Weiss, W. (1996), *Mecklenburg-Vorpommern, Brücke zum Norden und Tor zum Osten.,* first ed., Justus Perthes Verlag Gotha GmbH, Gotha.

Wood, E.M., Pidgeon, A.M., Radeloff, V.C. and Keuler, N.S. (2012), "Image texture as a remotely sensed measure of vegetation structure", *Remote Sensing of Environment*, Vol. 121 No. 0, pp. 516–526.

Woodhouse, I.H. (2006), *Introduction to Microwave Remote Sensing*, CRC Press, Boca Raton.

Yates, C.J., McNeill, A., Elith, J. and Midgley, G.F. (2010), "Assessing the impacts of climate change and land transformation on Banksia in the South West Australian Floristic Region", *Diversity and Distributions*, Vol. 16 No. 1, pp. 187–201.

Yu, L., Zhou, L., Liu, W. and Zhou, H.-K. (2010), "Using Remote Sensing and GIS Technologies to Estimate Grass Yield and Livestock Carrying Capacity of Alpine Grasslands in Golog Prefecture, China", *Pedosphere*, Vol. 20 No. 3, pp. 342–351.

Zha, Y. and Gao, J. (2011), "Quantitative detection of change in grass cover from multi-temporal TM satellite data", *International Journal of Remote Sensing*, Vol. 32 No. 5, pp. 1289–1302.

Zhao, F., Xu, B., Yang, X., Jin, Y., Li, J., Xia, L., Chen, S. and Ma, H. (2014), "Remote Sensing Estimates of Grassland Aboveground Biomass Based on MODIS Net Primary Productivity (NPP): A Case Study in the Xilingol Grassland of Northern China", *Remote Sensing*, Vol. 6 No. 6, p. 5368.

Zillmann, E., Gonzalez, A., Montero Herrero, Enrique J., van Wolvelaer, J., Esch, T., Keil, M., Weichelt, H. and Garzon, A.M. (2014), "Pan-European Grassland Mapping Using Seasonal Statistics From Multisensor Image Time Series", *Selected Topics in Applied Earth Observations and Remote Sensing, IEEE Journal of*, Vol. 7 No. 8, pp. 3461–3472.

Zlinszky, A., Mücke, W., Lehner, H., Briese, C. and Pfeifer, N. (2012), "Categorizing Wetland Vegetation by Airborne Laser Scanning on Lake Balaton and Kis-Balaton, Hungary", *Remote Sensing*, Vol. 4 No. 6, p. 1617.

Zlinszky, A., Schroiff, A., Kania, A., Deák, B., Mücke, W., Vári, Á., Székely, B. and Pfeifer, N. (2014), "Categorizing Grassland Vegetation with Full-Waveform Airborne Laser Scanning: A Feasibility Study for Detecting Natura 2000 Habitat Types", *Remote Sensing*, Vol. 6 No. 9, p. 8056.